Structure of slowly rotating magnetized neutron stars in a perturbative approach

Struktur langsam rotierender magnetisierter Neutronensterne in einem störungstheoretischem Ansatz

Master's thesis of Martin Jakob Steil

July 2017

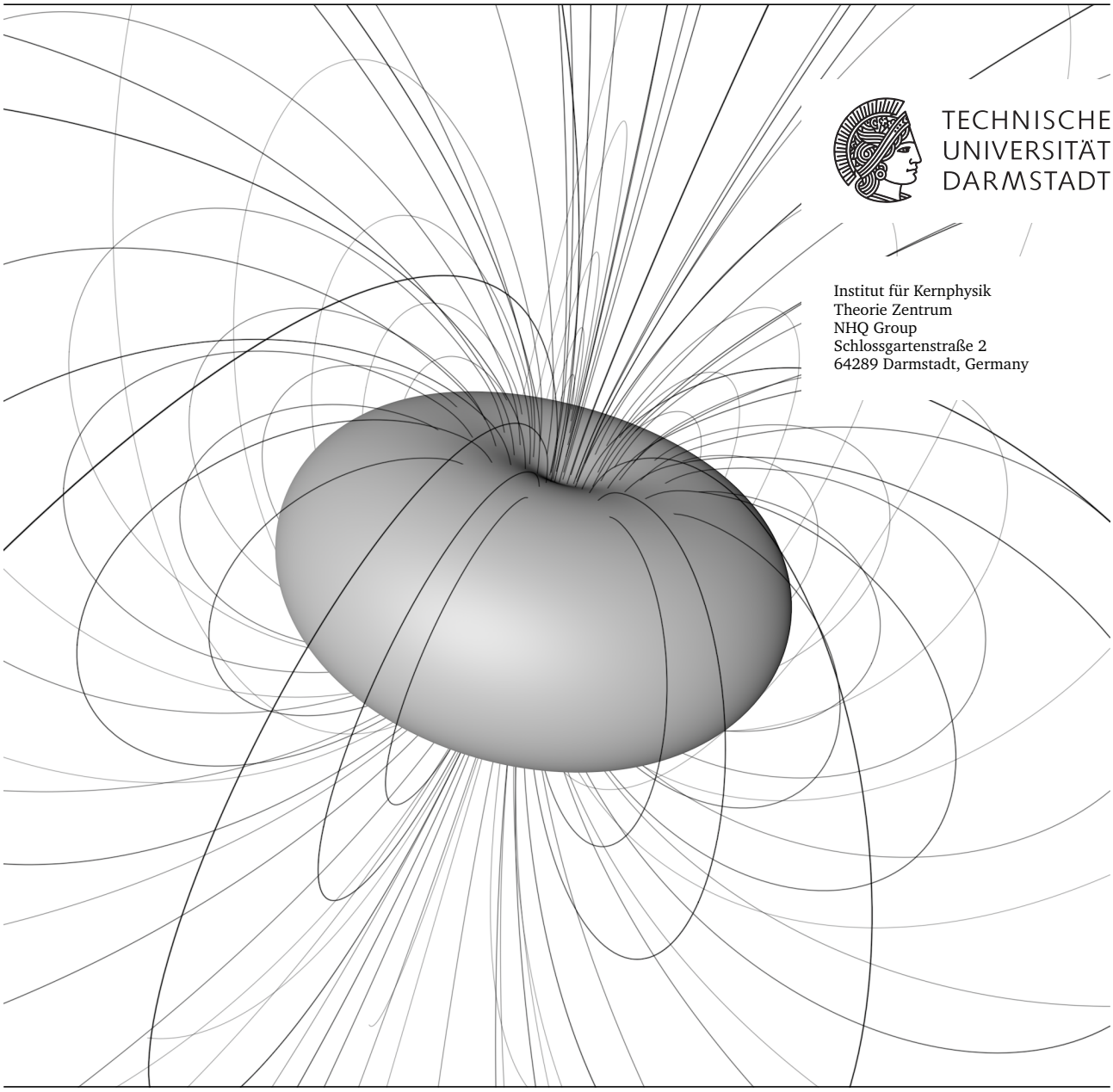

TECHNISCHE UNIVERSITÄT DARMSTADT

Institut für Kernphysik
Theorie Zentrum
NHQ Group
Schlossgartenstraße 2
64289 Darmstadt, Germany

Structure of slowly rotating magnetized neutron stars in a perturbative approach
Struktur langsam rotierender magnetisierter Neutronensterne in einem störungstheoretischem Ansatz

Vorgelegte Master-Thesis von Martin Jakob Steil

1. Gutachten: Priv.-Doz. Dr. Michael Buballa
2. Gutachten: Prof. Dr. Guy Moore

Tag der Einreichung: 27.07.2017

1. Korrigierte Fassung vom 22.06.2018

Abstract

In the scope of this Master's thesis we will discuss the structure of slowly rotating neutron stars (NS) with strong electro-magnetic fields. To compute NS deformed by electro-magnetic fields in a relativistic framework, one needs to solve the *Einstein-Maxwell* equations. The Einstein-Maxwell equations are a system of coupled partial differential equations (PDEs) and solving them is in general a rather involved task.

We will solve the Einstein-Maxwell equations perturbatively by expanding the system in the magnetic field B and in the angular velocity Ω up to $O\left(B^2\Omega^1\right)$. The resulting structure equations are not a system of coupled PDEs but a set staggered ordinary differential equation (ODE) systems. In $O\left(B^0\Omega^0\right)$ we recover the *Tolman-Oppenheimer-Volkoff* equations and in $O\left(B^1\right)$ we derive a relativistic *Grad-Shafranov* equation and a related $O\left(B^1\Omega^1\right)$ induction equation. In $O\left(\Omega^1\right)$ we recover an equation governing the *frame-dragging* frequency. In $O\left(B^2\Omega^0\right)$ and $O\left(B^2\Omega^1\right)$ we find sets of ODEs governing the electro-magnetic deformation of the NS. In our numerical computations we will only consider magnetic fields with purely dipolar structure and the related induced electric fields. Deformations resulting from this simple field geometry can be described up to $\mathrm{O}\left(B^2\Omega^1\right)$ using methods of the classical *Hartle-Throne* formalism, which was originally developed as a perturbative model for rotationally deformed NS up to third-order in the angular velocity.

We discuss the structure of electro-magnetically deformed NS within our perturbative approach. Furthermore we compare our perturbative solutions of $O\left(B^2\Omega^1\right)$ to numerically exact solutions of the Einstein-Maxwell equations, which we computed using the `magstar` code from the LORENE software library. In general we can report that for central magnetic fields below $\sim 10^{13}\,\mathrm{T}$ results from both methods are in good agreement.

In the scope of this work we furthermore discuss the possibility to model realistic NS with analytical interior solutions. We will present novel analytic solutions of the $\mathrm{O}\left(B^1\Omega^1\right)$ equations for those analytic interior solutions in form of series in compactness. Throughout this work we will identify the Tolman VII solution as a potent tool for effectively describing realistic NS.

After a summary of our key results we will conclude this thesis with an outlook on possible extensions, improvements and applications of the approach used in this Master's thesis.

Zusammenfassung

Im Rahmen dieser Master Thesis werden wir die Struktur von langsam rotierenden Neutronensternen (NS) mit starken elektro-magnetischen Feldern diskutieren. Um durch elektro-magnetische Felder deformierte NS in einem relativistischen Rahmen zu berechnen, müssen die *Einstein-Maxwell* Gleichungen gelöst werden. Die Einstein-Maxwell Gleichungen sind ein System gekoppelter partieller Differentialgleichungen (PDEs) und sie zu lösen ist im Allgemeinen eine ziemlich aufwendige Aufgabe.

Wir werden die Einstein-Maxwell Gleichungen perturbativ lösen, indem wir das System im magnetischen Feld B und der Winkelgeschwindigkeit Ω bis zur $O\left(B^2\Omega^1\right)$ entwickeln. Die aus dieser Entwicklung resultierenden Strukturgleichungen sind kein System gekoppelter PDEs sondern ein Satz von gestaffelten Systemen gewöhnlicher Differentialgleichungen (ODEs). In $O\left(B^0\Omega^0\right)$ finden wir die *Tolman-Oppenheimer-Volkoff* Gleichungen und in $O\left(B^1\right)$ leiten wir eine relativistische *Grad-Shafranov* Gleichung sowie eine dazugehörige $O\left(B^1\Omega^1\right)$ Induktions Gleichung ab. In $\mathrm{O}\left(\Omega^1\right)$ finden wir eine Gleichung für die *frame-dragging* Frequenz. In $O\left(B^2\Omega^0\right)$ und $O\left(B^2\Omega^1\right)$ finden wir Sätze von ODEs, welche die elektro-magnetischen Deformationen des NS beschreiben. In unseren numerischen

Berechnungen werden wir nur reine Dipol Magnetfelder und die dazugehörigen induzierten elektrischen Felder betrachten. Deformationen basierend auf der einfachen Geometrie solcher Felder können bis zur O $\left(B^2\Omega^1\right)$ mit Methoden des klassischen *Hartle-Thorne* Formalismuses behandelt werden, welche ursprünglich zur störungstheoretischen Beschreibung von durch Rotation deformierten NS bis zur dritten Ordnung in der Winkelgeschwindigkeit entwickelt wurden.

Wir diskutieren die Struktur elektro-magnetisch deformierter NS im Rahmen unseres perturbativen Modells. Des Weiteren vergleichen wir unsere perturbativen Lösungen der $O\left(B^2\Omega^1\right)$ mit numerisch exakten Lösungen der Einstein-Maxwell Gleichungen, welche wir mit dem `magstar` Code aus der LORENE Softwarebibliothek berechnet haben. Im Allgemeinen können wir berichten, dass für zentrale Magnetfelder unter $\sim 10^{13}$ T die Ergebnisse beider Methoden gut übereinstimmen.

Im Rahmen dieser Arbeit diskutieren wir des Weiteren die Möglichkeit realistische NS mit analytischen Innenraumlösungen zu beschreiben. Wir werden neuartige analytische Lösungen der O $\left(B^1\Omega^1\right)$ Gleichungen für diese analytischen Lösungen in Form von Reihen in der Kompaktheit präsentieren. Im Verlauf dieser Arbeit werden wir die Tolman VII Lösung als mächtiges Werkzeug zur effektiven Beschreibung realistischer NS identifizieren.

Nach einer Zusammenfassung unserer wichtigsten Resultate werden wir diese Arbeit mit einem Ausblick auf mögliche Erweiterungen, Verbesserungen und Anwendungen des in dieser Master Thesis verwendeten Ansatzes abschließen.

Acknowledgements

I would like to thank Prof. Dr. Wambach for giving me the opportunity to conduct research in the NHQ group and for his excellent lectures on general relativity and neutron stars. I am especially very grateful to my supervisor Priv.-Doz. Dr. Michael Buballa for his continuous assistance and support during my thesis project. I thank Prof. Dr. Guy Moore for the second assessment of this thesis.

Special thanks goes to Dr. Micaela Oertel for her invaluable contributions throughout this work. Without her expertise on the topics of magnetized neutron stars and general purpose equations of state this work in its current shape would have been impossible. Furthermore I am very thankful for her introduction into the usage of the LORENE-library and for her help with the online service COMPOSE.

Moreover, I would like to thank the members and alumni of the NHQ group: Eduard Alert, Philipp Isserstedt, Dominic Kraatz, Marco Schramm, Tobias Schulz, Matthias Seubert and Steven Vereeken, for their valuable input during various discussions and group meetings.

Furthermore I thank my colleagues at the Theory Center of IKP for the excellent working environment and atmosphere: especially Alexander Eller, Thomas Jahn, Vincent Klaer, Guy Moore, Daniel Robaina, Philipp Scior and all the previously mentioned members of the NHQ group.

I am very grateful to Sebastian Reinig for proofreading the final manuscript and for his expertise on programming related issues and questions.

Last but most certainly not least, I would like to express my deep gratitude towards my family and friends for their continuous support throughout my studies.

I dedicate this work to my late grandmother Anna Seethaler.

Erklärung zur Eigenständigkeit

Hiermit versichere ich, die vorliegende Master-Thesis ohne Hilfe Dritter nur mit den angegebenen Quellen und Hilfsmitteln angefertigt zu haben. Alle Stellen, die aus Quellen entnommen wurden, sind als solche kenntlich gemacht. Die schriftliche und elektronische Fassung stimmen überein. Diese Arbeit hat in gleicher oder ähnlicher Form noch keiner Prüfungsbehörde vorgelegen.

Darmstadt, den 27.07.2017

(Martin Jakob Steil)

Contents

1 Introduction

Neutron stars (NS) are the densest objects in the universe which can be observed directly. They are compact objects with masses between 1.4 and ~ 2 solar masses ($M_\odot$) and radii of only 10 to 15 km. The baryon number densities inside a NS reach from $n_{\mathrm{B,Fe}} = 4.730 \times 10^{-15}\,\mathrm{fm}^{-3}$ at the stellar surface up to multiple times nuclear baryon density $n_{\mathrm{B},0} = 0.16\,\mathrm{fm}^{-3}$ at the core. For most discussions NS can be considered cold [1]. A review on recent experimental constrains on NS masses, radii and equation of state (EoS) was given by F. Özel and P. Freire in [2].

In nature NS are supernova remnants and apart from being very dense objects they are also rotating and have strong electromagnetic fields. Rotation frequencies of NS can be as high as 716 Hz (PSR J1748-2446ad) and surface magnetic fields may exceed 10^{11} T (SGR 1806-20) [3].

Extreme densities, fast rotation and strong electromagnetic fields make NS ideal laboratories for extreme physics. The complication that NS are astronomical objects, which are thousands of light years away from earth, presents a huge challenge for probing their properties with experiments. With a new generation of X-ray telescopes (ASTROSAT-LAXPC, NICER, LOFT, SKA,...) and gravitational wave detectors (adv. LIGO, adv. Virgo, eLISA, KAGRA) astrophysicists are trying to probe NS and their properties in detail and precision to a degree never achieved before [2, 4, 5].

From a theoretical point of view a lot of aspects concerning NS structure and physics are still in very active research. The equation of state of neutron star matter and in general the detailed composition and properties of NS matter at high densities beyond $n_{\mathrm{B},0}$ is still unknown. We can not access such densities at low temperatures in experiments and a theoretical description of matter at densities above $n_{\mathrm{B},0}$ has proven to be very difficult. For the foreseeable future NS are the only laboratories which can provide experimental data for the low temperature, high density regime of the phase diagram of strongly interacting matter.

Extracting experimental data on NS composition and EoS requires a detailed understanding and description of NS structure. With upcoming precision measurements of orbital parameters, masses, radii, moments of inertia, burst oscillations, mergers and maybe even gravitational wave signals of isolated NS a detailed theoretical description of NS structure will be necessary to extract precise data on EoS and composition. A description beyond spherical symmetric stars involving the effects of rotation and electromagnetic fields will be important. In Chap. 2 we will discuss the theoretical framework needed for a description of NS structure.

In the following chapters we will focus on a very special class of NS: we will discuss NS with very strong surface magnetic fields of $\sim 10^{11}$ T so called *magnetars*. At least 10% of the NS population fall into this category after their birth in a supernova explosion [6]. The ultra strong magnetic fields are believed to decay on time scales of a few thousand years [6]. We observe magnetars in this active stage as either *Soft Gamma Repeaters* (SGRs) or *Anomalous X-ray Pulsars* (AXPs). Both sub classes have low rotation frequencies $\lesssim 1$ Hz (Periods P of a few seconds) but very high spin down rates $\dot{P}$ of $\sim 10^{-13}$ to $10^{-10}\,\mathrm{s\,s}^{-1}$ [3]. Those spin down rates are associated with the so called *dipole braking* mechanism: the magnetar's magnetic axis precesses around its rotation axis and the star emits dipole radiation. The energy loss by this radiation is compensated by a spin down of the magnetar's rotation. Using a simple classical description of this process and typical NS scales [7] the surface magnetic fields of SGRs and AXPs are expected to reach up to 10^{11} T [3]. The fields in the stellar center might exceed the surface field by a few orders of magnitude but the classical scalar virial theorem gives an upper limit of 10^{14} T [8, 9].

Magnetic fields of those magnitudes have effects on the stellar structure, since the electromagnetic contribution to the star's energy-momentum tensor becomes significant. Apart from those effects on the stellar structure the prospect of very high magnetic fields $\sim 10^{14}\,\mathrm{T}$ has recently lead to numerous papers (e.g. [10–13]) concerning the effect of strong magnetic fields on the EoS. The magnetic field affects the EoS due to Landau quantization of the constituent particles [14] and other effects. A self-consistent study of both structure and EoS effects of strong magnetic field was presented by D. Chatterjee et al. in 2014 [15]. They came to the conclusion that at field strengths of $\sim 10^{14}\,\mathrm{T}$ the effects on stellar structure are orders of magnitude bigger than the EoS effects when considering a magnetic field dependent MIT bag model quark matter EoS. The method developed by D. Chatterjee et al. was recently used to study effects of magnetic field dependent hadronic [16] and hybrid [17] EoS on the stellar structure self-consistently. R. O. Gomes et al. in [16] and B. Franzon et al. in [17] could confirm that EoS effects are minor at field strengths of $\sim 10^{14}\,\mathrm{T}$ when using hadronic or hybrid EoS.

The effects of electro-magnetic field on NS structure have been studied by Bonazzola et al. [18], Bocquet et al. [19] and Cardall et al. [20] within the framework of numerical relativity. They have solved the Einstein-Maxwell equations numerically exact for stationary, axisymmetric NS with rotation and magnetic fields.

Apart from studies within the framework of numerical relativity, Konno et al. [21] and later Ioka et al. and Colaiuda et al. [22–24] have studied slowly rotating, magnetically deformed stars in a perturbative approach. Those studies are based on an expansion of the Einstein-Maxwell equations in the magnetic field strength B and angular velocity Ω up to $O\left(B^2\Omega^1\right)$.

1.1 Structure this thesis

In the scope of this work we will study the effects of electro-magnetic fields on the structure and global properties of NS.

We will introduce the theoretical framework necessary to describe rotating NS with strong electromagnetic fields in Chap. 2. To describe the structure of rotating magnetized NS one faces the problem of solving the Einstein-Maxwell equations. In Sec. 2.2 we will summarize the approach of Bonazzola et al. [18] (BGSM) to solve this system iteratively, numerically exact in the frame work of numerical relativity. With Sec. 2.1 we will give a very short introduction of the key concepts of numerical relativity.

In Chap. 3 we will discuss in detail how to expand the Einstein-Maxwell equations in the magnetic field strength B and the rotation frequency around the metric of a spherical symmetric background star up to first-order in the angular velocity and second-order in the magnetic field. Konno et al. presented such an expansion in [21] using the Hartle-Thorne (HT) formalism [25]. We do not start from the HT metric but rather derive it as a special case of a more general expansion of the BGSM line element. During the derivation of our structure eqs. we keep a close connection between the perturbative model in construction and the BGSM model. We derive our central structure equations from the expanded field equations of Appendix A.

In Sec. 3.2 we discuss the O $\left(B^0\Omega^0\right)$ spherical symmetric background star and the *Tolman-Oppenheimer-Volkoff* (TOV) equations governing its structure. In this thesis we will use a reformulation of the TOV equation in terms of the logarithm of the enthalpy per baryon (log-enthalpy) h. We will discuss the advantages of this reformulation and in general the log-enthalpy as very convenient thermodynamic quantity in general relativistic calculations. We will discuss two analytical solutions of the TOV eqs.: the *Tolman VII* and *Schwarzschild interior* solution. In the following parts of this

thesis we will evaluate their potential to model the structure of realistic slowly rotating, magnetized NS.

We will briefly discuss the O $\left(B^0\Omega^1\right)$ frame-dragging effect of the classical HT formalism in Sec. 3.3 to then study electro-magnetic fields on the curved space time of TOV background stars in sections 3.4 and 3.5. We will again start with rather general expressions but then limit ourselves to purely dipolar magnetic field and induced quadrupolar electric fields.

In sections 3.6 and 3.7 we will discuss the O $\left(B^2\Omega^0\right)$ and O $\left(B^2\Omega^1\right)$ deformations caused by such fields. At the end of those two sections we will have derived all structure equations of our model, initial and matching conditions for their numerical integration and completely analytical exterior solutions for all of them.

In Sec. 3.8 we introduce a new model to study magnetized, non-rotating but with net charge Q globally charged NS. We will consider additional perturbations of O $\left(Q^2\right)$ and O $\left(B^1Q^1\right)$.

We will conclude our central theory Chap. 3 by discussing the global parameters related to our model.

In Chap. 4 we will briefly discuss the implementation of our structure equations. We give a short introduction into the implementation of the BGSM formalism within the LORENE library in Sec. 4.1. In this chapter we will also discuss and compare the performance and accuracy of both the perturbative and exact approach.

In Chap. 5 we will present numerical results. We will discuss results order by order as derived in Chap. 2.

Apart from numerical results for the two analytical background stars, we will present results for a polytropic and three realistic, hadronic EoS. We present information on all the used EoS in our second appendix B. For all EoS we will use the log-enthalpy as central thermodynamic quantity.

We will continuously check our results for numerical self-consistency and compare them to the results obtained with LORENE . To the best of our knowledge, a detailed quantitative comparison and evaluation of the potency of a perturbative general relativistic O $\left(B^2\Omega^1\right)$ magnetar model has not been done in literature so far.

In Chap. 6 we present a novel technique to construct analytical series solutions of the O $\left(B^1\Omega^1\right)$ structure equations for the two types of analytical background stars introduced earlier. We will also use this section to discuss related Newtonian results and expressions.

In Chap. 7 we will conclude this thesis by summarizing our results and by giving an outlook of possible extensions and applications related to our work.

1.2 Conventions, Notations and Units

Throughout this work we use the following conventions, notations and units.

We use Einstein summation convention, where we sum over contracted index pairs e.g.

$$A^\mu A_\mu \equiv \sum_{\mu=0}^{3} A^\mu A_\mu. \tag{1.1}$$

Greek letters $\alpha, \beta, \ldots$ are used for spacetime indices ranging from 0 to 3, where $\mu, \nu, \ldots$ are usually used for contracted spacetime summation indices. Latin indices $i, j, \ldots$ are used for spatial components only and therefore range from 1 to 3.

Indices are lowered e.g. $A_\alpha = g_{\alpha\mu} A^\mu$ and raised e.g. $A^\alpha = g^{\alpha\mu} A_\mu$ with the metric tensor $g_{\alpha\beta}$ and its inverse $g^{\alpha\beta}$ for which we use a space-like signature $(-,+,+,+)$. For partial derivatives we use the compact notation $\partial_\alpha \equiv \partial / \partial x^\alpha$. We typeset vectors in boldface e.g. $\mathbf{A}$, where $\mathbf{A} = A^\mu \mathbf{e}_\mu$.

We denote the symmetric parts of a tensor with parentheses () and antisymmetric parts with square brackets [] around the indices. Explicit symmetrization and anti-symmetrization can be performed in the usual way. The most important special cases within the scope of this work are

$$A_{(\alpha\beta)\gamma\ldots} = \frac{1}{2!}\left(A_{\alpha\beta\gamma\ldots} + A_{\beta\alpha\gamma\ldots}\right) \tag{1.2}$$

$$A_{[\alpha\beta]\gamma\ldots} = \frac{1}{2!}\left(A_{\alpha\beta\gamma\ldots} - A_{\beta\alpha\gamma\ldots}\right) \tag{1.3}$$

$$A_{[\alpha\beta\gamma]\delta\ldots} = \frac{1}{3!}\left(A_{\alpha\beta\gamma\delta\ldots} + A_{\gamma\alpha\beta\delta\ldots} + A_{\beta\gamma\alpha\delta\ldots} - A_{\alpha\gamma\beta\delta\ldots} - A_{\gamma\beta\alpha\delta\ldots} - A_{\beta\alpha\gamma\delta\ldots}\right) \tag{1.4}$$

We will use a similar notation for the permutation symbol: $[\alpha\beta\gamma\delta]$ is the completely antisymmetric perturbation symbol with $[0123] = 1$.

For the equations and numerical computations of this work we use a geometrized unit system (GU) in which the magnetic constant μ_0 divided by 4π, the Boltzmann constant k_B, the gravitational constant G and the speed of light c are taken as unity

$$\left[\mu_0/(4\pi)\right]_\mathrm{GU} \stackrel{!}{=} \left[k_\mathrm{B}\right]_\mathrm{GU} \stackrel{!}{=} [G]_\mathrm{GU} \stackrel{!}{=} [c]_\mathrm{GU} \stackrel{!}{=} 1. \tag{1.5}$$

We chose $\mu_0 = 4\pi$ to resemble a Gaussian unit system for the electromagnetic units since this system is quite common in astrophysics. In our GU system the dimensions of all physical quantities are powers of only one base dimension. We choose this dimension to be a length. This makes the equations and the numerical computations easier since they are not cluttered with physical constants. However for most discussions and figures we present our numerical results in more common units.

For the fundamental constants in our numerical computations we use the recommended values of CODATA [26] and for the astronomical constants we use values given by USNO [27].

2 Theoretical Framework: The Einstein-Maxwell equations

Neutron stars are rather small ($R \sim 15\,\mathrm{km}$) but quite massive ($M \sim 1.5\,M_\odot$), which means they have a large compactness ($Z \equiv M/R \sim 0.15$) and strong gravitational fields. Because of that fact, among other properties like strong electromagnetic fields or fast rotation, they need to be treated in a fully relativistic framework. The conventional theory to describe fully relativistic bodies with strong gravitational fields is Albert Einstein's theory of *general relativity* (GR).

Albert Einstein presented his geometric theory of gravitation, *general relativity*, in its final form in three papers in November 1915 [28–30]. We will only give a short introduction of GR, in which we will present the central equations and concepts important and related to this work. For a detailed discussion of GR we recommend, apart from Einstein's original papers, the textbooks [31–33].

Most of our central equations of the following chapters are derived from Einstein's field equations

$$\mathscr{E}_{\alpha\beta} \equiv G_{\alpha\beta} - 8\pi T_{\alpha\beta} = 0 \tag{2.1}$$

which relate curvature of four-dimensional spacetime, encoded in the Einstein tensor $G_{\alpha\beta}$, to the Einstein-Hilbert energy-momentum tensor $T_{\alpha\beta}$. This set of equations are the central point of GR. The Einstein tensor can be expressed in terms of the Ricci tensor $R_{\alpha\beta}$ and the scalar curvature R as

$$G_{\alpha\beta} \equiv R_{\alpha\beta} - \frac{1}{2} g_{\alpha\beta}\, R. \tag{2.2}$$

The scalar curvature is the contraction of the Ricci tensor $R \equiv R^{\mu}{}_{\mu}$ and the latter can be constructed from the metric and its first and second derivatives as

$$R_{\alpha\beta} \equiv \partial_\mu \Gamma^{\mu}{}_{\alpha\beta} - \partial_\beta \Gamma^{\mu}{}_{\mu\alpha} + \Gamma^{\mu}{}_{\mu\nu}\Gamma^{\nu}{}_{\beta\alpha} - \Gamma^{\mu}{}_{\beta\nu}\Gamma^{\nu}{}_{\mu\alpha}, \tag{2.3}$$

with the affine connection/Christoffel symbols

$$\Gamma^{\alpha}{}_{\beta\gamma} \equiv \frac{1}{2} g^{\alpha\mu}\Big[\partial_\gamma g_{\mu\beta} + \partial_\beta g_{\mu\gamma} - \partial_\mu g_{\beta\gamma}\Big]. \tag{2.4}$$

$g_{\alpha\beta}$ is the metric of the four-dimensional spacetime manifold $\mathcal{M}$. Given a coordinate grid $\{\mathbf{x}^\alpha\}$ with a set of associated basis vectors $\{\mathbf{e}_\alpha\}$ the metric tensor is given by the scalar product

$$g_{\alpha\beta} \equiv \mathbf{e}_\alpha \cdot \mathbf{e}_\beta = \mathbf{e}_\beta \cdot \mathbf{e}_\alpha = g_{\beta\alpha}. \tag{2.5}$$

The metric together with its first and second derivatives encodes the curvature of the spacetime manifold $\mathcal{M}$ completely. $g_{\alpha\beta}$ is essential for the line element/spacetime interval

$$ds^2 = \mathbf{e}_\mu \cdot \mathbf{e}_\nu dx^\mu dx^\nu = g_{\mu\nu} dx^\mu dx^\nu, \tag{2.6}$$

which is the measure for the separation of spacetime events. On a timelike ($ds^2 < 0$) world line the line element and the infinitesimal proper time interval $d\tau$ are related by $d\tau = \sqrt{-ds^2}$.

In GR free falling particles move along geodesics in $\mathcal{M}$ which are governed by the geodesic equation

$$\frac{d^2 q^\alpha}{ds^2} = -\Gamma^{\alpha}{}_{\mu\nu} \frac{dq^\mu}{ds} \frac{dq^\nu}{ds}, \tag{2.7}$$

with d^2q^α/ds^2 as the four acceleration of the particle. The geodesic eq. is the GR analogue to Newton's laws of motion and it can easily be extended to include external forces like the Lorentz force.

From the symmetry of the metric, and Schwarz's theorem follows the symmetry of the Ricci tensor and from it the symmetry of the Einstein tensor. The Ricci tensor is the only non-trivial contraction of the Riemann curvature tensor $R^\alpha{}_{\beta\gamma\delta}$, which can be defined by the Ricci identity

$$\nabla_\alpha \nabla_\beta A_\gamma - \nabla_\beta \nabla_\alpha A_\gamma = A_\mu R^\mu{}_{\gamma\beta\alpha} \tag{2.8}$$

as the commutator of the covariant derivative (2.11) of an arbitrary covector with components A_γ. The Riemann tensor $R_{\alpha\beta\gamma\delta}$ has a multitude of symmetries and properties when using the torsion free connection (2.4):

$$\begin{aligned}
&\text{Skew symmetry:} && R_{\alpha\beta\gamma\delta} = -R_{\beta\alpha\gamma\delta} = -R_{\alpha\beta\delta\gamma} = R_{\beta\alpha\delta\gamma}, && \text{(2.9a)}\\
&\text{Interchange symmetry:} && R_{\alpha\beta\gamma\delta} = R_{\gamma\delta\alpha\beta}, && \text{(2.9b)}\\
&\text{First Bianchi identity:} && 3R_{\alpha[\beta\gamma\delta]} = R_{\alpha\beta\gamma\delta} + R_{\alpha\gamma\delta\beta} + R_{\alpha\delta\beta\gamma} = 0, && \text{(2.9c)}\\
&\text{Second Bianchi identity:} && 3\nabla_{[\epsilon} R_{\gamma\delta]\alpha\beta} = \nabla_\epsilon R_{\alpha\beta\gamma\delta} + \nabla_\delta R_{\alpha\beta\epsilon\gamma} + \nabla_\gamma R_{\alpha\beta\delta\epsilon} = 0. && \text{(2.9d)}
\end{aligned}$$

For the compact notation of the first Bianchi identity we use screw symmetry in the last two indices to transform the uneven permutations which then add up with the even ones. For the compact notation of the second Bianchi identity we use interchange symmetry and then screw symmetry in the last two indices. An extremely useful contraction of the second Bianchi identity is

$$\nabla_\mu R^\mu{}_\alpha = \frac{1}{2}\nabla_\alpha R = \frac{1}{2}\partial_\alpha R. \tag{2.10}$$

The covariant derivative of a tensor field $\mathbf{T}$ of rank $\binom{m}{n}$ in direction $\mathbf{e}_\gamma$ is given by

$$\begin{aligned}
\nabla_\gamma T^{\alpha_1\ldots\alpha_m}{}_{\beta_1\ldots\beta_n} &= \partial_\gamma T^{\alpha_1\ldots\alpha_m}{}_{\beta_1\ldots\beta_n}\\
&\quad + \Gamma^{\alpha_1}{}_{\mu\gamma} T^{\mu\alpha_2\ldots\alpha_m}{}_{\beta_1\ldots\beta_n} + \ldots + \Gamma^{\alpha_m}{}_{\mu\gamma} T^{\alpha_1\ldots\alpha_{m-1}\mu}{}_{\beta_1\ldots\beta_n}\\
&\quad - \Gamma^{\mu}{}_{\beta_1\gamma} T^{\alpha_1\ldots\alpha_m}{}_{\mu\beta_2\ldots\beta_n} - \ldots - \Gamma^{\mu}{}_{\beta_n\gamma} T^{\alpha_1\ldots\alpha_m}{}_{\beta_1\ldots\beta_{n-1}\mu}.
\end{aligned} \tag{2.11}$$

A fundamental property of the covariant derivative of a rank $\binom{m}{n}$ tensor is, that it is a rank $\binom{m}{n+1}$ tensor. For a scalar S, which is a tensor of rank $\binom{0}{0}$, the covariant derivative is just the partial derivative $\nabla_\gamma S = \partial_\gamma S$ and $\partial_\gamma S$ is the component of a rank $\binom{0}{1}$ covector.

With the contraction (2.10) one can show another fundamental property of the Einstein tensor: its covariant divergence vanishes $\nabla_\mu G^{\alpha\mu} = 0$. Using this on the field eqs. (2.1) leads to

$$\nabla_\mu \mathscr{E}^{\alpha\mu} = \nabla_\mu G^{\alpha\mu} - \nabla_\mu T^{\alpha\mu} = 0 \Leftrightarrow \nabla_\mu T^{\alpha\mu} = 0, \tag{2.12}$$

which is the general relativistic form of energy-momentum conservation. If one is dealing with a moving perfect fluid one can project this equation orthogonally to the fluid rest frame, in which eq. (2.12) has the form of a relativistic Euler equation [24]. The fundamental law of baryon number conservation for a perfect fluid with proper baryon number density n_B and fluid four-velocity u^α takes the form

$$\nabla_\mu (n_\mathrm{B} u^\mu) = \partial_\mu (n_\mathrm{B} u^\mu \sqrt{-g}) = 0, \tag{2.13}$$

where the second identity uses the volume element of the metric $\sqrt{-g} = \sqrt{-\det g}$ and the identity $\Gamma^\mu{}_{\alpha\mu} = \partial_\alpha \log(\sqrt{-g})$.

In order to incorporate electromagnetic fields one has to solve the Einstein equations with the electromagnetic contribution to the energy-momentum tensor as well as the Maxwell equations since they govern the electromagnetic field. The Maxwell equations have to be solved on the curved four-dimensional spacetime governed by the Einstein equations.

A modern approach to formulate the Maxwell equations in a general relativistic framework is presented in [34–36]: one can begin by formulating the Maxwell equations in a locally flat inertial frame. In such a frame the inhomogeneous Maxwell source equations (*Gauss-Ampère law*), not including a macroscopic material description, in their contravariant form

$$\partial_\mu F^{\alpha\mu} = 4\pi J^\alpha \tag{2.14}$$

describe the effects of electromagnetism. In agreement with the laws of special relativity those equations are Lorentz invariant. $F_{\alpha\beta}$ is the antisymmetric Faraday tensor

$$F_{\alpha\beta} = 2\partial_{[\alpha}A_{\beta]} = \partial_\alpha A_\beta - \partial_\beta A_\alpha, \tag{2.15}$$

A_α is the electromagnetic four-potential and J_α is the four-current. The homogeneous Maxwell equations (*Gauss-Faraday law*)

$$\partial_{[\mu}F_{\nu\lambda]} = 0 \tag{2.16}$$

are satisfied by construction when using a Faraday tensor of form (2.15) due to the antisymmetry of $F_{\alpha\beta}$ and Schwarz's theorem.

The effects of spacetime curvature can be incorporated by replacing all derivatives with their covariant counterparts ($\partial_\mu \to \nabla_\mu$), the Minkowski metric of flat spacetime with its GR counterpart describing the curved spacetime ($\eta_{\alpha\beta} \to g_{\alpha\beta}$) and the volume element d^4x by $\sqrt{-g}d^4x$. This way of connecting a physical interaction with the gravitational field described by spacetime curvature is called *minimal coupling* [35, 36]. Applying this scheme to the Maxwell source equations (2.14) yields

$$\nabla_\mu F^{\alpha\mu} = 4\pi J^\alpha, \tag{2.17}$$

where $\nabla_\mu F^{\alpha\mu}$ is now the covariant divergence of the Faraday tensor. The Faraday tensor itself keeps its form (2.15) because we use a torsion free metric connection: the Levi-Civita connection. The Christoffel symbols we defined in eq. (2.4) satisfy the torsion freeness condition $\Gamma^\alpha_{(\beta\gamma)} = 0$ which leads to $\nabla_{[\alpha}A_{\beta]} = \partial_{[\alpha}A_{\beta]}$. Electric charge conservation takes the form of a covariant divergence

$$\nabla_\mu J^\mu = \partial_\mu(J^\mu\sqrt{-g}) = 0. \tag{2.18}$$

and the electromagnetic contribution to the energy-momentum tensor is

$$T^{(\mathrm{EM})}_{\alpha\beta} = \frac{1}{4\pi}\left(F_{\alpha\mu}F_\beta{}^\mu - \frac{1}{4}g_{\alpha\beta}F_{\mu\nu}F^{\mu\nu}\right). \tag{2.19}$$

Since $T^{(\mathrm{EM})}_{\alpha\beta}$ is one of the source terms of Einstein's field equations (2.1), the Maxwell equations (2.17) and the Einstein equations form a coupled system of nonlinear partial differential equations (PDEs). This system is sometimes referred to as Einstein-Maxwell equations and in general it can only be solved numerically using an iterative approach [18–20].

Noether's theorem relates symmetry properties of physical systems to conservation laws. We have already encountered charge (2.18) and baryon number (2.13) conservation which are related to internal symmetries. The $U(1)$ symmetry of electromagnetism implies electric charge conservation and similarly the $U(1)$ symmetry of QCD implies baryon number conservation.

The gauge invariance under general coordinate transformations of GR is the reason for the covariant conservation (2.12) of the energy-momentum tensor. We only presented the derivation of this conservation law from Einstein's field equations. It is also possible to derive $\nabla_\mu T^{\alpha\mu} = 0$ using the definition of the energy-momentum tensor as functional derivative of the matter action with respect to the metric, see e.g. [36]. By doing the latter, the connection to gauge invariance under general coordinate transformations becomes obvious.

Apart from those symmetries spacetime manifolds can have global symmetries which also lead to conservation laws. A way to encode spacetime symmetries in a coordinate-independent way is to use group actions on the spacetime manifold $\mathcal{M}$, see e.g. [37] for details. By using Lie groups it is possible to encode continuous transformations. A spacetime manifold $\mathcal{M}$ with metric $\mathbf{g}$ is invariant under such transformations if

$$2\nabla_{(\alpha}K_{\beta)} = \nabla_\alpha K_\beta + \nabla_\beta K_\alpha = 0, \tag{2.20}$$

where $\mathbf{K}$ is the generator of the symmetry group. Eq. (2.20) is called *Killing equation* and $\mathbf{K}$ *Killing vector*. When using a coordinate system adapted to such a Killing vector field, derivatives of the metric in the $\mathbf{K}$-direction vanish. This can be used to dramatically reduce the complexity of the field equations.

Noether's theorem implies that a Killing vector field has an associated conserved current. This current is

$$J^\alpha_{(K)} \equiv K^\mu R^\alpha{}_\mu \tag{2.21}$$

and its conservation $\nabla_\mu J^\mu_{(K)} = 0$ follows from the Killing eq. (2.20) and the fact that the directional derivative of the curvature scalar along a Killing vector field vanishes.

2.1 Numerical relativity and the 3+1 formalism

Solving Einstein's equations in dynamical scenarios with only a few or even no spacetime symmetries is in general a very difficult task due to the complicated nature of the coupled field equations. The field of *numerical relativity* (NR) has this task at its core. Again we will only give a short introduction of the basic points of NR and refer the interested reader to the various textbooks, lecture notes and papers on the topic. We can recommend the textbooks [34, 38] and the excellent lecture notes [39] for a first introduction to NR. After considerable ground work done by G. Darmois, A. Lichnerowicz and Y. Choquet-Bruhat between 1920 and 1950, P. A. M. Dirac and R. Arnowitt et al. presented a *Hamiltonian formulation of GR*, see e.g. [39] for references.

The formal foundation of the central equations of NR was laid 1962 by R. Arnowitt, S. Deser and C. W. Misner (ADM) in their paper "*The dynamics of general relativity*" [40]. The key idea of ADM and the authors mentioned previously was to decompose the four-dimensional spacetime manifold $\mathcal{M}$ into three-dimensional, space-like hypersurfaces Σ_t orthogonal to a time coordinate t. This *slicing of spacetime* is often referred to as *3+1 decomposition* and Fig. 2.1 shows the concept and some central objects.

The LHS of Fig. 2.1 depicts the foliation of the spacetime manifold while the RHS shows some central geometrical objects of the 3+1 formalism. The basis vector $\partial_\mathbf{t}$, given by the coordinate line of constant spatial points, can be decomposed into a spacelike part β (shift) and a timelike part $N\mathbf{n}$ (lapse): $\partial_\mathbf{t} = N\mathbf{n} + \beta$. $\mathbf{n}$ is the timelike unit normal ($n_\mu n^\mu = -1$) of the hypersurfaces Σ_t. In the following we will use coordinates adapted to this foliation: on Σ_t we introduce spatial coordinates $\{x^i\} = \{x^1, x^2, x^3\}$ and constant spatial points are connected by a temporal coordinate t. The basis vectors associated with those coordinates are $\partial_\mathbf{t} = \partial/\partial_t$ and $\partial_\mathbf{i} = \partial/\partial_{x^i}$.

From the geometry of the foliation it is possible to derive the components of $\mathbf{n}$ and β

$$\beta^\alpha = (0, \beta^i)^T, \tag{2.22}$$

$$n^\alpha = \frac{1}{N}(1, -\beta^i)^T, \tag{2.23}$$

$$n_\alpha = (-N, 0, 0, 0), \tag{2.24}$$

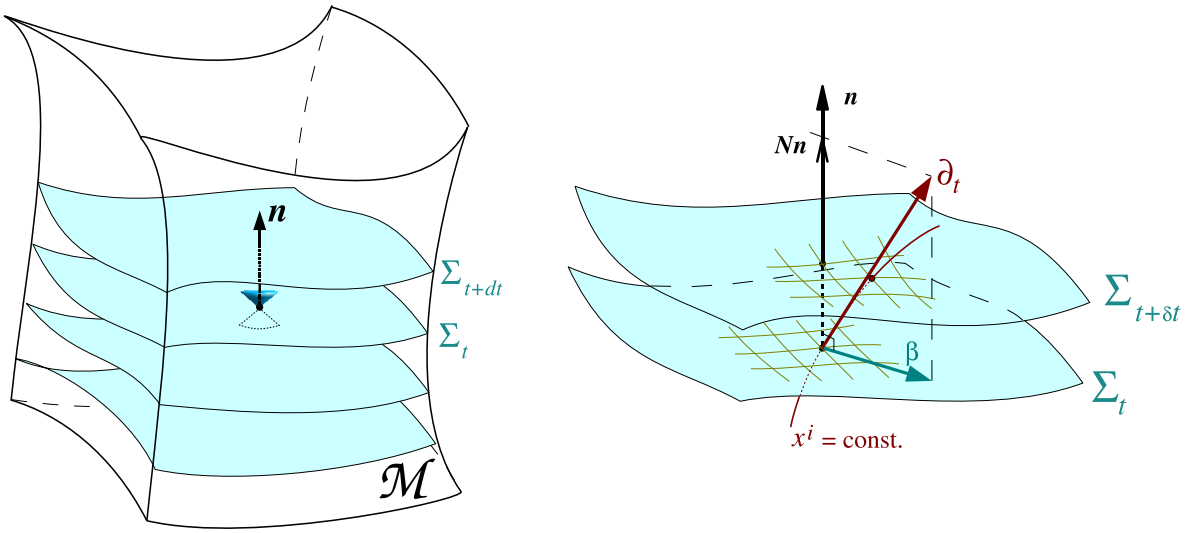

Figure 2.1: Foliation of the spacetime manifold $\mathcal{M}$ in space-like hypersurfaces Σ_t (left) and coordinates (x^i) on the hypersurfaces Σ_t and $\Sigma_{t+\delta t}$ (right). *Source: E. Gourgoulhon (2007) [39], p. 40 Fig. 3.1 (left) and p. 55 Fig. 4.1 (right).*

where the form of the covector component n_α follows directly from the normalisation condition and the vector component n^α. $\mathbf{n}$ can be interpreted as the four-velocity of the so called *Eulerian observer* $\mathcal{O}_n$ [18, 39]. For the Eulerian observer events on the hypersurface Σ_t are simultaneous. The lapse function N relates coordinate time t to the physical time τ measured by $\mathcal{O}_n$

$$d\tau = N dt. \tag{2.25}$$

Using coordinates adapted to this foliation it is possible to decompose the metric $\mathbf{g}$ of $\mathcal{M}$. The metric γ on Σ_t is the spatial part of the 4-metric $\mathbf{g}$, when using adapted coordinates

$$\gamma_{ij} = g_{ij}. \tag{2.26}$$

The full metric $\mathbf{g}$ can be decomposed as

$$\left(g_{\alpha\beta}\right) = \left(\begin{array}{c|c} -N^2 + \beta_k\beta^k & \beta_j \\ \hline \beta_i & \gamma_{ij} \end{array}\right), . \tag{2.27}$$

with the corresponding line element

$$ds^2 = g_{\mu\nu}dx^\mu dx^\nu = -N^2dt^2 + \gamma_{mn}\left(dx^m + \beta^m dt\right)\left(dx^n + \beta^n dt\right). \tag{2.28}$$

The volume elements of $\mathbf{g}$ and γ are related by $\sqrt{-\det g} = N\sqrt{-\det\gamma}$. The identities (2.26) and (2.27) can be obtained using the projection operator

$$\gamma^\alpha{}_\beta \equiv \delta^\alpha{}_\beta + n^\alpha n_\beta \tag{2.29}$$

and the eqs. (2.22) and (2.24). $\gamma^\alpha{}_\beta$ is purely spatial and can be used to project into Σ_t.

Using the 3+1 decomposition one can reformulate Einstein's field equation (10 coupled PDEs) into a constrained initial value problem of 6 evolution equations and 4 constrain equations (ADM equations). The constrain equations are four time-independent PDEs which specify the curvature on a given spatial hypersurface and the evolution equations are PDEs which describe how the curvature of the hypersurfaces changes in time, advancing from one time slice to the next. The ADM equations relate components of the spatial metric γ_{ij} and of the extrinsic curvature K_{ij} to source terms projected into Σ_t and t-direction. The extrinsic curvature K_{ij} encodes how Σ_t is embedded into $\mathcal{M}$. The *evolution equation of the spatial metric* encodes the relation between the time derivative of the induced metric components γ_{ij} and the components of the extrinsic curvature

$$\partial_t\gamma_{ij} = -2NK_{ij} + 2\nabla_{(i}\beta_{j)} = -2NK_{ij} + \nabla_i\beta_j + \nabla_j\beta_i, \tag{2.30}$$

where ∇_i are the covariant derivatives in Σ_t.

J. W. York played a primordial role in the development of modern NR by providing a general method to solve the initial data problem [41] and by reformulating the ADM equations into their modern form [42]. The field equations in this form (e.g. [34, p. 43, Box 2.1]) have several practical advantages over the classical GR field equations regarding implementation and numerical solution [34]. Apart from that the slicing of the four dimensional space time into three dimensional spatial hypersurfaces and an orthogonal time direction allows for an easier interpretation of results and central objects.

A lot of research and development by various groups alongside with the rapid development of powerful computer systems in the last decades made today's computations and simulations in the scope of NR possible. Today numerically exact solutions of fully general relativistic complex systems are possible. In this work we will limit our discussions on isolated compact stars but there are a lot of other, mostly astrophysical, applications and scenarios which use NR.

In the following section 2.2 we will give a short overview of the so called BGSM formalism which can be seen as an application of the formal concepts of NR to stationary, axisymmetric compact stars.

2.2 Exact solutions of Einstein-Maxwell equations in the BGSM formalism

In the introduction of Chap. 2 we presented the overall theoretical framework needed to describe compact objects with electromagnetic fields in a fully general relativistic setting. In this section we will introduce the formalism presented by S. Bonazzola, E. Gourgoulhon, M. Salgado and J. A. Marck (BGSM) in 1993 [18] for treating stationary, axisymmetric compact stars in a self-consistent way. We will present the equations of this formalism in the notation chosen by [37]. We can recommend the lecture notes [37] for a detailed presentation of the original BGSM formalism.

The metric of stationary, axisymmetric, circular and asymptotically flat spacetime can be expressed as

$$ds^2 = g_{\mu\nu}dx^\mu dx^\nu = -N^2dt^2 + A^2\left(d\tilde{r}^2 + \tilde{r}^2 d\theta^2\right) + B^2\tilde{r}^2\sin^2\theta\left(d\phi - N^\phi dt\right)^2, \tag{2.31}$$

where the metric potentials N, A, B and N^ϕ are functions of $(\tilde{r},\theta)$ only. t and ϕ are ignorable coordinates, meaning that all derivatives with respect to those two coordinates vanish.

The metric of this line element is

$$\left(g_{\alpha\beta}\right) = \left(\begin{array}{c|ccc} -N^2 + B^2N_\phi N^\phi\tilde{r}^2\sin^2\theta & 0 & 0 & -N^\phi B^2\tilde{r}^2\sin^2\theta \\ \hline 0 & A^2 & 0 & 0 \\ 0 & 0 & A^2\tilde{r}^2 & 0 \\ -N^\phi B^2\tilde{r}^2\sin^2\theta & 0 & 0 & B^2\tilde{r}^2\sin^2\theta \end{array}\right). \tag{2.32}$$

The form of this metric follows directly from the assumed symmetries, which can be encoded mathematically by two, commuting Killing vector fields $\xi = \partial/\partial_t$ and $\chi = \partial/\partial_\phi$. ξ is the generator of unidimensional translations in t and ξ is orthogonal to the hypersurfaces of constant time Σ_t. χ is the generator of rotations around the z-axis/in ϕ-direction. The t and ϕ coordinates are adapted to the Killing vector fields and therefore to the symmetries of the problem. The components of ξ and χ are trivial by construction

$$(\xi^\alpha) = (1,0,0,0)^T \tag{2.33}$$

$$(\chi^\alpha) = (0,0,0,1)^T. \tag{2.34}$$

ξ and χ commute

$$\xi^\mu\partial_\mu\chi_\alpha - \chi^\mu\partial_\mu\xi^\alpha = \xi^\mu\nabla_\mu\chi_\alpha - \chi^\mu\nabla_\mu\xi^\alpha = 0, \tag{2.35}$$

which means that the order in which both transformations are applied does not matter. A spacetime manifold with ξ and χ as Killing vectors is stationary and axisymmetric. Circularity refers to the vanishing of $g_{t\tilde{r}}$, $g_{t\theta}$, $g_{\tilde{r}\phi}$ and $g_{\theta\phi}$ and requires

$$\xi^\mu T_\mu{}^{[\alpha}\xi^\beta\chi^{\gamma]} = 0, \tag{2.36}$$

$$\chi^\mu T_\mu{}^{[\alpha}\xi^\beta\chi^{\gamma]} = 0. \tag{2.37}$$

Circularity limits the BGSM to sources with vanishing meridional flows: four-currents, four-velocities and the four-potential can not have non-vanishing $\tilde{r}$ and θ components. The metric components $g_{t\phi}$ and $g_{\phi\phi}$ are directly related to the scalar products of the corresponding killing vectors when using an adapted coordinate system

$$g_{t\phi} = \xi_\mu\chi^\mu, g_{\phi\phi} = \chi_\mu\chi^\mu. \tag{2.38}$$

The ϕ-component of the shift vector can then be identified as

$$N^{\phi} = -\frac{g_{t\phi}}{g_{\phi\phi}} = -\frac{\xi_{\mu}\chi^{\mu}}{\chi_{\mu}\chi^{\mu}}. \tag{2.39}$$

$g_{t\phi}$ or in the sense of eq. (2.39) N^{ϕ} is a measure of the spacetime vorticity. Configurations with vanishing N^{ϕ} are not only stationary, they are also static. Static spacetimes are stationary and the killing vector ξ is orthogonal to the family of hypersurface Σ_t.

The BGSM formalism uses so called MSQI (*Maximal Slicing - Quasi-Isotropic*) spherical coordinates $(t, \tilde{r}, \theta, \phi)$. Maximal slicing means that the volume element of the spatial metric γ_{ij} is maximal and the trace $K \equiv \gamma^{mn}K_{mn}$ of the extrinsic curvature tensor, from eq. (2.30), vanishes. Quasi-isotropic refers to the special choice of radial coordinates $(\tilde{r}, \theta)$ for which $g_{\tilde{r}\theta} = 0$ and $g_{\theta\theta} = \tilde{r}^2 g_{\tilde{r}\tilde{r}}$. The isotropic radius $\tilde{r}$ differs from the one used in the Hartle-Thorne formalism. The Hartle-Thorne formalism or in general most analytical approaches in classical GR use the flat space *areal radius* r, for which the area $\mathcal{A}_r$ of a 2-sphere at constant time and areal radius r is simply given by

$$\mathcal{A}_r = 4\pi r^2. \tag{2.40}$$

In the special case of spherical symmetry the same area in isotropic radial coordinates is given by

$$\mathcal{A}_r = 4\pi A(\tilde{r})^2 \tilde{r}^2, \tag{2.41}$$

in the BGSM formalism. The ADM eqs. of the BGSM formalism (2.44) do not reduce to the canonical TOV eqs. (3.48) when describing a spherical symmetric star without rotation and electromagnetic fields. They reduce to three second-order ordinary differential equations in $\tilde{r}$ [37]. Those structure equations in isotropic coordinates where first found by R. C. Tolman as early as 1930 [43].

A big advantage of the BGSM formalism is that it works with very general sources, energy-momentum tensors, as long as they do not break the symmetries of the model. For the following we will consider an energy-momentum tensor composed of a part for an ideal fluid $T^{(\mathrm{M})}_{\alpha\beta}$ and a part from the electromagnetic field $T^{(\mathrm{EM})}_{\alpha\beta}$:

$$T_{\alpha\beta} = T^{(\mathrm{M})}_{\alpha\beta} + T^{(\mathrm{EM})}_{\alpha\beta}. \tag{2.42}$$

Within the BGSM approach the fluid is allowed to rotate in ϕ-direction with an angular velocity Ω. The four-velocity of such a fluid is given by

$$u^{\alpha} = \left(u^t, 0, 0, u^{\phi}\right)^T = u^t \left(1, 0, 0, \Omega\right)^T, \tag{2.43}$$

with $\Omega = u^{\phi}/u^t$. For an observer moving with $\mathbf{u}$ the fluid is at rest and the corresponding reference frame $\mathcal{O}_u$ is called *fluid rest frame*. With respect to the symmetries of the model the vector potential and currents have only the following non-vanishing components A_t, A_{ϕ}, J_t and J_{ϕ}.

Using the metric of eq. (2.31) and the 3+1 decomposition of energy-momentum tensor of eq. (2.42) with the ADM equations, Einstein's field equations reduce to the following set of coupled, elliptic partial differential equations:

$$\Delta_3\left[\nu\right] = \sigma_{\nu}, \tag{2.44a}$$

$$\widetilde{\Delta}_3\left[N^{\phi}\tilde{r}\sin\theta\right] = \sigma_{N^{\phi}}, \tag{2.44b}$$

$$\Delta_2\left[(NB-1)\,\tilde{r}\sin\theta\right] = \sigma_{NB}, \tag{2.44c}$$

$$\Delta_2\left[\log A + \nu\right] = \sigma_{\nu A}, \tag{2.44d}$$

where $\nu \equiv \log N$. Δ_2, Δ_3 and $\widetilde{\Delta}_3$ are the scalar 2D flat space Laplacian, the scalar Laplacian and the ϕ-component of the vector Laplacian in 3D flat space:

$$\Delta_2 = \frac{\partial^2}{\partial \tilde{r}^2} + \frac{1}{\tilde{r}}\frac{\partial}{\partial \tilde{r}} + \frac{1}{\tilde{r}^2}\frac{\partial^2}{\partial \theta^2}, \tag{2.45a}$$

$$\Delta_3 = \frac{\partial^2}{\partial \tilde{r}^2} + \frac{2}{\tilde{r}}\frac{\partial}{\partial \tilde{r}} + \frac{1}{\tilde{r}^2}\frac{\partial^2}{\partial \theta^2} + \frac{1}{\tilde{r}^2 \tan\theta}\frac{\partial}{\partial \theta}, \tag{2.45b}$$

$$\widetilde{\Delta}_3 = \Delta_3 - \frac{1}{\tilde{r}^2 \sin^2\theta}. \tag{2.45c}$$

The source terms σ are complicated, nonlinear functions of the metric potentials, their derivatives and of components of the 3+1 decomposition of the energy-momentum tensor. They can be found in [37, eqs. (3.14)-(3.17)]. The field equations are therefore coupled and very complex but a numerical implementation is possible [18, 20].

The field equations are coupled to a set of Maxwell equations

$$\Delta_3 A_t = \sigma_{A_t}, \tag{2.46a}$$

$$\widetilde{\Delta}_3 \left[\frac{A^\phi}{r \sin\theta} \right] = \sigma_{A^\phi}, \tag{2.46b}$$

where the source terms σ_{A_t} and σ_{A^ϕ} are again complicated nonlinear functions of the metric potentials, their derivatives and of components of the 3+1 decomposition of the energy-momentum tensor. For a formulation of the BGSM formalism with electromagnetic fields we refer to the paper "*Rotating neutron stars models with magnetic field*" of M. Boncquet, S. Bonazzola, E. Gourgoulhon and J. Novak (BBGN) from 1995 [19]. The original BGSM paper included a discussion of electromagnetic fields but in a slightly different notation: they implemented the Maxwell equations for *electric* and *magnetic potentials* $\Phi \equiv -\mathbf{n}\cdot\mathbf{A} = -1/N\left(A_t + N^\phi A_\phi\right)$ and $\Psi \equiv \mathbf{e_3}\cdot\mathbf{A} = (A\tilde{r}\sin^2\theta)^{-1}A_\phi$ and not for the vector potentials.

The timelike four-velocity of $\mathscr{O}_n$ is

$$n^\mu = \frac{1}{N}\left(1,0,0,N^\phi\right)^T. \tag{2.47}$$

Projecting the momentum conservation equation into $\mathscr{O}_n$ leads to

$$\partial_i\left[h + \log N - \log\Gamma\right] = \frac{1}{\rho + P}\left(J^\phi - \Omega J^t\right)\partial_i A_\phi, \tag{2.48}$$

with the logarithm of the enthalpy per baryon (log-enthalpy) $h \equiv \log\left[\frac{\rho+P}{n_B m_B}\right]$, the Lorentz factor

$$\Gamma \equiv -\mathbf{n}\cdot\mathbf{u} = Nu^t = \frac{A\tilde{r}\sin\theta}{N}\left(\Omega - N^\phi\right) \tag{2.49}$$

relating the fluid rest frame and the Eulerian observer $\mathscr{O}_n$. The integrability condition for the system (2.48) requires the RHS to be expressible as a gradient $\partial_i M$. For non-constant A_ϕ BGSM have shown that this condition implies the following relation between the currents and A_ϕ

$$J^\phi - \Omega J^t = (\rho + P) f(A_\phi), \tag{2.50}$$

where $f(A_\phi)$ is the so called *current function*. We will discuss the relation between J^ϕ and A_ϕ and the notion of a current function further in Sec. 3.4. Using this result the equation of motion (2.48) can be integrated to a first integral of motion

$$h(\tilde{r},\theta)+\log\left[N(\tilde{r},\theta)\right]-\log\left[\Gamma(\tilde{r},\theta)\right]+M(\tilde{r},\theta)=\text{const.}, \tag{2.51}$$

with an electromagnetic Lorentz force term

$$M(\tilde{r},\theta)\equiv-\int_0^{A_\phi(\tilde{r},\theta)} f(x)dx. \tag{2.52}$$

Eq. (2.51) is the general relativistic equivalent to the classical Bernoulli theorem. To show this one can expand eq. (2.51) in the non-relativistic limit ($c\to\infty$). This is done in [37] for non-magnetic configurations and expressions for classical rotating and magnetic configurations are discussed in [44]. To briefly summarize the result: In the non-relativistic limit eq. (2.51) looks very similar but the relativistic enthalpy is replaced by the classical one, $\log N$ is replaced by the Newtonian gravitational potential, the Lorentz factor is replaced by the fluid velocity squared and the Lorentz force term is replaced with a classical analogon.

In the stellar interior the BGSM and BBGN approach assumes infinite conductivity. For cold NS this assumption is a good first approximation since the electrical transport properties of cold NS are mainly determined by the degenerate, relativistic electron gas, which has an electrical conductivity of the order 10^{24}s^{-1} [45] in the majority of the interior volume. According to Ohm's law the electric field measured in the fluid rest frame must vanish

$$E^{(u)}_\alpha = F_{\alpha\mu}u^\mu = 0, \tag{2.53}$$

when assuming an interior with infinite conductivity. Eq. (2.53) is commonly referred to as *ideal magnetohydrodynamics (MHD) condition* [34]. Projecting this relation into $\mathscr{O}_n$ leads to a simple relation between A_t and A_ϕ:

$$\frac{\partial A_t}{\partial x^i}=-\Omega\frac{\partial A_\phi}{\partial x^i}. \tag{2.54}$$

In case of rigid rotation $\Omega=\text{const.}$ eq. (2.54) can be integrated to

$$A_t=-\Omega A_\phi+C, \tag{2.55}$$

where C is related to the total charge of the star. We will refer to eq. (2.55) as *induction equation*. Eqs. (2.54) and (2.55) only hold in the stellar interior in the stellar exterior the second Maxwell equation for the A_t eq. (2.46b) needs to be solved.

The electric and magnetic fields measured in $\mathscr{O}_n$ are given by

$$E^{(n)}_\alpha = F_{\alpha\mu}n^\mu, \tag{2.56}$$

$$B^{(n)}_\alpha = -\frac{1}{2}\epsilon_{\alpha\mu\nu\xi}n^\mu F^{\nu\xi}. \tag{2.57}$$

$\epsilon_{\alpha\mu\nu\xi}=\sqrt{-g}[\alpha\mu\nu\xi]$ is the pseudo-tensorial Levi-Civita symbol associated with the metric [32] and $\sqrt{-g}$ is the proper measure for the volume element

$$\sqrt{-g}=\sqrt{-\det\mathbf{g}}=NA^2B\tilde{r}^2\sin\theta. \tag{2.58}$$

The electromagnetic fields described by (2.56) and (2.57) are purely spatial $E^{\mu}_{(n)} n_{\mu} = B^{\mu}_{(n)} n_{\mu} = 0$ and in the following we will drop the label (n): if not explicitly stated otherwise we will measure all electromagnetic quantities in $\mathcal{O}_n$.

Using the volume element (2.58) and the velocity of $\mathcal{O}_n$ (2.47) the non-vanishing field components are

$$E_{\tilde{r}} = \frac{1}{N}\left(\partial_{\tilde{r}} A_t + N^{\phi}\partial_{\tilde{r}} A_{\phi}\right), \tag{2.59a}$$

$$E_{\theta} = \frac{1}{N}\left(\partial_{\theta} A_t + N^{\phi}\partial_{\theta} A_{\phi}\right), \tag{2.59b}$$

$$B_{\tilde{r}} = \frac{1}{A\tilde{r}^2 \sin\theta}\partial_{\theta} A_{\phi}, \tag{2.59c}$$

$$B_{\theta} = -\frac{1}{A\sin\theta}\partial_{\tilde{r}} A_{\phi}. \tag{2.59d}$$

As a consequence of the ideal MHD condition the Faraday tensor in the stellar interior is completely determined by the magnetic field

$$F^{\alpha\beta} = \epsilon^{\alpha\beta\mu\nu} u_{\mu} B^{(u)}_{\nu}, \tag{2.60}$$

which implies for the electric field

$$E_i = -\epsilon_{ijk}\left(\frac{u^j}{u^t} + \beta^j\right)\frac{B^k}{N}, \tag{2.61}$$

with $\epsilon_{ijk} = \sqrt{\gamma}[ijk] = n^{\mu}\epsilon_{\mu ijk}$.

All global quantities, like gravitational and baryonic mass, angular momentum, flat space radii and more can be obtained by integrals or analytic relations in terms of the metric potentials and source terms. Most formulas can be found in the original BGSM paper [18] and for a detailed discussion we refer to [37, Chap. 4, p. 59].

We will briefly describe a scheme for the numerical implementation of the BGSM formalism in Sec. 4.1. Apart from numerical errors the solutions of the BGSM/BBGM structure equations are exact solutions of the Einstein-Maxwell equations. Good measures of those numerical errors and the self-consistency of a numerical solution are the general relativistic virial identities GRV3 [46] and GRV2 [47].

In the scope of the current work we will focus our discussions on slowly rotating NS with constant Ω and magnetic fields modeled by a current function $f(x) = \text{const.}$. As we discuss in Sec. 3.4 choosing such a constant current function will limit the magnetic field geometry to purely dipolar magnetic fields.

3 Perturbative Magnetar model

In this chapter we discuss a perturbative expansion of the Einstein-Maxwell equations in the magnetic field up to $O\left(B^2\right)$ and in angular velocity up to $O\left(\Omega^1\right)$. We will do so using an approach similar to the one proposed by J. B. Hartle and K. S. Thorne (HT) in the 1970s. In 1967 Hartle presented an approach in his paper "*Slowly Rotating Relativistic Stars I. Equations of Structure*" [25], which in its core is based on an expansion of Einstein's field equations for rotating fluid spheres in the angular velocity Ω. In the following years HT published a series of papers related to this formalism, e.g. [48, 49].

In 1999 Konno et al. [21] used the HT ansatz to describe the deformations of NS with polytropic EoS by a dipole magnetic field. In the following years several authors picked up this idea and used it to solve the Einstein-Maxwell equations for magnetized NS perturbatively. In 2003 and 2004 K. Ioka and M. Sasaki discussed magnetic fields of NS extensively using a perturbative approach [22, 23]. Influenced by the work of Konno, A. Colaiuda et al. presented their work on magnetized NS in 2008 [24].

The general motivation to describe magnetic deformations of the NS perturbatively is simple: even in magnetars the electromagnetic contribution to the total energy-momentum tensor is in general rather small compared to the matter contributions. A magnetic field of $B = 4 \times 10^{12}\,\mathrm{T}$ has a corresponding energy density

$$B^2 = (4 \times 10^{12}\,\mathrm{T})^2 \sim 1\,\mathrm{MeV\,fm^{-3}}. \tag{3.1}$$

Contributions from pressure and energy density to the energy-momentum tensor are well above $100\,\mathrm{MeV\,fm^{-3}}$ in the central regions of NS. Compared to these contributions $1\,\mathrm{MeV\,fm^{-3}}$ from the magnetic field is a very small perturbation to the energy-momentum tensor of the fluid. So for magnetars with weak or even intermediate magnetic fields one can expect only small deformations away from spherical symmetry.

Similarly one can expect that for small rotation frequencies the deformations related to rotation are minor. An expansion only up to linear order in the rotation frequency should give reasonable results for slowly rotating magnetars. For this class of NS the magnetic deformations are expected to exceed rotational deformations by some orders of magnitude [18, 50].

In the following sections of this chapter we will formulate a theoretical framework to describe magnetars perturbatively.

3.1 Ansatz

In this section we will expand the metric and source terms around the ones of a spherical symmetric, non-rotating NS without electro-magnetic fields.

We will begin with expanding the BGSM line element (2.31) around the metric of a spherical symmetric background star. The line element of such a star can be given in the form

$$ds^2_{(00)} \equiv g^{(00)}_{\mu\nu} dx^\mu dx^\nu \equiv -\mathrm{e}^{\nu(r)} dt^2 + \mathrm{e}^{\lambda(r)} dr^2 + r^2 \left(d\theta^2 + \sin^2\theta d\phi^2\right) \tag{3.2a}$$

$$= -\mathrm{e}^{\nu(r)} dt^2 + \mathrm{e}^{\lambda(r)} dr^2 + r^2 d\Omega^2. \tag{3.2b}$$

For our magnetar model we use the areal radius, since it is better suited than the isotropic radius for our computations using the classical Einstein field eqs. (2.1). The angular dependency of the lapse function $N(r,\theta)$ can be expanded in zonal ($m=0$) scalar harmonics around $\mathrm{e}^{\nu(r)}$ as

$$N(r,\theta) \equiv \mathrm{e}^{\nu(r)/2}\left(1+2\sum_l n_l(r)\,\mathrm{P}_l(\cos\theta)\right)^{1/2} = \mathrm{e}^{\nu(r)/2}\left(1+\sum_l n_l(r)\,\mathrm{P}_l(\cos\theta)\right)+O\left(B^4\Omega^2\right), \quad (3.3)$$

where we consider $n_l(r)$ as $O\left(B^2\Omega^0\right)$ corrections.

The shift vector β or specifically its only non-vanishing component $N^\phi(r,\theta)$ has to be expanded in vector harmonics to preserve its transformation properties. For vector and tensor harmonics we use the notations and definitions given in [34, 51]. Our expansion in general is very similar to the one performed by K. Ioka and M. Sasaki [23] but we will keep a close connection to the quantities of the 3+1 formalism introduced in Sec. 2.1. For the expansion of $N^\phi(r,\theta)$ we use odd parity zonal vector harmonics

$$S^\phi_{l0} = \sigma^{\phi N} S^{l0}_N = \sigma^{\phi\phi} S^{l0}_\phi = \sum_l \sqrt{\frac{2l+1}{4\pi}}\frac{1}{\sin\theta}\frac{d\mathrm{P}_l(\cos\theta)}{d\theta}, \quad (3.4)$$

with the inverse metric σ^{AB} on the surface of the two-dimensional unit sphere S^2 and $S^{l0}_A = \nabla_A Y_{l0}$, where ∇_A is the covariant derivative on S^2. The expansion $N^\phi(r,\theta)$ reads

$$N^\phi(r,\theta) \equiv \sum_l w_l(r)\frac{1}{\sin\theta}\frac{d\mathrm{P}_l(\cos\theta)}{d\theta}, \quad (3.5)$$

where we have absorbed the normalisation factor $\sqrt{(2l+1)/(4\pi)}$ in the expansion coefficients, as we will do so with most such factors in the following.

What remains in terms of the metric is to expand the spatial metric γ_{ij}. For that task we use even parity tensor harmonics and a convenient ansatz [23] is

$$\gamma_{rr} \equiv \mathrm{e}^{\lambda(r)}\left(1+2\frac{\mathrm{e}^{\lambda(r)}}{r}\sum_l m_l(r)\,\mathrm{P}_l(\cos\theta)\right), \quad (3.6a)$$

$$\gamma_{\theta\theta} \equiv r^2\left(1+2\sum_l k_l(r)\,\mathrm{P}_l(\cos\theta)\right), \quad (3.6b)$$

$$\gamma_{\phi\phi} \equiv \sin^2\theta\,\gamma_{\theta\theta}, \quad (3.6c)$$

$$\gamma_{ij} \equiv 0 \quad \forall i \neq j. \quad (3.6d)$$

T. Regge and J. A. Wheeler [52] and F. J. Zerilli [53] developed this ansatz and particular gauge choice for metric perturbation in a spherical spacetime.

Similar to the metric we also need to expand the source terms in orders of B and Ω. We consider the following source term

$$T_{\alpha\beta} = T^{(\mathrm{F00})}_{\alpha\beta} + \Delta T^{(\mathrm{F})}_{\alpha\beta} + T^{(\mathrm{EM})}_{\alpha\beta} + O\left(B^4\Omega^2\right), \quad (3.7)$$

where $T^{(\mathrm{F00})}_{\alpha\beta}$ is the $O\left(B^0\Omega^0\right)$ source term of the background star, $T^{(\mathrm{EM})}_{\alpha\beta}$ is the energy-momentum tensor of the electro-magnetic field and and $\Delta T^{(\mathrm{F})}_{\alpha\beta}$ are corrections due to magnetic deformation of the fluid.

As matter source term we will consider an ideal fluid which has the energy-momentum tensor

$$T^{(\mathrm{F})}_{\alpha\beta} = (P+\rho)u_\alpha u_\beta + P g_{\alpha\beta}, \quad (3.8)$$

with pressure P, energy density ρ and fluid four-velocity $\mathbf{u}$. The fluid four-velocity $\mathbf{u}$ is a normalized time-like vector $u_\mu u^\nu = -1$. With this normalization condition, eq. (2.43) and the metric one can find an explicit expression for u^t and u^ϕ

$$u^t = \frac{1}{\sqrt{-\left(g_{tt} + 2g_{t\phi}\Omega + g_{\phi\phi}\Omega^2\right)}} = \mathrm{e}^{\nu(r)/2}\left(1 - \sum_l n_l(r)\,\mathrm{P}_l(\cos\theta)\right) + O\left(B^4\Omega^2\right), \tag{3.9a}$$

$$u^\phi = \Omega u^t. \tag{3.9b}$$

The pressure and energy density iso-surfaces of the background star $P(r)$ and $\rho(r)$ are spherical shells. Those are deformed in presence of a magnetic field. We describe this deformations as corrections to the background star values $P(r)$ and $\rho(r)$. To do so we first recall the logarithm of the enthalpy per baryon

$$h \equiv \log\left[\frac{\rho + P}{n_\mathrm{B} m_\mathrm{B}}\right] = \log\left[\frac{\mu}{\mu_0}\right] \tag{3.10}$$

as introduced early with eq. (2.51). μ_0 is the value of the baryon chemical potential at zero pressure and it is given by the mean baryon rest mass m_B. The Gibbs-Duhem relation at zero temperature

$$\rho = -P + \mu n_\mathrm{B} = -P + \frac{dP}{d\mu}\mu \tag{3.11}$$

can be rearranged to yield a differential identity for h

$$dh = \frac{d\mu}{\mu} = \frac{dP}{\rho + P} \tag{3.12}$$

which can be integrated to the definition we gave earlier. The identity

$$\frac{dP}{dh} = \rho + P \tag{3.13}$$

is extremely useful. In the following sections we identify the logarithm of the enthalpy per baryon h as the most convenient thermodynamic base quantity to work with. Identifying and working with the log-enthalpy within the HT is a unique feature of our derivation. Most authors work in the pressure as base thermodynamic quantity and at some point introduce a dimensionless "*pressure perturbation factor*" [21, 25]. The pressure perturbation factor in the classical HT approach is in fact the deformation log-enthalpy h grid and introducing h as corresponding fundamental thermodynamic property for the background star makes derivation and interpretation of results much easier. For the following we will consider a one-parameter EoS in h: the EoS relates all thermodynamic quantities to h. In the present work the relevant quantities are pressure $P(h)$, energy density $\rho(h)$, baryon density $n_\mathrm{B}(h)$ and their derivatives with respect to h. Using the EoS we can relate the deformations of the log-enthalpy grid $h(r)$ to the deformations of the pressure and density surfaces as

$$h(r,\theta) \equiv h(r) + \sum_l h_l(r)\,\mathrm{P}_l(\cos\theta) + O\left(B^4\Omega^2\right), \tag{3.14a}$$

$$P(r,\theta) \equiv P(h(r,\theta)) = P(r) + (P(r) + \rho(r))\sum_l h_l(r)\,\mathrm{P}_l(\cos\theta) + O\left(B^4\Omega^2\right), \tag{3.14b}$$

$$\rho(r,\theta) \equiv \rho(h(r,\theta)) = \rho(r) + \frac{d\rho}{dh}\sum_l h_l(r)\,\mathrm{P}_l(\cos\theta) + O\left(B^4\Omega^2\right), \tag{3.14c}$$

$$n_\mathrm{B}(r,\theta) \equiv n_\mathrm{B}(h(r,\theta)) = n_\mathrm{B}(r) + \frac{dn_\mathrm{B}}{dh}\sum_l h_l(r)\,\mathrm{P}_l(\cos\theta) + O\left(B^4\Omega^2\right), \tag{3.14d}$$

where we have expanded the $O\left(B^2\right)$ corrections to the background stars log-enthalpy in harmonics.

Using eqs. (3.14b), (3.14c), (3.9a) and (3.9b) the fluid energy-momentum tensors of the background star reads

$$T^{(\mathrm{F}00)\alpha}{}_{\beta} = -\left[\rho(r) + P(r)\right]\delta^{\alpha}_{t}\delta^{t}_{\beta} + P(r)\,\delta^{\alpha}_{\beta}. \tag{3.15}$$

The corrections $\Delta T^{(\mathrm{F})}_{\alpha\beta}$ can be constructed using the four-velocity, and eqs. (3.14b)-(3.14c). We introduced the energy-momentum tensor of the electro-magnetic field $T^{(\mathrm{EM})}_{\alpha\beta}$ in terms of the four-potential in eq. (2.19). In Sec. 3.4 we will discuss the expansion of the four-potential in harmonics in detail.

In terms of deformations we will only consider dipolar ($l = 1$) magnetic fields and the corresponding induced $l = 0$ and $l = 2$ electric fields. Matching the angular dependence of the resulting electro-magnetic source term requires only two non-vanishing $h_l(r)$ coefficients: h_0 and h_2. The whole problem has reflexion symmetry in the $\theta = \pi/2$-plane which excludes odd expansion coefficients in γ_{ij} and N and even coefficients in N^{ϕ}. For an expansion up $O\left(B^2\Omega^1\right)$ the only non-vanishing expansion coefficients are n_0, n_2, w_1, w_3, m_0, m_2, k_0 and k_2 because higher-order coefficients have no matching source terms. Further we choose our radial coordinate such that $k_0(r) \stackrel{!}{=} 0$. This coordinate gauge choice is very convenient and in terms of the HT formalism known as k-gauge [54].

Order by order the corrections to $ds^2_{(00)}$ read

$$ds^2_{(01)} = g^{(01)}_{\mu\nu}dx^{\mu}dx^{\nu} \equiv -2r^2\sin^2\theta\,\omega(r)\,dt\,d\phi, \tag{3.16}$$

$$\begin{aligned} ds^2_{(20)} = g^{(20)}_{\mu\nu}dx^{\mu}dx^{\nu} \equiv{}& 2\mathrm{e}^{\nu(r)}\left(n_0(r) + n_2(r)\,\mathrm{P}_2(\cos\theta)\right)dt^2 \\ &+ 2\frac{\mathrm{e}^{2\lambda(r)}}{r}\left(m_0(r) + m_2(r)\,\mathrm{P}_2(\cos\theta)\right)dr^2 \\ &+ 2r^2k_2(r)\,\mathrm{P}_2(\cos\theta)\left(d\theta^2 + \sin^2\theta\,d\phi^2\right) \end{aligned} \tag{3.17}$$

$$\begin{aligned} ds^2_{(21)} = g^{(21)}_{\mu\nu}dx^{\mu}dx^{\nu} \equiv{}& -2r^2\sin^2\theta\Big[W_1(r) + W_3(r)\left(1 + 5\mathrm{P}_2(\cos\theta)\right) \\ &+ 2k_2(r)\,\omega(r)\,\mathrm{P}_2(\cos\theta)\Big]dt\,d\phi, \end{aligned} \tag{3.18}$$

where $ds^2_{(01)}$ is $O\left(B^0\Omega^1\right)$, $ds^2_{(20)}$ is $O\left(B^2\Omega^0\right)$ and $ds^2_{(21)}$ is $O\left(B^2\Omega^1\right)$. The complete line element up to $O\left(B^2\Omega^1\right)$ reads

$$ds^2 = ds^2_{(00)} + ds^2_{(01)} + ds^2_{(20)} + ds^2_{(21)} + O\left(B^4\Omega^2\right). \tag{3.19}$$

All expansion coefficients are $O\left(B^2\Omega^0\right)$ apart form $\omega(r)$, $W_1(r)$ and $W_3(r)$. $W_3(r)$ and $W_1(r)$ are $O\left(B^2\Omega^1\right)$ and $\omega(r)$ is $O\left(B^0\Omega^1\right)$. We have split $w_1(r)$ from eq. (3.5) into $W_1(r)$ and $\omega(r)$ to realize that all expansion coefficients are of proper order in B and Ω. In the following we will not discuss the metric potential k_2 itself but rather a highly convenient axillary potential $v_2 \equiv k_2 + n_2$. Working in terms of v_2 makes the field equations and their solutions much easier.

This line element is identical to the one used by Hartle and Thorne [25, 48, 49]. The only modification in the scope of this work is the inclusion of an elector-magnetic source term and the fact that we consider deformations originating from such an EM field. In the classical HT formalism up to $O\left(\Omega^3\right)$ the higher-order deformations are caused by rotational deformations originating form the $l = 1$ frame-dragging term $\omega(r)$. A dipolar magnetic field has the same angular dependence which is the reason for the equality of the line elements. The field equations we will derive will be very similar to the ones found by HT. To be specific the homogeneous parts of the ODEs will be identical, since we use the same line element.

We now have a line element and source terms expanded up to second-order in B and up to first-order in Ω. With them we compute Einstein's field equations (2.1) up to $O\left(B^2\Omega^1\right)$ in the appendix A. By using the expansion of this section to describe deformations away from spherical symmetry we are left with a one dimensional problem in r. We expanded the entire angular dependency with low order Legendre polynomials and the only derivatives which we can not compute analytically are the radial ones. This makes the problem mathematically much easier because we are now dealing with ODEs instead of PDEs. From now on we will stop writing out the radial dependence of the metric potentials explicitly (e.g. $n_0(r) \equiv n_0$) and denote radial derivatives with an apostrophe.

Expanding the field equations in B and Ω decouples the field equations of different orders. The higher-order eqs. only depend on the lower-order ones but higher and lower order eqs. are not coupled. This allows us to solve the eqs. order by order and a self-consistent iterative solution scheme is no longer necessary. By expanding angular dependency explicitly in harmonics and by expanding the field eqs. in proper orders in B and Ω we reduced the coupled set of PDEs of the BGSM formalism into a set of staggered ODEs.

There are no Einstein equations of $O\left(B^1\right)$, since the energy-momentum tensor of the magnetic field is of $O\left(B^2\right)$ but the Maxwell equations are of $O\left(B^1\Omega^1\right)$ and we will discuss them in detail in Sec. 3.4. Sec. 3.2 we will discuss the structure equations of $O\left(B^0\right)$ and in Sec. 3.6 the ones of $O\left(B^2\right)$. Field eqs. related to rotation will be treated in Sec. 3.3 and Sec. 3.7.

3.1.1 Matching of interior and exterior manifolds

We will treat the stellar exterior and interior separately. In the stellar exterior matter support vanishes $T^{(\mathrm{F})}_{\alpha\beta} = 0, \forall r > R$ which simplifies the field equations. The interface between the stellar interior and exterior is the stellar surface. For a spherical symmetric background star this surface is determined by the stellar radius R, which is defined as the radius at which $P(R) = 0$. In contrast to the classical HT formalism the exterior we deal with is not outright source free: the electromagnetic contributions $T^{(\mathrm{EM})}_{\alpha\beta}$ are non-zero in the stellar exterior. This makes our higher-order $O\left(B^2\Omega^0\right)$ and $O\left(B^2\Omega^1\right)$ exterior solutions not vacuum but electro-vacuum solutions of Einstein's field equations.

Matching interior and exterior solutions has to be done by imposing junction conditions on the stellar surface. We use a variation of the *Israel-Darmois junction conditions* (IDJC), see e.g. [55] for a short overview and further references. Israel-Darmois junction conditions require continuity of the induced metric and induced extrinsic curvature on the interface between the two space-time manifolds, to be matched. Such a matching preserves spacetime symmetries and lengths on the interface.

We will not go into details on how to formally enforce these conditions, instead we refer the interested reader to the recent work of B. Reina and R. Vera [54]. B. Reina and R. Vera discussed the matching of interior and exterior solutions in detail for the HT-metric. We will summarize their key results. For the background star the matching conditions are

$$\nu_<(R) - \nu_>(R) = 0, \tag{3.20a}$$
$$\nu'_<(R) - \nu'_>(R) = 0, \tag{3.20b}$$
$$\lambda_<(R) - \lambda_>(R) = 0, \tag{3.20c}$$
$$\lambda'_<(R) - \lambda'_>(R) = 8\pi R \mathrm{e}^{\lambda(R)}\rho(R). \tag{3.20d}$$

The first discontinuity rises in the derivative of the g_{rr} potential λ' and it is proportional to the residual surface density $\rho(R)$. For most EoS $\rho(R)$ is either zero or very low. When matching potentials on the

stellar surface we will explicitly denote interior solutions with the sub- or superscript $<$ and exterior solutions with $>$. We will also use those sub- or superscripts when discussing results and equations which are only valid in one regime.

In first-order in Ω the frame-dragging frequency and its derivative have to be continuous

$$\omega_<(R) - \omega_>(R) = 0, \tag{3.21a}$$
$$\omega'_<(R) - \omega'_>(R) = 0, \tag{3.21b}$$

to realize the IDJC.

For the electro-magnetic fields we employ magneto- and electrostatic matching conditions, which we discuss briefly in Sec. 3.4 and Sec. 3.5.

The $O\left(B^2\right)$ metric potentials can all be chosen continuous across the stellar surface with the exception of the g_{rr} monopole perturbation m_0.

$$n_0^<(R) - n_0^>(R) = 0, \tag{3.22a}$$
$$n_2^<(R) - n_2^>(R) = 0, \tag{3.22b}$$
$$m_2^<(R) - m_2^>(R) = 0, \tag{3.22c}$$
$$v_2^<(R) - v_2^>(R) = 0, \tag{3.22d}$$

The discontinuity of m_0 is proportional to discontinuities in the source terms: in $O\left(B^2\right)$ namely to the residual surface density $\rho(R)$, similar to the case for λ'. We will discuss this discontinuity and the matching of m_0 in detail in Sec. 3.6.2. In their classical papers HT constructed m_0 continuously across the stellar surface. This works in the case of vanishing residual surface density $\rho(R) = 0$ but fails to give self-consistent results otherwise.

The $O\left(B^2\Omega^1\right)$ metric potentials are higher-order corrections to the frame-dragging frequency and must obey the same matching conditions as ω

$$W_1^<(R) - W_1^>(R) = 0, \tag{3.23a}$$
$$W_1^{<\prime}(R) - W_1^{>\prime}(R) = 0, \tag{3.23b}$$
$$W_3^<(R) - W_3^>(R) = 0, \tag{3.23c}$$
$$W_3^{<\prime}(R) - W_3^{>\prime}(R) = 0. \tag{3.23d}$$

Matching conditions of the higher-order metric potentials in $O\left(B^2\Omega^1\right)$ are always imposed at the background star's radius. The deformation $\delta R(\theta)$ of this surface is an $O\left(B^2\right)$ effect, see eq. (3.262). Expanding a matching condition for an $O\left(B^2\right)$ potential, e.g. n_2, reveals

$$\begin{aligned} n_2^<(R^*(\theta)) - n_2^>(R^*(\theta)) &= n_2^<(R + \delta R(\theta)) - n_2^>(R + \delta R(\theta)) \\ &= n_2^<(R) - n_2^>(R) + (n_2^{<\prime}(R) - n_2^{>\prime}(R))\delta R(\theta) \\ &= n_2^<(R) - n_2^>(R) + O\left(B^4\Omega^2\right). \end{aligned} \tag{3.24}$$

$n_2^{>\prime}(R)\delta R(\theta)$ is an $O\left(B^4\right)$ term and we consider only perturbations up to $\mathrm{O}\left(B^2\Omega^1\right)$.

3.1.2 Orthonormal tetrad of the Eulerian observer

The orthonormal tetrad $\{\mathbf{e}_{\hat{\alpha}}\}$ carried by the Eulerian observer $\mathscr{O}_n$ can be extracted from the corresponding projection operator

$$\gamma^\alpha{}_\beta \equiv \delta^\alpha{}_\beta + n^\alpha n_\beta \tag{3.25}$$

and its four-velocity $\mathbf{n}$ [34]. For the following we will only need the tetrad up to $O\left(B^1\Omega^1\right)$ and in this order

$$(n^\alpha) = \mathrm{e}^{-\nu/2}\,(1,0,0,\omega)^T\,, \tag{3.26a}$$
$$(n_\alpha) = \mathrm{e}^{\nu/2}\,(1,0,0,0)\,. \tag{3.26b}$$

As the notation suggest the projector $\gamma^\alpha{}_\beta$ is the mixed tensor form of the spatial metric.

The orthogonal and normalized basis vectors of the tetrad carried by $\mathcal{O}_n$ are given by

$$\mathbf{e}_{\hat{k}} \cdot \mathbf{e}_{\hat{l}} = \gamma_{kl}, \tag{3.27}$$
$$e^\alpha_{\hat{t}} = n^\alpha. \tag{3.28}$$

The components of the tetrad in terms of the basis vectors up to $O\left(B^1\Omega^1\right)$ read

$$(e^\alpha_{\hat{t}}) = \mathrm{e}^{-\frac{\nu}{2}}\,(1,0,0,\omega)^T\,, \tag{3.29a}$$
$$(e^\alpha_{\hat{r}}) = \mathrm{e}^{-\frac{\lambda}{2}}\,(0,1,0,0)^T\,, \tag{3.29b}$$
$$(e^\alpha_{\hat{\theta}}) = \frac{1}{r}\,(0,0,1,0)^T\,, \tag{3.29c}$$
$$(e^\alpha_{\hat{\phi}}) = \frac{1}{r\sin\theta}\,(0,0,0,1)^T\,. \tag{3.29d}$$

The information about spacetime curvature, which in the present case is reduced to the length of the basis vectors, is encoded completely in components when using the tetrad (3.29) as basis. We use the scalar product $\mathbf{A}\cdot\mathbf{e}_{\hat{\alpha}}$ to extract tetrad components $A_{\hat{\alpha}}$ of an arbitrary vector $\mathbf{A}$:

$$A_{\hat{\alpha}} = A_\mu e^\mu_{\hat{\alpha}}. \tag{3.30}$$

The components $A_{\hat{\alpha}}$ are very useful for displaying GR effects on vector fields and for the discussion of non-relativistic/Newtonian limits since the length of $\mathbf{e}_{\hat{\alpha}}$ is constant 1. Further more all components $A_{\hat{\alpha}}$ have the same dimensions as the vector field $\mathbf{A}$ which makes plotting components together much easier.

In principle the choice of the tetrad carried by $\mathcal{O}_n$ as basis is arbitrary but in terms of the 3+1 formalism it is a natural one. Asymptotically the Eulerian observer coincides with a Newtonian one at spatial infinity.

3.2 $O\left(B^0\Omega^0\right)$: Spherical symmetric background star

In zeroth-order in the magnetic field and angular velocity our ansatz describes a spherical symmetric compact star. Once an EoS is chosen, the two metric potentials ν and λ together with the log-enthalpy gradient $h(r)$ describe the spherical symmetric, cold compact star completely. Using the unperturbed energy-momentum tensor of the ideal fluid one can compute the $O\left(B^0\Omega^0\right)$ field equations. Using the two field equations (A.2) and (A.3) together with the Euler equation in $O\left(B^0\right)$ (A.5) we will derive the analytical *Schwarzschild solutions* [56, 57] and the *Tolman-Oppenheimer-Volkoff* (TOV) equation(s) [43, 58]. Starting from eq. (A.4) and a specific density profile we will derive a class of analytical *Tolman VII* solutions [59].

3.2.1 Vacuum solution: Exterior Schwarzschild solution

Outside the compact star, $r > R$, pressure and density vanish and eq. (A.2) becomes

$$\begin{aligned} 0 &= 1 - \mathrm{e}^{\lambda_>} - r\lambda'_> \\ &= -1 + \mathrm{e}^{-\lambda_>} - r\lambda'_> \mathrm{e}^{-\lambda_>} \\ &= \frac{d}{dr}\left(r\mathrm{e}^{-\lambda_>} - r\right). \end{aligned} \tag{3.31}$$

This equation can be integrated to yield

$$\begin{aligned} -2M &= r\mathrm{e}^{-\lambda_>} - r \\ 1 - \frac{2M}{r} &= \mathrm{e}^{-\lambda_>}, \end{aligned} \tag{3.32}$$

where we have chosen the constant of integration as $-2M$. From eq. (3.32) follows:

$$\lambda'_> = -\frac{2M}{r(r-2M)}. \tag{3.33}$$

Equation (A.3) becomes

$$0 = -1 + \mathrm{e}^{\lambda_>} - r\nu'_>, \tag{3.34}$$

$$\begin{aligned} \nu'_> &= \frac{\mathrm{e}^{\lambda_>} - 1}{r} \\ &= \frac{2M}{r(r-2M)}. \end{aligned} \tag{3.35}$$

Comparing eqs. (3.33) and (3.35) reveals $\nu'_>(r) = -\lambda'_>(r)$ and therefore

$$\nu_>(r) = -\lambda_>(r) + c_\nu. \tag{3.36}$$

From the asymptotic flatness condition ($g_{\mu\nu} \to \eta_{\mu\nu}$ for $r \to \infty$) follows $c_\nu = 0$ and the exterior Schwarzschild solution (ESS) [56] reads:

$$\mathrm{e}^{\lambda_>} = \frac{1}{1 - \frac{2M}{r}}, \tag{3.37a}$$

$$\lambda'_> = -\frac{2M}{r(r-2M)}, \tag{3.37b}$$

$$\mathrm{e}^{\nu_>} = \mathrm{e}^{-\lambda_>} = 1 - \frac{2M}{r}, \tag{3.37c}$$

$$\nu'_> = -\lambda'_>. \tag{3.37d}$$

Up until now M is only a constant of integration and only in that sense the gravitational mass of the configuration, that it is the single parameter that governs the gravitational field/curvature outside the configuration. Using the asymptotic expansion of the ESS at large distances, one can identify M as the classical gravitational mass seen by a quasi Newtonian observer [60]. Further is can be identified as the Komar mass, see eq. (3.242).

3.2.2 Interior solution: Tolman-Oppenheimer-Volkoff equations in standard form

Inside the compact star, $r \leq R$, pressure and density do not vanish and in order to solve the equations of hydrostatic equilibrium, one has to specify an equation of state which relates the thermodynamic quantities.

We begin our derivation of the TOV equation with eq. (A.2):

$$-8\pi r^2 \rho = -1 + \mathrm{e}^{-\lambda}\left(1 - r\lambda'\right). \tag{3.38}$$

By defining

$$M'(r) \equiv 4\pi r^2 \rho(r) \tag{3.39}$$

one can integrate eq. (3.38) to:

$$-2M(r) = r\mathrm{e}^{-\lambda(r)} - r + c_M, \tag{3.40}$$

$$\mathrm{e}^{-\lambda(r)} = 1 - \frac{2M(r) + c_M}{r}. \tag{3.41}$$

At the surface of the star the exterior and interior solution have to be equal. Using this one can identify the gravitational mass of the ESS, M, as

$$M = M(R) = 4\pi \int_0^R dr r^2 \rho(r), \tag{3.42}$$

with $c_M = 0$.

In order to derive a differential equation for the pressure gradient we first rewrite eq. (A.3) to get an expression for ν':

$$\nu' = \frac{8\pi r^2 P \mathrm{e}^{\lambda} + \mathrm{e}^{\lambda} - 1}{r}. \tag{3.43}$$

Inserting this into the Euler eq. (A.5) leads to

$$P' = -\frac{\left(8\pi r^2 P \mathrm{e}^{\lambda} + \mathrm{e}^{\lambda} - 1\right)(P + \rho)}{2r}. \tag{3.44}$$

With eq. (3.41) this can be rewritten into the well known form

$$P'(r) = -\frac{\left(M(r) + 4\pi r^3 P(r)\right)(P(r) + \rho(r))}{r(r - 2M(r))} \tag{3.45}$$

$$= -\frac{\rho(r) M(r)}{r^2}\left(1 + \frac{P(r)}{\rho(r)}\right)\left(1 + \frac{4\pi r^3 P(r)}{M(r)}\right)\left(1 - \frac{2M(r)}{r}\right)^{-1}, \tag{3.46}$$

which is usually referred to as *Tolman-Oppenheimer-Volkoff* equation or by some authors just as *Oppenheimer-Volkoff* equation [61]. It is the general relativistic equivalent of the classical, Newtonian equation of hydrostatic equilibrium: $P'(r) = -\rho(r)M(r)/r^2$. The three GR correction factors in eq. (3.46) are all positive and therefore increase the pressure gradient, which leads to equilibrium configurations with smaller masses compared to the Newtonian case.

To fully describe the star we need the last metric potential ν inside the star. Having derived an expression for the pressure gradient the most convenient differential equation for ν is the plain relativistic Euler eq. (A.5):

$$\nu' = -\frac{2P'}{P + \rho}. \tag{3.47}$$

In summary we have derived three differential equations which govern the structure inside a spherical symmetric, cold, compact star:

$$M'(r) = 4\pi r^2 \rho(r), \tag{3.48a}$$

$$P'(r) = -\frac{\big(M(r) + 4\pi r^3 P(r)\big)\big(P(r) + \rho(r)\big)}{r(r - 2M(r))}, \tag{3.48b}$$

$$\nu'(r) = -\frac{2P'(r)}{P(r) + \rho(r)}. \tag{3.48c}$$

Equations (3.48a) and (3.48b) are coupled and eq. (3.48c) is decoupled from the first two. The stellar surface is defined as the surface of zero pressure. The boundary conditions at the stellar surface, $r = R$, are given in eqs. (3.20) with the ESS (3.37) as exterior solution. At the center, $r = 0$, all metric potentials and thermodynamic quantities need to be finite for non-singular configurations. Given an EoS, which in case of the canonical TOV eqs. is necessary to relate pressures to energy densities, there is a unique solution of the TOV equations for every chosen central pressure. For the vast majority of EoS the TOV eqs. need to be integrated numerically.

The explicit form (3.46) and the definition of $M(r)$ goes back to the paper "*On Massive Neutron Cores*" of Oppenheimer and Volkoff published 1939 [58]. They not only formulated this popular equation, they also solved it numerically for a physical, microscopic EoS: namely the one of a degenerated, cold neutron gas. They followed the same steps for the formulation of eq. (3.46) as we did here based on field equations from Tolman [62]. Tolman derived the structure equations eqs. (A.2)-(A.5) in isotropic coordinates as early as 1930 [43] and he identified eq. (3.47) as the general relativistic equivalent to the Newtonian equation of hydrostatic equilibrium. For a modern understanding and for the implementation using realistic EoS, Oppenheimer and Volkoff's work was essential but Tolman's contribution to the derivation of this equation should not be underestimated [63]. We will refer to the entire system (3.48) as TOV equations.

This canonical form of the structure eqs. is very popular and used by most authors but it has major shortcomings in terms of implementability, stability and even theoretical insight into the problem as we will discuss in the next subsection.

3.2.3 Interior solution: Lindblom's form of the Tolman-Oppenheimer-Volkoff equations

There are three major shortcomings of the TOV eqs. in their canonical form (3.48).

The first one is the fact that they give ν only in differential form and explicit integration to obtain ν would be necessary without further insight.

The last two are more technical problems when integrating the coupled system eqs. (3.48a) and (3.48b). The integration domain is not known prior to integration, since the stellar radius is not known. It is defined as the radius R where $P(R) = 0$. To determine this point during integration can be problematic especially when using tabulated EoS or analytical EoS which do not approach $P = 0$ asymptotically, like e.g. the EoS of an incompressible fluid with constant density. Furthermore eqs. (3.48a) and (3.48b) form a stiff ODE system: the pressure and energy density vary strongly in order of magnitude. Numerical integration of the TOV eqs. in their standard form is certainly possible with a good adaptive method and special care at the stellar surface but it is not unproblematic [64].

In this subsection we will derive the TOV equations in the log-enthalphy which will solve all three problems.

Recalling the differential definition of h from the Gibbs-Duham relation in eq. (3.12) it is possible to rewrite the Euler eq. (A.5) as

$$\frac{d\nu(r)}{dr} = -\frac{2}{P(r)+\rho(r)}\frac{dP(r)}{dr} = -2\frac{dh(r)}{dr}. \tag{3.49}$$

This equation can be trivially integrated to

$$\nu(r) = -2h(r) + c_{\nu h} \tag{3.50}$$

This integral form of the Euler equation is the general relativistic Bernoulli theorem for a static, spherical symmetric star. The g_{tt} metric potential is directly related to the log-enthalpy h. The constant $c_{\nu h}$ can be found by matching the interior solution to the ESS

$$\nu_{>}(R) \overset{!}{=} \nu_{<}(R) \Rightarrow c_{\nu h} = \log\left[1 - \frac{2M}{R}\right], \tag{3.51}$$

since $h(R) = 0$. The latter can be derived from the definition (3.10) of h. At the stellar surface $P = 0 \Rightarrow \mu = \mu_0 = m_{\mathrm{B}}$ and $h(R) = \log(\mu_0/\mu_0) = 0$.

Eq. (3.48a) can be reformulated as

$$\frac{dh(r)}{dr} = \frac{dP(r)}{dr}\frac{dh(r)}{dP(r)} = -\frac{\left(M(r) + 4\pi r^3 P(r)\right)}{r(r-2M(r))}. \tag{3.52}$$

"Inverting" this equation and integrating the system $\{dr(h)/dh, dM(h)/dh\}$ is possible and solves all the three problems mentioned above, since the integration domain is known as $h \in \left[h_c, 0\right]$ and the ODE $dr(h)/dh$ is regular at $h = 0$. This reformulation was first proposed by L. Lindblom in 1992 [65]. We will use a slightly modified version of Lindblom's original eqs. by rewriting the system $\{dr(h)/dh, dM(h)/dh\}$ into

$$\frac{dr(h)^2}{dh} = -\frac{2r(h)^2\left(1-2z(h)\right)}{4\pi r(h)^2 P(h) + z(h)}, \tag{3.53a}$$

$$\frac{dz(h)}{dh} = \left(2\pi\rho(h) - \frac{z(h)}{2r(h)^2}\right)\frac{dr(h)^2}{dh}, \tag{3.53b}$$

with $z \equiv M(r)/r$. This form was brought forward by L. Lindblom [66] and S. Postnikov discussed it in detail in [67]. It has an increased numerical stability when compared to the system in $r(h)$ and $M(h)$ and it allows for a proper NLO expansion around $r \to 0 \Leftrightarrow h \to h_c$:

$$r(h)^2 \xrightarrow[h\to h_c]{} \frac{3(h_c-h)}{2\pi(3P_c+\rho_c)}\left(1 + \frac{3\frac{d\rho}{dh}|_{h_c} + 15P_c - 5\rho_c}{10(3P_c+\rho_c)}(h_c-h)\right) + O\left(h^3\right), \tag{3.54a}$$

$$z(h) \xrightarrow[h\to h_c]{} \frac{2\rho_c(h_c-h)}{3P_c+\rho_c}\left(1 - \frac{5\rho_c(\rho_c-3P_c) + 3\frac{d\rho}{dh}|_{h_c}(6P_c+\rho_c)}{10\rho_c(3P_c+\rho_c)}(h_c-h)\right) + O\left(h^3\right). \tag{3.54b}$$

With this expansion one can make the first integration step of the system (3.54) explicitly with a controlled error by comparing the LO(h^1) step with the NLO(h^2) step. This expansion in proper orders in the integration variable is unique to the $\{dr^2(h)/dh, dz(h)/dh\}$ system.

The system (3.53) together with an EoS and the two algebraic identities for the metric potentials

$$\nu(h) = -2h + \log\left[1 - \frac{2M}{R}\right], \tag{3.55a}$$

$$\lambda(h) = -\log\left[1 - 2z(h)\right], \tag{3.55b}$$

encode the stellar structure completely.

In order to expand the following higher-order structure eqs. we invert (3.54) to get expansions of the metric potentials and thermodynamic quantities in r

$$\lambda(r) \xrightarrow[r\to 0]{} \frac{8}{3}\pi\rho_c r^2 + O\left(r^3\right), \tag{3.56a}$$

$$\nu(r) \xrightarrow[r\to 0]{} \nu_c + \frac{4}{3}\pi(3P_c+\rho_c)r^2 + O\left(r^3\right), \tag{3.56b}$$

$$P(r) \xrightarrow[r\to 0]{} P_c - \frac{2}{3}\pi(\rho_c+P_c)(3P_c+\rho_c)r^2 + O\left(r^3\right), \tag{3.56c}$$

$$\rho(r) \xrightarrow[r\to 0]{} \rho_c - \frac{2}{3}\pi(3P_c+\rho_c)\left.\frac{d\rho}{dh}\right|_{h_c} r^2 + O\left(r^3\right). \tag{3.56d}$$

For using the EoS and the Euler eq. (3.50) to compute ν analytically it is not necessary to integrate in h. Using the identity (3.50) or its equivalent in terms of the chemical potential [1] is possible independent of the scheme used for the system $\{(3.48a),(3.48b)\}$. In Tab. 4.1 we will compare numerical performance of different forms of the TOV eqs. but to anticipate the results: the system (3.53) is overall the best choice in terms of performance and stability.

The close relation of the log-enthalpy to the baryon chemical potential, $h = \log\mu/\mu_0$, makes it a rather natural base variable for an EoS. A lot of analytical, zero temperature, microscopic EoS can be given in closed form in μ. To mention the some prominent examples: degenerate fermi gas, npe-gas, constant speed of sound and MIT bag model EoS can be given analytically in terms of μ and therefore also in terms of h. At $T = 0$ the chemical potential and the Fermi energy are equal. First-order phase transitions have continuous pressures and chemical potentials so h is also continuous at such transitions. For realistic tabulated EoS the chemical potential is often directly tabulated or it can be constructed using the Gibbs-Duham relation. In computations of realistic EoS from more involved interacting models for hadrons or quarks the baryon chemical potential is an important quantity.

Due to its simplicity, numerical advantages and close connection to the Bernoulli theorem we can strongly recommend Lindblom's system $\{dr^2(h)/dh, dz(h)/dh\}$ over the classical one of Oppenheimer Volkoff.

3.2.4 Interior Schwarzschild solution

In 1916 K. Schwarzschild presented not only his famous solution of Einstein's field equations outside a spherical, static body, he also presented an analytical solution for the interior of an incompressible fluid sphere [57]. This solution is referred to as *interior Schwarzschild solution* (ISS). We use it in the scope of this work to check the accuracy of our numerical implementation and to compare configurations of constant density to ones with a more realistic density gradient.

The ISS is the solution of the TOV equations for an incompressible fluid sphere of constant density. This central density is related to the total gravitational mass M and the radius R of the star by

$$\rho(r) = \rho_c = \frac{3M}{4\pi R^3}. \tag{3.57}$$

Eq. (3.39) can be integrated analytically to

$$M(r) = \frac{M}{R^3}r^3 = \frac{4}{3}\pi\rho_c r^3. \tag{3.58}$$

With the EoS of an incompressible relativistic fluid (IRF), eq. (B.2), and the expression (3.58) the differential eq. (3.53a) for $r(h)$ becomes separable

$$\frac{r(h)r'(h)}{3-8\pi\rho_c r(h)^2} = \frac{1}{4\pi\rho_c}\frac{1}{2-3\mathrm{e}^h} \tag{3.59}$$

and can be integrated by parts to

$$-\frac{\log\left[3-8\pi r^2\rho_c\right]}{16\pi\rho_c} = \frac{h}{8\pi\rho_c} - \frac{\log\left[2-3\mathrm{e}^h\right]}{8\pi\rho_c} + c_{rh}. \tag{3.60}$$

Using the boundary condition of vanishing radius at the stellar center $r(h_c) = 0$ one can fix the integration constant c_{rh} to get

$$r^2(h) = \frac{3}{8\pi\rho}\left[1-\left(\frac{(3\mathrm{e}^h-2)\mathrm{e}^{h_c-h}}{3\mathrm{e}^{h_c}-2}\right)^2\right], \tag{3.61}$$

$$z(h) = \frac{4}{3}\pi\rho r^2(h). \tag{3.62}$$

The central log-enthalpy h_c is related to the ISS star's compactness $Z \equiv M/R$ by

$$h_c = \log\left[\frac{3-6Z+\sqrt{1-2Z}}{4-9Z}\right], \tag{3.63}$$

which results in an expression for the central pressure

$$P_c = \rho_c\frac{3Z+\sqrt{1-2Z}-1}{4-9Z}. \tag{3.64}$$

Mass and radius in terms of h_c and ρ_c are given by

$$M = \frac{1}{12\sqrt{2\pi\rho_c}}\left[3-\frac{3\mathrm{e}^{2h_c}}{(2-3\mathrm{e}^{h_c})^2}\right]^{3/2}, \tag{3.65}$$

$$R = \frac{1}{2\sqrt{2\pi\rho_c}}\left[3-\frac{3\mathrm{e}^{2h_c}}{(2-3\mathrm{e}^{h_c})^2}\right]^{1/2}. \tag{3.66}$$

For our purposes the ISS in h is ideal since we also integrate the TOV eqs. in h. Especially eqs. (3.61) and (3.62) can be used to test numerical solutions for accuracy. Fixing just two of the parameters out of $\left[M,R,Z,\rho_c,P_c,h_c\right]$ plus a mean baryon rest mass, if $n_{\mathrm{B}}(s)$ is of interest, completely determines the structure of an equilibrium configuration and we have analytic expressions for all quantities and gradients of such an IRF background star.

The ISS in terms of h is not very common but it can be used together with the IRF EoS to construct metric potentials and thermodynamic quantities in terms of the radius. For our purposes the ISS

solution in terms of the dimensionless radial variable $s \equiv r/R$ and the configurations compactness Z and radius R is best suited:

$$\lambda(s) = -\log\left[1-2s^2Z\right], \tag{3.67a}$$

$$\nu(s) = -2\log\left[\frac{\sqrt{1-2Z}\sqrt{1-2s^2Z}-6Z+3}{(s^2-9)Z+4}\right] + \log\left[1-2Z\right], \tag{3.67b}$$

$$P(s) = \frac{3Z}{4\pi R^2}\left[\frac{\sqrt{1-2Z}\sqrt{1-2s^2Z}-6Z+3}{(s^2-9)Z+4} - 1\right], \tag{3.67c}$$

$$\rho(s) = \frac{3Z}{4\pi R^2} = \text{const.}, \tag{3.67d}$$

$$n_{\mathrm{B}}(s) = \frac{\rho(s)}{m_{\mathrm{B}}} = \frac{3Z}{4\pi R^2 m_{\mathrm{B}}} = \text{const.}. \tag{3.67e}$$

The metric potentials $\nu(s)$ and $\lambda(s)$ are independent of the configuration's central density. Pressure, energy- and baryon density scale trivially in ρ_c. The internal structure only depends on Z in a non-trivial way. We will make use of this fact in Chap. 6.

The expression for the baryonic mass $M_{\mathrm{B}} = m_{\mathrm{B}}\mathscr{B}_0$ from eq. (3.250a) is analytical for the ISS and can be integrated to yield

$$M_{\mathrm{B}} = \frac{3R}{4}\left[\frac{1}{\sqrt{2Z}}\arcsin\left(\sqrt{2Z}\right) - \sqrt{1-2Z}\right]. \tag{3.68}$$

Using eq. (3.64) we can derive two interesting limits for compact objects.

The first one is the so called *Schwarzschild-Buchdahl* (SB) limit [57, 68]: There is a maximum compactness Z_{SB} for incompressible fluid spheres in GR

$$Z_{\mathrm{SB}} = \frac{4}{9}, \tag{3.69}$$

given by the $P_c \to \infty$ limit of eq. (3.64). S. Weinberg showed in 1972 [69] that this limit holds independently of the EoS for all stars with $\partial\rho/\partial r \leq 0$ and g_{rr} not singular. In GR no compact star can have a compactness beyond 4/9 without collapsing into a black hole. This limit is special to GR since it does not exist in the Newtonian theory.

Requiring $\rho_c = P_c$ leads to the second limit

$$Z_{\mathrm{C}} = \frac{3}{8}. \tag{3.70}$$

Z_{C} is called causality limit for ISS stars. In 1964 H. Bondi showed that for arbitrary EoS with $P > 0$, $\rho > 0$ and $dP/d\rho < 1$ a similar limit of $Z_{\mathrm{B}} = 0.38$ holds [1, 70].

The ISS is one and arguably the simplest and most popular analytic interior solution for relativistic compact objects. The simplicity of the ISS however comes at a cost; it is not very well suited to describe realistic compact objects or to be specific neutron stars. A constant density profile is not realistic and the IRF EoS is not physical in the sense that its sound speed is at all densities infinite. For modeling self-bound stars with high residual surface densities, like pure quark stars, the ISS provides a somewhat viable effective model for some global parameters but for primarily hadronic NS it is not well suited.

3.2.5 Tolman VII solution

We already discussed the ISS as one analytic interior solution and pointed out its shortcomings when it comes to describing NS. In this subsection we will introduce another analytic interior solution which will be better suited for describing realistic NS. M. S. R. Delgaty and K. Lake (DL) list 127 analytic interior solutions for isolated, static, spherically symmetric, perfect fluid spheres [71]. They found that only 16 can be considered physical meaning that they

1. have isotropic pressure,
2. are regular at the origin,
3. have positive definite pressures and densities at the origin,
4. have a finite stellar radius with a vanishing surface pressure,
5. have decreasing pressure and density gradients
6. and causal sound speeds.

The ISS meets all but the last of these six requirements. From those 16 physical perfect fluid interior solutions one is particularly interesting: the Tolman VII [59] solution. In his famous 1939 paper *Static Solutions of Einstein's Field Equations for Spheres of Fluid* R. C. Tolman discussed eight analytic interior solutions. Among those a solution constructed by him, which he referred to as *Solution VII* (TVII). He only presented this solution and immediately disregarded it. In his words:

> "*The dependence of p on r, with* $e^{-\lambda/2}$ *and* e^{ν} *explicitly expressed in terms of r, is so complicated that the solution is not a convenient one for physical considerations.*" – R.C. Tolman, 1939 [59].[(1)]

It is true that the algebraic structure of TVII solution is complicated but this does not a priori disqualifies it as unphysical. In fact the TVII solution satisfies all six requirements of DL and quite a few analytic interior solutions are of TVII-type or include it as a limit [55]. Tolman's statement of it being not convenient still holds to some extent but with modern computer algebra systems, the analytic complexity of the solution can be handled.

In this subsection we will derive a class of TVII solutions, using the same steps Tolman used in his original derivation but a different notation. We will discuss and reason through out this work that the TVII solution can be a very potent tool to model realistic NS.

To construct the TVII solution the following form for the g_{rr} metric potential is assumed

$$e^{-\lambda} \stackrel{!}{=} 1 + \frac{r^2}{A^2} + \frac{r^4}{B^4} \equiv 1 + \frac{8}{15}\pi\rho_c r^2 \left(\frac{3r^2\mu}{R^2} - 5 \right), \tag{3.71}$$

where we introduced three constants μ, ρ_c and R instead of the two originally used by Tolman. ρ_c is the configuration's central density and R its radius. The density gradient inside the star can be constructed from eq. (3.71) with eq. (A.2)

$$\rho(r) = \rho_c \left(1 - \mu \frac{r^2}{R^2} \right). \tag{3.72}$$

The free parameter μ classifies families of TVII solutions. μ controls the density gradient: the energy density inside a TVII configuration is strictly monotonically decreasing for $\mu \in (0, 1]$. $(1-\mu)\rho_c$ is the

(1) Tolman uses lowercase p as variable name for the pressure, while we use uppercase P.

residual density on the stellar surface and for $\mu = 0$ the ansatz is the one for the ISS. For $\mu = 0$ the density is constant and for $\mu \in (0, 1]$ it quadratically decreases towards the surface.

The total mass of a TVII configuration is given by

$$M = \frac{4}{15}\pi R^3 \rho_c \left(5 - 3\mu\right) \tag{3.73}$$

and with this expression we can rewrite our ansatz in terms of the dimensionless radial variable $s \equiv r/R$ and the compactness $Z \equiv M/R$ as

$$\mathrm{e}^{-\lambda(s)} = 1 + \frac{2s^2 Z\left(5 - 3\mu s^2\right)}{3\mu - 5}, \tag{3.74a}$$

$$\rho(s) = \frac{15Z\left(\mu s^2 - 1\right)}{4\pi(3\mu - 5)R^2}. \tag{3.74b}$$

The next step towards a complete interior solution is deriving an expression for the g_{tt} metric potential ν. For that endeavour we rewrite eq. (A.4) using eq. (A.3) as

$$\frac{d}{ds}\left(\frac{\mathrm{e}^{-\lambda(s)} - 1}{s^2}\right) + \frac{d}{ds}\left(\frac{\mathrm{e}^{-\lambda(s)}\nu'(s)}{2s}\right) + \mathrm{e}^{-\lambda(s)-\nu(s)}\frac{d}{ds}\left(\frac{\mathrm{e}^{\nu(s)}\nu'(s)}{2s}\right) = 0, \tag{3.75}$$

which can be integrated twice to yield

$$\mathrm{e}^{\nu(s)} = \frac{5Z + 6\mu - 15Z\mu}{6\mu}\cos^2\phi(s), \tag{3.76}$$

with the auxiliary functions

$$\phi(s) = \arctan\left[\frac{\sqrt{5-\mu}}{\sqrt{(6/Z - 12)\mu}} + \frac{W(s) - W(1)}{2}\right], \tag{3.77a}$$

$$W(s) = \log\left[\frac{6\sqrt{2}\mu s^2 - 5\sqrt{2} + 2\sqrt{3}\sqrt{(5-3\mu)\mu \mathrm{e}^{-\lambda(s)}/Z}}{6\sqrt{(5-3\mu)\mu}}\right], \tag{3.77b}$$

where we already fixed the constants of integration with the boundary conditions $P(s = 1) = 0$ and $\mathrm{e}^{\nu(s=1)-\lambda(s=1)} = 1$.

Using the field eq. (A.3) and the expressions for the metric potentials we can find an expression for the pressure

$$P(s) = \frac{2sZ\left(5 - 3\mu s^2\right) + \left(3\mu - 6\mu s^4 Z + 10 s^2 Z - 5\right)\nu'(s)}{8\pi(3\mu - 5)R^2 s} \tag{3.78}$$

and with it expressions for the baryon density and the log-enthalpy

$$n_{\mathrm{B}}(s) = \frac{\cos\phi(s)}{\phi(1)}\frac{P(s) + \rho(s)}{m_{\mathrm{B}}}, \tag{3.79}$$

$$h(s) = \log\frac{\cos\phi(1)}{\cos\phi(s)}. \tag{3.80}$$

The expression for the speed of sound reads

$$c_s^2(s) = \frac{1}{15}\tan\phi(s)\left(3\tan\phi(s) - \frac{\sqrt{6}Z\left(6\mu s^2 - 5\right)}{\sqrt{\mu(5-3\mu)Z\mathrm{e}^{-\lambda(s)}}}\right). \tag{3.81}$$

μ	h_c	$P_c\,[\mathrm{MeV\,fm^{-3}}]$	$\rho_c\,[\mathrm{MeV\,fm^{-3}}]$	$n_\mathrm{B}(0)\,[\mathrm{fm^{-3}}]$	$c_s(0)$	$M\,[M_\odot]$	$R\,[\mathrm{km}]$	Z	$M_\mathrm{B}\,[M_\odot]$
0	0.103	51.214	473.444	0.508	∞	0.768	7.559	0.150	0.851
1/4	0.112	48.967	473.444	0.502	0.714	0.833	8.199	0.150	0.921
1/2	0.125	47.734	473.444	0.494	0.554	0.918	9.035	0.150	1.013
3/4	0.147	48.503	473.444	0.484	0.512	1.035	10.192	0.150	1.138
1	0.189	54.170	473.444	0.469	0.530	1.214	11.952	0.150	1.321

Table 3.1: Global parameters related to the configurations plotted in Fig. 3.1 and Fig. 3.2. The column with $\mu = 0$ corresponds to the ISS configuration, while columns with $\mu > 0$ are TVII configurations. All share the same compactness and central density.

While the expressions for λ and ρ are reasonably simple the expression for ν and the thermodynamic quantities P, n_B and h are highly complicated nested expressions.

In Sec. B.2 of the appendix we will discuss the EoS related to TVII configurations. In the remainder of this subsection we will discuss the structure of TVII equilibrium configuration, related limits and compare both to the ISS.

Fig. 3.1 displays the pressure, energy- and baryon density gradients in five configurations of the same central density and compactness. Four TVII configurations and one ISS configuration are plotted. The energy density gradients show the quadratic decay of the ansatz and the increasing residual surface density for decreasing μ. The baryon density gradients look similar to $\rho(s)$ for TVII configurations but the functional dependence of the monotonic decrease is highly complicated. The residual surface baryon density is

$$n_\mathrm{B}(s=1) = \frac{\rho_c}{m_\mathrm{B}}(1-\mu). \tag{3.82}$$

For $\mu \to 0$ the TVII solutions approach their ISS counterparts, as expected from the ansatz.

Fig. 3.2 depicts the metric potentials and the speed of sound. The metric potentials of all five solutions are identical in the stellar exterior with this choice of radial coordinate. In $s = r/R$ the ESS for $\lambda_>$ and $\nu_>$ depends on the compactness only and we choose five configurations with the same compactness. The ISS as $(\mu \to 0)$-limit of the TVII solutions is again evident.

The speed of sound in the right panel of Fig. 3.2 shows a very interesting feature of TVII solutions: the speed of sound is not only causal it is also monotonically decreasing form the stellar center to the stellar surface. This behavior is expected in realistic NS and only 9 of the 127 solutions listed by DL have this feature. Especially the TVII_1 solution is extremely interesting since it has vanishing sound speed, pressure and density at the stellar surface. Very low or in terms of central values vanishing surface sound speeds and densities are also expected for NS with a realistic, non-relativistic crust.

Tab. 3.1 shows the global parameters related to the configurations plotted in Fig. 3.1 and Fig. 3.2. Central log-enthalpy, radii and masses increase while central baryon densities decrease for TVII configurations with increasing μ at fixed Z and ρ_c. For the central speed of sound and the pressure the hierarchy has not a simple linear relation to μ. The functional dependence of both quantities is to complicated for that.

Using the expression (3.81) for the sound speed and the expressions for pressure (3.78) and energy density (3.74b) one can discuss three extreme configurations. Depending on μ we can derive compactness limits for configurations with infinite central pressure, configurations with $P_c = \rho_c$ and configurations at the causal limit $c_s(s=0) = 1$. Fig. 3.3 shows these limits and the corresponding ones for ISS solutions. There are no ISS solutions with causal sound speeds so it is not surprising that in the $(\mu \to 0)$-limit TVII configurations aproach zero compactness/ vanish. The Schwarzschild-Buchdahl limit for the TVII solution lies below 4/9 for all $\mu \in (0,1]$. The $(P_c = \rho_c)$-limit lies below

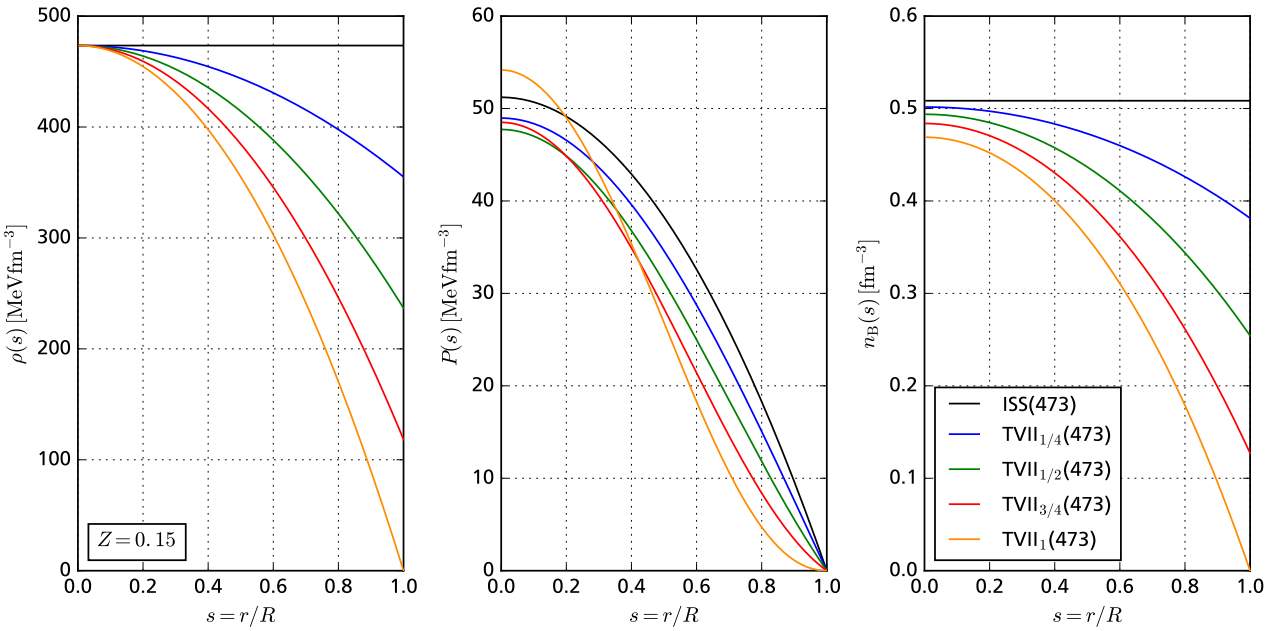

Figure 3.1: Thermodynamic gradients inside four TVII configurations and one ISS configuration. All share the same central density of $473.444\,\mathrm{MeV\,fm^{-3}}$ and compactness of $Z = 0.15$.

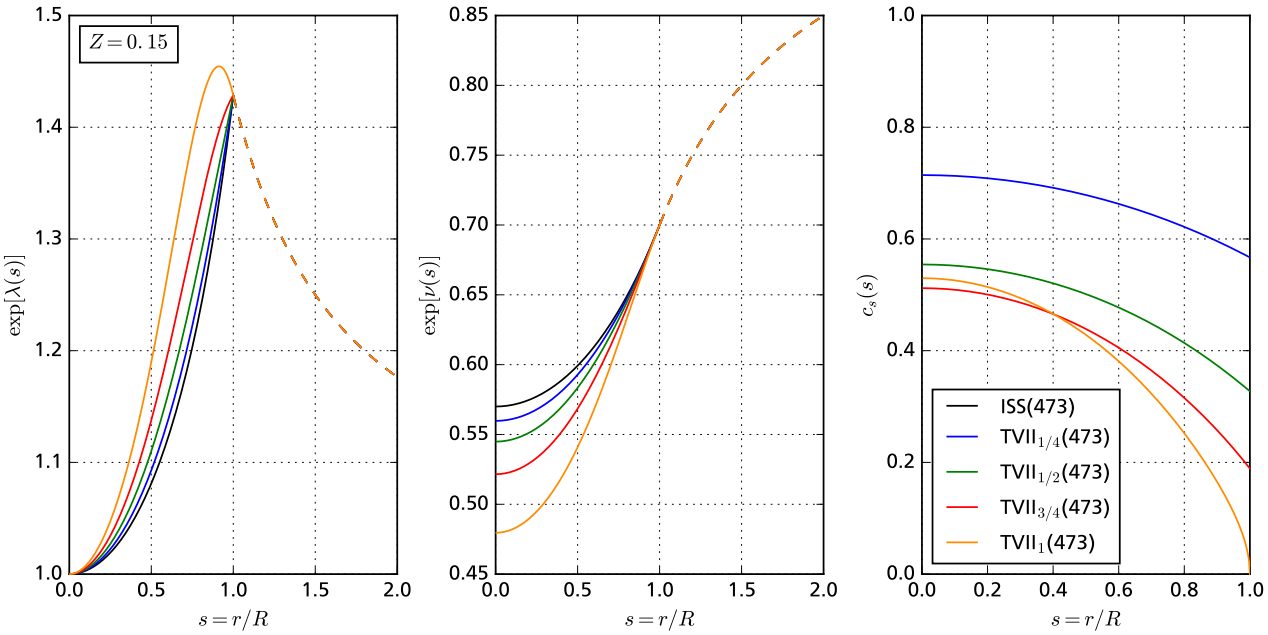

Figure 3.2: Metric potentials (left) and sound speed gradient (right) for four TVII configurations and one ISS configuration. All share the same central density of $473.444\,\mathrm{MeV\,fm^{-3}}$ and compactness of $Z = 0.15$. Dashed lines mark the exterior solutions.

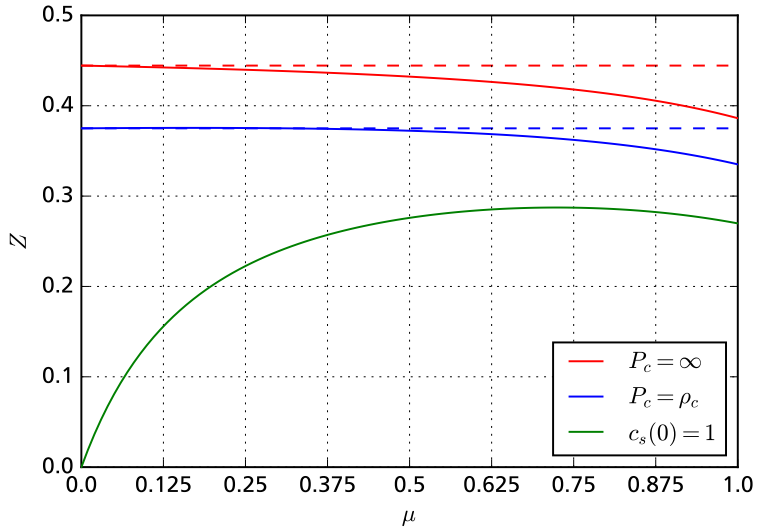

Figure 3.3: Compactness limits for extremal TVII configurations for different μ: Configurations with maximal compactness (red) are the ones with $P_c = \infty$, TVII stars with $P_c = \rho_c$ (blue) have lower compactnesses and causal configurations (green) have compactnesses below 0.3. The dashed lines correspond to the Schwarzschild-Buchdahl limit (red) and causality limit (blue) of the ISS solution.

3/8 for TVII configurations with large μ, slightly above (too slightly to be visible in Fig. 3.3) 3/8 for low μ and approaches the ISS value for $\mu \to 0$.

For $\mu = 1$, meaning vanishing surface density, the numerical values for those limit are

$$Z^{\mathrm{TVII}}_{\mathrm{SB}}(\mu = 1) \approx 0.386, \tag{3.83a}$$

$$Z^{\mathrm{TVII}}_{P_c=\rho_c}(\mu = 1) \approx 0.335, \tag{3.83b}$$

$$Z^{\mathrm{TVII}}_{c_s(0)=1}(\mu = 1) \approx 0.270. \tag{3.83c}$$

Fig. 3.4 shows the binding energy $M_{\mathrm{B}} - M$ divided by M for sequences of different μ and Z. $M_{\mathrm{B}}/M - 1 > 0$ for all configurations on the displayed sequences, meaning that all configurations are bound. The expression for the baryonic mass is an integral over analytic functions but the integrand is too complicated for analytic integration. We obtained the values for M_{B} in this subsection by numerical integration of

$$M_{\mathrm{B}} = 4\pi R^3 m_{\mathrm{B}} \int_0^1 n_{\mathrm{B}}(s) \mathrm{e}^{\lambda(s)/2} s^2 ds. \tag{3.84}$$

For more details regarding the properties and structure of TVII configuration, we refer the interested reader to the work of A. M. Raghoonundun [55, 72].

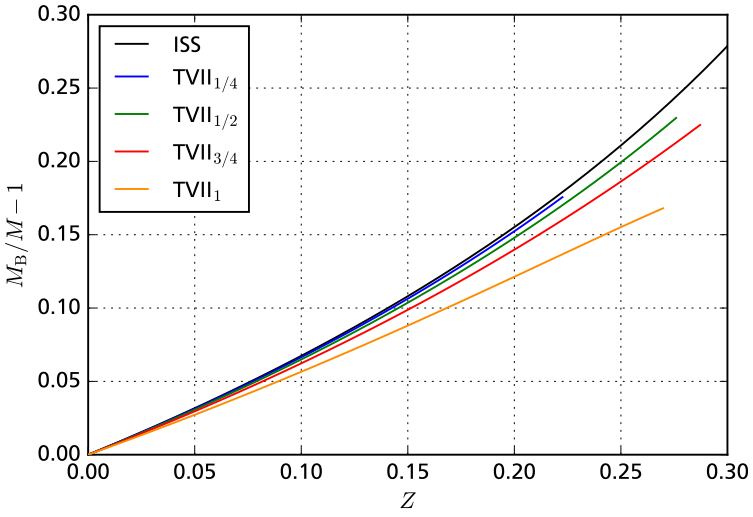

Figure 3.4: Binding energy divided by gravitational mass as a function of compactness for four TVII sequences and one corresponding ISS sequences. Only causal TVII configurations are plotted.

3.3 $O\left(B^0\Omega^1\right)$: Frame-dragging

The only non-trivial field equation linear in Ω is eq. (A.6), which becomes the homogeneous second-order ODE

$$\bar{\omega}'' + \frac{1}{2r}\left(r(\nu'+\lambda') - 8\right)\bar{\omega}' + \frac{2}{r}(\nu'+\lambda')\bar{\omega} = 0. \tag{3.85}$$

when using

$$\bar{\omega}(r) \equiv \Omega - \omega(r). \tag{3.86}$$

Eq. (3.85) is the classical HT frame-dragging (FD) equation and it is discussed in detail in [25, 48]. The difference between the four-velocity of the fluid rest $\mathbf{u}$ and the one of the Eulerian observer $\mathbf{n}$ is given by

$$(u^\alpha - n^\alpha) = (0,0,0,\mathrm{e}^{-\nu/2}\bar{\omega})^T + O\left(B^2\Omega^1\right). \tag{3.87}$$

Apart from $O\left(\Omega^1\right)$ effects, $\bar{\omega}(r)$ and $\omega(r)$ are also needed for the deduction of the induced electric field and for the higher-order corrections W_1 and W_3.

The Eulerian observer rotates around the z-axis with an angular velocity smaller than Ω which gives the effect its name. This effect in general is also known as *Lense-Thirring precession* or the *Lense-Thirring effect* and it is a purely general relativistic effect.

Fig. 3.5 shows the trajectory of a free falling particle in the $(\theta = \pi/2)$-plane. The particle gets dragged in positive ϕ-direction.

Around the coordinate singularity at the origin the FD eq. (3.85) can be expanded and solved to yield

$$\bar{\omega}(r)/\Omega \underset{r\to 0}{\longrightarrow} c_{\bar{\omega}}\left(1 + \frac{8}{5}\pi(P_c+\rho_c)r^2\right) + O\left(r^4\right). \tag{3.88}$$

In the stellar exterior eq. (3.85) becomes

$$\bar{\omega}_>'' + \frac{4}{r}\bar{\omega}_>' = 0, \tag{3.89}$$

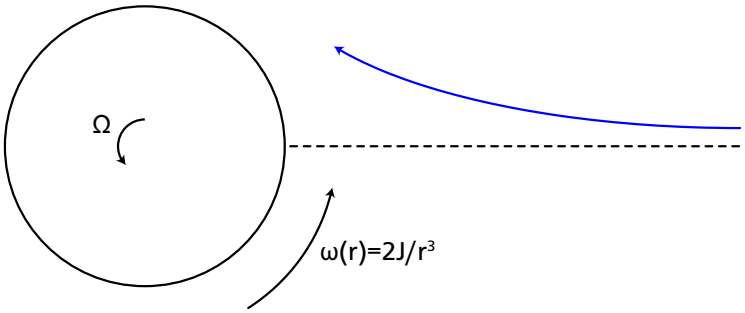

Figure 3.5: Dragging of local inertial frames in the $(\theta = \pi/2)$-plane: The trajectory of a free falling particle (blue) dropped from spatial infinity with vanishing initial velocity and its angular velocity $d\phi/dt = \omega(r)$ are depicted in the field of a slowly rotating star (black circle). *This illustration is based on Fig. 6.1 of [1].*

which can be integrated trivially. The asymptotically flat solution is

$$\bar{\omega}_{>}(r) = \Omega - \frac{2J}{r^3}, \tag{3.90}$$

where J can be identified as the angular momentum of the rotating configuration in $O\left(B^0\Omega^1\right)$. We will discuss J and alternate expressions for it in Sec. 3.9. Introducing the moment of inertia $I \equiv J/\Omega$ eq. (3.90) implies

$$\omega_{>}(r) = \frac{2I}{r^3}\Omega. \tag{3.91}$$

The angular momentum J and the scale of the homogeneous system $c_{\bar{\omega}}$ can be determined by imposing the junction condition (3.21).

In $O\left(B^0\Omega^1\right)$ the line element (3.19) in the stellar exterior takes the form

$$ds^2_{>} = -\left(1-\frac{2M}{r}\right)dt^2 + \left(1-\frac{2M}{r}\right)^{-1}dr^2 + -\frac{4J\sin^2\theta}{r}dtd\phi + r^2d\Omega^2 + O\left(B^2\Omega^2\right). \tag{3.92}$$

Expanding the Kerr metric [73] in the Kerr parameter $a = J/M$ up to first-order in a leads to the same line element (3.92).

3.4 $O\left(B^1\Omega^0\right)$: Magnetic field of a spherical background star

One of two non-trivial Maxwell equations is the one governing the magnetic field

$$\nabla_\mu F_\phi{}^\mu = 4\pi J_\phi, \tag{3.93}$$

which is of $O\left(B^1\Omega^0\right)$. For the covariant divergence we can use the metric of the background star (3.2), since we are only interested in the magnetic field up to order $O\left(B^1\right)$. Solving the Maxwell equations with the metric of the magnetically deformed star would involve terms of order $O\left(B^3\right)$. With the $O\left(B^0\Omega^0\right)$ metric (3.2) eq. (3.93) becomes

$$4\pi J_\phi = \nabla_\mu F_\phi{}^\mu \tag{3.94a}$$

$$4\pi J_\phi(r,\theta) = -\mathrm{e}^{-\lambda}\partial_r^2 A_\phi(r,\theta) + \frac{1}{2}\mathrm{e}^{-\lambda}\left(\lambda'-\nu'\right)\partial_r A_\phi(r,\theta) + \frac{\cot\theta\,\partial_\theta A_\phi(r,\theta)}{r^2} - \frac{\partial_\theta^2 A_\phi(r,\theta)}{r^2} \tag{3.94b}$$

$$-4\pi J_\phi(r,\theta) = \mathrm{e}^{-\lambda}\partial_r^2 A_\phi(r,\theta) + \frac{1}{2}\mathrm{e}^{-\lambda}\left(\nu'-\lambda'\right)\partial_r A_\phi(r,\theta) + \frac{\sin\theta}{r^2}\partial_\theta\left[\frac{1}{\sin\theta}\partial_\theta A_\phi(r,\theta)\right] \tag{3.94c}$$

The angular part of this second-order PDE can be solved by expanding $A_\phi(r,\theta)$ and $J_\phi(r,\theta)$ in odd parity zonal ($m=0$) vector harmonics S_ϕ^{l0} as introduced in eq. (3.4)

$$A_\phi(r,\theta) \equiv \sum_{l=1}^{\infty} a_{\phi l}(r) S_\phi^{l0} = \sum_{l=1}^{\infty} a_{\phi l}(r) \sin\theta \frac{d\mathrm{P}_l(\cos\theta)}{d\theta} = -\sum_{l=1}^{\infty} a_{\phi l}(r)\left(1-\tilde{y}^2\right)\frac{d\mathrm{P}_l\left(\tilde{y}\right)}{d\tilde{y}}, \tag{3.95}$$

$$J_\phi(r,\theta) \equiv \sum_{l=1}^{\infty} j_{\phi l}(r) S_\phi^{l0} = \sum_{l=1}^{\infty} j_{\phi l}(r) \sin\theta \frac{d\mathrm{P}_l(\cos\theta)}{d\theta} = -\sum_{l=1}^{\infty} j_{\phi l}(r)\left(1-\tilde{y}^2\right)\frac{d\mathrm{P}_l\left(\tilde{y}\right)}{d\tilde{y}}, \tag{3.96}$$

with $\tilde{y} \equiv \cos\theta$ and the Legendre polynomials $\mathrm{P}_l(\tilde{y})$. This expansion corresponds to a multipole expansion of the fields $A_\phi(r,\theta)$ and $J_\phi(r,\theta)$. Equating eq. (3.94c) with this expansion and using the Legendre differential equation

$$\frac{d}{d\tilde{y}}\left[\left(1-\tilde{y}^2\right)\mathrm{P}_l'(\tilde{y})\right] + l(l+1)\mathrm{P}_l(\tilde{y}) = 0, \tag{3.97}$$

leads to l second-order ODEs in r for the expansion coefficients $a_{\phi l}(r)$ and $j_{\phi l}(r)$:

$$\mathrm{e}^{-\lambda} a_{\phi l}'' + \frac{1}{2}\mathrm{e}^{-\lambda}\left(\nu'-\lambda'\right)a_{\phi l}' - \frac{l(l+1)}{r^2}a_{\phi l} = -4\pi j_{\phi l}. \tag{3.98}$$

Up until now our discussion holds for arbitrary, purely poloidal magnetic fields and currents. The expansion coefficients of the current density $j_{\phi l}(r)$ are not independent of $a_{\phi l}(r)$. In order to describe a star in hydrostatic equilibrium the configuration must obey the relativistic Euler equation. This equation includes Lorentz force terms $\sim J_\mu F^{\mu\alpha}$ and one can derive a relation between J_α and A_α. A. Colaiuda et al. [24] derived such a relation from the relativistic Euler equation in a differential from. In case of vanishing toroidal fields and decoupled harmonic components there is just one non-vanishing $j_{\phi l}(r)$ coefficient [23, 24]:

$$j_{\phi l}(r) = c_{j\phi} r^2 \left(P(r) + \rho(r)\right)\delta_{l1}, \tag{3.99}$$

where $c_{j\phi}$ is a constant of $O\left(B^1\right)$. We will derive this result from the relativistic Euler equation in Sec. 3.6.1 for the special case ($l=1$). Combining this result from the Euler eq. with the Maxwell eq. leads to

$$\mathrm{e}^{-\lambda} a_{\phi l}'' + \frac{1}{2}\mathrm{e}^{-\lambda}\left(\nu'-\lambda'\right)a_{\phi l}' - \frac{l(l+1)}{r^2}a_{\phi l} = -4\pi c_{j\phi} r^2\left(P+\rho\right)\delta_{l1}. \tag{3.100}$$

Eq. (3.100) is called *relativistic Grad-Shafranov* (GS) equation on a spherical-symmetric background star [21–23]. Fields satisfying this equation result in hydrostatic equilibrium configuration satisfying the Bernoulli theorem (3.174). The *classical Grad-Shafranov* equation [74] describes the equilibrium of a classical two dimensional plasma in ideal MHD. For the special case of purely dipolar fields we recover the classical GS eq. as the non-relativistic limit of eq. (3.100) in Sec. 6.2.2, eq. (6.47).

For the following discussions of this subsection we will limit ourselves to configurations with pure dipolar magnetic fields, meaning that we only consider vector potentials A_ϕ and current densities J_ϕ with just one non-vanishing expansion coefficient $a_{\phi 1}(r) \equiv a_\phi(r)$ and respectively $j_{\phi 1}(r) \equiv j_\phi(r)$:

$$A_\phi(r,\theta) \stackrel{!}{=} a_{\phi 1}(r)\sin\theta\frac{d\mathrm{P}_1(\cos\theta)}{d\theta} \equiv -a_\phi(r)\sin^2\theta, \tag{3.101}$$

$$J_\phi(r,\theta) \stackrel{!}{=} j_{\phi 1}(r)\sin\theta\frac{d\mathrm{P}_1(\cos\theta)}{d\theta} \equiv -j_\phi(r)\sin^2\theta. \tag{3.102}$$

Considering only dipolar magnetic fields simplifies the problem. In this case the magnetic configuration is governed by only one second-order ODE

$$\mathrm{e}^{-\lambda}a_\phi'' + \frac{1}{2}\mathrm{e}^{-\lambda}\left(\nu' - \lambda'\right)a_\phi' - \frac{2}{r^2}a_\phi = -4\pi j_\phi. \tag{3.103}$$

Using the relativistic Euler equation we will derive the functional form of j_ϕ in eq. (3.172) and eq. (3.103) becomes

$$\mathrm{e}^{-\lambda}a_\phi'' + \frac{1}{2}\mathrm{e}^{-\lambda}\left(\nu' - \lambda'\right)a_\phi' - \frac{2}{r^2}a_\phi = -4\pi c_{j\phi} r^2 (P+\rho). \tag{3.104}$$

Eq. (3.104) is singular at $r = 0$ because of the coordinate singularity at that point but physically its solutions for a_ϕ have to be regular. To guaranty regularity of the solutions and to find initial conditions we expand eq. (3.104) in a Taylor series around $r = 0$, using the TOV asymptotic from eqs. (3.56). In leading-order the ODE (3.104) becomes

$$a_\phi''(r) - 2a_\phi(r) + O\left(r^3\right) = 0, \tag{3.105}$$

which has the regular solution

$$a_\phi(r) \overset{r\to 0}{\to} -\frac{1}{2}B_0 r^2 + O\left(r^3\right). \tag{3.106}$$

B_0 is an integration constant of $O\left(B^1\right)$, which we have chosen this way so that eq. (3.119a) becomes

$$B_{\hat{r}}(r=0,\theta=0) = B_0 \tag{3.107}$$

at the stellar center: B_0 is the magnetic field strength at the stellar center and a free input parameter of our model. All constants of $O\left(B^1\right)$ and $O\left(B^2\right)$ can be expressed in terms of this constant e.g.

$$c_{j\phi} \equiv B_0 c_{j\phi 0}, \tag{3.108}$$

where $c_{j\phi 0}$ is of $O\left(B^0\right)$ and depends only on the background star.

$c_{j\phi 0}$ is not a free parameter: it has to be fixed by imposing magnetostatic boundary conditions [21, 75] on the stellar surface. The components of the magnetic field tangential to the stellar surface are continuous in the case of vanishing surface currents and the component normal to the surface is always continuous. We will only consider configurations with vanishing surface currents and therefore completely continuous fields. Translating those matching conditions to the vector potential using eqs. (3.118) it becomes obvious that the expansion coefficients $a_{\phi l}(r)$ and their derivatives $a'_{\phi l}(r)$ have to be continuous at $r = R$

$$a^<_{\phi l}(R) \overset{!}{=} a^>_{\phi l}(R), \tag{3.109a}$$

$$a^{<\prime}_{\phi l}(R) \overset{!}{=} a^{>\prime}_{\phi l}(R). \tag{3.109b}$$

In the purely dipolar case we have two matching conditions in $l = 1$.

For a given background star and field strength the matching conditions (3.109) can only be realized with unique $c_{j\phi 0}$ and an unique exterior solution. The latter depends on the background star and the $\mathrm{O}\left(B^1\right)$ magnetic dipole moment μ, see Sec. 3.4.1. With the expansion (3.106) and with the matching conditions the ODE for a_ϕ (3.104) has to be solved as a boundary value problem. We use the following procedure: We integrate eq. (3.104) with a guess for $c_{j\phi 0}$ and then we fix the dipole moment μ by imposing $a^<_{\phi l}(R) \overset{!}{=} a^>_{\phi l}(R)$. We optimize our guess for $c_{j\phi 0}$ by finding the root of the second matching condition $a^{<\prime}_{\phi l}(R) - a^{>\prime}_{\phi l}(R)$.

3.4.1 Exterior solution for the vector potential

Outside the star the metric is given by the ESS encoded in eqs. (3.37) and the current density vanishes $j_{\phi l} = c_{j\phi} r^2 (P+\rho)\delta_{l1} = 0$ since P and ρ vanish for $r > R$. This simplifies the GS eq. (3.104) for $a_{\phi l}$ significantly:

$$0 = \left(1 - \frac{2M}{r}\right) r^2 a^{>}_{\phi l}{}''(r) + 2M a^{>}_{\phi l}{}'(r) - l(l+1) a^{>}_{\phi l}(r) \tag{3.110a}$$

$$0 = r^2 \frac{d}{dr}\left[\left(1 - \frac{2M}{r}\right)\frac{d a^{>}_{\phi l}(r)}{dr}\right] - l(l+1) a^{>}_{\phi l}(r)\,. \tag{3.110b}$$

A change of variables with $x \equiv r/(2M) > 1$ transforms eq. (3.110b) into

$$-(x-1)x a^{>}_{\phi l}{}''(x) - a^{>}_{\phi l}{}'(x) + l(l+1) a^{>}_{\phi l}(x) = 0. \tag{3.111}$$

This ODE has the form of a *hypergeometric equation* [76] with $a = l$, $b = -l-1$ and $c = -1$ and the solution with the correct $(r \to \infty)$-asymptotic is

$$a^{>}_{\phi l}(x) = -\frac{\mu_l}{(2M)^a} x^{-a}\, {}_2F_1\left[a, a-c+1, a-b+1; x^{-1}\right] = -\frac{\mu_l}{(2M)^l} x^{-l}\, {}_2F_1\left[l, l+2, 2l+2; x^{-1}\right], \tag{3.112}$$

with the Gauss hypergeometric function ${}_2F_1\left[a, a-c+1, a-b+1; x^{-1}\right]$ analytically continued on the $x > 1$ branch, the multipole moment μ_l and the asymptotic

$$a^{>}_{\phi l}(x) \xrightarrow[x\to\infty]{} -\frac{\mu_l}{(2M)^l} x^{-l}\left(1 + O\left(x^{-1}\right)\right). \tag{3.113}$$

In our geometrized unit system μ_l has the dimensions length to the power of $l+1$ and $\left[\mu_l\right]_{\mathrm{SI}} = \mathrm{A\,m}^{l+1}$.

In our numerical computations we only consider configurations with purely dipolar fields, $\mu_l = \mu\delta_{l1}$, with

$$a^{>}_{\phi}(r) = \frac{3\mu r^2}{8M^3}\left(\frac{2M}{r} + \frac{2M^2}{r^2} + \log\left[1 - \frac{2M}{r}\right]\right), \tag{3.114a}$$

$$a^{>}_{\phi}{}'(r) = \frac{3\mu}{2M^2}\left(\frac{M-r}{2M-r} + \frac{r}{2M}\log\left[1 - \frac{2M}{r}\right]\right). \tag{3.114b}$$

The dipole moment μ is fixed by matching interior and exterior solutions as described at the end of Sec. 3.4.

3.4.2 The magnetic field

The magnetic field measured by the Eulerian observer $\mathcal{O}_n$ (moving with n^α) is given by

$$B_\alpha = -\frac{1}{2}\epsilon_{\alpha\mu\nu\xi} n^\mu F^{\nu\xi}, \tag{3.115}$$

with

$$\epsilon_{\alpha\mu\nu\xi} = \mathrm{e}^{(\nu+\lambda)/2} r^2 \sin\theta\left[\alpha\mu\nu\xi\right], \tag{3.116}$$

and n^α from eq. (3.26a), the non-vanishing components of the magnetic field measured in $\mathcal{O}_n$ are

$$B_r(r,\theta) = \frac{e^{\lambda(r)/2}}{r^2 \sin\theta} \partial_\theta A_\phi(r,\theta), \tag{3.117a}$$

$$B_\theta(r,\theta) = e^{-\lambda(r)/2} \sin\theta \partial_r A_\phi(r,\theta). \tag{3.117b}$$

For discussion and the non-relativistic limiting case the components of B_α with respect to the orthonormal tetrad carried by $\mathcal{O}_n$ are advantageous as discussed in Sec. 3.1.2. Using eq. (3.29) and the scalar product $B_{\hat{\alpha}} = \mathbf{B} \cdot \mathbf{e}_{\hat{\alpha}}$, the tetrad components of the magnetic field follow as

$$B_{\hat{r}}(r,\theta) = -\frac{1}{r^2 \sin\theta} \partial_\theta A_\phi(r,\theta) = -\sum_{l=0}^{\infty} \frac{l(l+1)}{r^2} a_{\phi l}(r) \mathrm{P}_l(\cos\theta), \tag{3.118a}$$

$$B_{\hat{\theta}}(r,\theta) = \frac{e^{-\lambda(r)/2}}{r \sin\theta} \partial_r A_\phi(r,\theta) = \sum_{l=0}^{\infty} \frac{e^{-\lambda(r)/2}}{r} a'_{\phi l}(r) \frac{d\mathrm{P}_l(\cos\theta)}{d\theta}, \tag{3.118b}$$

with the typical angular dependency expected for a multipole expansion of a purely poloidal magnetic field. When considering purely dipolar configurations eq. (3.118) reduces to

$$B_{\hat{r}}(r,\theta) = -\frac{2a_\phi(r)}{r^2} \cos\theta, \tag{3.119a}$$

$$B_{\hat{\theta}}(r,\theta) = \frac{e^{-\lambda(r)/2} a'_\phi(r)}{r} \sin\theta. \tag{3.119b}$$

Inserting the exterior solution $a^>_\phi$ and the ESS, the magnetic field outside the star can be given analytically as

$$B^>_{\hat{r}}(r,\theta) = -\sum_{l=0}^{\infty} \frac{l(l+1)}{r^{2+l}} \mu_l \, {}_2F_1\left[l, l+2, 2l+2, \frac{2M}{r}\right] \mathrm{P}_l(\cos\theta), \tag{3.120a}$$

$$\begin{aligned} B^>_{\hat{\theta}}(r,\theta) = -\sqrt{1-\frac{2M}{r}} \sum_{l=0}^{\infty} \frac{l(l+1)}{r^{3+l}} \mu_l \Bigg(& (l+1) r \, {}_2F_1\left[l, l+2, 2l+2, \frac{2M}{r}\right] \\ & + M(l+2) \, {}_2F_1\left[l+1, l+3, 2l+3, \frac{2M}{r}\right] \Bigg) \frac{d\mathrm{P}_l(\cos\theta)}{d\theta}. \end{aligned} \tag{3.120b}$$

Asymptotically those complicated expressions reduce to the flat space multipole expansion of a purely poloidal magnetic field

$$B^>_{\hat{r}}(r,\theta) \xrightarrow[r\to\infty]{} \sum_{l=0}^{\infty} \frac{l(l+1)}{r^{2+l}} \mu_l \left(1 + O\left(\frac{1}{r}\right)^1\right) \mathrm{P}_l(\cos\theta), \tag{3.121a}$$

$$B^>_{\hat{\theta}}(r,\theta) \xrightarrow[r\to\infty]{} -\sum_{l=0}^{\infty} \frac{l}{r^{2+l}} \mu_l \left(1 + O\left(\frac{1}{r}\right)^1\right) \frac{d\mathrm{P}_l(\cos\theta)}{d\theta}, \tag{3.121b}$$

with the characteristic r^{-l-2} LO. The far field is dominated by the dipolar ($l = 1$) part of the magnetic field decaying in LO as r^{-3}. When considering such a field exclusively, $\mu_l = \mu\delta_{l1}$, the magnetic field takes the explicit form

$$B^>_{\hat{r}}(r,\theta) = -\frac{3\mu}{4M^3} \left(\log\left[1 - \frac{2M}{r}\right] + \frac{2M}{r} + \frac{2M^2}{r^2} \right) \cos\theta, \tag{3.122a}$$

$$B^>_{\hat{\theta}}(r,\theta) = \frac{3\mu}{4M^3} \left(\sqrt{1-\frac{2M}{r}} \log\left[1 - \frac{2M}{r}\right] + \frac{2M(M-r)}{r\sqrt{r(r-2M)}} \right) \sin\theta. \tag{3.122b}$$

Expanding in the non-relativistic limit ($c \to \infty \Leftrightarrow M \to 0$) yields

$$B^{>}_{\hat{r}}(r,\theta) = \frac{2\mu}{r^3}\left(1+\frac{3M}{2r}+\frac{12M^2}{5r^2}+O\left(M^3\right)\right)\cos\theta, \tag{3.123a}$$

$$B^{>}_{\hat{\theta}}(r,\theta) = \frac{\mu}{r^3}\left(1+\frac{2M}{r}+\frac{37M^2}{10r^2}+O\left(M^3\right)\right)\sin\theta, \tag{3.123b}$$

where the terms beyond $O\left(M^0\right)$ are higher-order corrections to the non-relativistic limit. The higher-order terms account for the effects of spacetime curvature. At the surface of the sun M/R is of the order 10^{-6} and at the surface of a compact star ($M = 2\,M_\odot$, $R = 15\,\mathrm{km}$) it is around 10^{-1}. So even in relativistic scenarios the corrections to the magnetic field outside the star are rather small but inside a compact star they become significant. The non-relativistic, flat space expressions for the magnetic dipole field

$$B^{>}_{\hat{r},\mathrm{cl.}}(r,\theta) = \frac{2\mu}{r^3}\cos\theta, \tag{3.124a}$$

$$B^{>}_{\hat{\theta},\mathrm{cl.}}(r,\theta) = \frac{\mu}{r^3}\sin\theta, \tag{3.124b}$$

are the standard textbook expressions [77] which arise from purely classical calculations.

3.5 $O\left(B^1\Omega^1\right)$: Electric field of a spherical background star

The non-trivial Maxwell equation governing the electric field is

$$\nabla_\mu F_t{}^\mu = 4\pi J_t \tag{3.125}$$

and it is of $O\left(B^1\Omega^1\right)$. For the covariant divergence we use the metric $g^{(00)}_{\alpha\beta} + g^{(01)}_{\alpha\beta}$ of the rotating background star of $O\left(B^0\Omega^1\right)$. Computing the covariant divergence leads to

$$4\pi J_t = \nabla_\mu F_t{}^\mu \tag{3.126a}$$

$$\begin{aligned} -4\pi J_t(r,\theta) = {}& \mathrm{e}^{-\lambda(r)}\partial_r^2 A_t(r,\theta) - \frac{\mathrm{e}^{-\lambda(r)}\left(-4+r\lambda'(r)+r\nu'(r)\right)}{2r}\partial_r A_t(r,\theta) + \frac{1}{r^2}\partial_\theta^2 A_t(r,\theta) \\ & + \frac{\cot\theta}{r^2}\partial_\theta A_t(r,\theta) - \frac{\mathrm{e}^{-\lambda(r)}\left(\omega(r)\left(-2+r\nu(r)'\right)-r\omega'(r)\right)}{r}\partial_r A_\phi(r,\theta) \\ & + \frac{2\omega(r)\cot\theta}{r^2}\partial_\theta A_\phi(r,\theta) \end{aligned} \tag{3.126b}$$

which can be rewritten to

$$\begin{aligned} & -4\pi J_t(r,\theta) + \frac{\mathrm{e}^{-\lambda(r)}\left(\omega(r)\left(-2+r\nu(r)'\right)-r\omega'(r)\right)}{r}\partial_r A_\phi(r,\theta) - \frac{2\omega(r)\cot\theta}{r^2}\partial_\theta A_\phi(r,\theta) = \\ & \mathrm{e}^{-\lambda(r)}\partial_r^2 A_t(r,\theta) - \frac{\mathrm{e}^{-\lambda(r)}\left(-4+r\lambda'(r)+r\nu'(r)\right)}{2r}\partial_r A_t(r,\theta) + \frac{1}{r^2\sin\theta}\partial_\theta\left[\sin\theta\,\partial_\theta A_t(r,\theta)\right]. \end{aligned} \tag{3.127}$$

Expanding $A_t(r,\theta)$ and $J_t(r,\theta)$ in scalar zonal ($m=0$) harmonics, Legendre polynomials $\mathrm{P}_l(\cos\theta)$, and using the expansion of A_ϕ the angular and radial dependencies decouple and eq. (3.127) decomposes into l inhomogeneous second-order ODEs in r for the expansion coefficients:

$$\begin{aligned} & -\frac{1}{r}\mathrm{e}^{-\lambda}\left(\omega(r\nu'-2)-r\omega'\right)\left[\sum_n a'_{\phi n}\sin\theta\frac{d\mathrm{P}_n(\cos\theta)}{d\theta}\right]_l + \frac{2}{r^2}\omega\left[\sum_n n(n+1)a_{\phi n}\cos\theta\,\mathrm{P}_n(\cos\theta)\right]_l \\ & = \mathrm{e}^{-\lambda}a''_{tl} - \frac{1}{2r}\mathrm{e}^{-\lambda}a'_{tl}\left(r\nu'+r\lambda'-4\right) - l(l+1)\frac{a_{tl}}{r^2} + 4\pi j_{tl}. \end{aligned} \tag{3.128}$$

In the following we will focus on the electric field corresponding to the dipolar field $a_{\phi l} = a_\phi \delta_{l1}$ for which eq. (3.128) simplifies to

$$\begin{aligned} &-4\pi j_{tl} - \frac{1}{r}\mathrm{e}^{-\lambda}\left(\omega(r\nu'-2) - r\omega'\right)a'_\phi\left[\frac{2}{3}\delta_{l0} - \frac{2}{3}\delta_{l2}\right] + \frac{2}{r^2}\omega a_\phi\left[\frac{1}{3}\delta_{l0} + \frac{2}{3}\delta_{l2}\right] \\ &= \mathrm{e}^{-\lambda}a''_{tl} - \frac{1}{2r}\mathrm{e}^{-\lambda}a'_{tl}\left(r\nu' + r\lambda' - 4\right) - l(l+1)\frac{a_{tl}}{r^2}. \end{aligned} \tag{3.129}$$

In the following subsections we will discuss interior and exterior solutions of this Maxwell equation and the corresponding electric fields, currents and potentials.

3.5.1 Interior solution for the electric potential and charge density

In the stellar interior we assume infinite conductivity (ideal MHD condition) as discussed in Sec. 2.2. The ideal MHD condition which requires the vanishing of the electric field in the fluid rest frame

$$E^{(u)}_\alpha = F_{\alpha\mu}u^\mu = 0 \tag{3.130}$$

leads to

$$\partial_{x_i}\left(A_t(r,\theta) + \Omega A_\phi(r,\theta)\right) = 0, \tag{3.131}$$

in case of $\Omega = \text{const.}$. The multipole expansions of the four potential and considering purely dipolar magnetic fields leads to

$$\sum_{l=0}^{\infty} a'_{tl}(r)\,\mathrm{P}_l(\cos\theta) = -\Omega\sin^2\theta\, a'_\phi(r), \tag{3.132}$$

$$\partial_\theta \sum_{l=0}^{\infty} a_{tl}(r)\,\mathrm{P}_l(\cos\theta) = -2\Omega\sin\theta\cos\theta\, a_\phi(r), \tag{3.133}$$

which requires

$$a_{tl}(r) = a_{t0}(r)\,\delta_{l0} + a_{t2}(r)\,\delta_{l2}. \tag{3.134}$$

In case of a purely dipolar magnetic fields the induced electric fields in the stellar interior have only mono and quadrupole components. With this fact we can integrate the induction equation to get explicit expressions for $a^<_{t0}$ and $a^<_{t2}$:

$$a^<_{t0}(r) = \frac{2}{3}\Omega a_\phi(r) + c_{at0}, \tag{3.135a}$$

$$a^<_{t2}(r) = -\frac{2}{3}\Omega a_\phi(r). \tag{3.135b}$$

The integration constant c_{at0} has no effect on the electric field. We fix c_{at0} to ensure continuity of a_{t0} over the stellar surface. We make this particular gauge choice because it makes plotting the four potential easier and more instructive. The particular expressions for the induced electric potentials result in a very simple overall expression for $A^<_t(r,\theta)$:

$$A^<_t(r,\theta) = \Omega a_\phi(r)\sin^2\theta + c_{at0}. \tag{3.136}$$

The electric potential in the interior is purely of $O\left(B^1\Omega^1\right)$.

Plugging the induced electric potentials into the Maxwell eq. (3.129) allows for a determination of the corresponding induced charge density $j_{tl} = j_{t0}\delta_{l0} + j_{t2}\delta_{l2}$ with

$$j^<_{t0}(r) = \frac{2\Omega j_\phi(r)}{3} - \frac{a_\phi(r)\,\bar\omega(r)}{3\pi r^2} + \frac{\mathrm{e}^{-\lambda(r)}a'_\phi(r)\left(\bar\omega(r)\left(-2 + r\nu'(r)\right) - r\bar\omega'(r)\right)}{6\pi r}, \tag{3.137a}$$

$$j^<_{t2}(r) = -\frac{2\Omega j_\phi(r)}{3} - \frac{2a_\phi(r)\,\bar\omega(r)}{3\pi r^2} - \frac{\mathrm{e}^{-\lambda(r)}a'_\phi(r)\left(\bar\omega(r)\left(-2 + r\nu'(r)\right) - r\bar\omega'(r)\right)}{6\pi r}. \tag{3.137b}$$

3.5.2 Exterior solution for the electric potential

We consider the stellar exterior as matter free. Currents, densities and pressures vanish outside the NS. In the stellar exterior the Maxwell eq. (3.129) simplifies to

$$-(x-1)x a_{tl}^{>\prime\prime}(x)-2(x-1)a_{tl}^{>\prime}(x)+l(l+1)a_{tl}^{>}(x)=J\mu\frac{\delta_{l0}+\delta_{l2}\left(2+3x-6x^2-6(x-1)x^2\log\left[\frac{x-1}{x}\right]\right)}{4M^4(x-1)x^3}, \tag{3.138}$$

where we used the ESS, the exterior solution for the frame-dragging frequency and the coordinate transformation $x\equiv r/(2M)>1$. For $l=0$ and $l=2$ this second-order ODE is inhomogeneous even in the stellar exterior.

The inhomogeneous RHS is a $a_\phi\omega$ cross term between the magnetic field and the frame-dragging frequency. The homogeneous LHS has again the form of a hypergeometric equation but in this case with $a=-l$, $b=l+1$, $c=2$. The homogeneous part of eq. (3.138) has two linearly independent solutions

$$a_{tl,\mathrm{H1}}^{>}(x)=x^l\,{}_2F_1\left[-1-l,-l,-2l;x^{-1}\right], \tag{3.139}$$

$$a_{tl,\mathrm{H2}}^{>}(x)=x^{-l-1}\,{}_2F_1\left[l,l+1,2+2l;x^{-1}\right], \tag{3.140}$$

with $x\to\infty$ asymptotics

$$a_{tl,\mathrm{H1}}^{>}(x)\xrightarrow[x\to\infty]{}x^l\left(1+O\left(x^{-1}\right)\right), \tag{3.141}$$

$$a_{tl,\mathrm{H2}}^{>}(x)\xrightarrow[x\to\infty]{}x^{-l}O\left(x^{-1}\right). \tag{3.142}$$

For $l=0$ and $l=2$ it is necessary to construct a particular solution of the inhomogeneous system. Using the two independent homogeneous solutions we construct a particular solution by the *variation of parameters* method, see e.g. [76]. For shorter expressions and the involved integrals it is convenient to work with a compactified, dimensionless radial coordinate $y=1-2M/r$ with $y\in[1-2M/R,1)$ and $1-2M/R\geq 1/9$ because of the SB-limit (3.69).

The solutions for $a_{tl}^{>}$ have two free parameters each which we fix using the following boundary conditions. At spatial infinity we require the potentials to vanish which fixes one constant and at the stellar surface we impose electrostatic boundary conditions [75, 78] which fixes the other one. At the stellar surface the tangential components of the electric field in the surface need to be continuous while the radial/normal component can be discontinuous. When considering the interior solutions related to a purely dipolar magnetic field, electrostatic boundary conditions require

$$a_{tl}^{>}=a_{t0}^{>}\delta_{l0}+a_{t2}^{>}\delta_{l2}, \tag{3.143}$$

$$a_{t2}^{<}=a_{t2}^{>}. \tag{3.144}$$

Electrostatic boundary conditions require that the exterior field related to the induced interior field has only non-vanishing $l=0$ and $l=2$ components. The quadrupolar component of the electric potential has to be continuous to ensure continuity of the tangential field components. The monopole components a_{t0} and its derivative can be discontinuous across the surface. We discuss this discontinuity and the physics behind it in the second part of Sec. 3.5.3. The exterior monopole component is given by

$$a_{t0}^{>}(y)=\frac{Q(y-1)}{2M}-\frac{J\mu}{8M^4}\left(-5+4y+y^2-2(1+2y)\log[y]\right), \tag{3.145}$$

which has the asymptotics

$$a^{>}_{t0}(r) \xrightarrow[r\to\infty]{} -\frac{Q}{r} + \frac{J\mu}{3r^4} + O\left(r^{-5}\right). \tag{3.146}$$

Q is the total electric charge of the star and it is not a constant of $O\left(B^1\Omega^1\right)$. The global electrical charge Q of the NS is a free input parameter. For the most part we will consider configurations with $Q = 0$ but we will discuss some theoretical aspects of globally charges NS in Sec. 3.8 and corresponding numerical results in Sec. 5.6.

The exterior quadrupolar potential is given by

$$\begin{aligned} a^{>}_{t2}(y) = -5\mathcal{Q}_{\mathrm{E}} &\frac{-1-9y+9y^2+y^3-6y(1+y)\log[y]}{2M^3(y-1)^2} \\ -J\mu &\frac{6+41y-39y^2-9y^3+y^4+\left(1+27y+33y^2-y^3\right)\log[y]}{4M^4(y-1)^2}, \end{aligned} \tag{3.147}$$

which has the asymptotics

$$a^{>}_{t2}(r) \xrightarrow[r\to\infty]{} 2\frac{\mathcal{Q}_{\mathrm{E}}}{r^3} + O\left(r^{-4}\right). \tag{3.148}$$

$\mathcal{Q}_{\mathrm{E}}$ can be identified as the asymptotic, electric quadrupole moment and its value is fixed by the matching conditions on the stellar surface. The non-vanishing tangential component $E_{\hat{\theta}}$ is governed by a_{t2} and requiring its continuity $E^{>}_{\hat{\theta}}(R) = E^{<}_{\hat{\theta}}(R)$ fixes $\mathcal{Q}_{\mathrm{E}}$ as

$$\begin{aligned} \mathcal{Q}_{\mathrm{E}} = \mu\Omega R^2 &\frac{(-1+Y)^2\left(3-4Y+Y^2+2\log(Y)\right)}{20\left(-1-9Y+9Y^2+Y^3-6Y(1+Y)\log(Y)\right)} \\ +\mu\Omega I &\frac{\left(6+41Y-39Y^2-9Y^3+Y^4+\left(1+27Y+33Y^2-Y^3\right)\log(Y)\right)}{5R(-1+Y)\left(-1-9Y+9Y^2+Y^3-6Y(1+Y)\log(Y)\right)}, \end{aligned} \tag{3.149}$$

where $Y \equiv 1-2M/R$ and I is the moment of inertia of the rotating star. In the non-relativistic limit this rather lengthy expression simplifies drastically to

$$\mathcal{Q}_{\mathrm{E}} = \frac{1}{3}\mu\Omega R^2 + O\left(M^1\right), \tag{3.150}$$

which resembles the textbook expression [77] for the electric quadrupole moment induced by the magnetic dipole moment μ of a with angular velocity Ω rotating star with radius R.

When considering configurations with global charge $Q = 0$, the electric field in the interior and exterior is purely $O\left(B^1\Omega^1\right)$.

3.5.3 The Electric field and induced charges

The tetrad components of the electric field measured by $\mathcal{O}_n$, $E^{(n)}_{\alpha} = F_{\alpha\mu}n^{\mu}$, are given by

$$E_{\hat{r}}(r,\theta) = \mathrm{e}^{-(\nu(r)+\lambda(r))/2}\left(\partial_r A_t(r,\theta) + \omega(r)\,\partial_r A_\phi(r,\theta)\right), \tag{3.151a}$$

$$E_{\hat{\theta}}(r,\theta) = \mathrm{e}^{-\nu(r)/2}\left(\partial_\theta A_t(r,\theta) + \omega(r)\,\partial_\theta A_\phi(r,\theta)\right). \tag{3.151b}$$

Using eqs. (3.135) the electric field in the stellar interior takes the explicit form

$$E^{<}_{\hat{r}}(r,\theta) = \mathrm{e}^{-(\nu(r)+\lambda(r))/2}\bar{\omega}(r)\,a'_{\phi}(r)\sin^2\theta, \tag{3.152a}$$

$$E^{<}_{\hat{\theta}}(r,\theta) = \frac{2\mathrm{e}^{-\nu(r)/2}\bar{\omega}(r)\,a_{\phi}(r)}{r}\sin\theta\cos\theta, \tag{3.152b}$$

which can be rewritten in terms of the magnetic tetrad components (3.118) as

$$E^{<}_{\hat{r}}(r,\theta) = \mathrm{e}^{-\nu(r)/2}\bar{\omega}(r)\,rB^{<}_{\hat{\theta}}(r,\theta)\sin\theta, \tag{3.153a}$$

$$E^{<}_{\hat{\theta}}(r,\theta) = -\mathrm{e}^{-\nu(r)/2}\bar{\omega}(r)\,rB^{<}_{\hat{r}}(r,\theta)\sin\theta. \tag{3.153b}$$

Eq. (3.153) highlights the fact that the interior electric field is induced in $O\left(\Omega^1\right)\times O\left(B^1\right)$ and that it is directly coupled to the magnetic field components. This result could be obtained without the help of the four-potential by using eq. (2.61). The angular structure in the interior is quite interesting. The polar-component is a pure $l=2$ quadrupole while the radial component has a pure $\sin^2\theta$-angular dependence. The mono and quadrupole components $a^{<}_{t0}$ and $a^{<}_{t2}$ interfere destructively as the θ-independent part of the $l=2$ term cancel with the $l=0$ term. We will visualize the geometry of the electro-magnetic fields with streamline plots in Sec. 5.3.1.

In the stellar exterior the electric field is given analytically by

$$E^{>}_{\hat{r}}(r,\theta) = \frac{Q}{r^2} + d_r(r)\,\mathrm{P}_2(\cos\theta), \tag{3.154a}$$

$$E^{>}_{\hat{\theta}}(r,\theta) = d_{\theta}(r)\sin\theta\cos\theta. \tag{3.154b}$$

where we used eqs. (3.145) and (3.147) and introduced the functions $d_r(r)$ and $d_{\theta}(r)$. The exterior electric field is a superposition of a pure $O\left(B^1\Omega^1\right)$ quadrupole field and a monopole field governed by the global charge of the configuration only. $d_r(r)$ and $d_{\theta}(r)$ are lengthy functions of r and given by

$$\begin{aligned} d_r(r) = &-5\mathcal{Q}_{\mathrm{E}}\frac{2M\left(M^2+3Mr-6r^2\right)+3(3M-2r)r^2\log\left(1-\frac{2M}{r}\right)}{2M^5r^2} \\ &+J\mu\frac{2M\left(6M^3+5M^2r+15Mr^2-30r^3\right)+\left(6M^3r+45Mr^3-30r^4\right)\log\left(1-\frac{2M}{r}\right)}{4M^6r^3}, \end{aligned} \tag{3.155a}$$

$$\begin{aligned} d_{\theta}(r) = &-15\mathcal{Q}_{\mathrm{E}}\frac{2M\left(M^2-6Mr+3r^2\right)+3r\left(2M^2-3Mr+r^2\right)\log\left(1-\frac{2M}{r}\right)}{2M^5r^{3/2}\sqrt{-2M+r}} \\ &-3J\mu\frac{2M\left(2M^4-5M^2r^2+30Mr^3-15r^4\right)-15r^3\left(2M^2-3Mr+r^2\right)\log\left(1-\frac{2M}{r}\right)}{4M^6r^{7/2}\sqrt{-2M+r}}. \end{aligned} \tag{3.155b}$$

Asymptotically the electric field takes the simple form

$$E^{>}_{\hat{r}}(r,\theta) \xrightarrow[r\to\infty]{} \frac{Q}{r^2} - \frac{6\mathcal{Q}_{\mathrm{E}}}{r^4}\mathrm{P}_2(\cos\theta) + O\left(\frac{1}{r}\right)^5, \tag{3.156a}$$

$$E^{>}_{\hat{\theta}}(r,\theta) \xrightarrow[r\to\infty]{} -\frac{6\mathcal{Q}_{\mathrm{E}}}{r^4}\sin\theta\cos\theta + O\left(\frac{1}{r}\right)^5. \tag{3.156b}$$

As expected we find the characteristic r^{-l-2} LO terms for the multipole components.

For the non-relativistic limit we can expand the electric field in M to get

$$E^{>}_{\hat{r}}(r,\theta) = \frac{Q}{r^2} - \frac{2\mu\Omega R^2}{r^4}\left(1-\left(\frac{1}{2}-\frac{8R}{3r}\right)\frac{M}{R}+\left(1-\frac{2R}{r}\right)\frac{I}{R^3}+O\left(M^2\right)\right)\mathrm{P}_2(\cos\theta), \tag{3.157a}$$

$$E^{>}_{\hat{\theta}}(r,\theta) = -\frac{2\mu\Omega R^2}{r^4}\left(1-\left(\frac{1}{2}-\frac{3R}{r}\right)\frac{M}{R}+\left(1-\frac{3R}{r}\right)\frac{I}{R^3}+O\left(M^2\right)\right)\sin\theta\cos\theta, \tag{3.157b}$$

where we considered the moment of inertia as $O\left(M^1\right)$ in LO. In the Newtonian limit these expressions reduce further to

$$E^{>}_{\hat{r},\mathrm{cl.}}(r,\theta) = \frac{Q}{r^2} - \frac{2\mu\Omega R^2}{r^4}\mathrm{P}_2(\cos\theta), \tag{3.158a}$$

$$E^{>}_{\hat{\theta},\mathrm{cl.}}(r,\theta) = -\frac{2\mu\Omega R^2}{r^4}\sin\theta\cos\theta, \tag{3.158b}$$

where we can identify the classical expression for $\mathcal{Q}_{\mathrm{E,cl.}} = \mu\Omega R^2/3$. The non-relativistic, flat space, electric field (3.158) resembles the textbook expression of the induced field of a rotating, aligned dipole [77].

The radial component of the electric field is discontinuous at the surface. This discontinuity is related to a surface charge density. Associated with the induced charge density is an induced interior charge. An expression relating global-, interior- and surface charge can be obtained by integrating the covariant law of current conservation (2.18). Integrating over a spatial slice of constant time and employing the Gauss-Ostrogradsky theorem leads to

$$Q = Q_< + Q_S, \tag{3.159}$$

with Q as the global electric charge, $Q_<$ as the induced interior charge

$$Q_< = 2\pi\int_0^R\int_0^\theta J^t(r,\theta)\sqrt{-g}\,d\theta\,dr = -4\pi\int_0^R \mathrm{e}^{\frac{\lambda(r)-\nu(r)}{2}} r^2\left(j_{t0}(r)-\frac{2j_\phi(r)\,\omega(r)}{3}\right)dr \tag{3.160}$$

and Q_S as the surface charge

$$Q_S = 2\pi R^2\int_0^\pi \sigma_S(\theta)\sin\theta\,d\theta, \tag{3.161}$$

where the surface charge density $\sigma_S(\theta)$ is given by

$$\sigma_S(\theta) = \frac{1}{4\pi}\left(E^{>}_{\hat{r}}(R,\theta) - E^{<}_{\hat{r}}(R,\theta)\right). \tag{3.162}$$

Eq. (3.159) can be used for checking the self-consistency of our expressions. The integral for the surface charge can be performed analytically, since all angular dependencies are analytical

$$Q_S = Q - \frac{2}{3}\mathrm{e}^{-(\nu(R)+\lambda(R))/2}R^2\bar{\omega}(R)a'_\phi(R) = Q - \frac{2}{3}R^2\bar{\omega}(R)a'_\phi(R) = Q - \frac{2}{3}\mu\Omega + O\left(M^1\right). \tag{3.163}$$

The total surface charge is made up of the global charge Q and an induced $\mathrm{O}\left(B^1\Omega^1\right)$ surface charge. The induced surface charge in the non-relativistic limit is simply given by $-2/3\mu\Omega$. The quadrupolar parts of the exterior field do not contribute to Q_S, since $\mathrm{P}_2(\cos\theta)\sin\theta$ integrates to zero over the interval $[0,\pi]$.

The integral (3.160) for $Q_<$ can be rewritten as

$$Q_< = 2\pi \int_0^R \frac{2}{3} e^{-(\lambda+\nu)/2} r^2 \bar{\omega} a_\phi'' - \frac{1}{3} e^{-(\lambda+\nu)/2} r a_\phi' \left(\bar{\omega}\left(-4 + r\lambda' + r\nu'\right) - 2r\bar{\omega}'\right) dr, \tag{3.164}$$

where we used the explicit expression for j_{t0} from eq. (3.137a) as well as the Maxwell eq. (3.103) to eliminate j_ϕ. Integrating the first summand under the integral by parts leads to a primitive function and an integral which cancels with the second summand what remains is

$$Q_< = \left[\frac{2}{3} e^{-(\nu(r)+\lambda(r))/2} r^2 \bar{\omega}(r) a_\phi'(r)\right]_0^R = \frac{2}{3} R^2 \bar{\omega}(R) a_\phi'(R). \tag{3.165}$$

The induced interior charge is equal to minus one times the induced surface charge. Induced charges do not contribute to the global electric charge as they should. Creating global net charge with induction would violate charge conservation.

The only way to describe charged configurations is to prescribe a global charge Q, which takes the form of a surface charge when we require purely dipolar magnetic fields.

3.5.4 Tetrad components of the four-current and four-potential

With the results of this section and the previous one we can give explicit expressions for the four-current and four-potential tetrad components. For purely dipolar magnetic fields and the corresponding induced electric fields the non-vanishing tetrad components of **J** and **A** read

$$J_{\hat{t}}(r,\theta) = e^{-\nu(r)/2}\left(j_{t0}(r) + j_{t2}(r) P_2(\cos\theta)\right), \tag{3.166a}$$

$$J_{\hat{\phi}}(r,\theta) = -\frac{j_\phi(r)}{r}\sin\theta, \tag{3.166b}$$

$$A_{\hat{t}}(r,\theta) = e^{-\nu(r)/2}\left(a_{t0}(r) + a_{t2}(r) P_2(\cos\theta)\right), \tag{3.167a}$$

$$A_{\hat{\phi}}(r,\theta) = -\frac{a_\phi(r)}{r}\sin\theta. \tag{3.167b}$$

3.6 $O\left(B^2\Omega^0\right)$: Magnetic deformations

In this section we discuss the $O\left(B^2\Omega^0\right)$ deformations caused by a magnetic dipole field discussed in Sec. 3.4.

3.6.1 Perturbations of the source terms

The Euler equations eqs. (A.22)-(A.21) can be rearranged to yield the following identities for the log-enthalpy deformations

$$\nabla_\mu \mathscr{E}^{\theta\mu} = 0 \Leftrightarrow h_2 = -n_2 - \frac{2a_\phi j_\phi}{3r^2(P+\rho)}, \tag{3.168}$$

$$\left(\nabla_\mu \mathscr{E}^{r\mu}\right)_{l=0} = 0 \Leftrightarrow h_0' = -n_0' + \frac{2j_\phi a_\phi'}{3r^2(P+\rho)}, \tag{3.169}$$

$$\left(\nabla_\mu \mathscr{E}^{r\mu}\right)_{l=2} = 0 \Leftrightarrow h_2' = -n_2' - \frac{2j_\phi a_\phi'}{3r^2(P+\rho)}. \tag{3.170}$$

Differentiating eq. (3.168) and comparing it to eq. (3.170) results in a simple ODE for the current density j_ϕ:

$$\frac{d}{dr}\left[\frac{2j_\phi(r)}{3r^2\left(P(r)+\rho(r)\right)}\right]=0, \tag{3.171}$$

which can be integrated trivially to

$$j_\phi(r)=c_{j\phi}r^2\left(P(r)+\rho(r)\right). \tag{3.172}$$

We used this result earlier to derive the GS eq. (3.100) for a pure ($l=1$) field, which guaranties that our magnetic fields are consistent with the equation of motion. Eq. (3.172) is not an $O\left(B^2\right)$ identity it is an $O\left(B^1\right)$ relation restricting the shape of the current density/current function. This restriction is a direct consequence of only considering $l=1$ magnetic fields. A. Colaiuda et al. [24] derived equivalent expressions for higher l and even for non-vanishing meridional currents and coupling multipole components. We just presented an explicit derivation of the pure $l=1$ identity because it is the only one we will use throughout this work.

The raw Euler equation $\nabla_\mu \mathscr{E}^{r\mu}=0$ including $O\left(B^0\Omega^0\right)$ and $O\left(B^2\Omega^0\right)$ terms reads

$$0=h'(r)+h_0'(r)+h_2'(r)\mathrm{P}_2(\cos\theta)+\nu'(r)/2+n_0'(r)+n_2'(r)\mathrm{P}_2(\cos\theta)-\frac{j_\phi(r)a_\phi'(r)}{r^2\left(P(r)+\rho(r)\right)}\sin^2\theta. \tag{3.173}$$

Using eq. (3.172) we can integrate the differential Euler equation to a first integral of motion

$$h(r)+h_0(r)+h_2(r)\mathrm{P}_2(\cos\theta)+\nu(r)/2+n_0(r)+n_2(r)\mathrm{P}_2(\cos\theta)-c_{j\phi}a_\phi(r)\sin^2\theta=\frac{c_{\nu h}}{2}+c_{n0h0}, \tag{3.174}$$

which is the $O\left(B^2\Omega^0\right)$ expansion of the equation of motion of the BGSM formalism (2.51). Where in our case $-c_{j\phi}a_\phi(r)\sin^2\theta$ can be identified as the Lorentz force term

$$M(r,\theta)=-c_{j\phi}a_\phi(r)\sin^2\theta=\int_0^{A_\phi(r,\theta)=-a_\phi(r)\sin^2\theta}c_{j\phi}dx. \tag{3.175}$$

Our restriction to purely dipolar magnetic fields is realized by a constant current function (2.50): $f(x)=$ const. in the BGSM/BBGN. The constant $c_{\nu h}$ is $O\left(B^0\Omega^0\right)$ and we introduced it in eq. (3.50) and the constant c_{n0h0} is $O\left(B^2\Omega^0\right)$.

Decomposing the angular parts of eq. (3.174) we can give algebraic relations between the g_{tt} metric potential and the source term deformations

$$h_0=-n_0+\frac{2}{3}c_{j\phi}a_\phi+c_{n0h0}, \tag{3.176}$$

$$h_2=-n_2-\frac{2}{3}c_{j\phi}a_\phi. \tag{3.177}$$

Solving the field eq. (A.14) for m_0' yields

$$\left(\mathcal{E}^t{}_t\right)_{l=0} = 0 \Leftrightarrow m_0' = 4\pi r^2 \frac{d\rho}{dh} h_0 + \frac{1}{3} e^{-\lambda} \left(a_\phi'\right)^2 + \frac{2a_\phi^2}{3r^2}. \tag{3.178}$$

Similarly solving the field eq. (A.16) for n_0' leads to

$$\left(\mathcal{E}^r{}_r\right)_{l=0} = 0 \Leftrightarrow n_0' = \frac{e^\lambda \left(1 + r\nu'\right)}{r^2} m_0 + 4e^\lambda \pi r (P+\rho) h_0 + \frac{\left(a_\phi'\right)^2}{3r} - \frac{2e^\lambda a_\phi^2}{3r^3}. \tag{3.179}$$

Making use of eqs. (3.179) and (3.169) one can derive an ODE for h_0:

$$h_0' = \frac{2}{3} c_{j\phi} a_\phi' - n_0' = -\frac{e^\lambda \left(1 + r\nu'\right)}{r^2} m_0 - 4e^\lambda \pi r (P+\rho) h_0 - \frac{\left(a_\phi'\right)^2}{3r} + \frac{2e^\lambda a_\phi^2}{3r^3} + \frac{2}{3} c_{j\phi} a_\phi'. \tag{3.180}$$

Since the ODE for m_0 (3.178) contains h_0 and not n_0 it is convenient to implement the coupled system of m_0' and h_0'. The n_0 metric potential then follows from the simple algebraic expression (3.176) between n_0 and h_0.

To implement the ODEs (3.178) and (3.180) for m_0 and h_0 the $r \to 0$ asymptotic of both functions is needed for the first explicit step of numerical integration. Using the TOV asymptotic (3.56) and the asymptotic of a_ϕ from eq. (3.106), we derive

$$h_0(r) \overset{r\to 0}{\to} c_{h0} - \frac{1}{6}\left(B_0^2 (1 + 2c_{j\phi 0}) + 4\pi \left(3P_c + \rho_c + \left.\frac{d\rho}{dh}\right|_{r=0} \right) c_{h0} \right) r^2 + O\left(r^3\right), \tag{3.181a}$$

$$m_0(r) \overset{r\to 0}{\to} \frac{1}{6}\left(B_0^2 + 8\pi \left.\frac{d\rho}{dh}\right|_{r=0} c_{h0} \right) r^3 + O\left(r^4\right). \tag{3.181b}$$

The constant c_{h0} corresponds to the scale of the homogeneous system and to the central value of h_0, since $h_0(r=0) = c_{h0}$. c_{h0} is the $\mathrm{O}\left(B^2\right)$ shift of the central log-enthalpy. In the scope of this work we will only consider configurations with $h_0(r=0) = 0$, which in turn implies that the central log-enthalpy is entirely provided by the background star. This scheme leads to magnetically deformed stars with non-constant baryonic mass (see eq. (3.251)) for different B_0. This choice is well suited for comparing NS sequences with variable magnetic field B_0 but constant central log-enthlaphy h_c.

Another scheme [23] for fixing c_{h0} is to enforce constant baryonic mass when changing the central magnetic field strength B_0. This requires negative c_{h0} to compensate for the magnetic deformations. Enforcing constant baryonic mass/ total baryon number on a variable B_c sequence this way works well for small magnetic deformations and equivalently small absolute values of c_{h0}. Once the deformations become larger describing the shift of central log-enthalphy in order $\mathrm{O}\left(B^2\right)$ becomes inaccurate. Realizing constant baryonic mass sequences for variable B_c by adjusting the central log-enthalphy h_c of the background star works better in this case.

Outside the star ($r > R$) the ODEs for m_0 and n_0 can be solved analytically. The deformations of the log-enthalpy grid have no meaning in the stellar exterior, since the enthalpy field vanishes outside the star. The first term of Eq. (3.178) vanishes since P and ρ vanish for $r > R$ and the remaining ODE can be integrated analytically

$$\begin{aligned} m_0^>(r) = \delta M &+ \frac{3\left(r^2 - M^2\right)\mu^2}{8M^4 r} - \frac{3\left(M^2 + Mr - r^2\right)\mu^2}{8M^5} \log\left[1 - \frac{2M}{r}\right] \\ &+ \frac{3r^2(r-2M)\mu^2}{32M^6} \log^2\left[1 - \frac{2M}{r}\right], \end{aligned} \tag{3.182}$$

by using the ESS (3.37) and the exterior solution $a_\phi^>(r)$ of eq. (3.114). The second term of Eq. (3.180) vanishes again because matter sources vanish outside the star and with $m_0^>(r)$, $n_0^>(r)$ can be obtained by analytical integration

$$\begin{aligned} n_0^>(r) = \frac{\delta M}{2M-r} - \frac{3\mu^2\left(M^2-6Mr+r^2\right)}{8M^4r(2M-r)} - \frac{3\mu^2\left(3M^2-4Mr+r^2\right)}{8M^5(2M-r)}\log\left[1-\frac{2M}{r}\right] \\ + \frac{3\mu^2r^2}{32M^6}\log^2\left[1-\frac{2M}{r}\right]. \end{aligned} \tag{3.183}$$

The integration constant δM and c_{n0h0} from eq. (3.176) can be determined by matching interior and exterior solutions. The matching condition for m_0 reads

$$\delta M = m_0^<(R) - m_0^>(R)|_{\delta M=0} + 4\pi R^3\frac{2M-R}{M-R}\rho(R)h_0^<(R), \tag{3.184}$$

where $m_0^<(R)$ and $h_0^<(R)$ are the surface values of the interior solutions. The discontinuity of m_0 scales with the residual surface density and will in the scope of this work only be significant when using IRF EoS or TVII EoS with $\mu < 1$. This subtlety is overlooked by most authors when using the HT formalism to describe rotational [25, 79] or magnetic [24] deformations. The $O\left(B^2\right)$ constant δM has a fundamental meaning: it is the shift/increase in gravitational mass due to magnetic deformations, as we will discuss and show in Sec. 3.9.

The constant c_{n0h0} relating n_0 and h_0 is fixed by imposing $n_0^>(R) \stackrel{!}{=} n_0^<(R)$.

3.6.3 Quadrupole metric perturbations

Solving the field eq. (A.19) for m_2 yields a simple analytical relation between m_2 and n_2:

$$\left(\mathscr{E}^\phi{}_\phi - \mathscr{E}^\theta{}_\theta\right) : m_2 = -e^{-\lambda}rn_2 + \frac{2}{3}e^{-2\lambda}r\left(a_\phi'\right)^2. \tag{3.185}$$

By equating the field eqs. (A.18) and (A.17) with this expression for m_2 one can derive a coupled ODE system for ν_2 and n_2:

$$\nu_2' = -\nu' n_2 + \frac{4a_\phi a_\phi'}{3r^2} + \frac{e^{-\lambda}\left(a_\phi'\right)^2\left(2+r\nu'\right)}{3r}, \tag{3.186}$$

$$\begin{aligned} n_2' = {} & \frac{\left(2+2e^\lambda\left(-1+4\pi r^2(P+\rho)\right)-r^2\left(\nu'\right)^2\right)}{r^2\nu'}n_2 - \frac{4e^\lambda}{r^2\nu'}\nu_2 \\ & + \left(a_\phi'\right)^2\left(\frac{2}{3r^2\nu'} + \frac{1}{3}e^{-\lambda}\nu'\right) + \frac{4a_\phi a_\phi'\left(2+r\nu'\right)}{3r^3\nu'} + \frac{8e^\lambda a_\phi^2}{3r^4\nu'} + \frac{16e^\lambda\pi a_\phi j_\phi}{3r^2\nu'}. \end{aligned} \tag{3.187}$$

The rather complicated structure of especially the second ODE (3.187) makes this system difficult to handle compared to the ones encountered previously. To work with this system it is convenient to introduce

$$y_2 \equiv \nu_2 - \frac{2}{3r^2}a_\phi^2 + \frac{2e^{-\lambda}}{3r}a_\phi' a_\phi + \frac{e^{-\lambda}}{6}(a_\phi')^2 \tag{3.188}$$

and to use y_2 instead of v_2 for the numerical integration in the stellar interior. The ODE system

$$y_2' = -n_2\nu' + \frac{1}{2}\mathrm{e}^{-\lambda}\left(a_\phi'\right)^2\nu' - \frac{\mathrm{e}^{-\lambda}a_\phi a_\phi'\left(-2+2\mathrm{e}^{\lambda}-r\lambda'-r\nu'\right)}{3r^2} + \frac{8\pi a_\phi j_\phi}{3r} + \frac{4}{3}\pi j_\phi a_\phi', \tag{3.189}$$

$$n_2' = -\frac{n_2\left(-2+2\mathrm{e}^{\lambda}-r\lambda'-r\nu'+r^2\left(\nu'\right)^2\right)}{r^2\nu'} - \frac{4\mathrm{e}^{\lambda}y_2}{r^2\nu'} + \frac{4a_\phi a_\phi'}{3r^2} + \frac{1}{3}\mathrm{e}^{-\lambda}\left(a_\phi'\right)^2\nu' + \frac{16\mathrm{e}^{\lambda}\pi a_\phi j_\phi}{3r^2\nu'}, \tag{3.190}$$

has regular homogeneous and particular expansions around $r = 0$

$$n_{2,H}(r) \overset{r\to 0}{\to} c_{n2H0}r^2 + O\left(r^3\right), \tag{3.191a}$$

$$y_{2,H}(r) \overset{r\to 0}{\to} -\frac{2}{3}c_{n2H0}\pi(3P_c+\rho_c)r^4 + O\left(r^5\right), \tag{3.191b}$$

$$n_{2,P}(r) \overset{r\to 0}{\to} c_{n2P0}r^2 + O\left(r^3\right), \tag{3.191c}$$

$$y_{2,P}(r) \overset{r\to 0}{\to} -\frac{2}{9}\pi(3P_c+\rho_c)(3c_{n2P0}+3c_{j\phi 0}-2)r^4 + O\left(r^5\right). \tag{3.191d}$$

Expanding the particular system $\left\{dn_2/dr, dv_2/dr\right\}$ around $r = 0$ is not possible, which is why we integrate $\left\{dn_2/dr, dy_2/dr\right\}$ in the stellar interior numerically.

In the stellar exterior we can use the ESS and the exterior solution $a_\phi^>$ to construct an analytical ODE for n_2. In the stellar exterior the second term of the RHS of eq. (3.190) becomes $2/My_2(r)$ which allows us to differentiate the entire eq. (3.190) once in r and then plug in eq. (3.189) to derive a decoupled second-order ODE for $n_2^>$

$$(1-p^2)n_2^{>\prime\prime}(p) - 2pn_2^{>\prime}(p) + \frac{2(3p^2-1)}{p^2-1}n_2^>(p) = \frac{3\mu^2\left(2\left(-1+p+p^2\right)+(-1+p)(1+p)^2\log\left(\frac{-1+p}{1+p}\right)\right)}{M^4\left(-1+p^2\right)^2}, \tag{3.192}$$

where we used the dimensionless radial variable $p \equiv r/M - 1$. Eq. (3.192) is an inhomogeneous second-order ODE, with a homogeneous LHS in form of a *associated Legendre differential equation* [76] with $l = 2$ and $m = 2$. The homogeneous system has two linearly independent solutions: the associated Legendre polynomials $P_2^2(p)$ and $Q_2^2(p)$. Using variation of parameters with those two solutions, we construct a particular solution in terms of the compactified exterior radial variable $y \equiv 1 - 2M/r$:

$$\begin{aligned} n_2^>(y) = &-\frac{5\left(-1+8y-8y^3+y^4+12y^2\log(y)\right)}{16M^3(-1+y)^2y}\mathcal{Q}_{\mathrm{M}} \\ &+\frac{3\mu^2\left(7-40y-4y^2+40y^3-3y^4+2\left(1-24y^2-8y^3+y^4\right)\log(y)+8y^2\log^2(y)\right)}{32M^4(-1+y)^2y}, \end{aligned} \tag{3.193}$$

where we already determined one integration constant by requiring asymptotic flatness. The remaining $O\left(B^2\right)$ constant $\mathcal{Q}_{\mathrm{M}}$ is the mass quadrupole moment of the deformed NS, as we will see in eq. (3.271).

The exterior solutions for y_2 and v_2 can be constructed by integrating eq. (3.189) or respectively eq. (3.186) after plugging in the exterior solution for n_2, since both ODEs have trivial homogeneous solutions, meaning no explicit v_2 or y_2 dependent terms. The exterior solutions are

$$\begin{aligned} y_2^{>}(y) = &-\frac{5\left(-1-9y+9y^2+y^3-6y(1+y)\log(y)\right)}{16M^3(y-1)y}\mathcal{Q}_{\mathrm{M}} - \frac{3\left(6+45y+8y^2+y^3\right)\mu^2}{32M^4y} \\ &+ \frac{3\left(1+12y+14y^2+3y^3\right)\mu^2\log(y)}{16M^4(y-1)y} - \frac{3(-1+3y)\mu^2\log^2(y)}{16M^4(y-1)}, \end{aligned} \tag{3.194}$$

$$\begin{aligned} v_2^{>}(y) = &-\frac{5\left(-1-9y+9y^2+y^3-6y(1+y)\log(y)\right)}{16M^3(y-1)y}\mathcal{Q}_{\mathrm{M}} - \frac{3\left(5+28y+9y^2+2y^3\right)\mu^2}{32M^4y} \\ &\frac{3\left(1+2y+6y^2+5y^3\right)\mu^2\log(y)}{16M^4(y-1)y} - \frac{3\left(-1-10y+3y^2\right)\mu^2\log^2(y)}{16M^4(y-1)^2}, \end{aligned} \tag{3.195}$$

where we used asymptotic flatness to determine the integration constants of the first-order systems. This makes $\mathcal{Q}_{\mathrm{M}}$ the only $O\left(B^2\right)$ constant governing the $l=2$ exterior metric potentials.

$\mathcal{Q}_{\mathrm{M}}$ and c_{n2H0} can be determined by imposing the junction conditions $n_2^{<}(R) - n_2^{>}(R) = 0$ and $v_2^{<}(R) - v_2^{>}(R) = 0$, while c_{n2P0} can be chosen arbitrarily since a general solution is given by an arbitrary particular solution plus a homogeneous one.

3.7 $O\left(B^2\Omega^1\right)$: Electro-magnetic deformations

The $O\left(B^2\Omega^1\right)$ metric potentials W_1 and W_3 are higher-order corrections to the frame-dragging frequency. The field eqs. (A.23) and (A.24) governing them are inhomogeneous second-order ODEs with rather complicated source terms. The source terms include $O\left(B^2\right)$ deformations coupled to the frame-dragging frequency, namely S_0 and S_2, as well as electro-magnetic sources S_1 and S_3 which are either $O(B)\times O(E)$ or $O(\Omega)\times O\left(B^2\right)$.

For implementation and numerical integration in the stellar interior we recast the second-order ODEs into coupled first-order systems by using the substitutions

$$U_i \equiv r^4 \mathrm{e}^{-(\nu+\lambda)/2} W_i', \tag{3.196}$$

$$V_i \equiv \mathrm{e}^{-(\nu+\lambda)/2} W_i. \tag{3.197}$$

The system for W_1 form eq. (A.23) becomes

$$U_1' = 2r^3\left(\nu'+\lambda'\right)V_1 - S_0 - S_1 + S_2, \tag{3.198a}$$

$$V_1' = \frac{U_1}{r^4} - \frac{1}{2}\left(\nu'+\lambda'\right)V_1, \tag{3.198b}$$

with the source terms of eqs. (A.25), (A.27) and (A.26). Expanding homogeneous and particular systems around the coordinate singularity $r=0$ reveals

$$U_{1,H}(r) \overset{r\to 0}{\to} c_{U1H0} r^5 + O\left(r^6\right), \tag{3.199a}$$

$$V_{1,H}(r) \overset{r\to 0}{\to} \left(\frac{5}{16\pi(P_c+\rho_c)} - \frac{1}{8}r^2\right)c_{U1H0} + O\left(r^3\right), \tag{3.199b}$$

$$U_{1,P}(r) \overset{r\to 0}{\to} c_{U1P0} r^5 + O\left(r^6\right), \tag{3.199c}$$

$$V_{1,P}(r) \overset{r\to 0}{\to} -\frac{2}{9}\pi(3P_c+\rho_c)(3c_{n2P0}+3c_{j\phi 0}-2)r^4 + O\left(r^5\right). \tag{3.199d}$$

In the stellar interior electro-magnetic source terms S_1 can be simplified using the induction eq. (3.135) to

$$S_1^< = \frac{16}{5} e^{-\frac{\lambda}{2}-\frac{\nu}{2}} \bar{\omega} \left(e^{\lambda} a_\phi^2 + r^2 (a_\phi')^2 \right). \tag{3.200}$$

In the stellar exterior it is possible to construct an analytical solution for W_1. The LHS of eq. (A.24) simplifies drastically in the stellar exterior to

$$W_1^{>\prime\prime}(r) + \frac{4 W_1^{>\prime}(r)}{r} = \frac{1}{r^4} \left(S_2 - S_1 - S_0 \right). \tag{3.201}$$

The homogeneous system of eq. (3.201) has to linearly independent solutions $W_{1,H1}^> = c_{W1H1} r^{-3}$ and $W_{1,H2}^> = c_{W1H2}$ and using them and the variation of parameters method we can construct an asymptotically flat exterior solution

$$\begin{aligned} W_1^>(r) = & -\frac{(y-1)^3}{4M^3}\delta J - \frac{3\mathcal{Q}_{\mathrm{M}} J (y-1)\left(3 - 3y^2 + \left(1 + 4y + y^2\right)\log(y)\right)}{8M^6} - \frac{3\mathcal{Q}_{\mathrm{E}}\mu y(7+5y)\log(y)}{2M^6(y-1)} \\ & + \frac{\mathcal{Q}_{\mathrm{E}}\mu\left(-(y-1)^2\left(11 - 69y - 15y^2 + y^3\right) + 36y(1+y)\log^2(y)\right)}{8M^6(y-1)^2} \\ & + \frac{J\mu^2\left(10133 - 24240y - 3900y^2 + 3400y^3 + 135y^4 + 72y^5\right)}{3200M^7} \\ & - \frac{3J\mu^2\left(54 - 283y - 302y^2 + 32y^3 + 13y^4 + 6y^5\right)\log(y)}{160M^7(y-1)} \\ & + \frac{9J\mu^2\left(1 - 26y - 13y^2 + y^3 - 4y^4 + y^5\right)\log^2(y)}{80M^7(y-1)^2}. \end{aligned} \tag{3.202}$$

The reason for the complicated and lengthy particular solution is the complexity of the expressions for the electro-magnetic field and metric potentials in the stellar exterior. Asymptotically $W_1^>$ decays as

$$W_1^>(r) \overset{r\to\infty}{\to} \frac{2\delta J}{r^3} - \frac{4(J\mathcal{Q}_{\mathrm{M}} + \mu\mathcal{Q}_{\mathrm{E}})}{5r^6} + O\left(\frac{1}{r}\right)^7, \tag{3.203}$$

where we can identify δJ as LO term and a r^{-6} NLO term proportional to the sum of the quadrupole moments multiplied by he angular momentum and dipole moment respectively. The constant δJ can be identified, see eq. (3.248), as the $O\left(B^2\Omega^1\right)$ correction to the angular momentum. In contrast to the situation in the classical $O\left(\Omega^3\right)$ HT formalism δJ is not just a correction associated with a higher-order correction to the moment of inertia. Our δJ has also purely electro-magnetic contributions but since we consider only $O(\Omega) \times O(B)$ electric fields in this section we can define an effective moment of inertia correction δI of pure $O\left(B^2\right)$ as

$$\delta I = \frac{\delta J}{\Omega}. \tag{3.204}$$

For electric fields which can not be considered as $O(\Omega) \times O(B)$ the angular momentum can not be related to such a correction of the moment of inertia. Will discuss this highly interesting situation in Sec. 3.8 for configurations with non-vanishing net charge.

The second-order ODE for W_3 (A.24) can be reformulated into two coupled first-order ODEs

$$U_3' = 2r^2\left(5\mathrm{e}^{\lambda} + r\left(\nu' + \lambda'\right)\right) - S_2 - S_3, \tag{3.205}$$

$$V_3' = \frac{U_3}{r^4} - \frac{1}{2}\left(\nu' + \lambda'\right)V_3, \tag{3.206}$$

using the ansatz of eq. (3.198). Around $r = 0$ this system has a rather simple expansion

$$U_{1,H}(r) \overset{r\to 0}{\to} c_{U3H0}r^5 + O\left(r^6\right), \tag{3.207a}$$

$$V_{1,H}(r) \overset{r\to 0}{\to} \frac{c_{U3H0}}{2}r^2 + O\left(r^3\right), \tag{3.207b}$$

$$U_{1,P}(r) \overset{r\to 0}{\to} c_{U3P0}r^5 + O\left(r^6\right), \tag{3.207c}$$

$$V_{1,P}(r) \overset{r\to 0}{\to} \frac{c_{U3P0}}{2}r^2 + O\left(r^5\right). \tag{3.207d}$$

In the stellar interior electro-magnetic source terms S_3 can be simplified using the induction eq. (3.135) to

$$S_3^{<} = \frac{8}{15}\mathrm{e}^{-\frac{\lambda}{2}-\frac{\nu}{2}}\bar{\omega}\left(4\mathrm{e}^{\lambda}a_\phi^2 - r^2(a_\phi')^2\right). \tag{3.208}$$

Even though the system for W_3 has one less source term compared to the W_1 system constructing an exterior solution for W_3 is more difficult. The homogeneous system has two linearly independent solutions which are on their own more complicated than the simple expressions for $W_{1,H}^{>}$ and the par-

ticular solution resulting from variation of parameters is rather lengthy and involves non-elementary functions:

$$
\begin{aligned}
W_3^{>}(r) = &-\frac{7\left(-6-125y+80y^2+60y^3-10y^4+y^5-60y(1+2y)\log(y)\right)}{64M^5(y-1)^2}W_3^{\infty} \\
&+\frac{\mathcal{Q}_{\mathrm{E}}\mu\left(3+481y+129y^2+18y^3-y^4\right)}{24M^6(y-1)}-\frac{\mathcal{Q}_{\mathrm{E}}\mu y\left(32+58y+15y^2\right)\log(y)}{4M^6(y-1)^2} \\
&+\frac{3\mathcal{Q}_{\mathrm{E}}\mu y(-1+4y)\log^2(y)}{4M^6(y-1)^2}-\frac{\mathcal{Q}_{\mathrm{M}}J\left(-6+3667y+3315y^2-837y^3+161y^4\right)}{192M^6(y-1)} \\
&+\frac{J\mathcal{Q}_{\mathrm{M}}\left(-6+49y+428y^2+72y^3-24y^4+6y^5\right)\log(y)}{16M^6(y-1)^2}-\frac{15J\mathcal{Q}_{\mathrm{M}}y(1+2y)\log^2(y)}{8M^6(y-1)^2} \\
&+\frac{J\mu^2\left(59460+1207739y+847797y^2-125163y^3+17617y^4-2358y^5-432y^6\right)}{19200M^7(y-1)} \\
&-\frac{J\mu^2\left(6+131y+51y^2-9y^3+y^4\right)\pi^2}{40M^7(y-1)}+\frac{3J\mu^2y(1+2y)\log(y)\pi^2}{2M^7(y-1)^2} \\
&+\frac{J\left(-234-7186y-20450y^2-6480y^3+1062y^4-159y^5+36y^6\right)\mu^2\log(y)}{320M^7(y-1)^2} \\
&+\frac{3J\mu^2\left(6+131y+51y^2-9y^3+y^4\right)\log(1-y)\log(y)}{20M^7(y-1)} \\
&-\frac{9J\mu^2\left(2+33y-6y^2-18y^3+2y^4\right)\mu^2\log^2(y)}{160M^7(y-1)^2}-\frac{3Jy(1+2y)\log^3(y)}{8M^7(y-1)^2} \\
&\frac{3J\mu^2\left(-6-125y+80y^2+60y^3-10y^4+y^5+60y(1+2y)\log(y)\right)\mathrm{Li}_2(y)}{20M^7(y-1)^2} \\
&-\frac{18J\mu^2y(1+2y)\mathrm{Li}_3(y)}{M^7(y-1)^2}+\frac{18J\mu^2y(1+2y)\zeta(3)}{M^7(y-1)^2},
\end{aligned}
\tag{3.209}
$$

with an integration constant W_3^{∞}, the dilogarithm $\mathrm{Li}_2(y)$ and the trilogarithm $\mathrm{Li}_3(y)$. We were not able to construct a more compact solution in terms of elementary functions but the solution we found is asymptotically flat by construction and solves the ODE for W_3 in the stellar exterior. The asymptotic of eq. (3.209) is again rather simple

$$
W_3^{>}(r) \overset{r\to\infty}{\to} \frac{W_3^{\infty}}{r^5}+\frac{18\mathcal{Q}_{\mathrm{M}}J+25MW_3^{\infty}-2\mathcal{Q}_{\mathrm{E}}\mu}{10r^6}+O\left(\frac{1}{r}\right)^7. \tag{3.210}
$$

We have four matching conditions (3.23) in $\mathrm{O}\left(B^2\Omega^1\right)$, which we can use to determine δJ, c_{U1H0}, W_3^{∞} and c_{U3H0}. For the particular solutions in the stellar interior we chose w.l.o.g. $c_{U1P0}=B_0^2\Omega^1$ and $c_{U3P0}=B_0^2\Omega^1$.

3.8 Effects of non-zero global net charge on non-rotating equilibrium configurations

While constructing the exterior solution for the monopole electric potential a_{t0} in Sec. 3.5.2 we first encountered the possibility of global net charge as a free input parameter. In this section we will discuss some effects of globally charged configurations. We will introduce global net charge in form of a surface charge density, see eq. (3.163). We will only consider non-rotating configurations with a charge free interior.

Realistic astrophysical objects do not posses significant global net charge, because the long range repulsion of the constituents of such a charge would destabilize the astrophysical object. When describing NS with atmospheres larger local charge differences between interior and atmosphere are possible. When compensated by a pulsar magnetosphere net interior charges of realistic NS can be of the order of 10^{12} C [80] but we are not considering NS with atmospheres. We will only discuss some interesting theoretical aspects of charged configurations within our perturbative approach. This section and the corresponding numerical results of Sec. 5.6 are meant as a qualitative/order of magnitude discussion of effects of global net charge.

Looking at units one can expect that even very large charges have only a minor effect on non-electromagnetic characteristics. An electric field of 1.2×10^{21} V/m has a corresponding energy density

$$E^2 = (1.2 \times 10^{21}\,\mathrm{V/m})^2 \sim 1\,\mathrm{MeV\,fm^{-3}}. \tag{3.211}$$

Even in charged or rotating magnetars 10^{21} V/m are gigantic values for electric fields. A global charge of around 10^{19} C would be necessary to realize 10^{21} V/m fields on the surface of a static 15 km NS. In terms of contributions to the energy-momentum tensor even very high charges and electric fields have only minor effects. Such fields and charges can not be realized in a realistic equilibrium configuration/ astrophysical object.

3.8.1 $O\left(B^1Q^1\right)$: Electromagnetically-induced frame-dragging

When considering non-rotating, configurations with global net charge Q and a non-vanishing magnetic field a very interesting GR effect occurs. The spacetime of such configurations is not static and possess a non-vanishing vorticity: the scalar product of the two killing vector fields χ and ξ is non-vanishing. The reason for that is a non-vanishing electro-magnetic Poynting vector around the source. In the case of a monopole electric and dipolar magnetic field the non-vanishing tetrad component of this Poynting vector in the stellar exterior is

$$S_{\hat{\phi}} = -\frac{Qa'_\phi(r)}{4\pi e^{\lambda(r)} r^3}\Theta(r-R)\sin\theta, \tag{3.212}$$

which is part of the energy-momentum tensor

$$T^{(\mathrm{EM}),>}_{t\phi} = S_{\hat{\phi}}\, r\sin\theta. \tag{3.213}$$

This source term implies the existence of a corresponding curvature term $G_{t\phi}/(8\pi)$ according to Einstein's field equations. It becomes necessary to introduce a $O\left(B^1Q^1\right)$ frame-dragging frequency ω_{BQ}. This FD frequency is purely of the order $O(B)\times O(Q)$ and is therefore known under the name *electromagnetically-induced frame-dragging*.

The line element of the O $\left(B^0Q^0\right)$ background star ds^2 from eq. (3.2) needs to be extended using

$$ds^2_{(BQ)} = g^{(BQ)}_{\mu\nu}dx^\mu dx^\nu \equiv -2r^2\sin^2\theta\,\omega_{BQ}(r)\,dt\,d\phi. \tag{3.214}$$

The $O\left(Q^1B^1\right)$ field eq. is very similar to the FD eq. (3.85):

$$\omega''_{BQ} - \frac{1}{2r}\left(r(\nu'+\lambda')-8\right)\omega'_{BQ} + \frac{2}{r}(\nu'+\lambda')\omega_{BQ} = -\frac{Qa'_\phi}{r^4}\Theta(r-R). \tag{3.215}$$

In the stellar interior both are identical, since the $O\left(Q^1B^1\right)$ source term is only non-vanishing in the stellar exterior. The homogeneous interior system is regular around the coordinate singularity $r=0$:

$$\omega_{BQ}(r) \xrightarrow[r\to 0]{} c_{BQ}\left(1+\frac{8}{5}\pi(P_c+\rho_c)r^2\right) + O\left(r^4\right). \tag{3.216}$$

In the stellar exterior the ODE (3.215) simplifies to

$$\omega_{BQ}^{>\,\prime\prime}(r)-\frac{1}{4r}\omega_{BQ}^{>\,\prime}(r)=-\frac{3Q\mu\left(2M(M-r)+(2M-r)r\log\left(1-\frac{2M}{r}\right)\right)}{M^3(2M-r)r^3}, \tag{3.217}$$

which can be integrated twice to the asymptotically flat expression

$$\omega_{BQ}^{>}(r)=\frac{2J_{BQ}}{r^3}+\frac{Q\mu\left(2M\left(2M^2+3Mr-3r^2\right)+3(2M-r)r^2\log\left(1-\frac{2M}{r}\right)\right)}{4M^4r^3}, \tag{3.218}$$

with the asymptotic

$$\omega_{BQ}^{>}(r)\overset{r\to\infty}{\to}\frac{2J_{BQ}}{r^3}-\frac{Q\mu}{r^4}-\frac{6Q\mu M}{5r^5}+O\left(\frac{1}{r}\right)^6. \tag{3.219}$$

The two $O\left(B^1Q^1\right)$ constants c_{BQ} and J_{BQ} can be determined by imposing the junctions conditions (3.21).

J_{BQ} can be identified as the angular momentum of the configuration, see eq. (3.248). This angular momentum of $O(B)\times O(Q)$ is electromagnetically-induced and not related to rotation of the fluid. Because of the coupling to the magnetic field even small or realistic charges can result in a significant increase of the total angular momentum.

The Komar integral expression

$$J_{BQ}=-\frac{8}{3}\pi\int_0^R \mathrm{e}^{\lambda/2-\nu/2}\left(P+\rho\right)\bar{\omega}_{BQ}r^4dr-\frac{\mu Q\left(R^2\log\left(1-\frac{2M}{R}\right)+2M(M+R)\right)}{4M^3}, \tag{3.220}$$

has an interior contribution similar to the expression for J in eq. (3.246) and an exterior contribution, which we already integrated.

The effect of electro-magnetically induced FD arises quite naturally in GR as consequence of Einstein's field equations when considering sources with elector-magnetic fields with non-zero Poynting vectors and we arguably discussed one of the simplest cases where it can occur. Just as the canonical Lense-Thirring effect, electromagnetically-induced frame-dragging is a purely GR effect with no direct Newtonian analogon. For a more general discussion of this GR effect we refer the interested reader to the work of A. F. Gutiérrez-Ruiz and L. A. Pachón [81] and L. Herrera et al. [82] and references therein.

3.8.2 $O\left(Q^2\right)$: Electric corrections to g_{tt} and g_{rr}

When allowing global net charge and considering corrections up to $O\left(Q^2\right)$ the electro-magnetic energy-momentum in the stellar exterior $T^{(\mathrm{EM}),>}$ has additional $O\left(Q^2\right)$ source terms

$$T_{tt}^{(\mathrm{EM}),>}=\frac{\mathrm{e}^{-\lambda}Q^2}{8\pi r^4}+\frac{\mathrm{e}^{\nu}a_\phi^2}{2\pi r^4}\cos^2\theta+\frac{\mathrm{e}^{-\lambda+\nu}\left(a_\phi'\right)^2}{8\pi r^2}\sin^2\theta, \tag{3.221a}$$

$$T_{rr}^{(\mathrm{EM}),>}=-\frac{\mathrm{e}^{-\nu}Q^2}{8\pi r^4}-\frac{\mathrm{e}^{\lambda}a_\phi^2}{2\pi r^4}\cos^2\theta+\frac{\left(a_\phi'\right)^2}{8\pi r^2}\sin^2\theta. \tag{3.221b}$$

The algebraic simplicity of this additional Q^2 sources allows for simple $O\left(Q^2\right)$ additions to the exterior solutions of n_0 and m_0

$$n_0^{>}(r) = (3.183) + \frac{Q^2}{2r^2 - 4Mr} \tag{3.222}$$

$$m_0^{>}(r) = (3.182) + -\frac{Q^2}{2r}. \tag{3.223}$$

The mass shift is increased by

$$\delta M = \delta M|_{O\left(B^2\right)} + \delta M|_{O\left(Q^2\right)} = \delta M|_{O\left(B^2\right)} + Q^2 \frac{2R-3M}{2R(R-M)} \equiv \delta M|_{O\left(B^2\right)} + \delta M_Q. \tag{3.224}$$

We derived the expression for this mass shift using the junction conditions on the stellar surface and the source term integral expression (3.240b) for the Komar mass shift. In the stellar interior h_0 and m_0 have no Q^2 source terms and the solutions are either the purely $O\left(B^2\right)$ expressions or for vanishing magnetic fields they are trivial solutions. The n_0 metric potential has an additional $O\left(Q^2\right)$ shift c_{n0Q} to satisfy $n_0^{<}(R) - n_0^{<}(R) = 0$:

$$c_{n0Q} = \frac{Q^2 - 2\delta M_Q R}{2R^2 - 4MR}. \tag{3.225}$$

This shift contributes $M c_{n0Q}$ to the Komar mass according to eq. (3.240b) and the electric field additionally contributes Q^2/R which leaves

$$\delta M_Q = \frac{Q^2}{R} + \frac{M\left(Q^2 - 2\delta M_Q R\right)}{2R^2 - 4MR} = Q^2 \frac{2R-3M}{2R(R-M)} = \frac{Q^2}{R}\frac{2-3Z}{2-2Z} \tag{3.226a}$$

$$\sim 5.0 \times 10^{-5} \left(\frac{Q}{1 \times 10^{18}\,\mathrm{C}}\right)^2 \left(\frac{R}{\mathrm{km}}\right)^{-1} \left(\frac{2-3Z}{2-2Z}\right) M_\odot \tag{3.226b}$$

for the electric contribution to the mass shift. δM_Q is equal to the electric contribution Q^2/R lowered by a compactness factor $(2-3Z)/(2-2Z)$ which is 1 for $Z = 0$ and $3/5$ at the Schwarzschild-Buchdahl limit. For a ($R = 15\,\mathrm{km} \mid Z = 0.2$) NS the massive charge of $10^{19}\,\mathrm{C}$ corresponds to an increase in gravitational mass of only $3.2 \times 10^{-4}\,\mathrm{M}_\odot$.

The correct overall mass shift is realized by imposing the modified junction condition for m_0

$$\delta M = m_0^{<}(R) - m_0^{>}(R)|_{\delta M = 0} + 4\pi R^3 \frac{2M-R}{M-R}\rho(R) h_0^{<}(R) + Q^2 \frac{R-2M}{2R(R-M)}. \tag{3.227}$$

Imposing the junction condition (3.227) guaranties self-consistent results for δM.

In the case of vanishing magnetic fields the only non-zero perturbations are m_0 and n_0 and they read

$$m_0^{<}(r) = 0 \tag{3.228}$$

$$m_0^{>}(r) = \delta M_Q - \frac{Q^2}{2r} = Q^2 \frac{2R-3M}{2R(R-M)} - \frac{Q^2}{2r} \tag{3.229}$$

$$n_0^{<}(r) = c_{n0Q} = \frac{Q^2 - 2\delta M_Q R}{2R^2 - 4MR} = \frac{Q^2}{2MR - 2R^2} \tag{3.230}$$

$$n_0^{>}(r) = \frac{2\delta M_Q r}{4Mr - 2r^2} - \frac{Q^2}{4Mr - 2r^2} = \frac{Q^2\left(3Mr - MR - 2rR + R^2\right)}{2rR(2M-r)(M-R)}. \tag{3.231}$$

The corresponding line element in the stellar exterior up to $O\left(Q^2\right)$ reads

$$ds^2_> = -\left(1-\frac{2(M+\delta M_Q)}{r}+\frac{Q^2}{r^2}\right)dtdt+\frac{r(2\delta M_Q-2M+r)-Q^2}{(r-2M)^2}drdr+r^2d\Omega^2+O\left(B^1Q^3\right) \tag{3.232}$$

$$= -\left(1-\frac{2\mathscr{M}}{r}+\frac{Q^2}{r^2}\right)dtdt+\left(1-\frac{2\mathscr{M}}{r}+\frac{Q^2}{r^2}\right)^{-1}drdr+r^2d\Omega^2+O\left(B^1Q^3\right), \tag{3.233}$$

where we introduced the total mass in $O\left(Q^2\right)$ $\mathscr{M}\equiv M+\delta M_Q$, used the fact that δM_Q is $O\left(Q^2\right)$ and that we only consider the metric up to $O\left(B^0Q^2\right)$. In the stellar interior the metric only differs by a constant shift in g_{tt} from the one of the background star:

$$ds^2_< = ds^2_{(00)}+2\mathrm{e}^{\nu}c_{n0Q}dt^2+O\left(B^1Q^3\right). \tag{3.234}$$

Eq. (3.232) is the $O\left(Q^2\right)$ weak field expansion of the *Reissner-Nordström metric* [83, 84] which has the form of (3.233). The Reissner-Nordström metric is a static solution to the Einstein-Maxwell field eqs., which corresponds to the gravitational field of a non-rotating, spherically symmetric body of mass M and charge Q. It is a trivial extension of the exterior Schwarzschild solution and we derived and discussed it in this section as the exterior solution of a NS with non-zero net surface charge.

3.9 Global parameters

In the previous sections of this chapter we extensively discussed the solutions and equations governing metric potentials and electro-magnetic fields of our perturbative magnetar model. In this section we will discuss associated global parameters which we will focus on when comparing numerical results.

3.9.1 Conserved charges

The spacetime manifold we use has two killing vectors ξ (2.33) and χ (2.34) associated with stationarity and axisymmetry. Associated with those two spacetime symmetries/ Killing vectors are two conserved currents, according to eq. (2.21). We will use the standard way to construct associated conserved charges. Integrating a conserved covariant divergence over a spatial slice of constant time Σ_t reveals

$$0=\int_{\Sigma_t}\nabla_\mu J^\mu_{(K)}dx^3=\int_{\Sigma_t}\partial_{x_\mu}\left(\sqrt{-g}J^\mu_{(K)}\right)dx^3 \tag{3.235a}$$

$$=\int_{\Sigma_t}\partial_{x_t}\left(\sqrt{-g}J^t_{(K)}\right)dx^3+\int_{\Sigma_t}\partial_{x_i}\left(\sqrt{-g}J^i_{(K)}\right)dx^3. \tag{3.235b}$$

In eq. (3.235a) we used the standard identity $\Gamma^\mu_{\alpha\mu}=\partial_\alpha\log(\sqrt{-g})$. The second integral of (3.235b) can be rewritten into the flux through the surface $\partial\Sigma_t$ using the Gauss-Ostrogradsky theorem. When considering asymptotically flat spacetimes and $\Sigma_t=\mathbb{R}^3$ this contribution vanishes. Using the fact that we integrate over a slice of constant time we can interchange the integration and the partial derivative and we can integrate over t introducing a conserved charge Q_K as integration constant:

$$Q_K=\int_{\Sigma_t}\sqrt{-g}J^t_{(K)}dx^3. \tag{3.236}$$

Using the identity (3.236) on the conserved current of ξ we get the expression for the Komar mass [85]

$$M_K = \frac{1}{4\pi}\int_{\Sigma_t}\sqrt{-g}J^t_{(\xi)}dx^3 = \frac{1}{4\pi}\int_{\Sigma_t}\sqrt{-g}\xi^\mu R^t{}_\mu dx^3 = 2\int_{\Sigma_t}\sqrt{\gamma}\left(T^\nu{}_\mu - \frac{1}{2}T\delta^\nu{}_\mu\right)n_\nu\xi^\mu dx^3, \quad (3.237)$$

where we used the field eqs. and the relation $\sqrt{-g}R^t{}_\mu = \sqrt{\gamma}n_\nu R^\nu{}_\mu$ to derive the last identity. $T = T^\mu{}_\mu$ is the trace of the energy momentum tensor. Using the expressions for ξ^ν from eq. (2.33), eq. (3.237) simplifies to

$$M_K = 2\int_{\Sigma_t}\sqrt{\gamma}\left(T^t{}_t - \frac{1}{2}T\right)n_t\xi^t dx^3 = 2\int_{\mathbb{R}^3}\sqrt{\gamma}\left(T^t{}_t - \frac{1}{2}T\right)n_t dx^3, \quad (3.238)$$

This general expression needs to be expanded into proper orders of B and Ω in the setting of our perturbative approach:

$$M_K \equiv \mathscr{M} \equiv M + \delta M + O\left(B^3\Omega^2\right), \quad (3.239)$$

with

$$M = 4\pi\int_0^R \left(3P+\rho\right)\mathrm{e}^{\lambda/2+\nu/2}r^2 dr, \quad (3.240a)$$

$$\begin{aligned}\delta M = 4\pi\int_0^R &\left[\left(3P+3\rho+\frac{d\rho}{dh}\right)h_0 + \left(3P+\rho\right)\left(n_0+\frac{\mathrm{e}^\lambda m_0}{r}\right)\right]\mathrm{e}^{\lambda/2+\nu/2}r^2 dr \\ &+ \int_0^\infty \left[\frac{4a_\phi^2}{3r^2}+\frac{2(a_\phi')^2}{3}\right]\mathrm{e}^{\lambda/2+\nu/2}dr,\end{aligned} \quad (3.240b)$$

where M is $O\left(B^0\Omega^0\right)$ and δM is $O\left(B^2\Omega^0\right)$. The second integral of eq. (3.240b) is the contribution of the magnetic field to the mass shift and it is non-vanishing in the stellar exterior. This integral can be split into an interior and exterior integral, where the latter can be performed analytically.

The integral (3.238) can be transformed into a surface integral over $\partial\Sigma_t$, see e.g. [37] for details, which in turn can be transformed into an asymptotic identity for the Komar mass

$$M_K = \frac{1}{2}\lim_{r\to\infty}\int_0^\pi \partial_r\sqrt{-g_{tt}(r,\theta)}r^2\sin\theta d\theta. \quad (3.241)$$

Using the explicit asymptotic of ν and n_0 from eqs. (3.37) and (3.183) we can confirm

$$M_K = \frac{1}{2}\lim_{r\to\infty}\int_0^\pi \frac{\partial\sqrt{-g^>_{tt}(r,\theta)}}{\partial r}r^2\sin\theta d\theta = M + \delta M + O\left(B^3\Omega^2\right). \quad (3.242)$$

This can also be shown using partial integration of eq. (3.240) and the field equations. We will use the source term integrals (3.240) to check self-consistency of our numerical results, by comparing the asymptotic and integrated expressions for M and δM. Eq. (3.240a) is not the canonical expression (3.42) for the gravitational mass of a static, spherical-symmetric NS. The expression for the Komar mass includes relativistic pressure contributions as well as effects of spacetime curvature. Using the field eqs. and the boundary conditions at $r = 0$ and $r = R$ one can show

$$M = M_K|_{O\left(B^0\Omega^0\right)} = 4\pi\int_0^R \left(3P+\rho\right)\mathrm{e}^{\lambda/2+\nu/2}r^2 dr = 4\pi\int_0^R \rho(r)r^2 dr. \quad (3.243)$$

The fact that the total gravitational mass of a static, spherical-symmetric NS can be expressed as a flat space integral over the density alone is a non-trivial consequence of the field eqs. and their boundary conditions. Pressure and curvature contributions only cancel when integrating from $r = 0$ to R. The notion of an inclosed mass is not unique since for $r < R$: $M_K(r) \neq M(r)$.

Using analogous steps on the conserved current associated with χ we can derive a source term integral expression for the Komar angular momentum [85]

$$J_K = -\int_{\Sigma_t} \sqrt{\gamma}\left(T^t{}_\phi\right) n_t \chi^\phi dx^3 = 2\int_{\mathbb{R}^3} \sqrt{\gamma}\left(T^t{}_\phi\right) n_t dx^3, \tag{3.244}$$

which again can be decomposed in terms of proper order in B and Ω

$$J_K \equiv \mathscr{J} \equiv J + \delta J + O\left(B^3\Omega^2\right), \tag{3.245}$$

where J is the $O\left(\Omega^1 B^0\right)$ angular momentum and δJ $O\left(\Omega^1 B^2\right)$ corrections to it. The source term integral for δJ is rather lengthy and involves all lower-order metric potentials and fields. The source term integral for J on the other hand is rather simple

$$J = \frac{8}{3}\pi \int_0^R \mathrm{e}^{\lambda/2-\nu/2}\left(P+\rho\right)\bar{\omega} r^4 dr. \tag{3.246}$$

Analogously to M_K one can also derive an asymptotic definition for J_K, see e.g. [37] for details,

$$J_K = -\frac{1}{8}\lim_{r\to\infty}\int_0^\pi \partial_r\left(-\frac{g_{t\phi}}{g_{tt}}\right) r^4 \sin^3\theta d\theta = -\frac{1}{8}\lim_{r\to\infty}\int_0^\pi \partial_r N^\phi(r,\theta)\, r^4 \sin^3\theta d\theta. \tag{3.247}$$

Using the explicit asymptotic of ω and W_1 from eqs. (3.90) and (3.203) we can confirm

$$J_K = -\frac{1}{6}\lim_{r\to\infty}\left(\omega'_>(r) + W_1^{>\prime}(r)\right) r^4 = J + \delta J + O\left(B^3\Omega^2\right). \tag{3.248}$$

W_3 does not contribute to the angular momentum since its angular dependency integrates to zero. The fact that the exterior solution for W_1 has δJ as free parameter is no coincidence. We constructed the particular solution for $W_1^>$ to guarantee this behavior. In the classical HT formalism this is not done and the exterior solution for W_1 has an integration constant which is only related to δJ. We tried to reduce the constants of our model as much as possible and choosing global parameters as integration constants is a good way to archive this goal.

Apart from the two conserved charges associated with the spacetime symmetries of our configurations we also have internal symmetries and related conservations laws, namely baryon number and electric charge conservation. We already discussed global net-charge in Sec. 3.5.3 and will now introduce an integral expression for the total baryon number.

Integrating the expression for the baryon number conservation (2.13) the same way as discussed for M_K we can derive an expression for the total baryon number $\mathscr{B}$ of a magnetically deformed star

$$\mathscr{B} = \int_{\Sigma_t} n_{\mathrm{B}}\sqrt{-g}u^t dx^3 = \mathscr{B}_0 + \delta\mathscr{B} + O\left(B^3\Omega^2\right), \tag{3.249}$$

with

$$\mathscr{B}_0 = 4\pi\int_0^R \mathrm{e}^{\lambda/2} n_{\mathrm{B}} r^2 dr \tag{3.250a}$$

$$\delta\mathscr{B} = 4\pi\int_0^R \mathrm{e}^{\lambda/2}\left[\frac{dn_{\mathrm{B}}}{dh}h_0 + \frac{\mathrm{e}^\lambda m_0}{r}n_{\mathrm{B}}\right] r^2 dr. \tag{3.250b}$$

Using the total baryon number we can construct the related baryonic mass $\mathscr{M}_{\mathrm{B}}$ and the gravitational binding energy $\mathscr{E}_{\mathrm{B}}$:

$$\mathscr{M}_{\mathrm{B}} \equiv M_{\mathrm{B}} + \delta M_{\mathrm{B}} \equiv m_{\mathrm{B}} \left(\mathscr{B}_0 + \delta \mathscr{B} \right), \tag{3.251}$$

$$\mathscr{E}_{\mathrm{B}} \equiv \mathscr{M}_{\mathrm{B}} - \mathscr{M} = \left(M_{\mathrm{B}} - M \right) + \left(\delta M_{\mathrm{B}} - \delta M \right). \tag{3.252}$$

3.9.2 Iso-surfaces and geometric measures of deformation

The surfaces of constant log-enthalphy $h(r)$ are spheres of radius r in the metric of the unperturbed background star. According to our ansatz (3.14a) these surfaces are deformed in $O\left(B^2\right)$ by $h_0(r)$ and $h_2(r)$. We are now looking for surfaces $\bar{r}\,(r,\theta)$ of constant log-enthalpy in $O\left(B^2\right)$

$$h(\bar{r}\,(r,\theta),\theta) \stackrel{!}{=} h(r) = \text{const.}. \tag{3.253}$$

For that task we make the following ansatz for the iso-surfaces $\bar{r}\,(r,\theta)$

$$\bar{r}\,(r,\theta) \equiv r + \xi\,(r,\theta) \equiv r + \xi_0(r) + \xi_2(r)\mathrm{P}_2(\cos\theta) + O\left(B^4\Omega^2\right). \tag{3.254}$$

Taylor expanding $h(\bar{r}\,(r,\theta))$ up to $O\left(B^4\Omega^2\right)$ results in

$$h\,(r) + \frac{dh}{dr}\Delta\bar{r}\,(r,\theta) + h_0\,(r) + h_2\,(r)\,P_2(\cos\theta) \stackrel{!}{=} h(r) + O\left(B^4\Omega^2\right), \tag{3.255a}$$

$$h_0\,(r) + h_2\,(r)\,P_2(\cos\theta) + O\left(B^4\Omega^2\right) \stackrel{!}{=} -h'\,(r)\,\Delta\bar{r}\,(r,\theta), \tag{3.255b}$$

$$h_0\,(r) + h_2\,(r)\,P_2(\cos\theta) + O\left(B^4\Omega^2\right) \stackrel{!}{=} -h'\,(r)\left(\xi_0\,(r) + \xi_2\,(r)\,P_2(\cos\theta)\right), \tag{3.255c}$$

and we can identify

$$\xi\,(r,\theta) = -\left(h'\,(r)\right)^{-1}\Delta h\,(r,\theta) + O\left(B^4\Omega^2\right). \tag{3.256}$$

The deformations of iso-surfaces of constant log-enthalpy are directly related to the deformations of the log-enthalpy grid. Using the Bernoulli theorem (3.50) in $O\left(B^0\Omega^0\right)$ we recover a classical HT result

$$\Delta h\,(r,\theta) = \frac{1}{2}\nu'\xi\,(r,\theta) = -h'\xi\,(r,\theta), \tag{3.257}$$

where our $\Delta h\,(r,\theta)$ is called $p^*\,(r,\theta)$ in the original HT paper [25]. Identifying $\Delta h\,(r,\theta)$ as deformations of the log-enthalpy grid and not as a convenient choice of a dimensionless pressure perturbation makes this derivation much more intuitive. $\bar{r}\,(r,\theta)$ describes a surface of constant log-enthalpy $h(r)$ in the coordinate system of the $O\left(B^2\Omega^1\right)$. Fig. 3.6 depicts such an iso-surface $\bar{r}\,(r,\theta)$.

$\bar{r}\,(r,\theta)$ describes surfaces in the curved space of the metric $g_{\mu\nu}$ with its non-orthonormal basis vectors, which makes direct interpretation of them rather difficult. It is much more convenient to work with surfaces in a flat space. It is possible to embed the two dimensional surface

$$ds^2_{(2)} = \left(g_{\theta\theta}(\bar{r},\theta) + g_{rr}(\bar{r},\theta)(\partial_\theta\bar{r})^2\right)d\theta^2 + g_{\phi\phi}(\bar{r},\theta)d\phi^2 \tag{3.258}$$

of constant time and radius $r = \bar{r}\,(r,\theta)$ into three dimensional flat space. An embedding can be constructed by imposing conservation of lengths

$$ds^2_{(2)} \stackrel{!}{=} ds^2_{(3)} = d\eta_x^2 + d\eta_y^2 + d\eta_z^2. \tag{3.259}$$

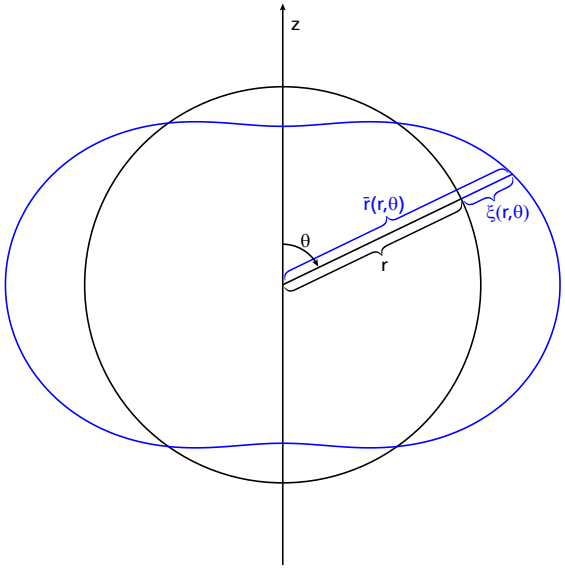

Figure 3.6: Coordinate systems (r,θ) in black and $(\bar{r}(r,\theta),\theta)$ in blue. *This illustration is based on Fig. 1 of [25].*

Such an embedding is not unique but a natural choice is an embedding which preserves axis symmetry. Equating (3.259) in $O\left(B^2\Omega^1\right)$ using cylindrical coordinates $\{\eta_\rho(\theta),\eta_\phi=\phi,\eta_z(\theta)\}$ reveals

$$\frac{\eta_\rho}{\eta_z}=\pm\tan\theta, \tag{3.260}$$

which allows us to choose spherical coordinates $\{\eta_r(\theta),\eta_\theta=\theta,\eta_\phi=\phi\}$ for $ds^2_{(3)}$. The flat space embedding of $\bar{r}(r,\theta)$ is given by

$$\eta_r(r,\theta)=r+\bar{r}_0(r)+\left(rk_2(r)+\bar{r}_2(r)\right)\mathrm{P}_2(\cos\theta)+O\left(B^4\Omega^2\right). \tag{3.261}$$

$\eta_r(r,\theta)$ describes a surface of constant log-enthalpy $h(r)$ in three dimensional flat space. Arguably the most interesting surface is the stellar surface $R^*(\theta)$ with $h(R)=0$:

$$R^*(\theta)\equiv\eta_r(R,\theta)\equiv R+\delta R(\theta)=R+\xi_0(R)+\left(Rk_2(R)+\xi_2(R)\right)\mathrm{P}_2(\cos\theta)+O\left(B^4\Omega^2\right). \tag{3.262}$$

In $O\left(B^0\Omega^0\right)$ we recover $R^*(\theta)=R$, which is expected since we work with the areal radius r, which is chosen to have this property. $\xi_0(R)$, $\xi_2(R)$ and $k_2(R)$ are $O\left(B^2\right)$ deformations of the background star surface.

Using the expression for $R^*(\theta)$ we can derive a variety of geometrical parameters. Polar and equatorial radius are given by

$$R^*_p\equiv R^*(0)=R+\xi_0(R)+\xi_2(R)+Rk_2(R)+O\left(B^4\Omega^2\right)\leq R, \tag{3.263}$$

$$R^*_e\equiv R^*(\pi/2)=R+\xi_0(R)-\frac{1}{2}\left(\xi_2(R)+Rk_2(R)\right)+O\left(B^4\Omega^2\right)\geq R. \tag{3.264}$$

The spheroids we encounter are oblate $R^*_p\leq R^*_e$. The surface area of the deformed spheroid described by $R^*(\theta)$ is given by

$$\mathscr{A}=2\pi\int_0^\theta R^*(\theta)\sqrt{R^*(\theta)^2+\left(\partial_\theta R^*(\theta)\right)^2}\sin^2\theta\,d\theta=4\pi R^2+8\pi R\xi_0(R)+O\left(B^4\Omega^2\right), \tag{3.265}$$

which in $O\left(B^2\Omega^1\right)$ allows us to identify the mean areal radius

$$R_m^* \equiv \sqrt{\frac{\mathscr{A}}{4\pi}} = R + \xi_0(R) + O\left(B^4\Omega^2\right). \tag{3.266}$$

Common measures of geometrical deformation of axisymmetric spheroids are the ellipticity e and the flattening/oblateness ε:

$$e \equiv \sqrt{1 - \left(\frac{R_p^*}{R_e^*}\right)^2} = \sqrt{3\left(k_2(R) - \xi_2(R)/R\right)}, \tag{3.267}$$

$$\varepsilon \equiv 1 - \frac{R_p^*}{R_e^*} = -\frac{3}{2}\left(k_2(R) + \xi_2(R)/R\right). \tag{3.268}$$

e and ε are in the interval $[0,1]$ and we will mainly use the oblateness ε to quantify geometrical deformation. ε has the nice property that it scales as a pure $O\left(B^2\right)$ term.

Using the oblateness we can introduce various thresholds for the magnetic field. In our approach the central magnetic field B_0 or in general the strength of the magnetic field is a free input parameter and all expressions, which we derived in this chapter scale in a well defined way in B_0. The geometry of the spheroid described by $R^*(\theta)$ only makes sense for $R_p^* \geq 0$. When the polar radius is zero the surface of revolution of $R^*(\theta)$ is similar to an elliptic torus with an overall diameter of $2R_e^*$. We will consider the $R_p^* = 0$ configuration as extremal and we will call the magnetic field strength realizing it $B_{\max}$. The geometry of such a configurations deviates significantly from the one of the background star and it should be expected that our perturbative approach fails to describe such configurations accurately.

A much more reasonable limit for the magnetic field can be derived from the definition of the oblateness. Looking at the relative difference between the exact definition of ε as $1 - R_p^*/R_e^*$ and the proper $O\left(B^2\right)$ expansion $-3/2\left(k_2(R) + \xi_2(R)/R\right)$ we can specify and relative error

$$\Delta\varepsilon \equiv \left| 1 - \frac{1 - R_p^*/R_e^*}{-\frac{3}{2}\left(k_2(R) + \xi_2(R)/R\right)} \right| \tag{3.269}$$

related to the geometrical deformation. If the deformation of the spheriod gets too big the $O\left(B^2\right)$ expansion $-3/2\left(k_2(R) + \xi_2(R)/R\right)$ will significantly differ from the definition. We will denote the magnetic field realizing a specific relative error $\Delta\varepsilon$ as $B_{\Delta\varepsilon}$. A priori it is not clear if $\Delta\varepsilon$ is a good measure for general derivations from the exact solution. We will test the viability of $\Delta\varepsilon$ as an intrinsic error estimate by comparing our perturbative results to exact results computed within the BGSM formalism throughout Chap. 5.

$B_{\max}$ and $B_{\Delta\varepsilon}$ depend on the background star only.

3.9.3 Asymptotic form of the external metric

In this chapter we derived analytical exterior solutions for all metric potentials. They are electro-vacuum solution of the Einstein-Maxwell eqs. and as those their analytic structure can be quite complicated. But since we describe an asymptotically flat exterior manifold their $r \to \infty$ asymptotics are rather simple.

The complete $O\left(B^2\Omega^1\right)$ line element has the following asymptotic

$$\begin{aligned} ds^2 = &-\left[1-\frac{2(M+\delta M)}{r}+\frac{2\mathcal{Q}_{\mathrm{M}}}{r^3}\mathrm{P}_2(\cos\theta)+O\left(\frac{1}{r}\right)^4\right]dt^2 \\ &+\left[1+\frac{2(M+\delta M)}{r}+\frac{8M^3+24M^2\delta M}{r^3}-\frac{2\mathcal{Q}_{\mathrm{M}}}{r^3}\mathrm{P}_2(\cos\theta)+O\left(\frac{1}{r}\right)^4\right]dr^2 \\ &+\left[1-\frac{2\mathcal{Q}_{\mathrm{M}}}{r^3}\mathrm{P}_2(\cos\theta)+O\left(\frac{1}{r}\right)^4\right]\left[r^2d\theta^2+r^2\sin^2\theta d\phi^2\right] \\ &-2\left[\frac{2(J+\delta J)}{r^3}+\frac{W_3^\infty}{r^5}\left(1+5\mathrm{P}_2(\cos\theta)\right)+O\left(\frac{1}{r}\right)^6\right]r^2\sin^2\theta dtd\phi. \end{aligned} \tag{3.270}$$

The NLO term in the asymptotic expansion of g_{tt}

$$-g_{tt}=1-\frac{2(M+\delta M)}{r}+\frac{2\mathcal{Q}_{\mathrm{M}}}{r^3}\mathrm{P}_2(\cos\theta)+O\left(\frac{1}{r}\right)^4 \tag{3.271}$$

is directly proportional to the configurations mass quadrupole moment $\mathcal{Q}_{\mathrm{M}}$ [25, 37]. For the deformed oblate spheroids we describe in our perturbative model $\mathcal{Q}_{\mathrm{M}}>0$. Prolate configurations have $\mathcal{Q}_{\mathrm{M}}<0$.

We have constructed the particular solution for $n_2^>$ such as

$$h_2^>(r)\overset{r\to\infty}{\to}\frac{\mathcal{Q}_{\mathrm{M}}}{r^3}+O\left(\frac{1}{r}\right)^4. \tag{3.272}$$

The specific choice of our particular solution relates the homogeneous part directly to the mass quadrupole moment. In the classical HT formalism [25] another particular solution is chosen and the amplitude of the homogeneous part is only related to $\mathcal{Q}_{\mathrm{M}}$ but not $\mathcal{Q}_{\mathrm{M}}$ itself. $\mathcal{Q}_{\mathrm{M}}$ is a very important measure of deformation [18] and we can access it very easily after imposing the junction conditions for n_2 and ν_2 on the stellar surface. Since we have analytical expressions for our exterior solutions in areal radius we are not forced to extract $\mathcal{Q}_{\mathrm{M}}$ from the asymptotic of a numerical solution. In the BGSM formalism the latter is necessary and in the isotropic radius not unproblematic [86].

The mass quadrupole moment can be used to study universality relations [87] and to construct simple gravitational wave emission models [88].

4 Implementation

4.1 Implementation of the BGSM formalism: `magstar` code and LORENE library

In Sec. 2.2 we gave a brief introduction into the BGSM and its central equations. To summarize: in the BGSM formalism the stellar structure is encoded by a set of $4+2$ coupled PDEs (four field equations (2.44a)-(2.44d) and two Maxwell equations (2.46a)-(2.46b)) and one analytic equation of motion (2.51). In this section we will briefly introduce the numerical resolution of those structure equations.

BGSM have developed "*Pseudo-spectral methods*" [89–91] to numerically solve the elliptic PDEs. Their methods are based on expanding the solutions on a set of basis functions. These functions are chosen with great care with regard to the symmetries and asymptotics of the problem as well as their numerical implementability. Using those basis functions on two two-dimensional adaptive grids the PDEs reduce to algebraic equations for expansion coefficients. It is necessary to use at least two $\left(\tilde{r}_i, \theta_i\right)$-grids: one for the stellar interior ($0 \leq \tilde{r}_i < \tilde{R}$) and one for the exterior ($\tilde{R} < \tilde{r} < \infty$), since there are no analytical exterior solutions, in the general case, and only asymptotic boundary conditions are know. The exterior grid is compactified for numerical implementability using $u \equiv 1/\tilde{r}$: $(\tilde{R} < \tilde{r}_i < \infty) \rightarrow (u_0 = 1/\tilde{R} > u_i > 0)$. Because of the complicated nature of the coupled, non-linear and inhomogeneous PDE system an iterative procedure is necessary to ultimately solve the structure equations.

This iterative procedure is called *self-consisten-field method* [39] and it works as follows:

1. Initial conditions for the integration have to be specified and they include: an EoS, a current function $f(x)$, an angular velocity Ω, a total charge Q and a central log-enthalpy h_c.
2. For the first step of the iteration very crude values for the metric potentials are chosen $N = A = B = 1$, $N^\phi = 0$ and $A^t = A^\phi = 0$. The initial enthalpy grid is modeled by a simple profile as $h(\tilde{r}) = h_c\left(1 - \tilde{r}^2/\tilde{R}^2\right)$ with an assumed stellar radius of $\tilde{R} = 10\,\mathrm{km}$.
3. From the enthalpy grid Γ, P, ρ and all the other source terms are computed.
4. Using the Pseudo-spectral methods the field and Maxwell equations are solved, using the current values of N, A, B, N^ϕ, A^t and A^ϕ on the right hand side of the elliptic PDEs, to obtain new values for N, A, B, N^ϕ, A^t and A^ϕ.
5. With those new values a new Lorentz factor Γ and a new electromagnetic Lorentz force term M are computed and the first integral of fluid motion (2.51)

$$h = h_c + \log N_c - \log N + \log \Gamma - M \tag{4.1}$$

   is used to compute new a enthalpy field and a new radial grid. Using adaptive grid methods the stellar radius is adjusted in each step by the condition $h(\tilde{R}) = 0$. Go to step 3.

This is only a sketch of the actual algorithm: there are a lot of complicated details involved in the actual code. Electromagnetic source terms and rotation are progressively increased. The iteration is stopped when the changes in log-enthalpy grid in step 5 of the sketch above are below a threshold value. A typical value for such a threshold is 10^{-12}.

For details involving the implementation of the Maxwell equations we refer to [19] and for general aspects we refer to the BGSM original paper [18] and references therein.

For completeness we should mention, that the formalism and methods developed by BGSM and BBGN for axisymmetric, static compact stars are used, improved and extended by various authors. To mention only two examples: D. Chatterjee et al. [15] extended the BGSM formalism to include the magnet field dependent EoS, magnetisation and anisotropies in the energy-momentum tensor in a self-consistent way. C. Y. Cardall et al. [20] studied configurations with very strong magnetic fields and deformations, numerical stability and EoS effects in the BGSM formalism. They developed their own method to solve the involved PDEs using Green's functions.

The LORENE , abbreviation for **L**angage **O**bjet pour la **RE**lativité **N**umériqu**E**, library [92] provides various C++ classes to numerically solve problems arising in NR and computational astrophysics. In the scope of this work the methods implemented in LORENE to solve the Einstein-Maxwell equations in the BGSM formalism are of primary interest. We use a slightly modified version of LORENE's MAGSTAR code to solve the Einstein-Maxwell equations for magnetized, rotating, stationary and axisymmetric stars numerically exact.

In the scope of the current work we will limit our discussions to slowly rotating stars with dipolar magnetic fields modeled by a current function $f(x) = \text{const.}$ and for most part zero net charge $Q = 0$.

We have only made minor modifications to the original[(2)] MAGSTAR code and the LORENE library-itself. The only significant modifications were changing the values for the fundamental constants in `unites.h`[(3)] to the recent recommended values of CODATA [26] and modifying and in case of TVII adding LORENE EoS classes. This was necessary in order to eliminate discrepancies between our numerical results and the ones obtained from LORENE arising from a difference in the value for the gravitational constant[(4)] and from slight differences in the implementation of the EoS. Apart from that we only added and modified some methods to output data and computational parameters. These latter modification however have no impact on the numerical results computed with the MAGSTAR code.

4.2 Perturbative Magnetar model

In Chap. 3 we derived a set of structure equations encoding the hydrostatic equilibrium of a deformed compact star up to $O\left(B^2\Omega^1\right)$. In this section we will very briefly describe how we implemented and solve these structure equations.

The free input parameters of the O $\left(B^2\Omega^1\right)$ magnetar model introduced in Chap. 3 are EoS, central log-enthalpy h_c, central magnetic field strength B_0 and angular velocity Ω. There are no other free input parameters in our model with the current assumptions.

In $O\left(B^0\Omega^0\right)$ we have derived the TOV eqs. (3.53) in h. For the background star we only need to solve the coupled first-order system $\{dr^2(h)/dh, dz(h)/dh\}$ for a specific EoS. For the first explicit step during numerical integration we use the NLO(h^2) expansion (3.54). By comparing the differences between NLO(h^2) and LO(h) for the first step we chose an initial step size in h which guarantees double precision in the first step. The O $\left(h^2\right)$ expansion is very potent and initial steps in h corresponding to radii of $\sim 10^{-7}$ km are possible without making a measurable error. For an integration in r much smaller steps are necessary to archive compatible precision.

We compare the numerical performance of different implementation of the TOV eqs. in Tab. 4.1. In terms of accuracy the systems in h work slightly better then the system in P. The TOV eqs. in their canonical from as ODE in r performs not very well compared to the systems in P and h. The plain system in h without introducing z and r^2 as variables needs the most steps. We have only taken

(2) v1.14 2014/10/13 08:53:57 J. Novak

(3) v1.8 2015/03/17 14:20:00 J. Novak

(4) The current 2014 CODATA value for G is about 0.04% bigger then the one from 1998, which was set in `unites.h`.

TOV system	steps(steps/tries)	r_1 [km]	$\lvert 1-M/M_{\rm ISS}\rvert$	$\lvert 1-R/R_{\rm ISS}\rvert$
$\{dr^2(h)/dh, dz(h)/dh\}$	59 (1.00)	1.20×10^{-6} km	1.42×10^{-14}	1.42×10^{-14}
$\{dr(h)/dh, dm(h)/dh\}$	446 (1.00)	1.20×10^{-6} km	1.45×10^{-14}	1.45×10^{-14}
$\{dr^2(P)/dP, dz(P)/dP\}$	41 (1.00)	5.18×10^{-18} km	1.13×10^{-13}	1.13×10^{-13}
$\{dP(r)/dr, dm(r)/dr\}$	298 (0.78)	1.00×10^{-20} km	3.76×10^{-11}	3.76×10^{-11}

Table 4.1: Performance comparison between different forms of the TOV eqs. We used our standard `gsl_odeiv2_step_rk8pd` integrator with adaptive step size control but without limiting the maximal step size to integrate the $Z = 0.15$ IRF(189) configuration. Used initial step size r_1, needed steps, steps over tries ratio and the discrepancies between numerically obtained and analytical ISS radii and masses are displayed.

rudimentary measures to solve the problems with the systems in P and r. We integrate the system in P from P_c to a very small residual pressure but make no attempts to make the last remaining step to $P = 0$. For the system in r and the IRF EoS the integrator overshoots the stellar surface and steps resulting in negative pressures occur. If such a step happens we discard it and try a new step with a significantly decreased step size. We continue this process until the relative changes in radius are below 1×10^{-16} km. With a bit more care especially the system in r might perform better. For the system (3.53) no modifications are necessary.

The two O $\left(B^0\Omega^0\right)$ metric potentials are algebraically related to z and h by eq. (3.55). After integrating the TOV eqs. in h we invert the numerical solution $r^2(h)$ to $h(r)$ and use this relation to provide the background quantities in terms of the radius. When limiting the maximal step size one can archive even better accuracies. The implementation we used to obtain the results of the next chapters integrate the TVII and IRF EoS with accuracies of around 1×10^{-15}.

In O $\left(\Omega^1\right)$ we have one second-order ODE system for the FD-frequency and in $O\left(B^1\right)$ we have the linear relativistic GS eq. (3.104) which describes the magnetic field in the stellar interior (one second-order inhomogeneous ODE). The induced electric field in O $\left(B^1\Omega^1\right)$ is analytically related to the magnetic field.

In O $\left(B^2\right)$ we have two separate ODE systems for mono- and quadrupole perturbations. To impose the $l = 2$ boundary condition without solving a boundary value problem we integrate the homogeneous and particular systems separately. In O $\left(B^2\Omega^1\right)$ we have two additional systems of two coupled ODEs for which we again solve the homogeneous and particular systems separately to impose the junction conditions for W_1 and W_3

To solve those ODE systems in the stellar interior we use the *Explicit embedded Runge-Kutta Prince-Dormand* $(8,9)$ *method* (`gsl_odeiv2_step_rk8pd`) of the *GNU Scientific Library* [93] with the `gsl_odeiv2_control_scaled_new` method for adaptive step size control. Since most of our structure equations are singular at $r = 0$, because of the coordinate singularity at that point, we perform the first step of numerical integration explicitly using the series expansions of the ODE systems and functions derived in Chap. 3. We chose a small initial steps size of 10^{-15} km and we limited the maximal step size to 1×10^{-3} R. In principle the `rk8pd` integrator would work with much bigger steps in intermediate radial regions but since we need the gradients of all our functions ($P(r)$, $M(r)$,...) for the integrations of the higher-order systems we limited the maximal step size to reduce errors due to interpolation.

The only real boundary value problem we have to solve is the one for a_ϕ. For that purpose we implemented a *Shooting method* [94] using our standard `rk8pd` integrator together with the `gsl_root_fsolver_brent` rootfinder. We use the same rootfinder to compute configurations with

certain global parameters like stars with specific masses or compactnesses.

To check the numerical self-consistency of our model we use the source term integral expressions for M, J, $Q_<$ and δM from Sec. 3.9 and eq. (3.160). Comparing results from those integrals to the values fixed by the matching conditions provides us with intrinsic error estimates in different orders.

$$O\left(B^0\Omega^0\right) : \Delta M \equiv |1 - M_{(3.240a)}/M| \tag{4.2a}$$
$$O\left(B^0\Omega^1\right) : \Delta J \equiv |1 - J_{(3.246)}/J| \tag{4.2b}$$
$$O\left(B^1\Omega^1\right) : \Delta Q \equiv |1 + Q_</Q_S| \tag{4.2c}$$
$$O\left(B^2\Omega^0\right) : \Delta\delta M \equiv |1 - \delta M_{(3.240b)}/\delta M| \tag{4.2d}$$

Those error estimates are typically around $\sim 10^{-6}$ for interpolated EoS and better then $\sim 10^{-10}$ for analytical EoS. The intrinsic error estimators of the `magstar` code GRV2 and GRV3 have similar magnitudes.

In total we have to solve only 18 ODEs as initial value problems where only pairs of two are coupled and the second-order system for a_ϕ as boundary value problem to have access to the entire structure of the deformed NS in O $\left(B^2\Omega^1\right)$. This is computationally extremely inexpensive when compared to the self-consistent iteration method of the `magstar` code. Depending on EoS and compactness computing a full solution for an equilibrium configuration takes between 0.5 and 2 seconds on a personal computer. A similar computation with the `magstar` code takes at least two orders of magnitude longer. For higher fields the iteration method of `magstar` needs a lot of steps to arrive at a self-consistent result where in our approach rotation frequency and magnetic field strengths are just scales and have no effect on runtime.

Once $h(r)$, $z(r)$, $a_\phi(r)$, $\omega(r)$, $m_0(r)$, $h_0(r)$, $n_2(r)$, $v_2(r)$, W_1 and W_3 are obtained by numerical integration and all the corresponding constants are fixed, the stellar structure of the deformed compact star is completely known up to $O\left(B^2\Omega^1\right)$. All other quantities can be obtained from analytical relations or by integration over the source terms and metric potentials.

5 Numerical Results

In this chapter we present the numerical results obtained from the implementation of our perturbative approach. We will discuss the structure of NS within this formalism up to $O\left(B^2\Omega^1\right)$ and we will present some results for charged, non-rotating NS up to $O\left(B^2Q^2\right)$.

We will compare our results obtained from the perturbative approach to results from the BGSM/BBGN formalism, computed with LORENE's `magstar` code.

5.1 $O\left(B^0\Omega^0\right)$: Spherical symmetric background stars

In this section we discuss numerical results for non-rotating configurations with no electro-magnetic fields. These are computations for $O\left(B^0\Omega^0\right)$ spherical symmetric background stars as discussed theoretically in the previous Sec. 3.2.

We will only present specific results related to the following discussion of magnetically deformed, slowly rotating stars. Studies of neutron star structure within the framework of the TOV equations have been done by many authors in the past decades. The references [1, 9, 60, 95] and [96, 97] are just a small sample of the many textbooks and papers on the topic.

5.1.1 Mass-radius curves and global parameters

To solve the TOV eqs. (3.53) in h it is necessary to supply an EoS relating pressure and energy density to the log-enthalpy h. To compute baryonic masses and binding energies it is further necessary to provide the relation between baryon number density to the log-enthalpy. In this work we discuss results for three realistic EoS, for a polytropic EoS and for two types of analytic EoS related to the ISS and TVII interior solutions.

We have chosen three realistic, tabulated, hadronic EoS: DD2 [98, 99], SFHo [100, 101] and FSG [102, 103]. We discuss the interpolation method we use as well as some details on those EoS in appendix B.4. We have chosen DD2 as an example for a stiff EoS: it generates a high pressure at a given energy density and has a high maximum mass. SFHo has a medium stiffness and a maximum mass of $2.06M_\odot$. SFHo is compatible with the latest NS mass-radius constraints [101]. FSG is an example for a rather soft EoS with a low maximum mass of $1.74M_\odot$, not compatible with $2M_\odot$ NS. We have included FSG anyway to discuss effects of such soft EoS on NS structure and fields.

We have chosen a polytrope with relativistic polytropic index $\gamma = 2$ and a dimensionless pressure coefficient $\kappa = 0.05$. Details and definitions for this type of analytic EoS can be found in appendix B.3. This choice of parameters allows NS with masses beyond $2M_\odot$. Radii of NS with this polytropic are rather large because Poly(0.05|2)has no realistic low pressure behavior to mimic a crust.

For most discussions we will use IRF(189) and $\text{TVII}_1(473)$. We have chosen the constant energy density of $189.377\,\text{MeV}\,\text{fm}^{-3}$ for the IRF EoS to realize NS with typical masses and radii and to have an IRF configuration with the same mass and radius as the SFHo configuration at a compactness of $Z = 0.15$. We have chosen the $\text{TVII}_1(473)$ EoS with $\mu = 1$ and $\rho_c = 473.444\,\text{MeV}\,\text{fm}^{-3}$ for the same reason. By construction both IRF(189) and $\text{TVII}_1(473)$ have identical Mass-radius curves for $M < M_{\text{max}}^{\text{TVII}}$. Choosing these two EoS to describe ISS and TVII configurations allows us to discuss ISS and TVII configurations of varying compactness and for $Z = 0.15$ we have three configurations of identical mass and radius, which only differ in EoS. This allows us to discuss the effect of different EoS on the NS structure without having to account for different masses and radii.

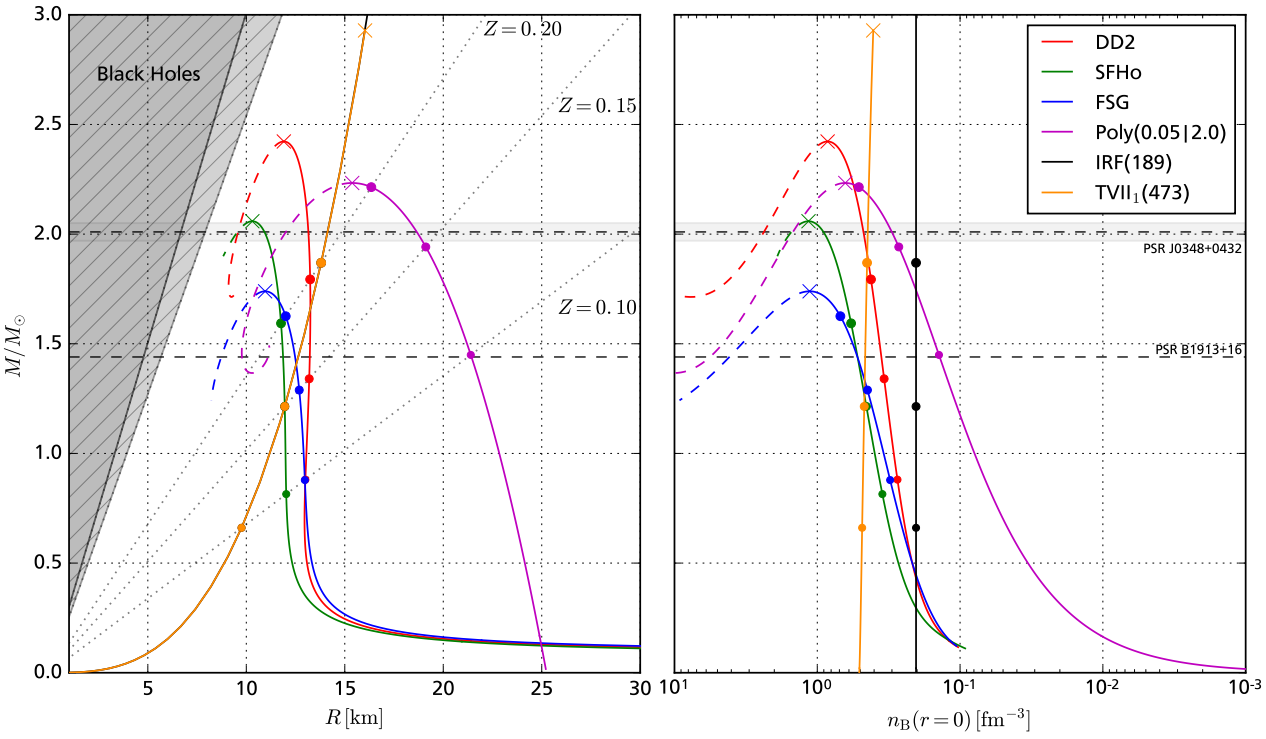

Figure 5.1: Mass over radius (left) and mass over central baryon density (right) for six different EoS. The crosses mark the configurations with maximum mass and the dots mark configurations with specific compactnesses. The dashed lines represent unstable configurations. The masses of PSR B1913+16(Hulse-Taylor-Pulsar) and PSR J0348+0432 are included for reference. The shaded areas depict the Schwarzschild-Buchdahl-limit and Bondi's causality limit, see Sec. 3.2.4 for details on both.

The mass-radius and mass over central baryon density curves of all six EoS are displayed in Fig. 5.1. Those particular plots focus on the NS region of the M-R plane. In Fig. B.3 we depict the full M-R range possible with the tabulated EoS. All EoS we have chosen have stable equilibrium configurations with compactnesses between 0.1 and 0.2. In the following we will frequently discuss results in this compactness range. A necessary condition for stability is $\partial M/\partial n_\mathrm{B} \geq 0$ [1] and NS with $\partial M/\partial n_\mathrm{B} = 0$ represent stable equilibrium configurations of maximum mass. By construction the M-R curves of IRF(189) and TVII$_1$(473) are identical below the maximum mass of TVII$_1$(473) . We consider only causal TVII configuration and have therefore chosen $Z_\mathrm{max}^{\mathrm{TVII}_1} = 0.386$, see eq. (3.83a), as maximal compactness on the TVII branch. As maximum mass for IRF(189) we have chosen its $P_c = \rho_c$ limit of $Z_\mathrm{C} = \frac{3}{8}$ but the corresponding mass of $4.80 M_\odot$ lies outside the plot range of Fig. 5.1. Only FSG is not able to produce NS with masses above $2M_\odot$.

Fig. 5.2 shows some selected central thermodynamic quantities related to the configurations of Fig. 5.1. The stiffness hierarchy between the tabulated EoS is clearly visible: FSG generates low pressures and has low central sound speeds, DD2 generates high pressures and has a high central speed of sound and SFHo lies between those two. Poly(0.05|2)has a medium stiffness between FSG and SFHo. In terms of central sound speeds TVII$_1$(473) is rather soft at low pressures, has a medium stiffness at intermediate pressures and becomes very stiff and causal for high pressures. IRF(189) has an infinite speed of sound as discussed in Sec. 3.2.4 but apart form that all EoS have causal, stable configurations. DD2, FSG and Poly(0.05|2)are causal for all pressures. DD2 and Poly(0.05|2)asymptotically approach the causal limit $c_s = c$, see Fig. B.4. Sound speeds of SFHo become superluminal for pressures beyond $\sim 1400\,\mathrm{MeV\,fm^{-3}}$ but for those pressures configurations are already unstable.

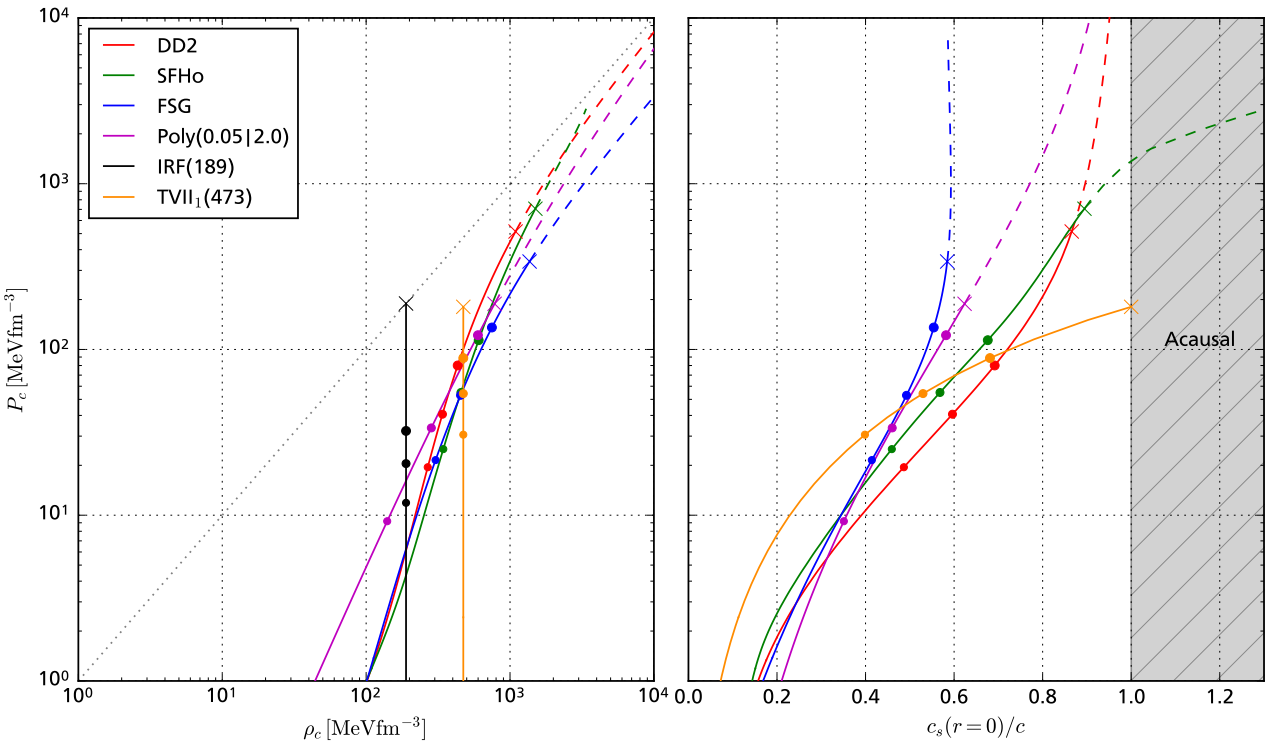

Figure 5.2: Central pressure over central energy density (left) and central pressure of centeral speed of sound (right) for the six different EoS and configurations of Fig. 5.1.

Tab. 5.1 lists global parameters and central thermodynamic quantities for special stable equilibrium configurations of Fig. 5.1. Together with the gravitational mass we give an estimate for intrinsic numerical errors ΔM, see eq. (4.2). The idea for our definition of ΔM is similar to the one behind the more sophisticated GR virial identities GRV3 and GRV2 used by the `magstar` code to measure intrinsic numerical errors. For the analytical Poly, IRF and TVII EoS the numerical errors are with an order of 10^{-14} extremely low. For the tabulated/interpolated EoS this error is significantly higher and typically of the order 10^{-6}.

By construction the $Z = 0.15$ configurations of SFHo, IRF(189) and TVII$_1$(473) have identical masses of $1.214 M_\odot$ and identical radii of 11.952 km. Comparing the remaining parameters of the $Z = 0.15$ star between the three EoS reveals that for IRF(189) the related thermodynamic quantities, the baryonic mass and binding energy differ significantly from the SFHo parameters. Baryonic mass and binding energy are off by $\sim 20\%$ and central density, pressure and baryon number density are only half of the SFHo values. As expected a constant density EoS is not very potent when it comes to modeling realistic NS. The situation is completely different for TVII$_1$(473) . The relative differences for all parameters lie below 7% for the TVII$_1$(473) and SFHo $Z = 0.15$ configuration.

In Fig. 5.3 we compare our results with results obtained with the `magstar` code. The results are in very good agreement for the analytical EoS with relative errors around $\sim 10^{-12}$. For the tabulated hadronic EoS the errors are around $\sim 10^{-6}$. The intrinsic error estimates of the `magstar` code GRV2 and GRV3 also predict errors of this magnitude. Interpolation errors prevent a higher accuracy. For tabulated EoS our intrinsic error estimates using ΔM are similar but for the analytic EoS we can archive slightly higher accuracies. For the following discussions these small differences in the background star parameters will be negligible.

EoS	h_c	$P_c\,[\mathrm{MeV\,fm^{-3}}]$	$\rho_c\,[\mathrm{MeV\,fm^{-3}}]$	$n_{\mathrm{B},c}\,[\mathrm{fm^{-3}}]$	$c_{s,c}/c$	Z	$M\,[M_\odot]\,(\Delta M)$	$R\,[\mathrm{km}]$	$M_\mathrm{B}\,[M_\odot]$	$E_B\,[M_\odot]$
DD2	0.118	19.475	267.968	0.274	0.487	0.100	$0.880\ (4.9\times10^{-6})$	13.000	0.928	0.047
SFHo	0.124	25.042	343.715	0.350	0.459	0.100	$0.815\ (1.6\times10^{-6})$	12.027	0.857	0.043
FSG	0.124	21.502	303.751	0.309	0.414	0.100	$0.879\ (1.1\times10^{-5})$	12.973	0.925	0.046
Poly(0.05|2)	0.132	9.197	140.072	0.141	0.351	0.100	$1.449\ (5.8\times10^{-14})$	21.398	1.525	0.075
IRF(189)	0.061	11.877	189.377	0.203	∞	0.100	$0.661\ (4.0\times10^{-14})$	9.758	0.705	0.045
TVII_1(473)	0.110	30.608	473.444	0.485	0.399	0.100	$0.661\ (1.8\times10^{-14})$	9.758	0.698	0.037
DD2	0.182	40.670	339.124	0.340	0.596	0.150	$1.340\ (3.9\times10^{-6})$	13.194	1.460	0.119
SFHo	0.192	55.001	455.824	0.453	0.568	0.150	$1.214\ (1.2\times10^{-6})$	11.952	1.319	0.105
FSG	0.200	52.890	453.128	0.445	0.493	0.150	$1.289\ (8.3\times10^{-6})$	12.688	1.399	0.110
Poly(0.05|2)	0.238	33.625	283.871	0.269	0.460	0.150	$1.942\ (5.5\times10^{-14})$	19.112	2.092	0.151
IRF(189)	0.103	20.486	189.377	0.203	∞	0.150	$1.214\ (1.2\times10^{-14})$	11.952	1.345	0.131
TVII_1(473)	0.189	54.170	473.444	0.469	0.530	0.150	$1.214\ (8.4\times10^{-15})$	11.952	1.321	0.107
DD2	0.270	80.054	432.764	0.421	0.692	0.200	$1.794\ (3.1\times10^{-6})$	13.242	2.022	0.229
SFHo	0.288	113.741	605.559	0.580	0.676	0.200	$1.593\ (9.1\times10^{-7})$	11.763	1.790	0.197
FSG	0.321	135.676	748.393	0.689	0.554	0.200	$1.626\ (6.1\times10^{-6})$	12.002	1.816	0.191
Poly(0.05|2)	0.413	121.882	598.317	0.512	0.582	0.200	$2.214\ (6.9\times10^{-14})$	16.347	2.429	0.214
IRF(189)	0.157	32.246	189.377	0.203	∞	0.200	$1.869\ (2.9\times10^{-14})$	13.801	2.159	0.290
TVII_1(473)	0.298	88.753	473.444	0.448	0.681	0.200	$1.869\ (6.9\times10^{-14})$	13.801	2.096	0.227
DD2	0.714	514.876	1092.647	0.846	0.866	0.300	$2.422\ (1.8\times10^{-6})$	11.906	2.899	0.477
SFHo	0.722	706.559	1500.325	1.152	0.894	0.295	$2.059\ (5.0\times10^{-7})$	10.306	2.435	0.376
FSG	0.483	339.297	1367.360	1.131	0.585	0.234	$1.739\ (4.6\times10^{-6})$	10.955	1.967	0.227
Poly(0.05|2)	0.493	188.619	781.308	0.636	0.624	0.214	$2.233\ (8.6\times10^{-14})$	15.377	2.453	0.220
IRF(189)	0.693	189.377	189.377	0.203	∞	0.375	$4.799\ (4.2\times10^{-14})$	18.897	6.807	2.008
TVII_1(473)	0.550	180.817	473.444	0.406	1.000	0.270	$2.929\ (5.4\times10^{-14})$	16.029	3.421	0.492

Table 5.1: Global parameters and central thermodynamic quantities for special stable equilibrium configurations of Fig. 5.1. For all six EoS we list three configurations with specific compactness $Z = 0.1, 0.15, 0.2$ and the configuration of maximum mass each.

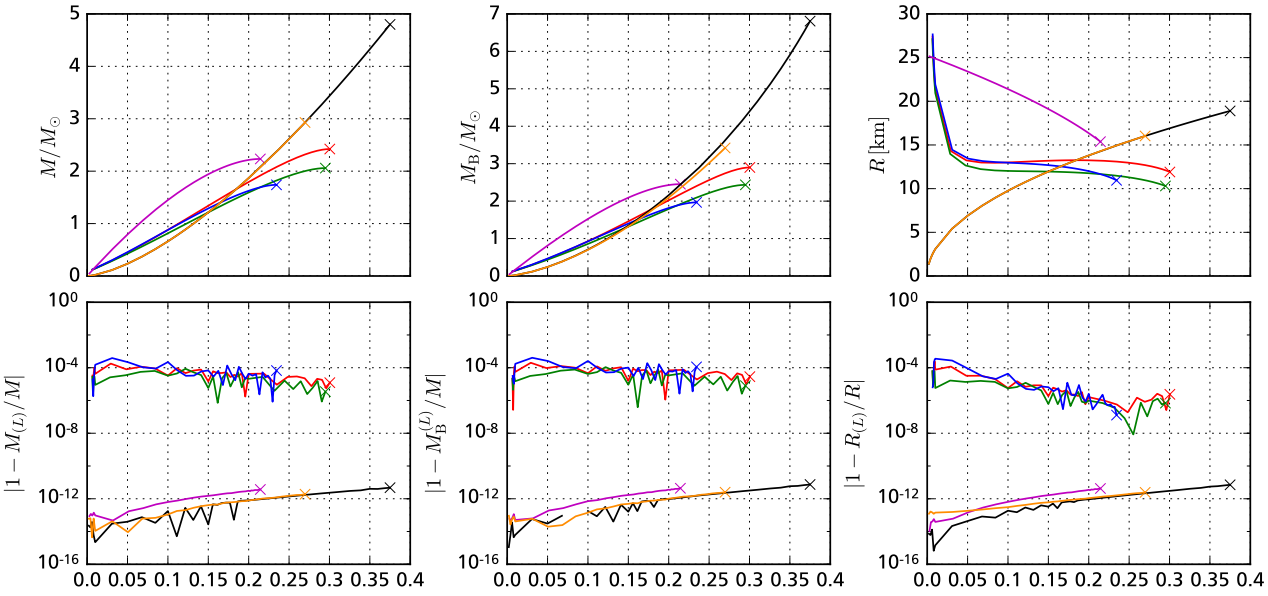

Figure 5.3: Comparison between global parameters obtained form integrating the TOV eqs. and results from the `magstar` code. We display results and errors for gravitational masses (left), baryonic masses (center) and radii (right).

5.1.2 Metric potentials and thermodynamic quantities

In Fig. 5.4 and Fig. 5.5 we display the metric potentials and thermodynamic quantities inside the $Z = 0.15$ configuration. The expected discontinuity of λ' at the stellar surface for IRF EoS is clearly visible. The density gradients of the hadronic EoS decay approximately quadratic in the stellar core. This general property of hadronic EoS is the main reason for the viability of TVII solutions as effective analytical models for realistic hadronic NS. ν and its derivative is continuous across the surface for all configurations and EoS.

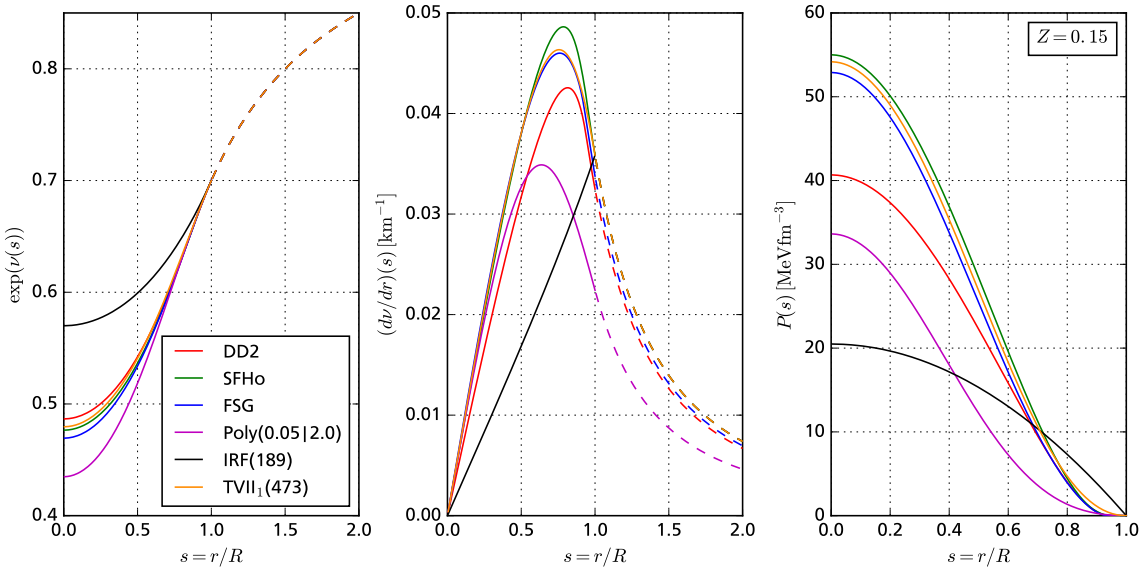

Figure 5.4: Metric potential ν (left),its derivative (center) and pressure (right) as functions of the dimensionless radius for all $Z = 0.15$ configurations. Dashed lines mark the analytic exterior solutions.

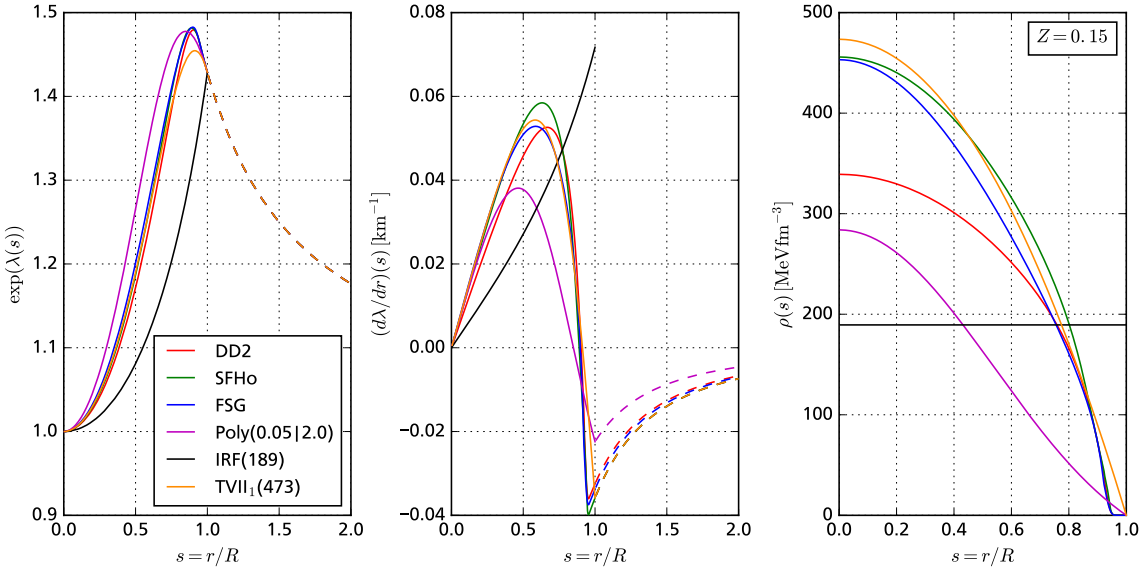

Figure 5.5: Metric potential λ (left), its derivative (center) and energy density (right) as functions of the dimensionless radius for all $Z = 0.15$ configurations. Dashed lines mark the analytic exterior solutions.

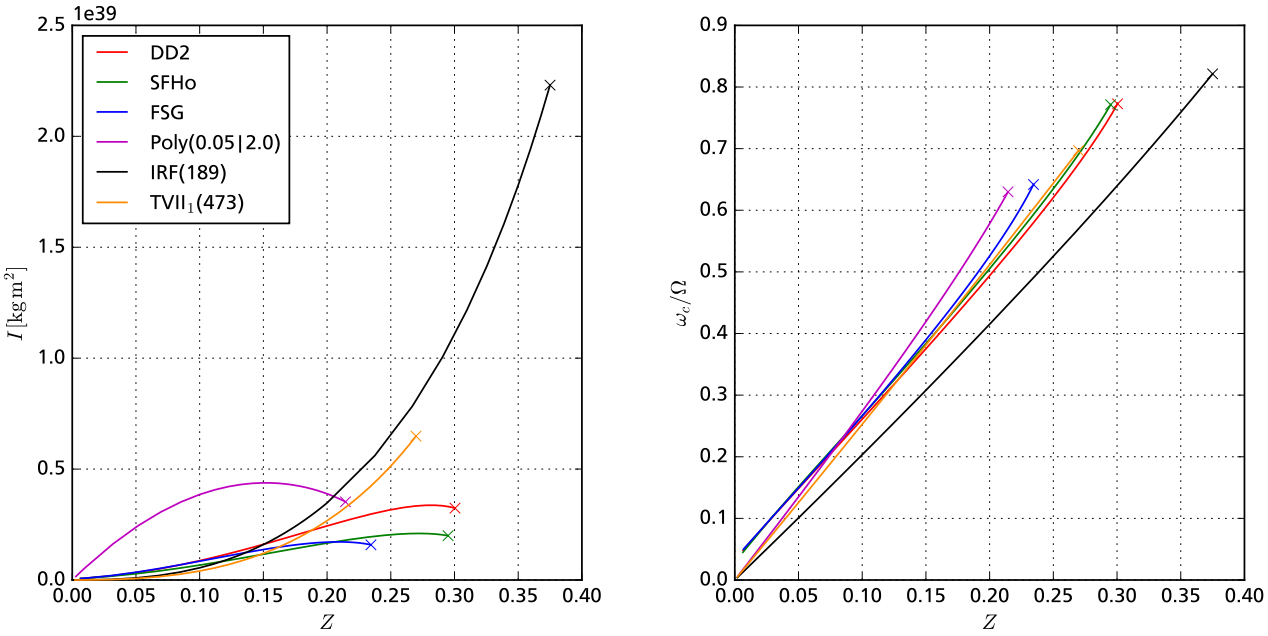

Figure 5.6: Moments of inertia (left) and central values for ω for different stable equilibrium configurations.

5.2 $O\left(B^0\Omega^1\right)$: Slowly rotating configurations

In this section we will discuss numerical solutions of the frame-dragging eq. 3.85. Fig. 5.7 displays solutions for $\omega(s)$ for all $Z = 0.15$ configurations. For the hadronic EoS as well as TVII$_1$(473) the solutions for $\omega(s)$ are very similar. The unique density gradient of IRF(189) is the reason for the distinct results for ω. The frame-dragging frequency is maximal at the stellar center and monotonically decreases towards 0. Outside the star this decrease is cubic and proportional to the moment of inertia as encoded in eq. (3.91). For configurations with zero residual surface density, here all except IRF(189) , the FD frequency and its first two derivatives are continuous across the stellar surface. For NS with IRF EoS only ω and ω' are on R by construction but ω'' changes signs at R.

In Fig. 5.6 we show moments of inertia as well as central values for ω for configurations with varying compactness and EoS. With increasing compactness the FD frequency increases. As a purely GR effect this behavior is to be expected. For TVII and IRF stars the moment of inertia monotonically increases with compactness. For Poly(0.05|2)the moment of inertia reaches a maximum around $Z \sim 0.15$ and then decreases for higher compactnesses. The moment of inertia for configurations with hadronic EoS also decreases after a certain compactness but for DD2, SFHo and FSG the maximal value for the moment of inertia is reached very close to the respective maximal compactness. The moments of inertia are of the order of $10^{38}\,\mathrm{kg\,m^2}$ for typical NS compactnesses.

For the moment of inertia it is quite common to display the dimensionless ratio $I/(MR^2)$ over Z and we do so in Fig. 5.8. This ratio is very similar for hadronic EoS in general, see e.g. [96]. In the typical NS regime $Z \sim 0.1 - 0.2$ the ratios $I/(MR^2)$ of TVII$_1$(473) and of the hadronic EoS are very similar. We will derive analytic series solutions for TVII and IRF EoS for the FD eq. in Chap. 6.

In Tab. 5.2 we present the important global parameters for some selected with $f = 0.01\,\mathrm{Hz}$ slowly rotating configurations. We use the relative difference between the asymptotic value for J and its Komar source term value to give an intrinsic error estimate δJ. For analytical EoS our numerical results are very accurate with relative errors of the order of $\sim 10^{-10}$. A comparison with `magstar` results

EoS	Z	$I\,[10^{38}\,\mathrm{kg\,m^2}]$	$J\,[10^{37}\,\mathrm{kg\,m^2\,s^{-1}}](\Delta J)$	ω_c/Ω	$\lvert 1-I_{(L)}/I\rvert$
DD2	0.100	0.871	0.547 (2.8×10^{-7})	0.261	3.0×10^{-6}
SFHo	0.100	0.672	0.422 (4.2×10^{-6})	0.267	1.8×10^{-5}
FSG	0.100	0.848	0.533 (3.6×10^{-6})	0.266	5.1×10^{-5}
Poly(0.05|2)	0.100	3.854	2.421 (1.4×10^{-11})	0.274	2.1×10^{-10}
IRF(189)	0.100	0.549	0.345 (2.3×10^{-14})	0.203	8.4×10^{-11}
TVII_1(473)	0.100	0.405	0.254 (1.6×10^{-10})	0.253	9.9×10^{-11}
DD2	0.150	1.607	1.010 (6.3×10^{-8})	0.375	4.4×10^{-5}
SFHo	0.150	1.161	0.730 (1.7×10^{-6})	0.384	5.7×10^{-5}
FSG	0.150	1.373	0.863 (3.7×10^{-4})	0.390	2.1×10^{-4}
Poly(0.05|2)	0.150	4.379	2.751 (4.5×10^{-11})	0.419	3.7×10^{-10}
IRF(189)	0.150	1.596	1.003 (2.0×10^{-13})	0.308	7.3×10^{-11}
TVII_1(473)	0.150	1.200	0.754 (8.0×10^{-10})	0.381	7.5×10^{-10}
DD2	0.200	2.439	1.532 (5.9×10^{-8})	0.494	4.0×10^{-5}
SFHo	0.200	1.664	1.045 (7.1×10^{-7})	0.505	5.7×10^{-5}
FSG	0.200	1.707	1.072 (2.7×10^{-6})	0.526	3.2×10^{-5}
Poly(0.05|2)	0.200	3.887	2.442 (4.3×10^{-10})	0.578	3.7×10^{-10}
IRF(189)	0.200	3.476	2.184 (5.9×10^{-12})	0.415	5.7×10^{-11}
TVII_1(473)	0.200	2.674	1.680 (1.6×10^{-10})	0.512	1.0×10^{-10}
DD2	0.300	3.240	2.036 (4.9×10^{-8})	0.773	4.5×10^{-5}
SFHo	0.295	1.999	1.256 (7.5×10^{-8})	0.771	2.0×10^{-5}
FSG	0.234	1.586	0.996 (5.9×10^{-6})	0.642	1.2×10^{-3}
Poly(0.05|2)	0.214	3.525	2.215 (2.0×10^{-10})	0.630	2.0×10^{-10}
IRF(189)	0.375	22.307	14.016 (1.1×10^{-11})	0.821	4.8×10^{-12}
TVII_1(473)	0.270	6.484	4.074 (1.8×10^{-10})	0.697	1.5×10^{-10}

Table 5.2: Global parameters for various slowly rotating ($f = 0.01\,\mathrm{Hz}$) NS. We have chosen this very low frequency in order to exclude higher-order corrections on I from the `magstar` results.

confirms this error estimate. For tabulated EoS our results as well as the one from the `magstar` code can not exceed the precision limit ($\sim 10^{-6}$) set by the errors in the background star.

In Tab. 5.3 we display `magstar` results for higher rotation frequencies. We have chosen the $Z = 0.15$ SFHo configuration as an example for a configuration with realistic NS values to discuss the order of magnitudes for rotational deformations. At typical magnetar rotation frequencies of $\sim 1\,\mathrm{Hz}$ contributions to the stellar mass are of the $O\left(10^{-7}\right)$ and corrections to the moment of inertia due to rotational deformation are of the $O\left(10^{-5}\right)$. Compared to electro-magnetic contributions for typical magnetars these are minor effects. An approach up to $O\left(\Omega^1\right)$ is sufficient for slowly rotating $f \lesssim 10\mathrm{Hz}$ magnetars.

f [Hz]	$M/M\|_{0\,\mathrm{Hz}} - 1$	$J/J\|_{0.02\,\mathrm{Hz}} - 1$
1	1.463×10^{-7}	-2.024×10^{-6}
10	1.463×10^{-5}	3.743×10^{-5}
100	1.461×10^{-3}	3.995×10^{-3}

Table 5.3: Rotational deformations of the initial $Z = 0.15$ SFHo configuration computed with the `magstar` code. The slight decrease of J for $f = 1\mathrm{Hz}$ is a numerical error. The intrinsic error estimate from GRV3 for this configuration is 4×10^{-5} and relative changes can not be computed accurately below this threshold.

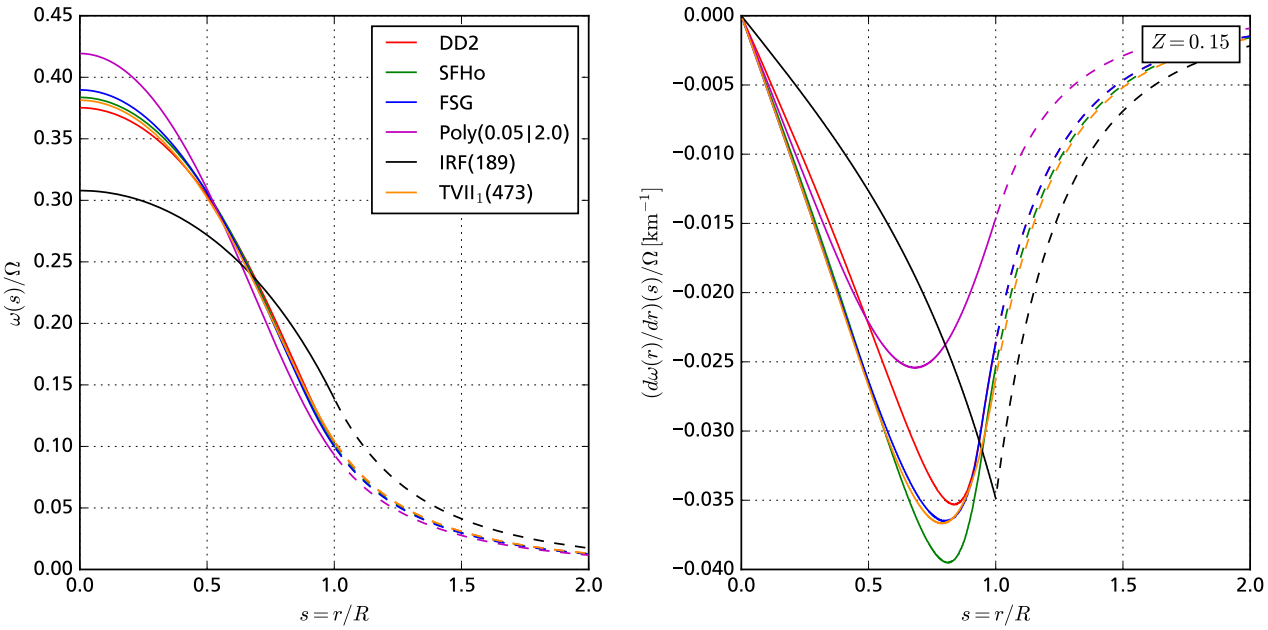

Figure 5.7: Reduced frame-dragging frequency $\bar{\omega}$ and its derivative over dimensionless radius for all $Z = 0.15$ configurations. Dashed lines mark the analytic exterior solutions.

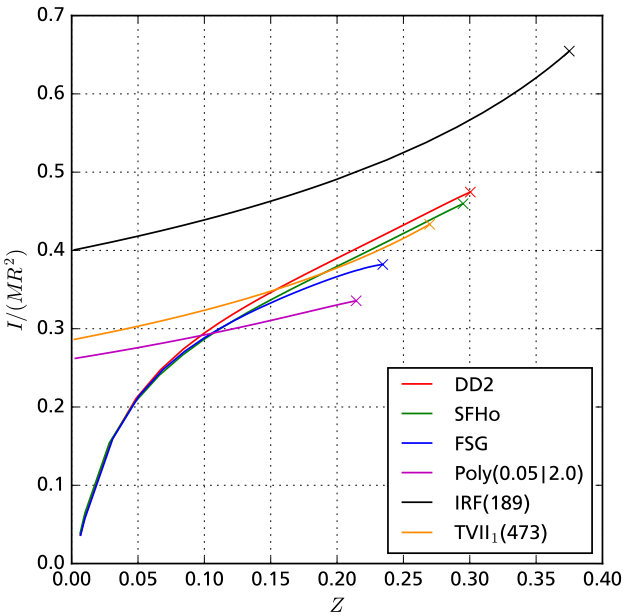

Figure 5.8: Moments of inertia divided by the stellar mass and the radius squared for different NS.

5.3 $O\left(B^1\Omega^1\right)$: The electro-magnetic field

In Sec. 3.4 we derived and discussed the relativistic Grad-Shafranov eq. (3.104) for a dipolar magnetic field on a spherical symmetric $O\left(B^0\right)$ background star. In this section we will present numerical solutions of the GS eq. (3.104) in the stellar interior and matching exterior solutions. Further we will present results for the induced electric field. First we will discuss the structure of those fields in general and then we will discuss the effects of EoS and compactness on the magnetic field.

For TVII and IRF background stars we derive classical limits and GR corrections in Chap. 6 analytically.

5.3.1 Structure of the electro-magnetic field

In this subsection we will discuss the structure of the electro-magnetic field for $Z = 0.15$ background stars. We will begin this discussion with the vector potential component a_ϕ, displayed in Fig. 5.9. Since we do not consider surface currents a_ϕ is continuously matched on the stellar surface. While the values for a_ϕ differ by quite a large amount between different EoS the resulting magnetic fields, see Fig. 5.10, are very similar. The slightly increased interior radial field component and decreased interior polar component for the IRF(189) are related to its high current density. Because of its constant density magnetic IRF(189) stars have very high current densities in the stellar interior, as can be seen in Fig. 5.11. For the hadronic EoS as well as $\text{TVII}_1(473)$ fields and currents are very similar. Stars with Poly(0.05|2)EoS are significantly bigger than its $Z = 0.15$ counter parts for the other EoS. The currents are much lower inside of Poly(0.05|2)stars.

Related to the magnetic quantities by the ideal MHD conditions we assume are the induced electric quantities. On the right of Fig. 5.11 we display the induced charge density, which is an analytical function of $\bar{\omega}$, a_ϕ and background star potentials, see eq. (3.137). The corresponding induced electric potentials are displayed in Fig. 5.12. By construction both mono and quadrupolar component of A_t are matched continuously across the stellar surface. The derivatives of a_{t0} and a_{t2} are not continuous at R, which in case of the monopole potential account to the surface charge density. The induced surface charge density is depicted in Fig. 5.13, it is angular dependent since interior and exterior electric fields have different geometries. The induced surface charges are highest at the pole caps of the magnetar and always negative. The gradient of the induced interior charge is also depicted in Fig. 5.13. For the IRF(189) star charge densities are very high as expected from its high J_t. The tetrad components of the corresponding induced electric field are displayed in Fig. 5.14. The discontinuity of the radial electric field, related to the induced surface charge density are clearly visible.

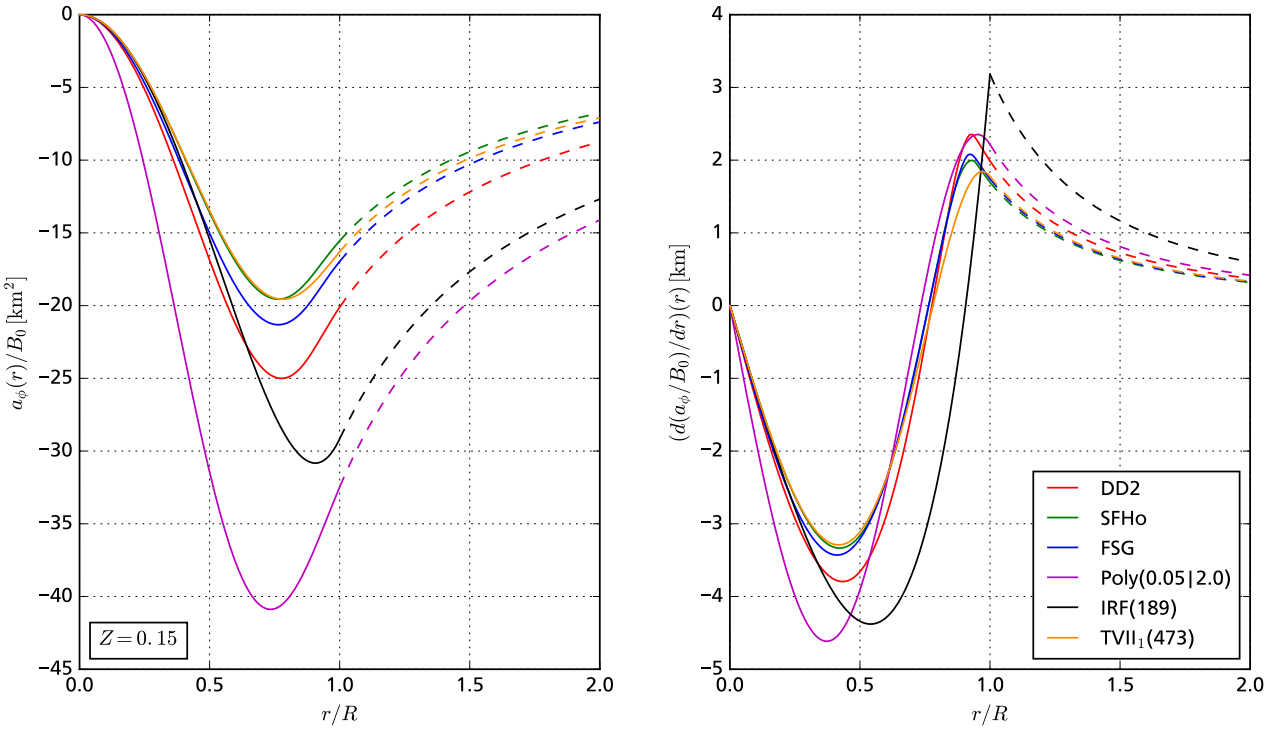

Figure 5.9: a_ϕ (left) and its derivative (right) for six different $Z = 0.15$ background stars, obtained from numerical integration of the GS eq.. Dashed lines mark the analytic exterior solutions.

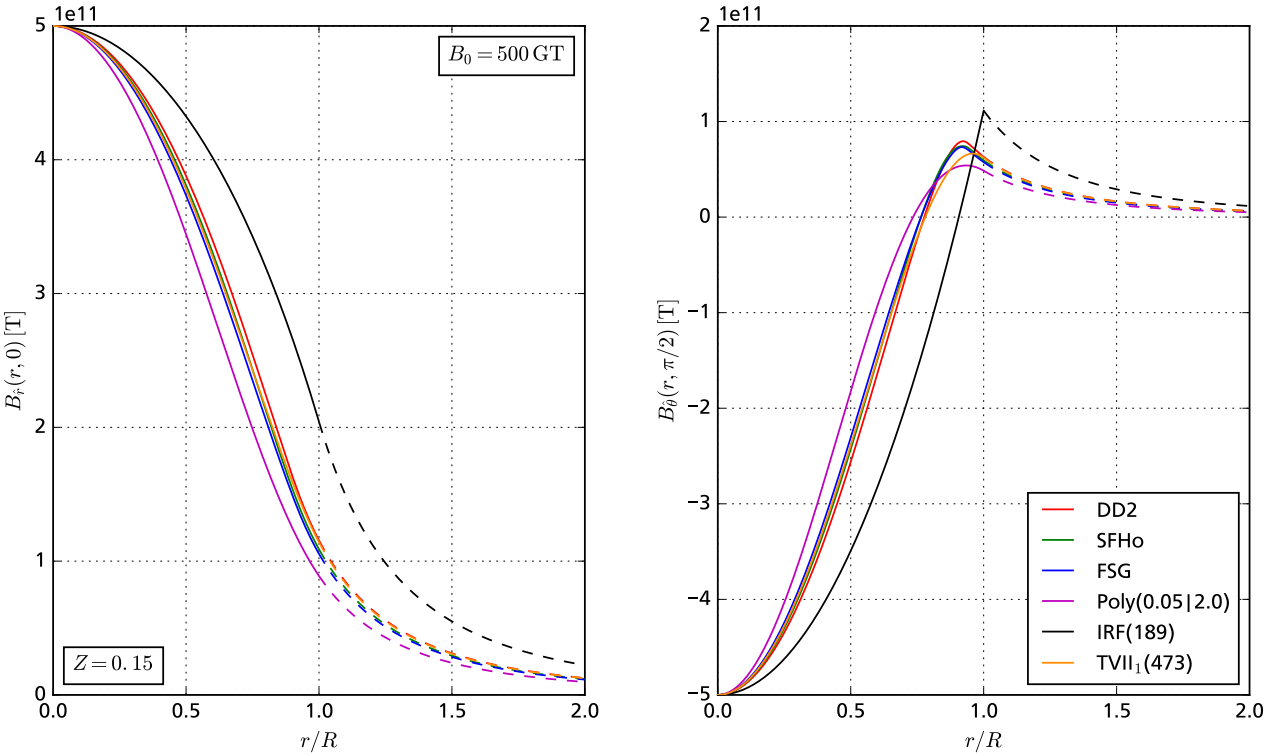

Figure 5.10: Radial (left) and polar tetrad components of the magnetic field (right) for six different $Z = 0.15$ background star. Dashed lines mark the analytic exterior solutions.

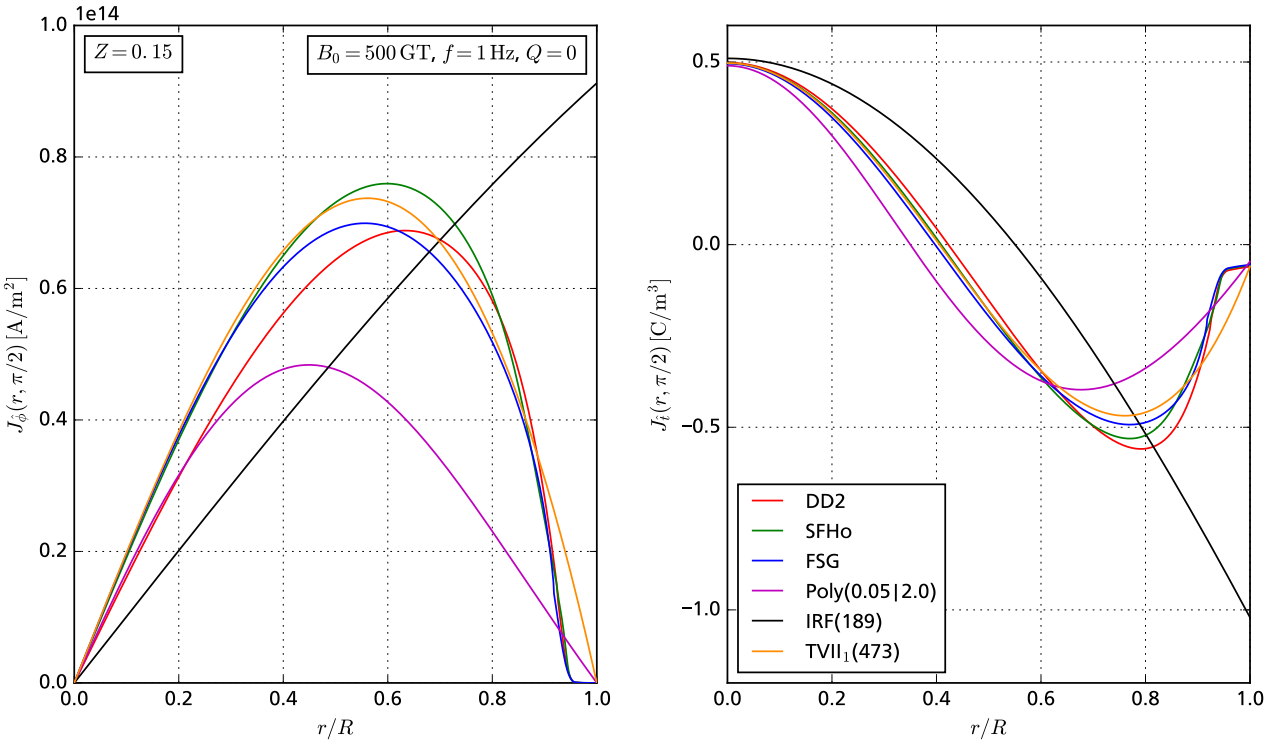

Figure 5.11: Current density (left) and induced charge density (right) for six different $Z = 0.15$ background star.

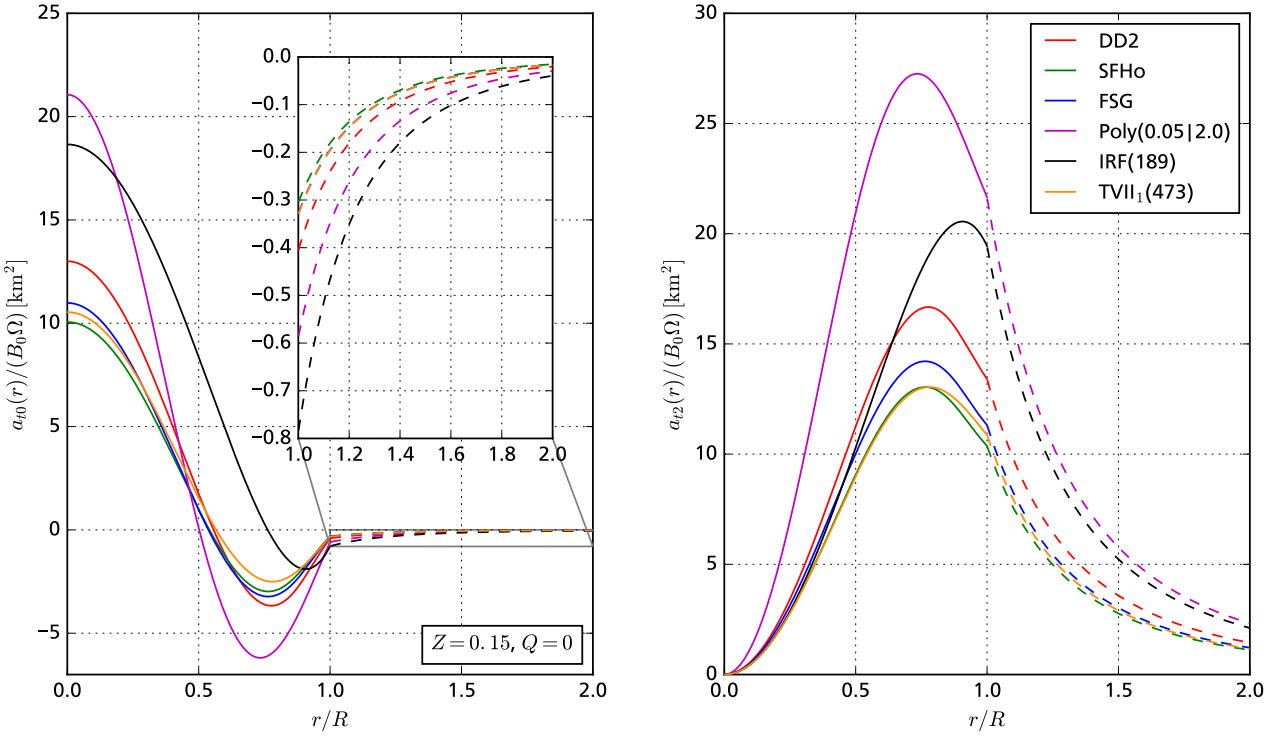

Figure 5.12: Components of the induced electric potential: a_{t0} (left) and a_{t2} (right) for six different $Z = 0.15$ background star. Dashed lines mark the analytic exterior solutions.

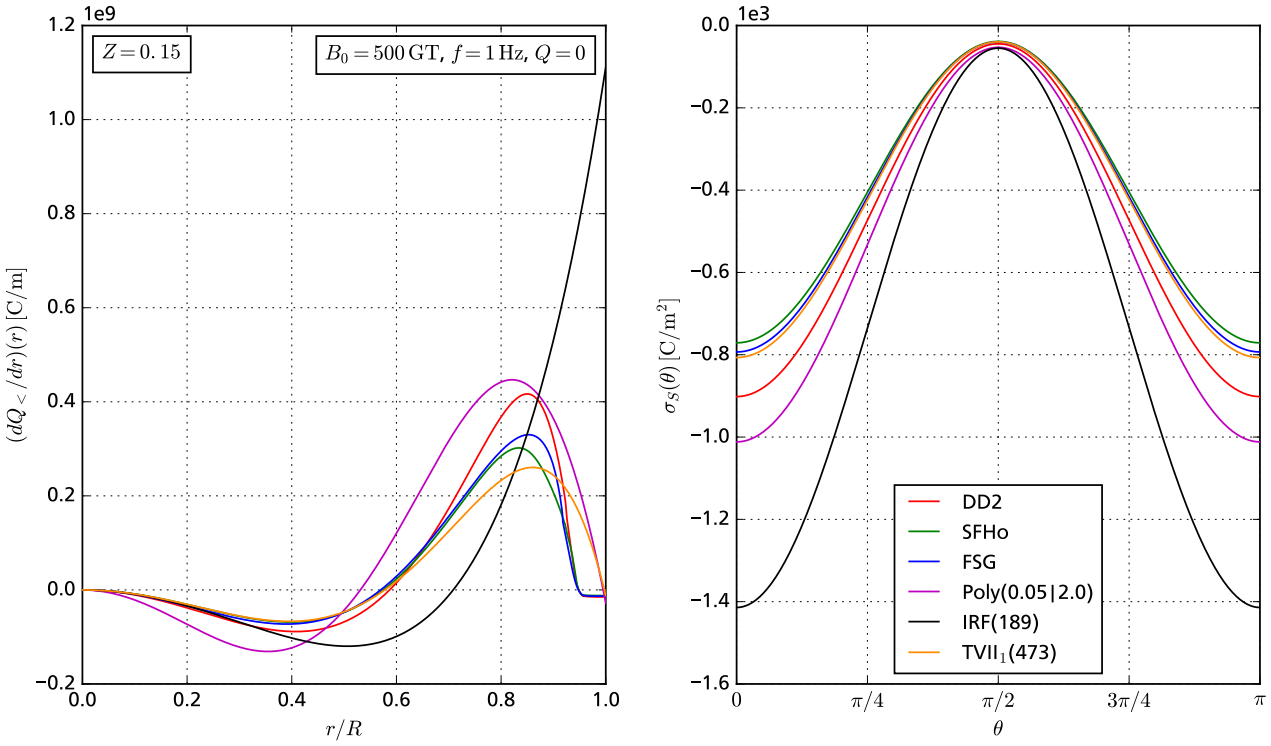

Figure 5.13: Induced O $\left(B^1\Omega^1\right)$ charges: Gradient of the interior charge (left) and angular distribution of the surface charge density (right) for six different $Z = 0.15$ background star.

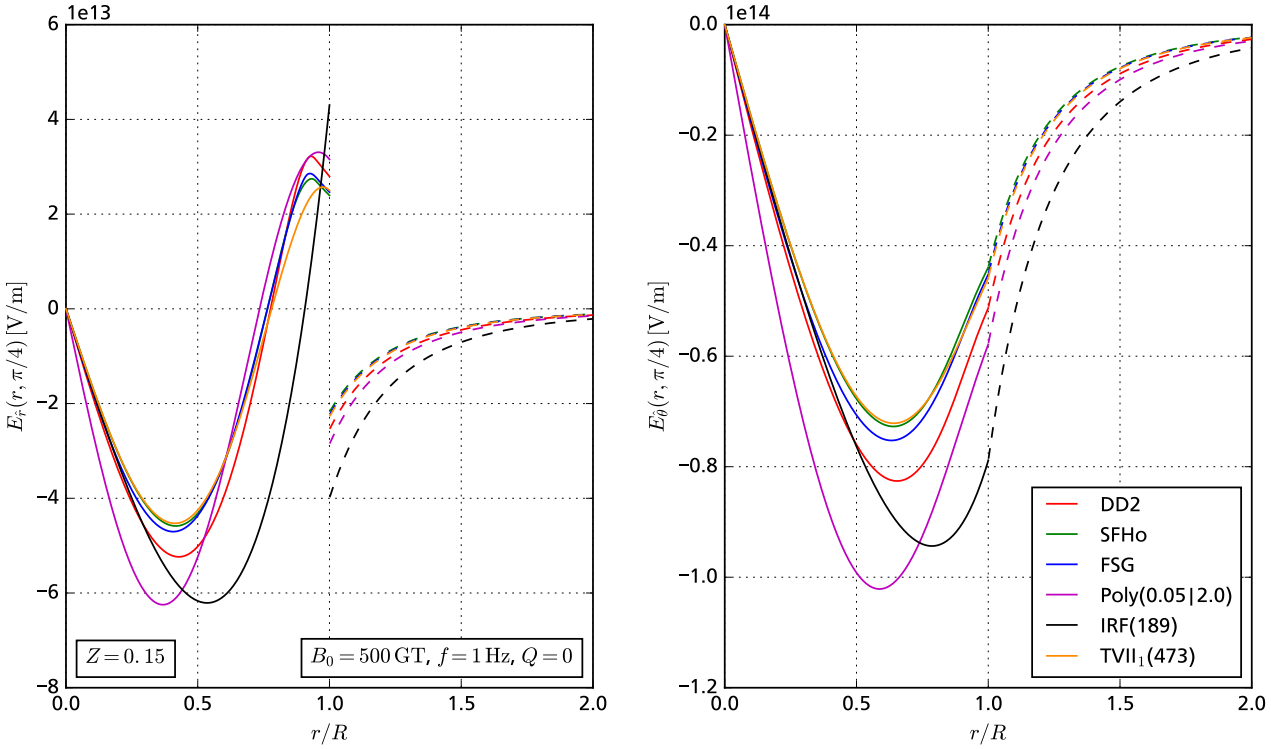

Figure 5.14: Radial (left) and polar tetrad components of the induced electric field (right) for six different $Z = 0.15$ background star at $\theta = \pi/4$. Dashed lines mark the analytic exterior solutions.

To visualize the geometry of the electro-magnetic field and the related quantities we include vector and density plots, Fig. 5.15-5.18, corresponding to the components of Fig. 5.9-5.14. The density plots share the same color map to allow for a direct comparison of magnitude. In the stellar exterior the induced electric field is purely quadrupolar. The induced interior field has a $\sin^2\theta$ angular dependence in the radial component which differs from the $P_2(\cos\theta)$ one in the exterior. The magnetic field is in the entire space purely $l = 1$ by construction and it is generated by a diffuse current loop in the stellar interior.

The fields for SFHo and $\text{TVII}_1(473)$ are extremely similar: we constructed $\text{TVII}_1(473)$ to model the SFHo $Z = 0.15$ configuration and it again succeeds as a very good effective model for realistic harmonic stars. By construction the IRF(189) $Z = 0.15$ NS shares mass and radius with its SFHo and $\text{TVII}_1(473)$ $Z = 0.15$ counter parts but the constant high energy density results in distinct and high currents and charges. The related fields are much stronger than the ones on SFHo or $\text{TVII}_1(473)$ configurations. Current- and charge densities do not decrease to zero towards the stellar surface because the density of $189\,\text{MeV}\,\text{fm}^{-3}$ provides constant support.

The Poly$(0.05\,|\,2)Z = 0.15$ NS is much bigger than its counter parts with different EoS and the electric fields is in magnitude comparable to the IRF(189) field. We did not include vector plots for DD2 and FSG configurations because their fields are so similar to the SFHo and $\text{TVII}_1(473)$ configurations.

The electric and vector potential tetrad components related to the fields of Fig. 5.15-Fig. 5.18 are displayed together in the panels of Fig. 5.19. Iso-surfaces of constant A_ϕ are surfaces of constant magnetic field strength and surfaces of constant A_t are iso-surfaces of constant electric field strength. Below the NS surface in the equatorial plane is a region where the magnetic and therefore the induced electric fields vanish. Magnetic field lines circle around this point and electric field line originate from it.

The overall geometry of the electro-magnetic field is encoded analytically by our multipole expansion but the explicit radial dependence is governed by numerical solutions of the GS eq. 3.104 and the induction eq. (3.135). The pure geometry of the electro-magnetic field does not change with compactness this is why we only showed results for one compactness in this section. In the following section we will discuss the effect of background star compactness on the electro-magnetic field.

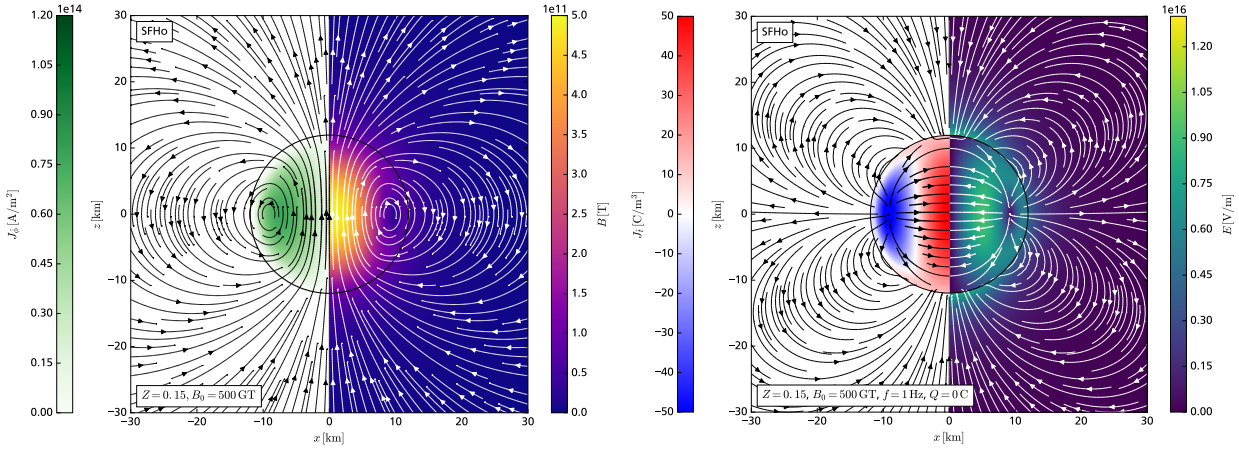

Figure 5.15: Magnetic (left) and electric field (right) for the $Z = 0.15$ SFHo background star with associated currents.

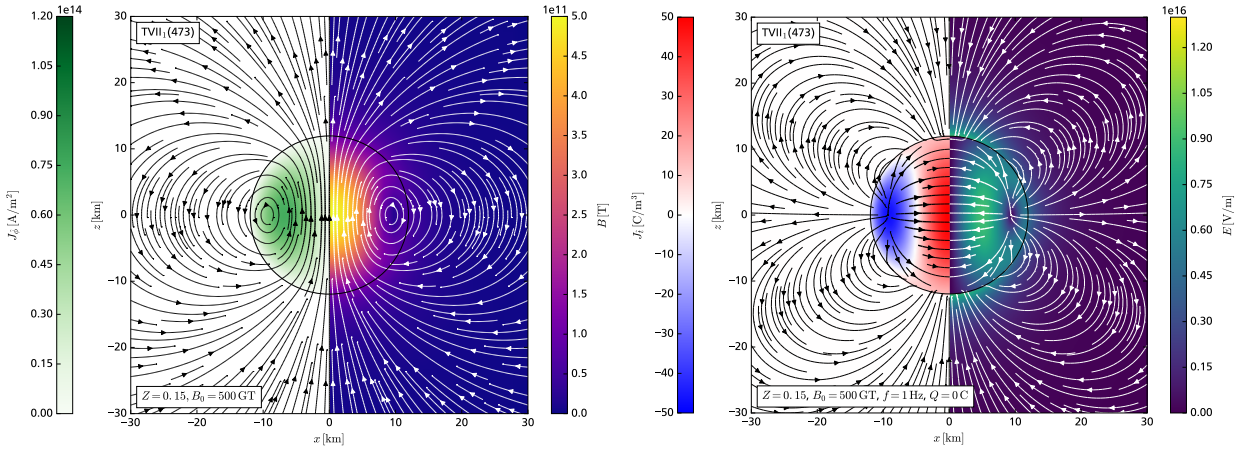

Figure 5.16: Magnetic (left) and electric field (right) for the $Z = 0.15$ TVII$_1$(473) background star with associated currents.

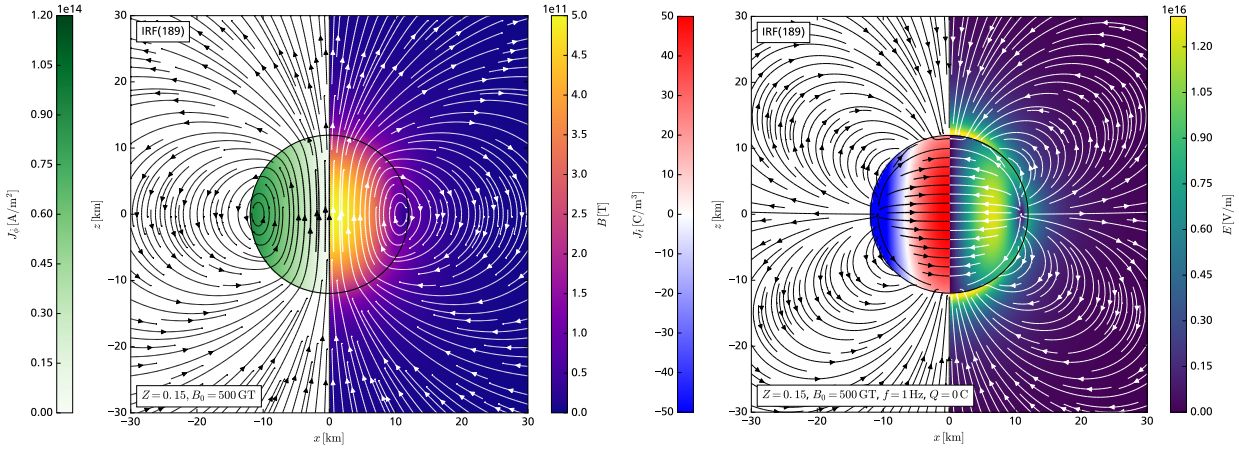

Figure 5.17: Magnetic (left) and electric field (right) for the $Z = 0.15$ IRF(189) background star with associated currents.

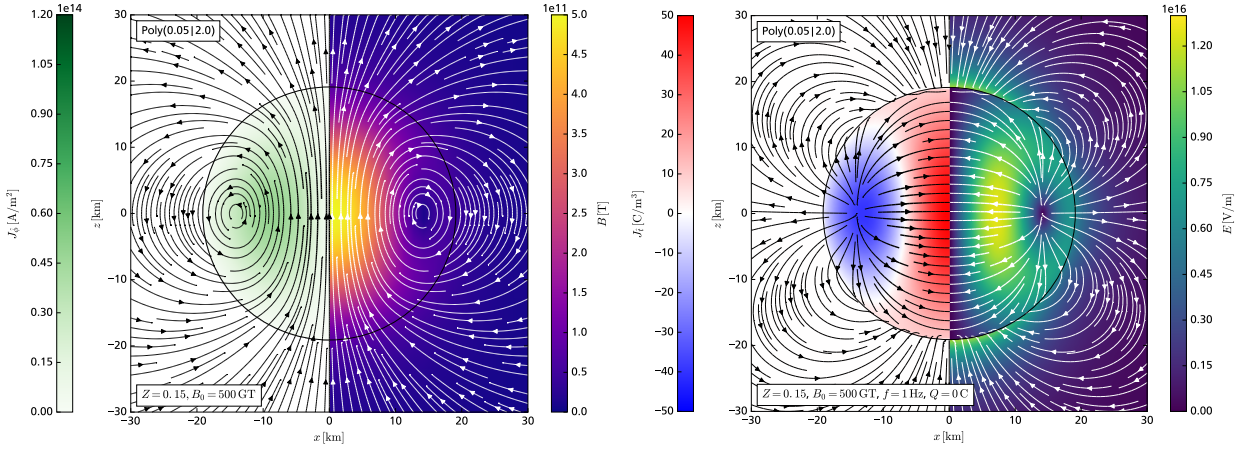

Figure 5.18: Magnetic (left) and electric field (right) for the $Z = 0.15$ Poly(0.05|2) background star with associated currents.

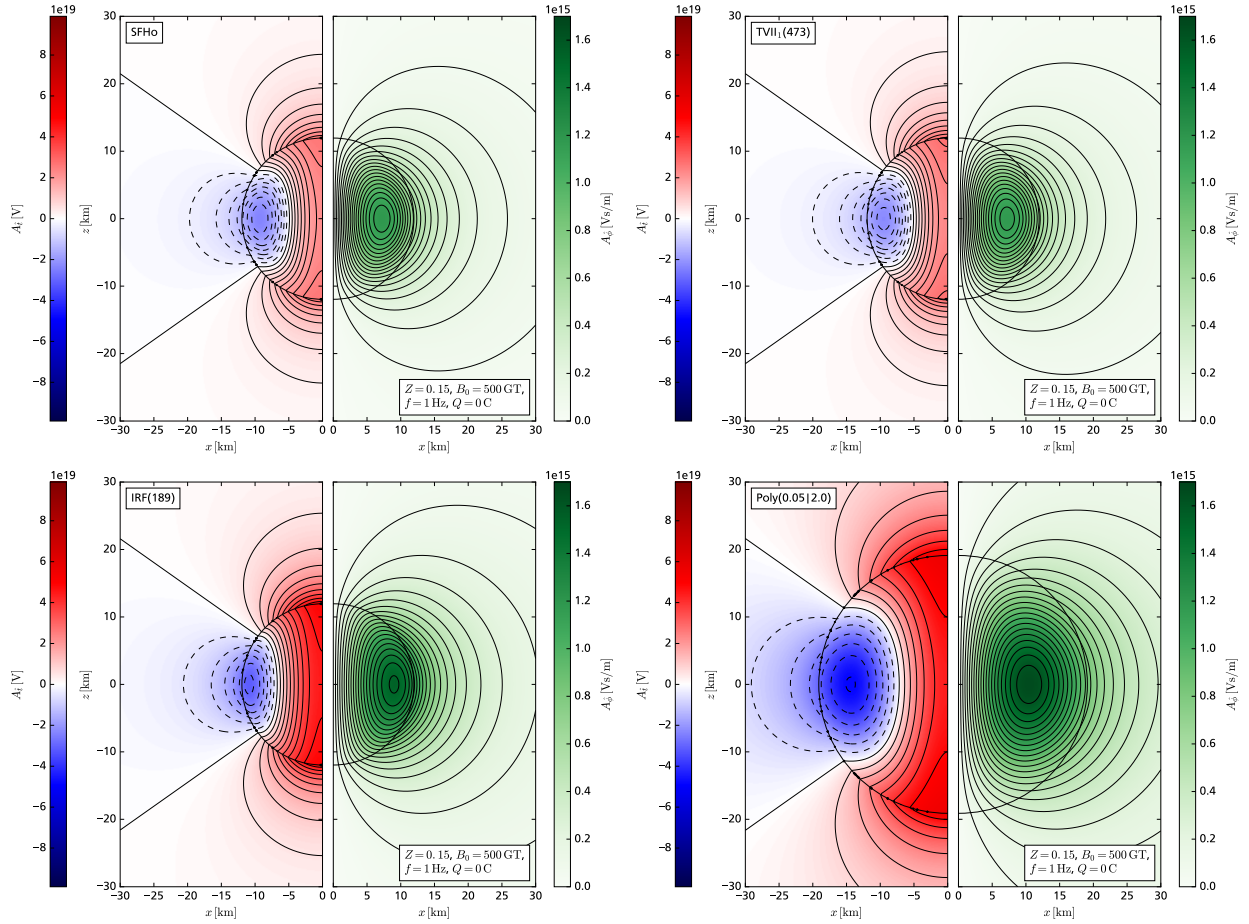

Figure 5.19: Density and iso-surface plots for the tetrad components of A_ϕ and A_t for $Z = 0.15$ SFHo (top left), TVII$_1$(473) (top right), IRF(189) (bottom left) and Poly(0.05|2)(bottom right) NS.

5.3.2 Effects of the background star on the global parameters of the EM field

In Fig. 5.20 we show the dependence of the relative dipole moment μ/B_0 and of the relative polar surface magnetic field B_p/B_0 on the background star. The relative surface field strength decreases for hadronic EoS with the compactness. The reason for that is the increase in radius for hadronic configurations with decreasing compactness.

The background stars of the analytical EoS TVII$_1$(473) and IRF(189) approach get smaller with decreasing compactness and the relative surface fields approach constant values of $8/35B_0$ and $2/5B_0$ respectively. For Poly(0.05|2)configurations B_p/B_0 approaches ~ 0.2 as Z goes to zero.

The relative dipole moment for the hadronic EoS are similar and lie around $1 \times 10^{18}\,\mathrm{A\,m^2/T}$. Related to its strong fields the IRF(189) EoS has large relative dipole moments at higer compactnesses. For small Z the dipole moments for TVII$_1$(473) and IRF(189) EoS decrease as the configurations get smaller.

Configurations with the stiff DD2 EoS have stronger fields and related dipole moments compared to configurations with softer FSG EoS. Stars with SFHo EoS have intermediate relative field strenghts and dipole moments. We have only plotted results for configurations with $Z > 1 \times 10^{-2}$. We do not discuss results on white dwarf or planet branch, see B.3, in the scope of this work.

In Fig. 5.21 we display results for the relative current function amplitude $-c_{j\phi}/B_0$ and the relative induced electric quadrupole moment $\mathcal{Q}_\mathrm{E}/(B_0\Omega)$. For $-c_{j\phi}/B_0$ we report an overall universal behavior for all considered EoS: the relative current function amplitude decreases as compactness increases.

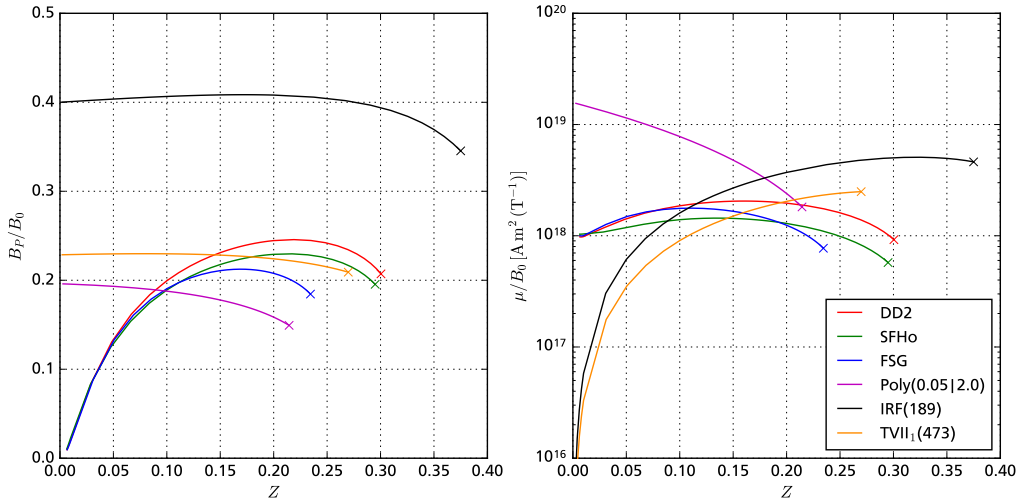

Figure 5.20: Relative polar surface magnetic field B_p/B_0 (left) and relative dipole moment μ/B_0 (right) for different background stars with varying compactness and EoS.

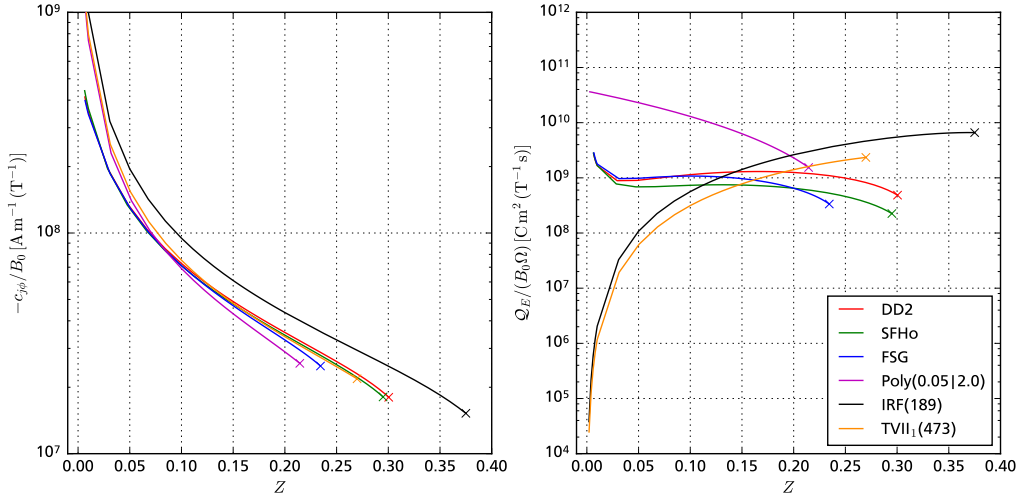

Figure 5.21: Relative current function amplitude $-c_{j\phi}/B_0$ (left) and relative electric quadrupole moment $\mathcal{Q}_\mathrm{E}/(B_0\Omega)$ (right) for different background stars with varying compactness and EoS.

The reason for that is simple with increasing compactness, density and pressures rise and since the current density is $\propto (P+\rho)\, c_{j\phi}$ has to decrease as pressures and densities increase to realize constant central magnetic fields. The TVII$_1$(473) relation is very similar to the hadronic relations for $-c_{a\phi}/B_0$.

The situation for $\mathcal{Q}_\mathrm{E}$ is very similar to the discussed situation for μ. The quadrupole moment is linear in μ and the Z dependent factor from eq. (3.149) does not change significantly with EoS and Z.

5.4 $O\left(B^2\right)$: Magnetic deformations

In this section we will discuss magnetic deformations within our perturbative approach. The $O\left(B^2\right)$ deformations are governed by the solutions of the structure equations of Sec. 3.6. We will limit the following discussion to global quantities, since they are more instructive than the gradients of the metric potentials. We will present results for the increase in gravitational mass δM, the mass quadrupole moment $\mathcal{Q}_{\mathrm{M}}$, the oblateness ε from eq. (3.268) and for the change of the polar radius.

We can draw several conclusions form the results displayed Fig. 5.22 and Fig. 5.23.

First of all we see that configurations with higher compactness are harder to deform: all figures show decreasing deformations for increasing compactness. In the sense of the term *compactness* this is easy to explain: compacter NS are bound stronger and therefore magnetic fields can only deform them slightly.

Another very dominant trend in all global quantities is that stars with softer EoS get deformed lesser than stars with stiffer EoS. In the sense of the term *stiff* this may sound counter intuitive but there is an easy explanation. NS with stiff EoS have lower pressures and energy density at given mass/compactness when compared to NS with softer EoS, see Fig. 5.4 and Fig. 5.5 . So for stiff EoS the contributions from the magnetic field to the energy-momentum tensor are bigger when compared to the energy density and pressure contributions.

The magnetic deformation computed within our perturbative magnetar model are in good agreement with the results obtained from the `magstar` code for magnetic fields below $1 \times 10^{13}\,\mathrm{T}$.

5.4.1 Intrinsic upper limit for the central magnetic field of the $O\left(B^2\Omega^1\right)$ model

In Sec. 3.9.2 we discussed the upper limit for the magnetic field in terms of the surface deformation. Fig. 5.24 shows the situation for a $M/R = 0.2$ Poly$(0.05|2.0)$ background star: with a central magnetic field of $2.128 \times 10^{14}\,\mathrm{T}$ the polar radius becomes zero. We plotted results for B_{max} for different compactnesses and EoS in Fig. 5.25. In general B_{max} is of the order $10^{14}\,\mathrm{T}$ which is in agreement with the estimate of the classical scalar virial theorem of $\sim 10^{14}\,\mathrm{T}$ [8, 9].

The magnetic fields corresponding to an error estimate of 1% are around $1 \times 10^{13}\,\mathrm{T}$ and we found a good agreement between our results and the one computed with the `magstar` code below this threshold.

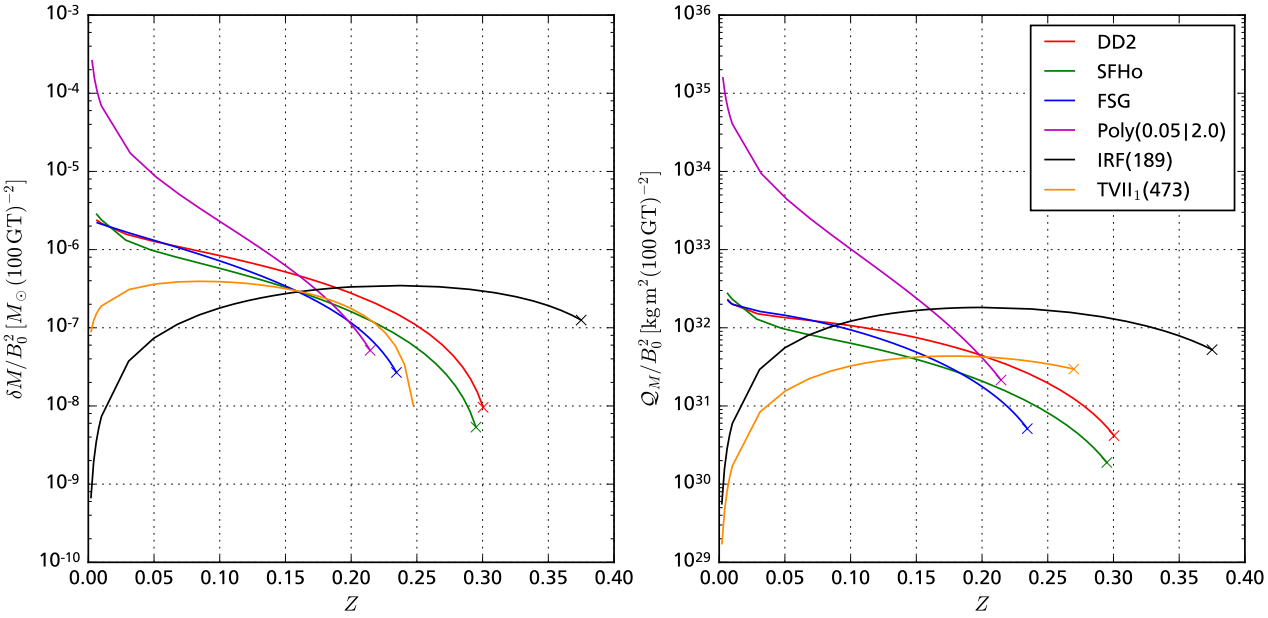

Figure 5.22: Relative O $\left(B^2\right)$ deformations $(\delta M)/B_0^2$ (left) and relative mass quadrupole moment $\mathcal{Q}_\mathrm{M}/B_0^2$ (right) for different background stars with varying compactness and EoS.

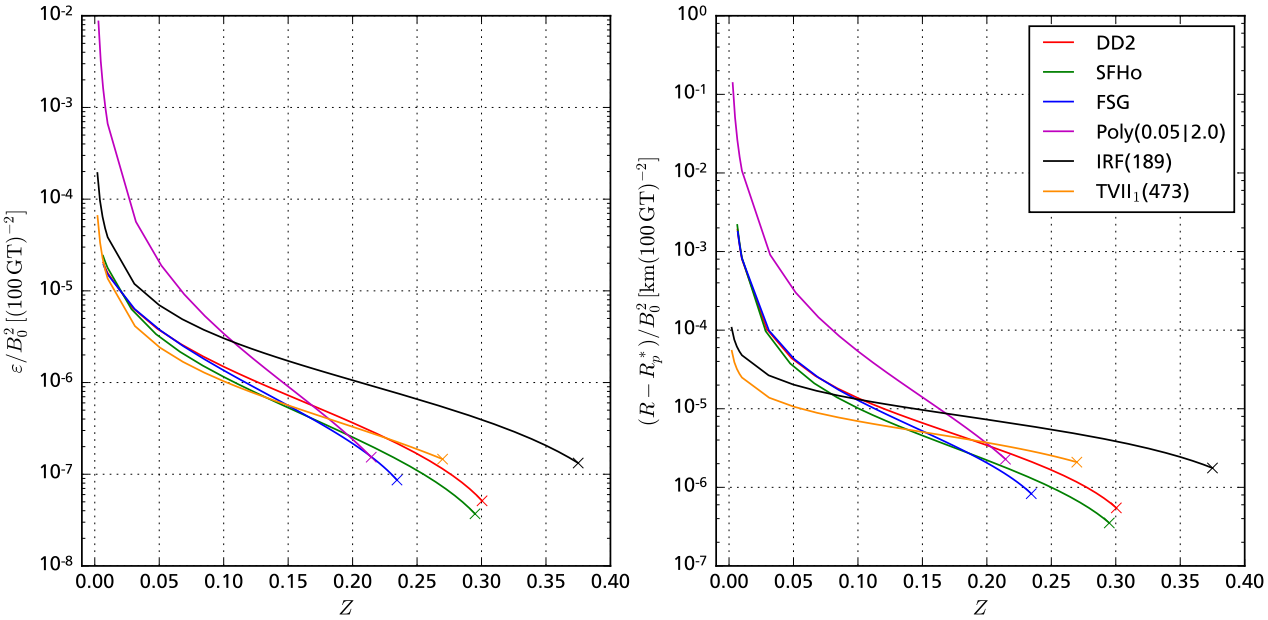

Figure 5.23: Reltaive oblateness ε/B_0^2 (left) and decrease in polar radius (right) for different background stars with varying compactness and EoS.

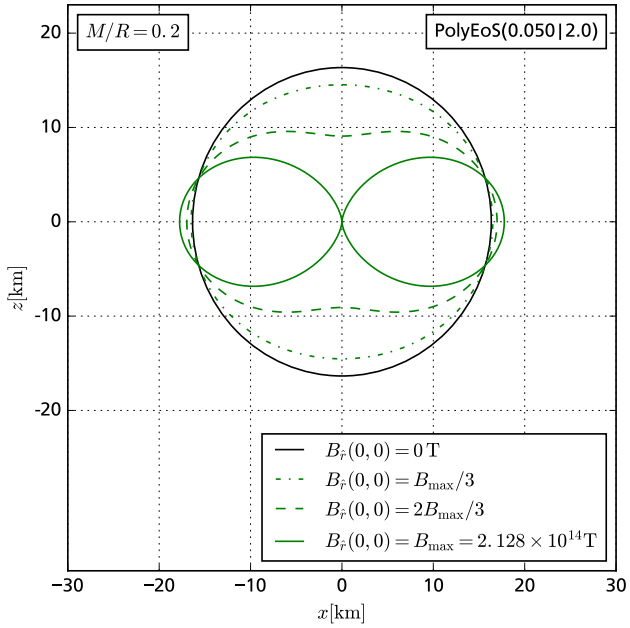

Figure 5.24: Extreme and maximal deformations of a $M/R = 0.2$ Poly(0.05|2.0) background star.

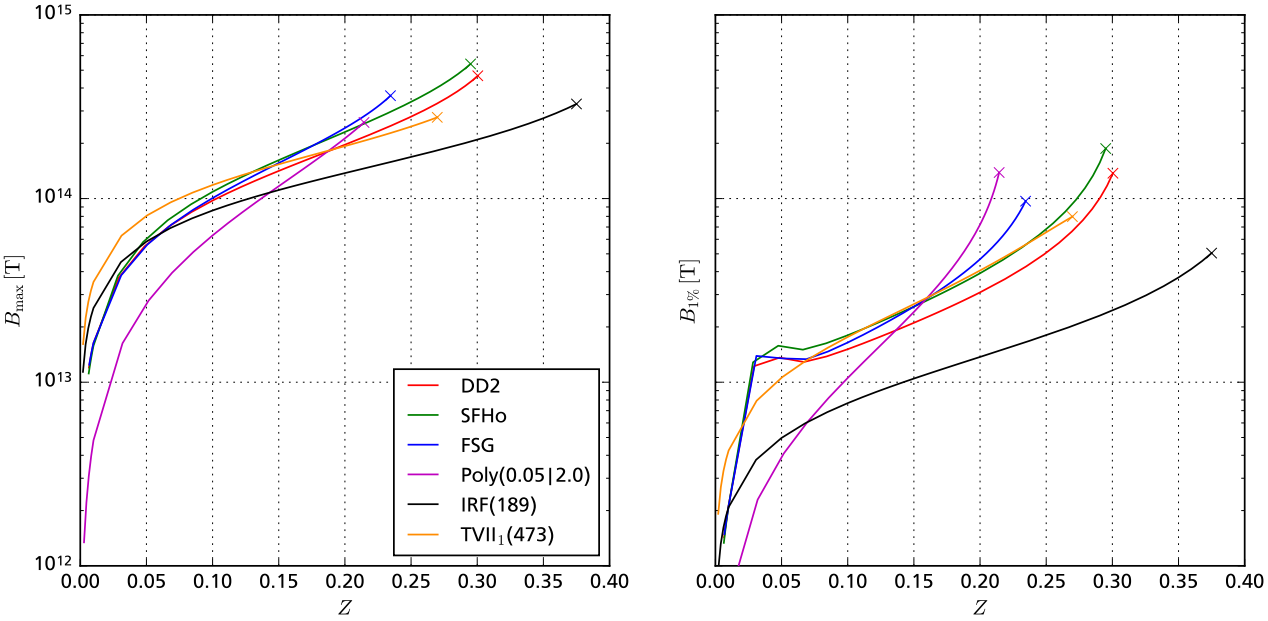

Figure 5.25: Maximal values for the central magnetic field (left) and values for $B_{1\%}$ from the error estimate (3.269) (right) for different background stars with varying compactness and EoS.

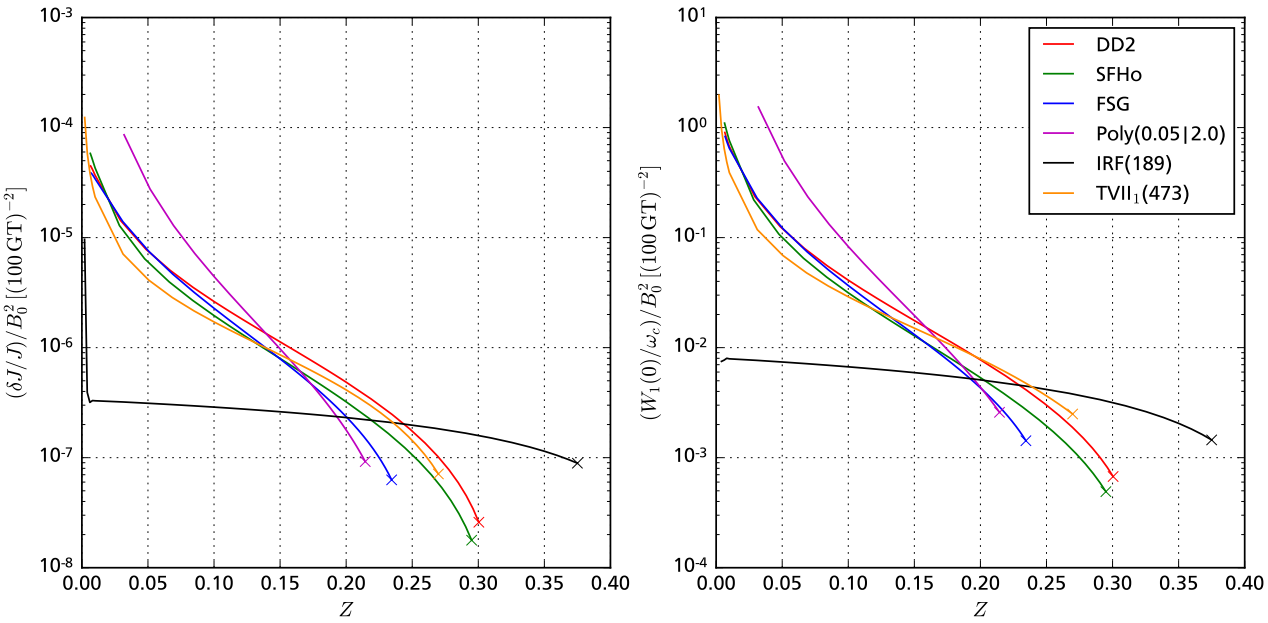

Figure 5.26: Relative O $\left(B^2\right)$ correction $(\delta J/J)/B_0^2$ to the angular momentum (left) and O $\left(B^2\right)$ corrections to the central value of the frame-dragging frequency (right) for different background stars with varying compactness and EoS.

5.5 $O\left(B^2\Omega^1\right)$: The electro-magnetic corrections to the angular momentum

The higher-order O $\left(B^2\Omega^1\right)$ corrections to the star's metric affect only the $g_{t\phi}$ component and represent higher-order correction to the frame-dragging frequency. W_3 has only a very small effect and is not directly related to an observable. W_1 on the other hand is an $l = 1$ correction to $\omega(r)$. In Fig. 5.26 we display corrections to the angular momentum and to the frame dragging frequency. With decreasing compactness the NS are easier to deform and O $\left(B^2\Omega^1\right)$ corrections become bigger except for the case of IRF(189) . Because of the distinct structure of the electric field inside the constant density IRF(189) star, see Sec. 5.3, the corrections to the frame-dragging frequency stay constant low.

In terms of EoS stiffness we find that corrections are slightly bigger for stiff EoS, like DD2, when compared to the softer SFHo and FSG results. But in general the O $\left(B^2\Omega^1\right)$ corrections for the hadronic EoS and the TVII$_1$(473) as effective model for SFHo configurations are very similar.

Again central magnetic fields beyond 100 GT are necessary for significant corrections. In Fig. 5.27 we show $W_1(r)$ and $W_3(r)$ for our canonical $Z = 0.15$ configuration. By construction both potentials are continuous across the surface. W_3 is always smaller negative and about one order of magnitude below W_1.

5.6 $O\left(Q^2\right)$ and $O\left(B^1Q^1\right)$: Configurations with global net charge

In this section we will discuss numerical results related to the theoretical discussions of Sec. 3.8.

We will begin with the purely electric contributions to the mass shift. On the left of Fig. 5.28 we plotted the mass shift of eq. (3.226) for different background stars. The only non-analytical dependence in the expression for δM_Q is $R[Z]$, the dependence of the stellar radius on the compactness for the different EoS shapes the relation for the electric mass shift.

For $Z \to 0$ the radii of IRF(189) and TVII$_1$(473) configurations approach zero and the electric mass shift increases rapidly in $O\left(1/R\right)$. More and more energy is stored in the electric field as the stellar surface becomes smaller and smaller. This can be understood quite intuitively: generating such

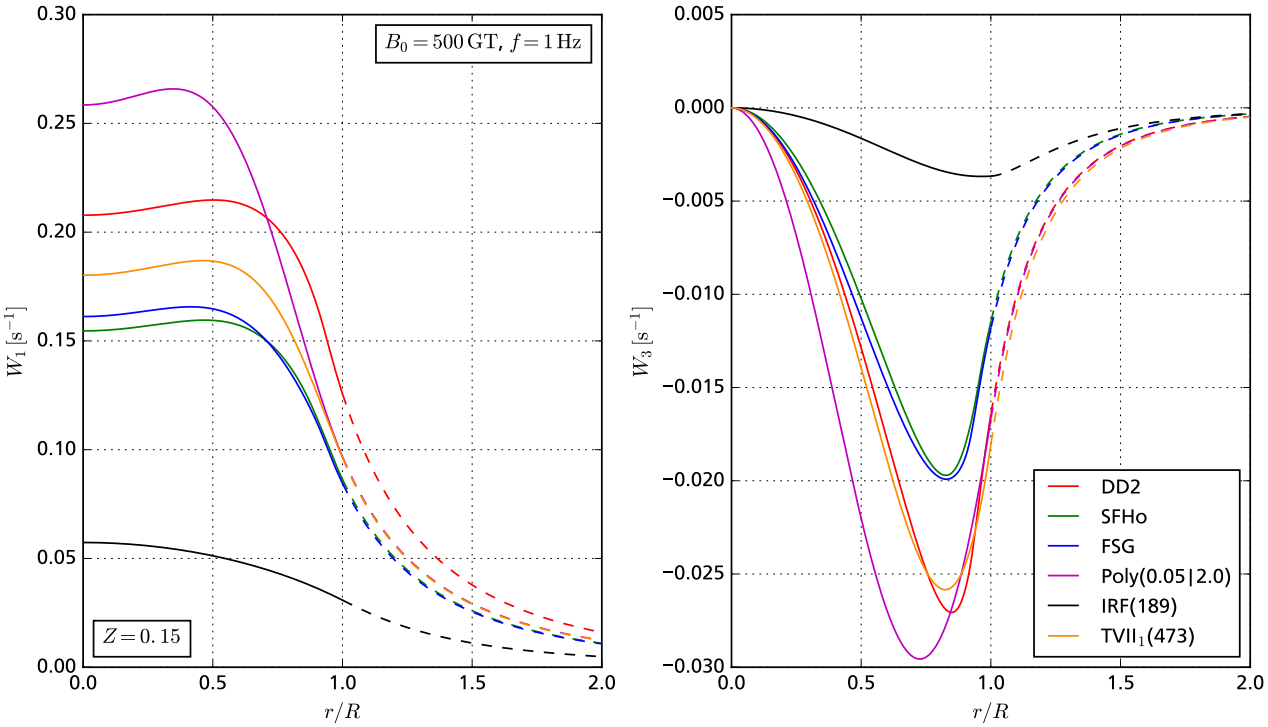

Figure 5.27: $W_1(r)$ and $W_3(r)$ for different $Z = 0.15$ configurations with a central magnetic field strength of 500 GT and a rotation frequency of 1 Hz. Dashed lines mark the analytic exterior solutions.

configurations takes more and more energy as the repulsive forces between equal charges increase with decreasing distance between them.

Poly(0.05|2)EoS NS approach a constant radius of $\sim 25\,\mathrm{km}$ as Z goes to zero, see Fig. 5.1, which results in a mass shift of $\delta M_Q \approx Q^2/25\,\mathrm{km}$ in that limit.

For hadronic EoS the electric mass shifts differ only slightly for configurations with intermediate and high compactnesses.

As discussed already in the theory section Sec. 3.8 δM_Q is very small even for large charges and in cases where magnetic fields are present the magnetic contributions to the mass shift are several orders of magnitude higher then the ones from δM_Q.

The electro-magnetically induced contributions from δJ_{BQ} can be significant when compared to the $O\left(\Omega^1\right)$ from Sec. 5.2. For charges of $1 \times 10^{12}\,\mathrm{C}$ and magnetic fields of around 500 GT the induced angular momentum is for typical NS of the order of $1 \times 10^{39}\,\mathrm{kg\,m^2\,s^{-1}}$, which is of the same order of magnitudes as the angular momentum for a 1Hz rotating star. The right panel of Fig. 5.8 shows the dependence of δJ_{QB} on EoS and background star compactness.

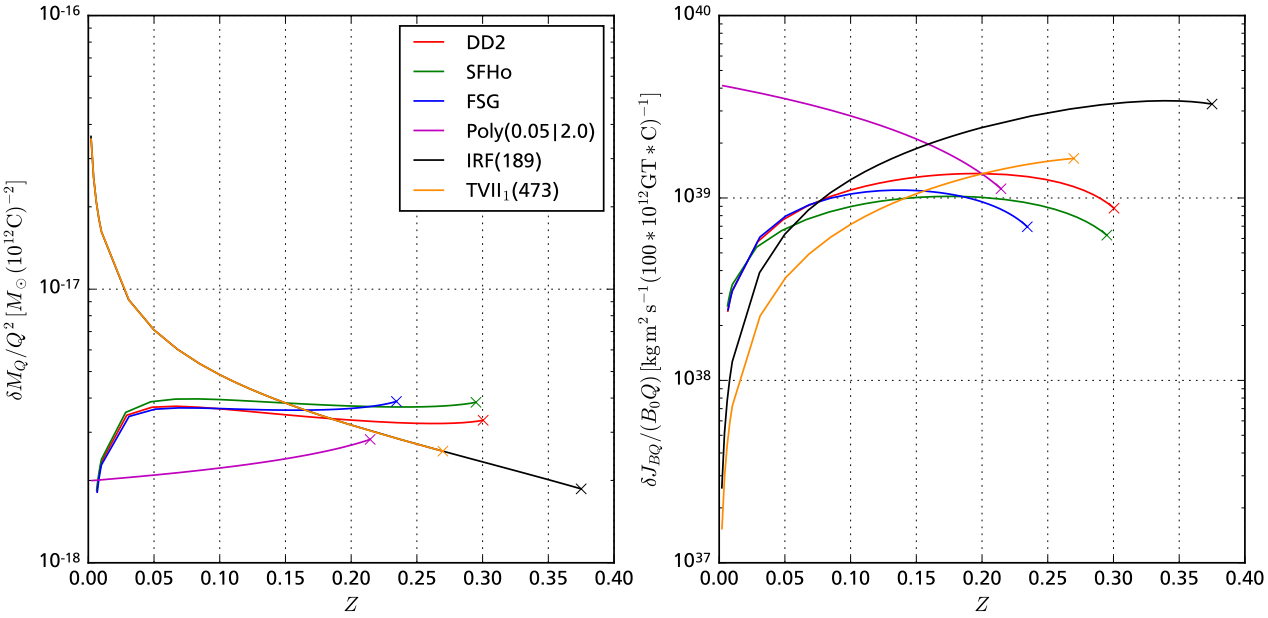

Figure 5.28: Electric mas shift (left) and electro magnetically induced angular momentum (right) for background stars with varying EoS and compactness.

6 Analytic series solutions of the $O\left(B^1\Omega^1\right)$ equations

For general EoS the $O\left(\Omega^1\right)$ frame-dragging eq. (3.85) and the $O\left(B^1\right)$ relativistic Grad-Shafranov eq. (3.104) for dipolar fields have to be solved numerically in the stellar interior. The ODEs themselves include the $O\left(B^0\Omega^0\right)$ background star's metric potentials and thermodynamic gradients which for general EoS can only be obtained by numerical integration of the TOV eqs. In Sec. 3.2.4 and Sec. 3.2.5 we introduced the interior Schwarzschild and Tolman VII solutions for which this is not the case. For ISS and TVII equilibrium configurations all metric potentials and thermodynamic gradients are known analytically. For ISS and TVII background stars the FD and GS eqs. are analytical ODEs but because of the complicated algebraic structure of both analytical solutions the task of finding exact analytical solutions for the interior FD and GS eqs. is difficult.

In this chapter we will derive and discuss analytic interior solutions for the GS and FD equation in form of a series in the background star compactness Z. There are several reasons why such an expansion is a priori not impossible.

An ISS equilibrium configuration is uniquely determined by specifying its compactness Z, its radius R and in principle the mean baryon rest mass of the IRF fluid m_{B}. The latter has only an effect on the number density and related parameters which are of no interest in this chapter. After choosing a family of TVII solutions by fixing μ, TVII equilibrium configurations are also determined by those $2+1$ parameters. The radius or related the central density appears in the ISS and TVII solutions only as a scale.

The metric potentials $\lambda(s)$ and $\nu(s)$ in terms of the dimensionless radial coordinate $s \equiv r/R$ are completely independent of central density or radius for TVII and ISS configurations. The functional form of both potentials depends only on the background star compactness Z. For the ISS $\lambda[Z](s)$ is given in eq. (3.67a) and $\nu[Z](s)$ is given in eq. (3.67a) and both are functions in s once a Z is chosen. When considering TVII solutions with fixed μ the situation is exactly the same, see eq. (3.74a) and eq. (3.76).

The thermodynamic quantities for configurations of the same Z, scale linear with the central density or equivalently R^{-2}, see eqs. (3.67c), (3.67d), (3.74b) and (3.78).

The only non-trivial parameter dependence of the ISS and fixed μ TVII solutions is their Z dependence. We already discussed, that in GR Z can not grow arbitrarily. In case of the ISS the Schwarzschild-Buchdahl limit $Z_{\mathrm{SB}} = 4/9$ represents the maximum compactness of any non singular configuration. For TVII configurations the maximum compactness is even lower as we displayed in Fig. 3.3. For physical/causal configurations the limiting compactnesses are even lower and realistic NS typically have values between 0.1 and 0.3. Z is dimensionless and for all non-singular configurations smaller then 1. This makes convergent expansions of the metric potentials and thermodynamic quantities around $Z = 0$ possible.

In the following we will expand and solve both the FD and GS eq. up to high-order in Z. We will compare results obtained from those expansions with numerical and analytical Newtonian results to validate them.

To the best of our knowledge, no one has considered such expansions in literature.

6.1 Compactness-series solutions of the Frame-dragging equation

6.1.1 Interior Schwarzschild solution

We will discuss the expansion of the frame-dragging eq. (3.85) for ISS background configurations in detail. The FD for an ISS star in the stellar interior reads

$$\begin{aligned} 0 = \bar{\omega}_<''(s) + \left(\frac{2sZ}{-2s^2Z - 3\sqrt{1-2Z}\sqrt{1-2s^2Z}+1} + \frac{2sZ}{2s^2Z-1} + \frac{4}{s} \right) \bar{\omega}_<'(s) \\ + \left(\frac{8Z}{-2s^2Z - 3\sqrt{1-2Z}\sqrt{1-2s^2Z}+1} + \frac{8Z}{2s^2Z-1} \right) \bar{\omega}_<(s) \end{aligned} \tag{6.1}$$

$$\equiv \mathscr{D}_i^{\bar{\omega}} v_{\bar{\omega}}^i, \text{ with } v_{\bar{\omega}}^i = \left(\bar{\omega}_<''(s), \bar{\omega}_<'(s), \bar{\omega}_<(s) \right)^{\mathrm{T}}. \tag{6.2}$$

The ODE $\mathscr{D}_i^{\bar{\omega}} v_{\bar{\omega}}^i = 0$ depends on the background star only by the Z dependence of $\mathscr{D}_i^{\bar{\omega}}$ which makes it possible to expand the ODE in this parameter. In the case of non singular IRF stars $Z \in [0, 4/9)$ which means an expansion around $Z = 0$ should converge against the exact solution. We use the following approach to expand and solve the ODE (6.2). First we make an ansatz for $\bar{\omega}_<(s)$ in form of power series in Z:

$$\bar{\omega}_<(s) \equiv \sum_{m=0}^{n} \bar{\omega}_{<,m}(s) Z^m. \tag{6.3}$$

We now construct $\bar{\omega}_{<,m}(s)Z^m$ as the solution of the ODE (6.2) in $O(Z^m)$. For that we need to expand $\mathscr{D}_i^{\bar{\omega}}$ up to $O(Z^m)$ which is possible up to arbitrarily high m since $\mathscr{D}_i^{\bar{\omega}}$ is $C^\infty\left(Z \in [0, 4/9)\right)$. We use the following notation for the $O(Z^m)$ expansion coefficients

$$(\mathscr{D}_i^{\bar{\omega}})_m \equiv \left. \frac{d^m \mathscr{D}_i^{\bar{\omega}}}{dZ^m} \right|_{Z=0}, \tag{6.4}$$

$$(v_{\bar{\omega}}^i)_m = \left(\bar{\omega}_{<,m}''(s), \bar{\omega}_{<,m}'(s), \bar{\omega}_{<,m}(s) \right)^{\mathrm{T}}. \tag{6.5}$$

Using those the pure $O(Z^m)$ term of the ODE (6.2) reads

$$\bar{\omega}_{<,m}''(s) - \frac{4}{s} \bar{\omega}_{<,m}'(s) = -\sum_{j=1}^{m} (\mathscr{D}_i^{\bar{\omega}})_j (v_{\bar{\omega}}^i)_{m-j} \equiv \mathscr{P}_m^{\bar{\omega}}(s). \tag{6.6}$$

Eq. (6.6) is an inhomogeneous second-order ODE for $\bar{\omega}_{<,m}(s)$. Its homogeneous system, the LHS of eq. (6.6), is extremely simple because it comes from the $O\left(Z^0\right)$ expansion of $\mathscr{D}_i^{\bar{\omega}}$. It is solved by the two linearly independent functions

$$\varphi_0(s) = C_0, \tag{6.7}$$

$$\varphi_1(s) = \frac{C_1}{s^3}. \tag{6.8}$$

From these two solutions we can construct the Green's function

$$G_{01}(s,t) = -\begin{vmatrix} \varphi_0(s) & \varphi_1(s) \\ \varphi_0(t) & \varphi_1(t) \end{vmatrix} \Big/ \begin{vmatrix} \varphi_0(t) & \varphi_1(t) \\ \varphi_0'(t) & \varphi_1'(t) \end{vmatrix} = \frac{1}{3} \left(\frac{1}{t^3} - \frac{1}{s^3} \right) t^4 \tag{6.9}$$

and with it a particular solution $\varphi_{P,m}^{\bar{\omega}}(s)$ of the $O(Z^m)$ FD system

$$\varphi_{P,m}^{\bar{\omega}}(s) = \int_0^s G_{01}(s,t) \mathscr{P}_m^{\bar{\omega}}(t) dt. \tag{6.10}$$

In practice this integral is an integral over polynomials in t which makes it very simple to perform even at high-orders.

What now remains is fixing the two constants C_0 and C_1 in $O(Z^m)$. The constraint of regularity at the center requires $C_1 = 0$. Using the expansion of exterior solution

$$\bar{\omega}_>(s)/\Omega = 1 - \frac{2}{s^3 R^3} \sum_{m=0}^{n} I_m Z^m, \tag{6.11}$$

we impose the junction conditions $\bar{\omega}_{>,m}(1) \overset{!}{=} \bar{\omega}_{<,m}(1)$ and $\bar{\omega}'_{>,m}(1) \overset{!}{=} \bar{\omega}'_{<,m}(1)$ in $O(Z^m)$ on the stellar surface $s = 1$ and with them we can fix C_0 and the $O(Z^m)$ correction I_m to the moment of inertia.

Using the method described it is straight forward to compute the Z-expansion of $\bar{\omega}_<(s)$ and the expansion of the moment of inertia order by order. For the interior Schwarzschild solution we obtain

$$I^{\text{ISS}} = \frac{2ZR^3}{5}\left[1 + \frac{6}{7}Z + \frac{106}{105}Z^2 + \frac{316}{231}Z^3 + \frac{351872}{175175}Z^4\right] + O\left(Z^6\right), \tag{6.12}$$

$$\frac{\omega_>^{\text{ISS}}(r)}{\Omega} = \frac{2I}{s^3 R^3} = \frac{2I}{r^3}, \tag{6.13}$$

$$\begin{aligned}\frac{\omega_<^{\text{ISS}}(s)}{\Omega} = &\left(2 - \frac{6s^2}{5}\right)Z + \left(-\frac{99s^4}{70} + \frac{9s^2}{5} + \frac{3}{10}\right)Z^2 + \left(-\frac{199s^6}{105} + \frac{72s^4}{35} + \frac{9s^2}{25} + \frac{2}{7}\right)Z^3 \\ &+ \left(-\frac{3403s^8}{1232} + \frac{11s^6}{4} + \frac{549s^4}{1400} + \frac{261s^2}{700} + \frac{2869}{8400}\right)Z^4 \\ &+ \left(-\frac{851547s^{10}}{200200} + \frac{1541s^8}{385} + \frac{373s^6}{700} + \frac{927s^4}{2450} + \frac{3439s^2}{7000} + \frac{1753}{3850}\right)Z^5 + O\left(Z^6\right),\end{aligned} \tag{6.14}$$

where we used $\omega/\Omega = 1 - \bar{\omega}/\Omega$.

The exterior solution is completely determined by the moment of inertia. In $O\left(Z^0\right)$ it vanishes since it is directly related to the mass distribution. In order $O\left(Z^1\right)$ we recover a well known expression: the classical moment of inertia of a slowly rotating sphere of constant density $2/5ZR^3 = 2/5MR^2$. The higher-order terms in Z are GR corrections to that classical expression, which are positive.

The interior solution is given in form of a power series in Z of simple polynomials in even powers of s. In order Z^m the corresponding polynomial is of order s^{2m}. In zeroth-order the frame dragging frequency vanishes, which can be considered the Newtonian limit. In Newtonian gravity there is no dragging of inertial frames/ Lense-Thirring precession.

The fact that the moment of inertia of a slowly rotating IRF can be expressed as $I = I[Z]$ is known in literature [96]. This is in fact true for all stable NS with one parameter EoS. One can make the following argument for it: For a given one parameter EoS the choice of a central pressure/log-enthalpy determines the structure of the background star completely. Compactness is a unique dimensionless parameter on a stable equilibrium sequence, which in turn means the mapping between compactness and central pressure/log-enthalpy is bijective. All global parameters for a given EoS can therefore be expressed as functions of Z. We use this fact throughout this work extensively as we often choose Z to specify configurations for a given EoS. In $O\left(\Omega^1\right)$ the moment of inertia is independent of Ω and therefore only depends on the background star. Which implies $I = I[Z]$. Since Z is dimensionless but I has dimensions L^3 in GU units it has to be possible to split $I[Z]$ into a dimensionless part $f[Z]$ and a part with dimensions L^3. In terms of SI units a natural choice is $I = M[Z]R[Z]^2 f[Z]$, but in GU units a proper power of every other dimensional background star parameter would work as well.

Fitting $f[Z]$ to numerical results for the moment of inertia is done frequently in literature. For IRF stars J. M. Lattimer and M. Prakash (LP) presented the fit

$$I_{\text{IRF}}^{\text{LP2000}} = \frac{2MR^2}{5}\left[1-0.87Z-0.3Z^2\right]^{-1} \tag{6.15}$$

in [96].

In Fig. 6.1 we compare numerical results for the moment of inertia and the central frame-dragging frequency to the analytical Z-series results. For the moment of inertia we have also included the LP-fit.

Our Z-series results converge uniformly to the numerical result for the moment of inertia when going to higher-orders in Z for all configurations below the Schwarzschild-Buchdahl limit. When using the $O\left(Z^{20}\right)$ expansion numerical and analytical results agree in double precision below $Z \sim 0.1$. This is the accuracy limit of our implementation. Above $Z \sim 0.2$ our $O\left(Z^5\right)$ series expansion for I from eq. (6.12) and the LP-fit have similar discrepancies to the numerical results. The LP-fit is inferior to our $O\left(Z^5\right)$ series expansion below $Z \sim 0.2$ and is not competitive to our higher-order expansions. To be fair the LP fit contains only 2 correction terms in Z so a higher-order fit might perform better.

For the central value of the frame-dragging frequency our Z-series solutions converge uniformly to the numerical result below the $P_c = \rho_c$ limit of $Z_{\text{C}} = 3/8$. For $Z \lesssim 0.15$ we can clearly see the numerical errors of our implementation. The high-order Z-series solutions are more accurate than our numerical implementation for low compactnesses. This shows the potency of the analytic series solutions as a means to benchmark numerics. The intrinsic error estimates for the $O\left(\Omega^1\right)$ angular momentum from comparing asymptotic and integral values ΔJ are of the same order of magnitude as the ones determined by comparison with the $O\left(Z^{20}\right)$ series. ΔJ turns out to be a robust error estimate in $O\left(\Omega^1\right)$.

For higher compactnesses the expansion does not converge against the numerical results. The reason for that is simple: as Z approaches the Schwarzschild-Buchdahl limit, central pressures increase rapidly and asymptotically approach infinity. To counter this pressure contribution and to keep masses finite the g_{tt} metric potential ν at the stellar center approaches zero. In this case the third coefficient of the ODE (6.2), $\mathscr{D}_3^{\bar{\omega}}$, approaches infinity. The Taylor series expansion of $\mathscr{D}_i^{\bar{\omega}}$ around $Z = 4/9$ can not reproduce this behavior and therefore the Z-Series for $\omega_<^{\text{ISS}}(s)$ does not converge against numerical results for small radii. This has however surprisingly little effect on $\omega_<^{\text{ISS}}(s)$ at larger $s \gtrsim 0.5$ and on the moment of inertia.

Slowly rotating, constant density configurations have been studied by numerous authors. One of the first papers using the classical HT formalism was the one of S. Chandrasekhar and J. C. Miller [104] in which they applied the HT formalism to constant density configurations. More recently, in 2017, C. Posada [105] also studied constant density stars in the HT formalism. But none of those authors have tried to construct a analytic solution for the $O\left(\Omega^1\right)$ FD equation. Quite surprisingly it seems that no one has tried such an expansion in Z of the ODE (6.2). LP claimed in their compendium "*Neutron Star Structure and Equation of State*" [96]:

> "*Unfortunately, an analytic representation of ω or the moment of inertia for any of the three exact solutions is not available.*" – J. M. Lattimer and M. Prakash, 2000 [96],

where they refer to the interior Schwarzschild solution, the TVII solution and the Buchdahl solution [106]. For the ISS we were able to find an analytical solution of the frame-dragging in the literature [107]: P. G. Whitman used complicated coordinate transformations to solve the FD eq. for the ISS using Heun functions. Our expansion results in much simpler expressions involving only powers of s and Z.

In this subsection we presented such an analytic representation for the ISS in form of a series in Z. In the following subsection we will present an analogous series solution for TVII configurations.

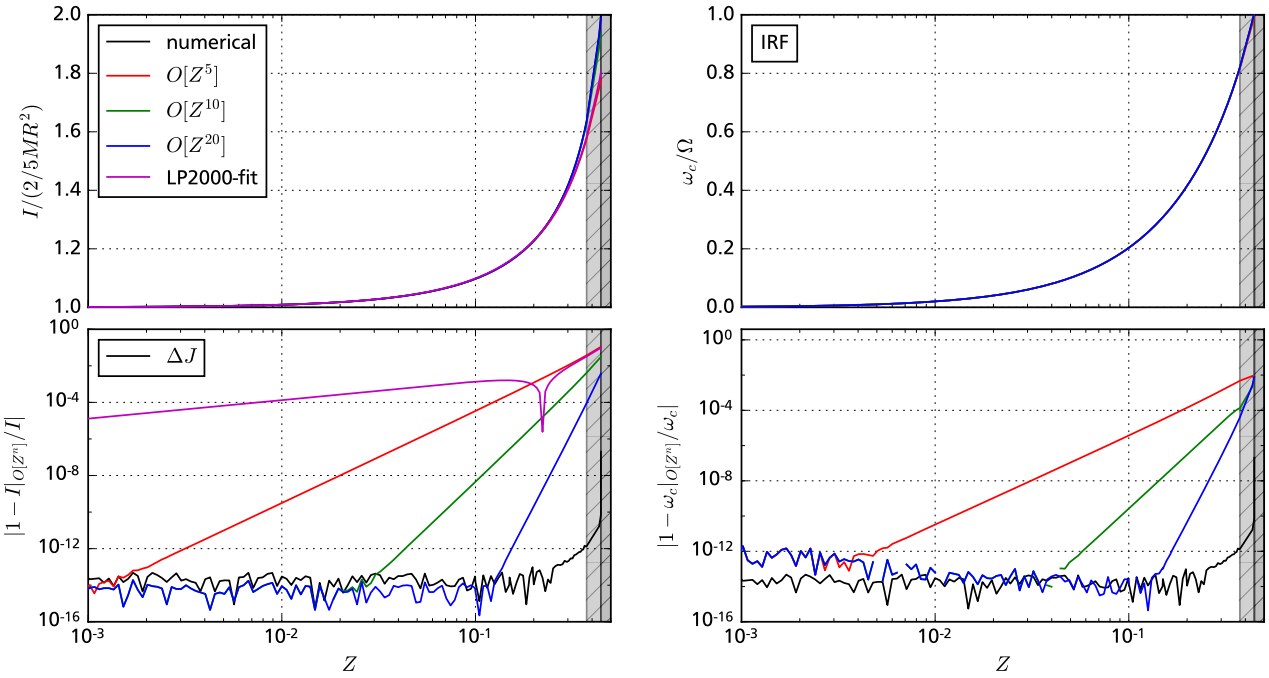

Figure 6.1: Comparison between numerical results and analytic Z-series solutions. In the plot for the moment of inertia (left) we included the LP-fit from eq. (6.15). On the right we display results for the central value of the frame dragging-frequency. As an intrinsic numerical error estimate we plotted ΔJ in black.

6.1.2 Tolman VII solution

Completely analogous to the expansion of the ISS solution a Z-series solution of the FD eq. is also possible for TVII background configurations. The ODE (6.6) holds also for TVII background configurations. For a fixed μ the expansion works completely similar. The fact that the algebraic structure of the TVII solution is much more complex makes series expanding ($\mathscr{D}_i^{\tilde{\omega}}$) more involved but it is still possible to do even to high orders in Z. We will give expressions for TVII configurations with $\mu = 1$, $3/4$, $1/2$ and $1/4$ but the expansion is possible for arbitrary $\mu \in [1,0)$. We derive the following expressions for the moment of inertia

$$I_{\mathrm{TVII}_1} = \frac{2ZR^3}{7}\left[1+\frac{112Z}{99}+\frac{72872Z^2}{45045}+\frac{22349744Z^3}{8729721}\right]+O\left(Z^5\right), \tag{6.16}$$

$$I_{\mathrm{TVII}_{3/4}} = \frac{26ZR^3}{77}\left[1+\frac{4798Z}{4719}+\frac{4475242Z^2}{3374085}+\frac{32413627628Z^3}{16783373607}\right]+O\left(Z^5\right), \tag{6.17}$$

$$I_{\mathrm{TVII}_{1/2}} = \frac{18ZR^3}{49}\left[1+\frac{5882Z}{6237}+\frac{2580394Z^2}{2207205}+\frac{3394223900Z^3}{2072972979}\right]+O\left(Z^5\right), \tag{6.18}$$

$$I_{\mathrm{TVII}_{1/4}} = \frac{46ZR^3}{119}\left[1+\frac{34570Z}{38709}+\frac{321357286Z^2}{299414115}+\frac{1452334671500Z^3}{986449743279}\right]+O\left(Z^5\right). \tag{6.19}$$

Again we recover in non-vanishing LO(Z^1) the corresponding classical moments of inertia. For a spherically symmetric body with radius R and density distribution $\rho(r)$ the Newtonian expression for the moment of inertia is

$$I_{\text{cl.}} = \int_0^{2\pi}\int_0^{\pi}\int_0^{R} \rho(r)(r^2\sin\theta)^2 r^2 \sin\theta\, dr d\theta d\phi = \frac{8}{3}\pi R^3 \int_0^1 \rho(s) s^4 ds, \tag{6.20}$$

which in case of a TVII configuration can be integrated, by using eq. (3.74b), to

$$I_{\text{cl.}}^{\text{TVII}}[\mu] = \frac{2ZR^3}{7}\frac{5\mu-7}{3\mu-5}. \tag{6.21}$$

The GR corrections are again positive and increase the moment of inertia.

The interior solutions for the FD eq. for TVII configurations are

$$\omega_<^{\text{TVII}_1}(s) = \left(\frac{15s^4}{14} - 3s^2 + \frac{5}{2}\right)Z + \left(-\frac{2055s^8}{1232} + \frac{955s^6}{126} - \frac{645s^4}{56} + 6s^2 + \frac{85}{336}\right)Z^2 + O\left(Z^3\right), \tag{6.22}$$

$$\omega_<^{\text{TVII}_{3/4}}(s) = \left(\frac{45s^4}{77} - \frac{24s^2}{11} + \frac{25}{11}\right)Z + \left(-\frac{18495s^8}{37268} + \frac{7640s^6}{2541} - \frac{5085s^4}{847} + \frac{477s^2}{121} + \frac{115}{484}\right)Z^2 + O\left(Z^3\right), \tag{6.23}$$

$$\omega_<^{\text{TVII}_{1/2})}(s) = \left(\frac{15s^4}{49} - \frac{12s^2}{7} + \frac{15}{7}\right)Z + \left(-\frac{2055s^8}{15092} + \frac{3820s^6}{3087} - \frac{1215s^4}{343} + \frac{141s^2}{49} + \frac{1055}{4116}\right)Z^2 + O\left(Z^3\right), \tag{6.24}$$

$$\omega_<^{\text{TVII}_{1/4}}(s) = \left(\frac{15s^4}{119} - \frac{24s^2}{17} + \frac{35}{17}\right)Z + \left(-\frac{2055s^8}{89012} + \frac{7640s^6}{18207} - \frac{4485s^4}{2023} + \frac{645s^2}{289} + \frac{6775}{24276}\right)Z^2 + O\left(Z^3\right). \tag{6.25}$$

In order Z^m the polynomial coefficient is of order s^{4m}.

In their paper [96] LP only discussed TVII configurations with vanishing residual surface density: in our nomenclature TVII_1 configurations. For TVII_1 LP give the following fit:

$$I_{\text{TVII}_1}^{\text{LP2000}} = \frac{2MR^2}{7}\left[1 - 1.1Z - 0.6Z^2\right]^{-1}. \tag{6.26}$$

In Fig. 6.2 we compare the TVII_1 series against numerical results and the corresponding LP fit. The overall situation is similar to the one encountered with the IRF EoS. For the angular momentum the Z-series converge uniformly against the numerical solution and below compactnesses of ~ 0.15 the $O\left(Z^{20}\right)$-series extends the accuracy of our numerical results. The numerical errors expected from the comparison between integral and asymptotic form of the angular momentum match the one found with aid of the analytic series. The LP fit works rather well at high compactnesses but ultimately can not keep up with higher-order analytic expansions. For the central frame-dragging frequency the Z-series converge uniformly against the numerical solution for causal configurations. When approaching the SB limit of TVII_1, see eq. (3.83a), the expansion of the ODE coefficients again fails to describe the extremal nature of the TVII_1 configuration approaching infinite central pressures.

The results for different μ are very similar to the ones for $\mu = 1$. In Fig. 6.7 we have included results for different values of μ. In case of the TVII solution it is not so surprising that such analytic series solutions are not known in literature, since interest in the solution in general increased only recently.

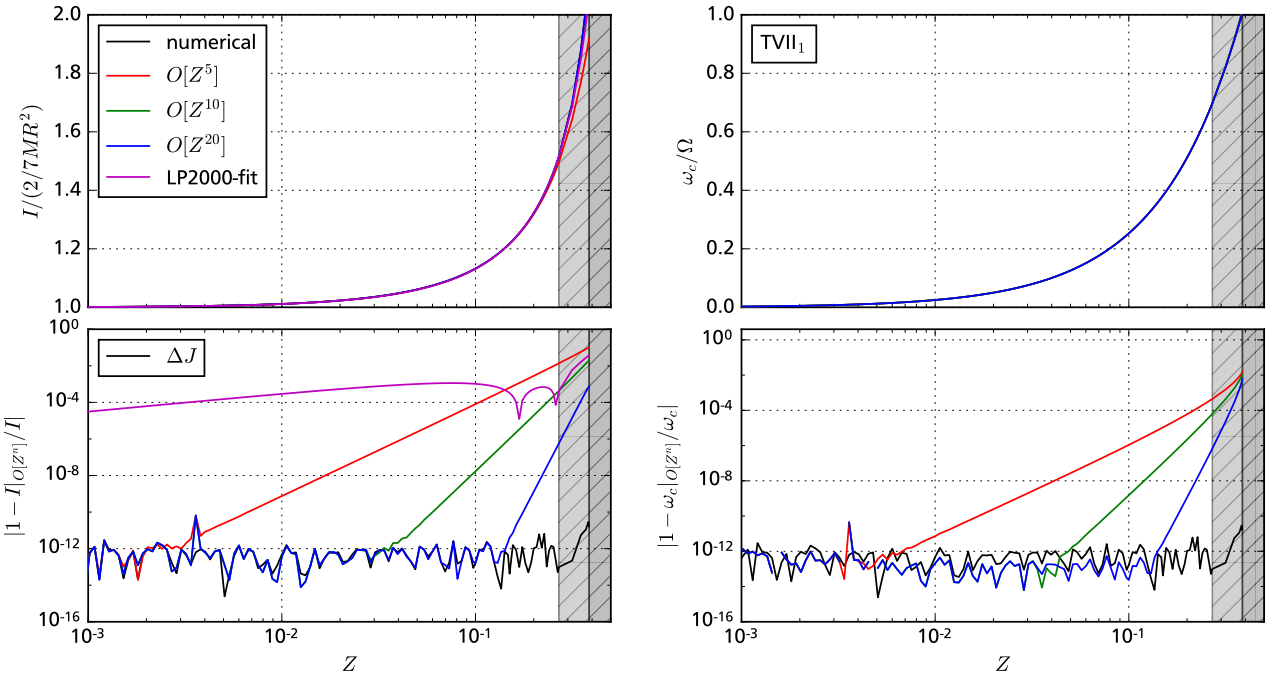

Figure 6.2: Comparison between numerical results and analytic Z-series solutions for TVII$_1$ stars. In the plot for the moment of inertia (left) we included the LP-fit from eq. (6.26). On the right we display results for the central value of the frame dragging-frequency. As an intrinsic numerical error estimate we plotted ΔJ in black.

6.2 Compactness-series solutions of the relativistic Grad-Shafranov equation

The $O\left(B^1\right)$ relativistic Grad-Shafranov eq. (3.104) for dipolar fields is algebraically very similar to the FD eq. Both are second-order ODEs for $l = 1$ quantities. In this section we will use the same techniques used in the previous Sec. 6.1, to construct analytic solutions in form of a series in Z for the relativistic Grad-Shafranov equation.

6.2.1 Interior Schwarzschild solution

The GS equation for an IRF star is a complicated but analytic inhomogeneous second-order ODE:

$$\begin{aligned} 0 = a_\phi^{<\prime\prime}(s) &+ \frac{2sZ\left(4s^2Z+3\sqrt{1-2Z}\sqrt{1-2s^2Z}-2\right)}{(2s^2Z-1)\left(2s^2Z+3\sqrt{1-2Z}\sqrt{1-2s^2Z}-1\right)}a_\phi^{<\prime}(s) \\ &- \frac{2}{s^2-2s^4Z}a_\phi^{<}(s) - c_{j\phi}R^2\frac{6s^2Z\sqrt{1-2Z}}{(2s^2Z-1)\left(3\sqrt{1-2Z}-\sqrt{1-2s^2Z}\right)} \end{aligned} \tag{6.27}$$

$$\equiv \mathscr{D}_i^{a\phi}\, v_{a\phi}^i - P_{a\phi}, \text{ with } v_{a\phi}^i = \left(a_\phi^<(s), a_\phi^<(s), a_\phi^<(s)\right)^{\mathrm{T}}. \tag{6.28}$$

The inhomogeneous part $P_{a\phi}$ scales with $c_{j\phi}R^2$ while the homogeneous system is naturally scale independent. The solution of eq. (6.28) will therefore be of the form $a_\phi^<(s) = c_{j\phi}R^2\tilde{a}_\phi^<(s)$, where the background star dependence of $\tilde{a}_\phi^<(s)$ is solely based on Z. Using the same technique discussed previously for the expansion of eq. (6.2) we derive the pure $O\left(Z^m\right)$ term of the ODE (6.28):

$$a^{<\prime\prime}_{\phi,m}(s) - \frac{2}{s^2} a^{<}_{\phi,m}(s) = P_{a\phi,m} - \sum_{j=1}^{m} (\mathscr{D}_i^{a\phi})_j (v^i_{a\phi})_{m-j} \equiv \mathscr{P}_m^{a\phi}(s). \tag{6.29}$$

The homogeneous system is solved by the two linearly independent functions

$$\varphi_2(s) = C_2 s^2, \tag{6.30}$$

$$\varphi_3(s) = \frac{C_3}{s}. \tag{6.31}$$

From these two solutions we can construct the Green's function

$$G_{23}(s,t) = -\begin{vmatrix} \varphi_2(s) & \varphi_3(s) \\ \varphi_2(t) & \varphi_3(t) \end{vmatrix} \Big/ \begin{vmatrix} \varphi_2(t) & \varphi_3(t) \\ \varphi_2'(t) & \varphi_3'(t) \end{vmatrix} = \frac{1}{3}\left(\frac{s^2}{t} - \frac{t^2}{s}\right) \tag{6.32}$$

and with it a particular solution $\varphi^{a\phi}_{P,m}(s)$ of the $O(Z^m)$ system

$$\varphi_{Q,m}(s) = \int_0^s G_{23}(s,t) \mathscr{P}_m^{a\phi}(t) dt. \tag{6.33}$$

The constraint of regularity at the center requires $C_3 = 0$. Using the $O(Z^m)$ expansion of exterior solution (3.114) we can impose the junction conditions $a^{<}_{\phi,m}(1) \stackrel{!}{=} a^{>}_{\phi,m}(1)$ and $a^{<\prime}_{\phi,m}(1) \stackrel{!}{=} a^{>\prime}_{\phi,m}(1)$ in $O(Z^m)$ on the stellar surface $s = 1$ and with them we can fix C_2 and the $O(Z^m)$ correction μ_m to the stars dipole moment.

For the interior Schwarzschild solution the expression for the dipole moment μ and the interior solution for a_ϕ read

$$\mu^{\mathrm{ISS}} = -\frac{c_{j\phi} Z R^3}{5}\left[1 - \frac{6Z}{7} - \frac{41Z^2}{105} - \frac{262Z^3}{825} - \frac{56517Z^4}{175175}\right] + O\left(Z^6\right), \tag{6.34}$$

$$\begin{aligned} \frac{a_\phi^{<,\mathrm{ISS}}(s)}{c_{j\phi} R^2} = {} & \left(\frac{s^2}{2} - \frac{3s^4}{10}\right) Z + \left(-\frac{69s^6}{280} + \frac{3s^4}{20} + \frac{9s^2}{40}\right) Z^2 + \left(-\frac{281s^8}{840} + \frac{3s^6}{8} - \frac{63s^4}{200} + \frac{587s^2}{1400}\right) Z^3 \\ & + \left(-\frac{2939s^{10}}{6160} + \frac{3s^8}{7} + \frac{117s^6}{700} - \frac{2637s^4}{3500} + \frac{7079s^2}{8400}\right) Z^4 \\ & + \left(-\frac{1459s^{12}}{2002} + \frac{199s^{10}}{308} - \frac{169s^8}{4200} + \frac{23847s^6}{49000} - \frac{12461s^4}{7000} + \frac{405373s^2}{231000}\right) Z^5 + O\left(Z^6\right). \end{aligned} \tag{6.35}$$

Again the non-vanishing LO terms are $O\left(Z^1\right)$. The magnetic field is directly coupled to the matter distribution. It is generated by the current function which in lowest-order in Z is proportional to the density gradient, which is an $O\left(Z^1\right)$ expression. Reintroducing the density one can rewrite the LO terms as

$$a^{<,\mathrm{ISS}}_{\phi,\mathrm{cl.}}(s) = \frac{2}{15} c_{j\phi} \rho_c \pi r^2 (5R^2 - 3r^2), \tag{6.36a}$$

$$a^{>,\mathrm{ISS}}_{\phi,\mathrm{cl.}}(s) = -\frac{\mu}{sR} = 4 c_{j\phi} \rho_c \pi R^5 \frac{1}{15r}, \tag{6.36b}$$

$$\mu^{\mathrm{ISS}}_{\mathrm{cl.}} = -\frac{4}{15} c_{j\phi} \rho_c \pi R^5. \tag{6.36c}$$

The central magnetic field and polar magnetic field on the stellar surface are related to $c_{j\phi}$ by

$$B^{\mathrm{ISS}}_{0,\mathrm{cl.}} = -Z c_{j\phi} = -\frac{4}{3} c_{j\phi} \rho_c \pi R^2, \tag{6.37a}$$

$$B^{\mathrm{ISS}}_{p,\mathrm{cl.}} = -\frac{2Z}{5} c_{j\phi} = -\frac{8}{15} c_{j\phi} \rho_c \pi R^2. \tag{6.37b}$$

The solution (6.36) was found in this form 1953 by V. C. A. Ferraro [108] as the classical solution for the dipole field of an incompressible fluid sphere. To the best of our knowledge we are the first to give GR corrections to this solution in form of an analytic series in the compactness. While searching for the Ferraro's solution as classical limit in our approach we discovered the possibility for a Z-series solution of the linearized, relativistic Grad-Shafranov equation. After constructing such a solution we successfully applied the technique to the frame-dragging equation. The order in which we discovered those solutions and in which we present them in this thesis are reversed.

Fig. 6.3 shows the surface and central polar magnetic field obtained from our series normalized to the $O\left(Z^1\right)$ values of Ferraro's solution as well as numerical results. Again we find a good agreement within the compactness bounds discussed in the previous section of this chapter. Fig. 6.4 shows corresponding results for the magnetic dipole moment and the electric quadrupole moment. For the latter we combined the results from Sec. 6.1.1 with the results of this section. In LO we recover the classical result for $\mathscr{Q}_{\mathrm{E}}$, which using eqs. (3.150) and (6.36c) reads

$$\mathscr{Q}^{\mathrm{ISS}}_{E,\mathrm{cl.}} = \frac{1}{3}\mu\Omega R^2 = -\frac{4}{45}\pi\rho_c R^7 c_{j\phi}\Omega. \tag{6.38}$$

Using the higher-order terms of our analytic series solution we can again check the numerical accuracy of our magnetar model. For compact NS relative numerical errors are of the order 10^{-12}, while for larger configurations with smaller compactness errors increase towards $\sim 10^{-6}$. We can compare this extrinsic error estimates to an intrinsic error estimate: for the $O\left(\Omega^1 B^1\right)$ quantities we use the relative difference between interior and surface charge ΔQ from eq. (4.2). We plotted the error estimate ΔQ in the lower panels of Fig. 6.3 and Fig. 6.4. For most quantities and compactnesses ΔQ turns out to be a rather conservative error estimate, when comparing it to the $\mathrm{O}\left(Z^{20}\right)$ extrinsic error estimate. Especially at higher compactnesses ΔQ overestimates numerical errors in other quantities by a few orders of magnitude. At low compactnesses ΔQ underestimates the errors in the electric quadrupole moment $\mathscr{Q}_{\mathrm{E}}$ significantly by four orders of magnitude.

6.2.2 Tolman VII solution

The expansion of the GS eq. with TVII background stars is technically completely analogous to the ISS case. In this subsection we use $\tilde{\mu}$ for the TVII parameter and μ for the magnetic dipole moment. We found the following GR corrections to the magnetic dipole moment

$$\mu_{\mathrm{TVII}_1} = -\frac{c_{j\phi} Z R^3}{7}\left[1 - \frac{8Z}{9} - \frac{6791Z^2}{15015} - \frac{940138Z^3}{2567565}\right] + O\left(Z^5\right), \tag{6.39}$$

$$\mu_{\mathrm{TVII}_{3/4}} = -\frac{13 c_{j\phi} Z R^3}{77}\left[1 - \frac{362Z}{429} - \frac{1365553Z^2}{3374085} - \frac{143395298Z^3}{448753305}\right] + O\left(Z^5\right), \tag{6.40}$$

$$\mu_{\mathrm{TVII}_{1/2}} = \frac{9 c_{j\phi} Z R^3}{49}\left[1 - \frac{478Z}{567} - \frac{2620763Z^2}{6621615} - \frac{25122795 82Z^3}{7926073155}\right] + O\left(Z^5\right), \tag{6.41}$$

$$\mu_{\mathrm{TVII}_{1/4}} = \frac{23 c_{j\phi} Z R^3}{119}\left[1 - \frac{130Z}{153} - \frac{39175933Z^2}{99804705} - \frac{92088336358Z^3}{290132277435}\right] + O\left(Z^5\right), \tag{6.42}$$

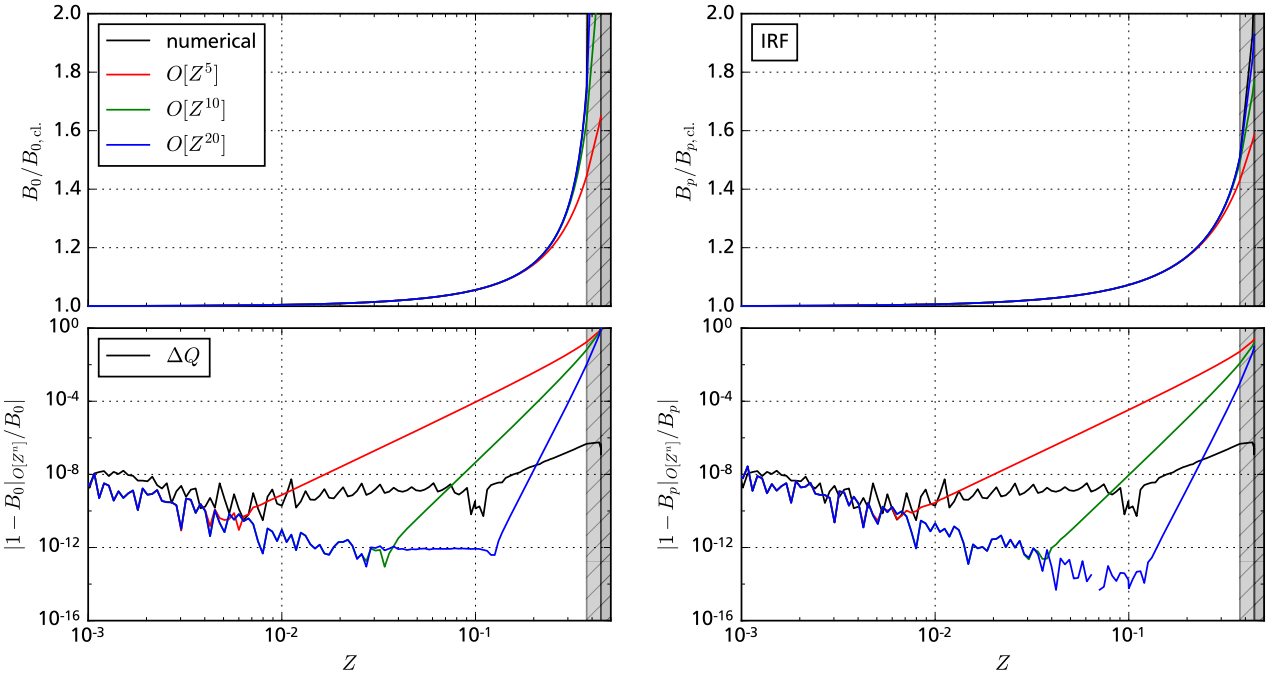

Figure 6.3: Comparison between numerical results and analytic Z-series solutions for IRF stars. Central magnetic field (left) and polar surface magnetic field (right) are normalized to the classical results. As an intrinsic numerical error estimate we plotted ΔQ in black.

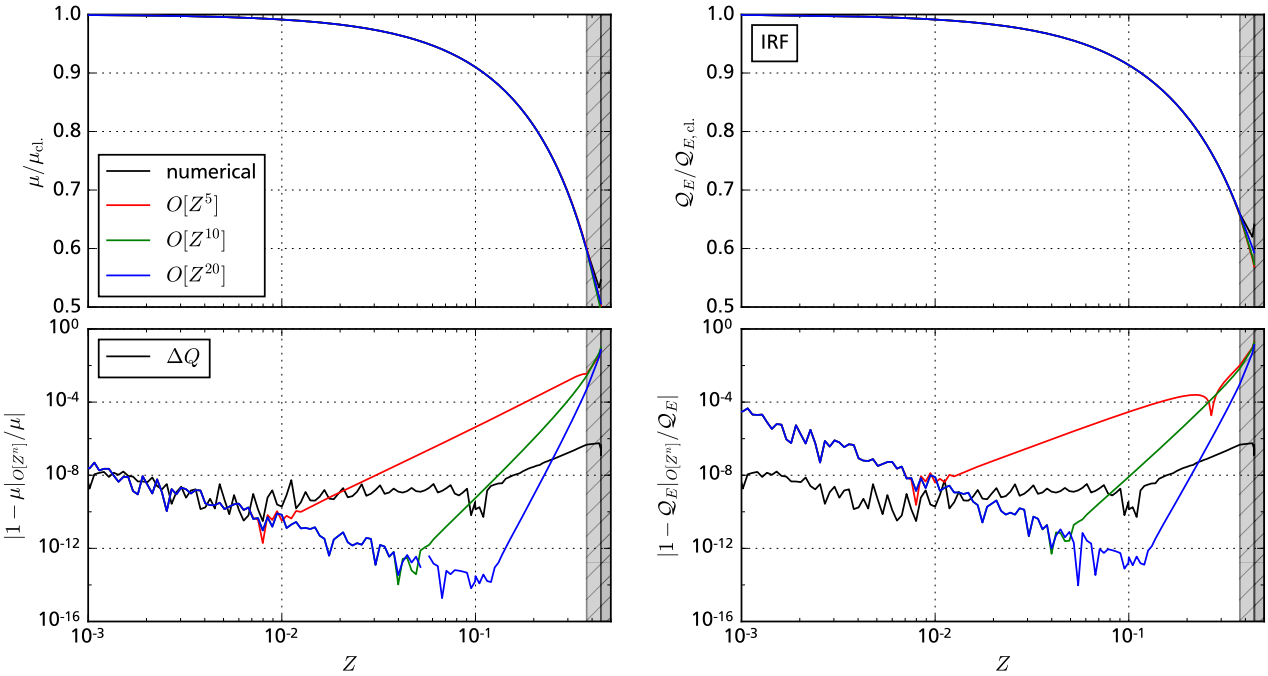

Figure 6.4: Comparison between numerical results and analytic Z-series solutions for IRF stars. On the left we show results for the magnetic dipole moment and on the right results for the electric quadrupole moment normalized to the classical results. To obtain the electric quadrupole moment we combined the results of the $O\left(\Omega^1\right)$ Z-series expansion and the $O\left(B^1\right)$ expansion of this section. As an intrinsic numerical error estimate we plotted ΔQ in black.

and for the interior solution we found

$$\frac{a_{\phi,<}^{\mathrm{TVII}_1}(s)}{c_{j\phi}R^2} = \frac{1}{56}s^2\left(15s^4-42s^2+35\right)Z - \frac{s^2\left(675s^8-2882s^6+3780s^4-1134s^2-615\right)Z^2}{2016} + O\left(Z^3\right), \tag{6.43}$$

$$\frac{a_{\phi,<}^{\mathrm{TVII}_{3/4}}(s)}{c_{j\phi}R^2} = \frac{1}{308}s^2\left(45s^4-168s^2+175\right)Z - \frac{s^2\left(2025s^8-11528s^6+19935s^4-7434s^2-5250\right)Z^2}{20328} + O\left(Z^3\right), \tag{6.44}$$

$$\frac{a_{\phi,<}^{\mathrm{TVII}_{1/2}}(s)}{c_{j\phi}R^2} = \frac{3}{196}s^2\left(5s^4-28s^2+35\right)Z - \frac{s^2\left(675s^8-5764s^6+14445s^4-6426s^2-5910\right)Z^2}{24696} + O\left(Z^3\right), \tag{6.45}$$

$$\frac{a_{\phi,<}^{\mathrm{TVII}_{1/4}}(s)}{c_{j\phi}R^2} = \frac{1}{476}s^2\left(15s^4-168s^2+245\right)Z, - \frac{s^2\left(675s^8-11528s^6+54405s^4-28350s^2-33510\right)Z^2}{145656} + O\left(Z^3\right). \tag{6.46}$$

In non-vanishing LO(Z^1) we again recover a classical solution. In the Newtonian limit $c \to \infty$ the metric gets flat and pressure contributions become negligible. The homogeneous part of eq. (3.100) simplifies to $a''_{\phi,\mathrm{cl}} - 2a_{\phi,\mathrm{cl}}/s^2$ while the inhomogeneous part is now only governed by the density distribution. The classical GS eq. for a pure dipole field reads

$$a''_{\phi,\mathrm{cl.}}(s) - \frac{2a_{\phi,\mathrm{cl.}}(s)}{s^2} = -s^2\rho(s). \tag{6.47}$$

For the TVII EoS constructing a solution to this ODE is a simple task with the method described in this section. A generalized version of Ferraro's solution for TVII density gradients reads

$$a_{\phi,\mathrm{cl.}}^{<,\tilde{\mu}}(s) = \frac{1}{105}\pi\rho_c R^4 s^2\left(70-42s^2+(15s^4-35)\tilde{\mu}\right)c_{j\phi}, \tag{6.48a}$$

$$a_{\phi,\mathrm{cl.}}^{>,\tilde{\mu}}(s) = -\frac{\mu_{\mathrm{cl.}}}{Rs} = -\frac{4\pi\rho_c R^4(7-5\tilde{\mu})c_{j\phi}}{105s}, \tag{6.48b}$$

$$\mu_{\mathrm{cl.}}^{\tilde{\mu}} = -\frac{4}{105}\pi\rho_c R^5(7-5\tilde{\mu})c_{j\phi} \tag{6.48c}$$

and related parameters are

$$B_{0,\mathrm{cl.}} = -\frac{5(2-\tilde{\mu})}{10-6\tilde{\mu}}Zc_{j\phi} = -\frac{2}{3}(2-\tilde{\mu})c_{j\phi}\rho_c\pi R^2, \tag{6.49a}$$

$$B_{p,\mathrm{cl.}} = -\frac{2(7-5\tilde{\mu})}{7(3\tilde{\mu}-5)}Zc_{j\phi} = -\frac{8}{105}(7-5\tilde{\mu})c_{j\phi}\rho_c\pi R^2, \tag{6.49b}$$

$$\mathcal{Q}_{E,\mathrm{cl.}} = \frac{1}{3}\mu_{\mathrm{cl.}}\Omega R^2 = -\frac{4}{315}(7-5\tilde{\mu})\pi\rho_c R^7 c_{j\phi}\Omega. \tag{6.49c}$$

As expected the generalized version of Ferraro's solution for TVII density gradients reduces to the classical one in the $\tilde{\mu} \to 0$-limit.

In Fig. 6.5 and Fig. 6.6 we show numerical results for TVII_1. In terms of accuracy and viability of ΔQ as an error estimate we come to the same conclusion as in the discussion for the IRF Z-series solution for the GS equation. In the right panel of Fig. 6.7 we display results for different values of μ. Again we find no surprising results.

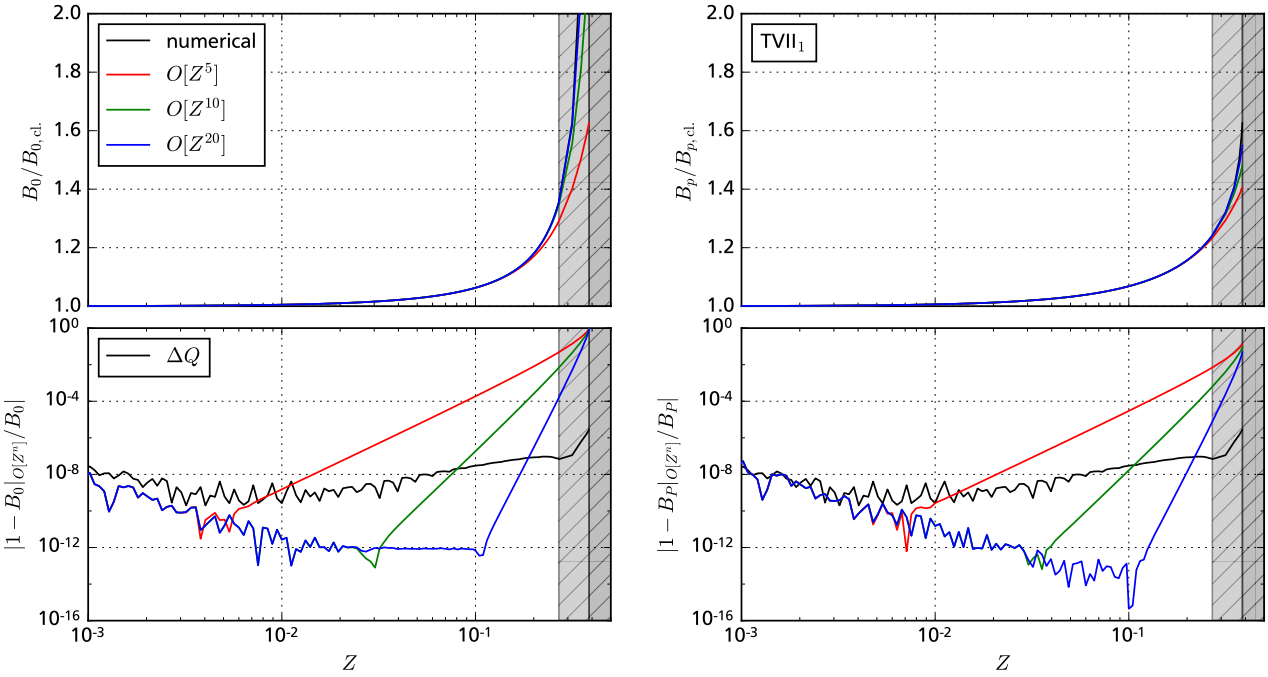

Figure 6.5: Comparison between numerical results and analytic Z-series solutions for TVII$_1$ stars. Central magnetic field (left) and polar surface magnetic field (right) are normalized to the classical results. As an intrinsic numerical error estimate we plotted ΔQ in black.

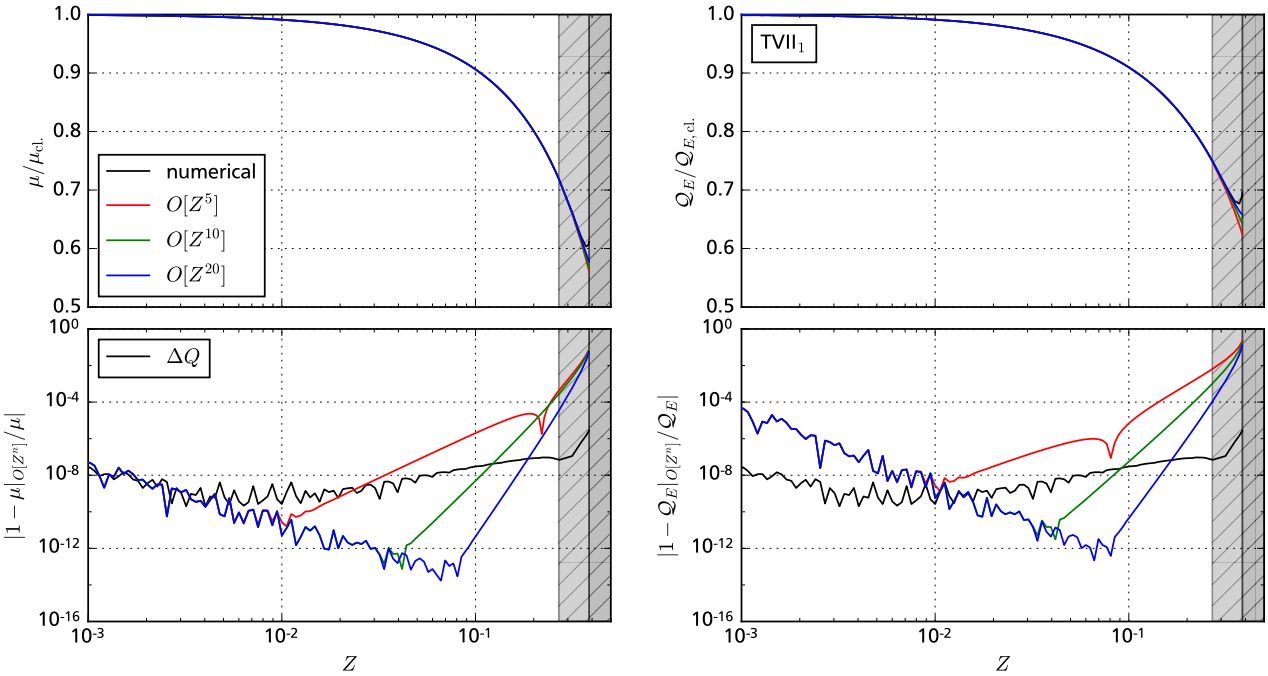

Figure 6.6: Comparison between numerical results and analytic Z-series solutions for TVII$_1$ stars. On the left we show results for the magnetic dipole moment and on the right results for the electric quadrupole moment normalized to the classical results. To obtain the electric quadrupole moment we combined the results of the $O\left(\Omega^1\right)$ Z-series expansion and the $O\left(B^1\right)$ expansion of this section. As an intrinsic numerical error estimate we plotted ΔQ in black.

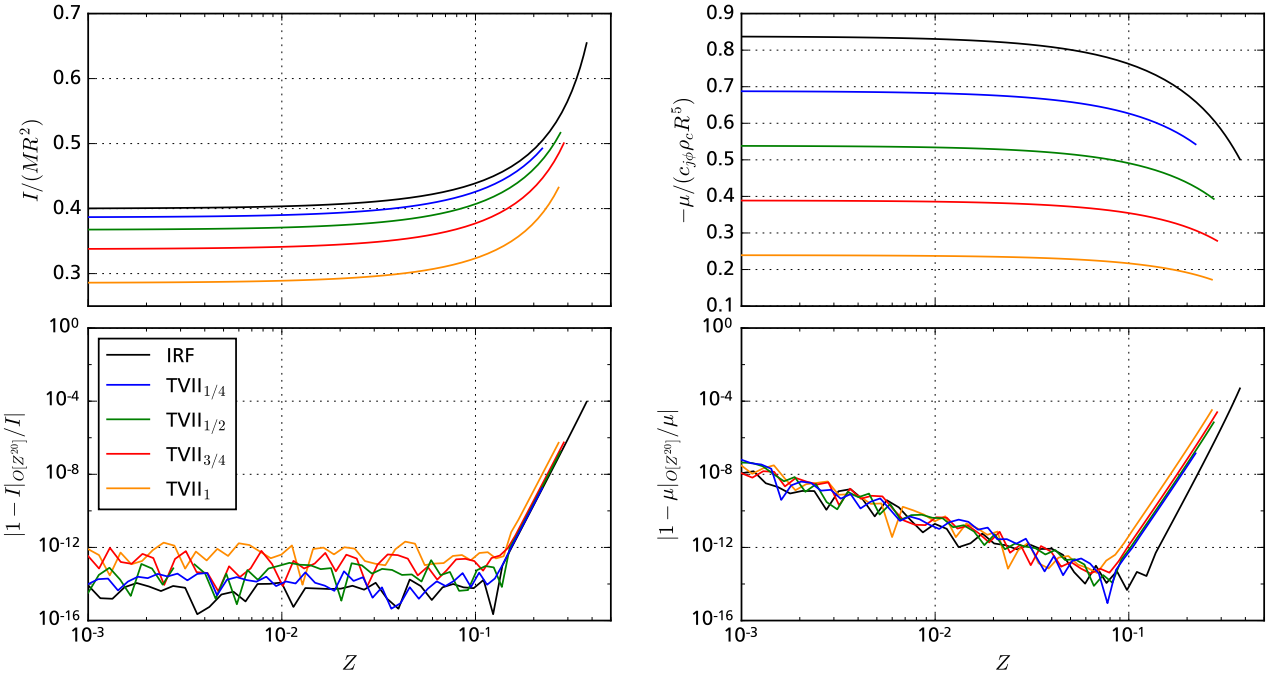

Figure 6.7: Comparison between numerical results and analytic Z-series solutions for four families of TVII configurations and for stars with IRF EoS. On the left we show results for moment of inertia and on the right results for the magnetic dipole moment.

7 Conclusion and outlook

After introducing the theoretical framework of the Einstein-Maxwell eqs., we gave a short introduction into the BGSM/BBGN formalism. Within the BGSM/BBGN formalism it is possible to solve the Einstein-Maxwell eqs. for magnetically deformed NS numerically exact.

In Chap. 3 we discussed in detail how to expand the Einstein-Maxwell equations in the magnetic field strength B and the rotation frequency around the metric of a spherical symmetric background star up to first-order in the angular velocity and second-order in the magnetic field. We discussed an ansatz which could be used to treat deformations originating from more complicated poloidal fields when considering higher multipole components in the metric perturbations. An extension to include toroidal fields by introducing additional metric perturbation would be possible for future research. During our discussion of the structure eqs. for the spherical symmetric background star we introduced the TOV eqs. in the log-enthalpy h. The TOV eqs. in h can be integrated very easily and the Bernoulli theorem in $O\left(B^1\Omega^1\right)$ describes a direct relation between h and the metric potential ν. We introduced two analytical interior solutions, the interior Schwarzschild and the Tolman VII solution, and derived the complete structure in O $\left(B^0\Omega^0\right)$ as well as the complete EoS for both.

Our treatment of electro-magnetic fields in the curved spacetime of an $O\left(B^0\Omega^0\right)$ could be extended to treat fields with higher multipole moments and for the exterior solutions and interior structure eqs. we already presented some expressions necessary for such an extension.

In our derivation of the HT structure eqs. in O $\left(B^2\Omega^1\right)$ we again used the log-enthalpy h as central thermodynamic quantity and identified it as a very convenient variable in the theory of perturbatively deformed NS. We kept a close connection during our derivation between the perturbative and exact model of the BGSM formalism. We solved the structure eqs. in the stellar exterior analytically and for the first step of numerical integration we derived $r \to 0$ expansions of all structure eqs. and metric potentials.

With the methods of Chap. 3 we discussed effects of non-vanishing net charge perturbatively. We presented expressions for the mass-shift and electro-magnetically induced frame-dragging effect.

We concluded Chap. 3 with a discussion of all important global parameters of the O $\left(B^2\Omega^1\right)$ model.

After a brief chapter about the implementation of the BGSM/BBGN formalism within the software library LORENE and about the numerical implementation of our structure eqs., we presented our numerical results.

In $O\left(B^0\right)$ we can report only very minor differences between results obtained with LORENE and solutions of the TOV eqs. We have tested our implementation of the TOV eqs. against the ISS and TVII solution with the conclusion that our implementation works with a very good accuracy. From the results for the background stars we could already see the potential of the TVII as an effective model of NS with realistic EoS.

For the classical $O\left(\Omega^1\right)$ HT frame-dragging frequency and the moment of inertia we presented perturbative results which are in very good agreement with the exact results from LORENE when considering low frequencies $f \lesssim 10\,\mathrm{Hz}$.

We discussed the effects of $O\left(B^0\right)$ background stars onto the electro-magnetic field described in $O\left(B^1\Omega^1\right)$. The electro-magnetic field configuration depends strongly on the EoS, since the current function is directly related to pressure and energy density.

With increasing compactness in the background star the magnetic deformations get weaker, since stars with increased compactness are much harder to deform. For stiff EoS the deformations are stronger compared to background stars with the same compactness but softer EoS. The main reason for this hierarchy is, that NS with stiff EoS have lower densities and pressures compared to NS with

softer EoS for stars with the same compactness. The magnetic contribution to the energy-momentum tensor is much more significant, when the pressure and energy density contributions from the fluid are smaller.

We have only recently discovered proficient parameter sets for the numerical iteration scheme of the `magstar` code, when considering configurations with electro-magnetic fields. We were not able to compute a lot of high accuracy results with our new parameter sets and we have not included specific results but nearly teased the conclusion we drew from our preliminary results. We plan to include and compute a sufficient amount of precise `magstar` results in the near future to round up this work.

In general we report a good agreement between the perturbative approach up to $O\left(B^2\Omega^1\right)$ and the numerically exact results obtained with LORENE up to central magnetic fields of $\sim 10^{13}\,\mathrm{T}$. This includes a good agreement for all measured SGR/AXP surface fields. We observe small deformations for central magnetic fields of $\lesssim 10^{13}\,\mathrm{T}$.

In Chap. 6 we derived novel compactness series solutions of the frame-dragging and relativistic Grad-Shafranov for TVII and IRF background stars. We used this expansion to benchmark the numerical accuracy of our O $\left(B^1\Omega^1\right)$ results and found a very good agreement between both. Especially the analytical solutions for TVII configurations are interesting since the TVII solution can be used to model realistic stars.

Applying this expansion approach to higher order rotational, magnetic or even tidal deformations could be very interesting. Studying the known universality relations [109] between moment of inertia/rotational quadrupole moment and tidal deformability with our analytic expansion approach for ISS and TVII could provide new insights into this phenomenon.

With our perturbative magnetar model, we present a numerically inexpensive option to study electro-magnetic fields and even deformations caused by such fields. This model is well suited to cover fast parameter spaces in terms of EoS and input parameters without the need for a lot of computing power. We have access to all global parameters and with the complete solution for the metric and the source terms we could implement and compute additional NS properties like tidal deformabilities.

The analytical exterior solutions of our O $\left(B^2\Omega^1\right)$ metric could be well suited to study geodetic motion of neutral or even charged particles.

Extending this model to include more complicated electro-magnetic fields would certainly be interesting but one should probably follow a different approach for implementation. Computing numerical exterior solutions would eliminate the need to compute them analytically which is a very time consuming task and might not be possible for higher-order corrections. With W_3 we already encountered a very complicated exterior solution and for terms with higher multipolarity the complexity will increase further. Using advanced numerical methods like a complex-plane strategy could eliminate the need to expand the structure equations around the coordinate singularity at $r = 0$.

While our perturbative approach is numerically inexpensive and rather easy to implement it is not very flexible. Including additional source terms, magnet field dependent EoS or non-zero temperature would be very difficult because the expansion assumes a one-parameter EoS.

Bibliography

[1] N. K. Glendenning, *Compact Stars - Nuclear Physics, Particle Physics and General Relativity*, 2nd ed., Springer, 2000.

[2] F. Özel and P. Freire, *Masses, Radii, and the Equation of State of Neutron Stars*, Annu. Rev. Astron. Astrophys. **54** (2016) 401–440, arXiv: 1603.02698 [astro-ph.HE].

[3] W. Lewin and M. van der Klis, *Compact Stellar X-ray Sources*, Cambridge University Press, Cambridge, 2006.

[4] D. Psaltis, F. Özel, and D. Chakrabarty, *Prospects for Measuring Neutron-star Masses and Radii with X-Ray Pulse Profile Modeling*, Astrophys. J. **787** (2014) 136, arXiv: 1311.1571 [astro-ph.HE].

[5] B. P. Abbott et al., *First Search for Gravitational Waves from Known Pulsars with Advanced LIGO*, Astrophys. J. **839** (2017) 12, arXiv: 1701.07709 [astro-ph.HE].

[6] *Isolated Neutron Stars: From the Surface to the Interior*, Sources of Gravitational Radiation, ed. by S. Zane, R. Turolla, and D. Page, Springer Netherlands, 2007.

[7] H. Tong, *Pulsar braking: magnetodipole vs. wind*, Science China Physics, Mechanics, and Astronomy **59**.1 (2016) 5752, arXiv: 1506.04605 [astro-ph.HE].

[8] D. Lai and S. L. Shapiro, *Cold equation of state in a strong magnetic field - Effects of inverse beta-decay*, Astrophys. J. **383** (1991) 745–751.

[9] S. Shapiro and S. Teukolsky, *Black Holes, White Dwarfs and Neutron Stars: The Physics of Compact Objects*, Wiley, 2008.

[10] A. Rabhi, C. Providencia, and J. Da Providencia, *Stellar matter with a strong magnetic field within density-dependent relativistic models*, J. Phys. **G35** (2008) 125201, arXiv: 0810.3390 [nucl-th].

[11] A. Rabhi et al., *Quark-hadron phase transition in a neutron star under strong magnetic fields*, J. Phys. **G36** (2009) 115204, arXiv: 0909.1114 [nucl-th].

[12] R. H. Casali, L. B. Castro, and D. P. Menezes, *Hadronic and hybrid stars subject to density-dependent magnetic fields*, Phys. Rev. **89**.1 (2014) 015805, arXiv: 1307.2651 [astro-ph.SR].

[13] M. Buballa and S. Carignano, *Inhomogeneous chiral symmetry breaking in dense neutron-star matter*, EPJ A **52** (2016) 57, arXiv: 1508.04361 [nucl-th].

[14] D. Bandyopadhyay, S. Chakrabarty, and S. Pal, *Quantizing Magnetic Field and Quark-Hadron Phase Transition in a Neutron Star*, Phys. Rev. Lett **79** (1997) 2176–2179, arXiv: astro-ph/9703066 [astro-ph].

[15] D. Chatterjee et al., *Consistent neutron star models with magnetic field dependent equations of state*, Mon. Not. Roy. Astron. Soc. **447** (2015) 3785, arXiv: 1410.6332 [astro-ph.HE].

[16] R. O. Gomes et al., *Highly magnetized neutron stars in a many-body forces formalism*, ArXiv e-prints (2017), arXiv: 1702.05685 [nucl-th].

[17] B. Franzon, V. Dexheimer, and S. Schramm, *A self-consistent study of magnetic field effects on hybrid stars*, Mon. Not. R. Astron. Soc. **456**.3 (2016) 2937–2945.

[18] S. Bonazzola et al., *Axisymmetric rotating relativistic bodies: A new numerical approach for 'exact' solutions*, Astron. Astrophys. **278** (1993) 421–443.

[19] M. Bocquet et al., *Rotating neutron star models with magnetic field*, Astron. Astrophys. **301** (1995) 757, arXiv: gr-qc/9503044 [gr-qc].

[20] C. Y. Cardall, M. Prakash, and J. M. Lattimer, *Effects of strong magnetic fields on neutron star structure*, Astrophys. J. **554** (2001) 322–339, arXiv: astro-ph/0011148 [astro-ph].

[21] K. Konno, T. Obata, and Y. Kojima, *Deformation of relativistic magnetized stars*, Astron. Astrophys. **352** (Dec. 1999) 211–216, arXiv: gr-qc/9910038 [gr-qc].

[22] K. Ioka and M. Sasaki, *Grad-Shafranov equation in noncircular stationary axisymmetric spacetimes*, Phys. Rev. **D67** (2003) 124026, arXiv: gr-qc/0302106 [gr-qc].

[23] K. Ioka and M. Sasaki, *Relativistic stars with poloidal and toroidal magnetic fields and meridional flow*, Astrophys. J. **600** (2004) 296–316, arXiv: astro-ph/0305352 [astro-ph].

[24] A. Colaiuda et al., *Relativistic models of magnetars: structure and deformations*, Mon. Not. Roy. Astron. Soc. **385** (2008) 2080–2096, arXiv: 0712.2162 [astro-ph].

[25] J. B. Hartle, *Slowly Rotating Relativistic Stars. I. Equations of Structure*, Astrophy. J. **150** (1967) 1005.

[26] National Institute of Standards and Technology, *CODATA Internationally recommended 2014 values of the Fundamental Physical Constants*, http://physics.nist.gov/cuu/Constants/, 2016.10.24 - 16:45.

[27] United States Naval Observatory (USNO), *Selected Astronomical Constants, 2014*, http://asa.usno.navy.mil/static/files/2014/Astronomical_Constants_2014.txt, 2016.10.24 - 16:45.

[28] A. Einstein, *Zur allgemeinen Relativitätstheorie*, Sitzungsber. preuss. Akad. Wiss. **47**.2 (1915) 799–801.

[29] A. Einstein, *Erklärung der Perihelbewegung des Merkur aus der allgemeinen Relativitätstheorie*, Sitzungsber. preuss. Akad. Wiss. **47**.2 (1915) 831–839.

[30] A. Einstein, *Die Feldgleichungen der Gravitation*, Sitzungsber. preuss. Akad. Wiss. **47**.2 (1915) 744–847.

[31] J. B. Hartle, *Gravity: An Introduction to Einstein's General Relativity*, Addison Wesley, 2003.

[32] H. Stephani, *Relativity: An Introduction to Special and General Relativity*, 3rd ed., Cambridge University Press, 2004.

[33] R. M. Wald, *General Relativity*, University of Chicago Press, 1984.

[34] T. W. Baumgarte and S. L. Shapiro, *Numerical Relativity - Solving Einstein's Equations on the Computer*, 3rd ed., Cambridge University Press, 2010.

[35] W. Cordeiro dos Santos, *Introduction to Einstein-Maxwell equations and the Rainich conditions* (2016), arXiv: 1606.08527 [gr-qc].

[36] R. Percacci, *General Relativity for Particle Physicists*, 2007, http://people.sissa.it/~percacci/lectures/genrel/, 2017.06.26 - 10:00.

[37] E. Gourgoulhon, *An Introduction to the theory of rotating relativistic stars*, CompStar 2010: School and Workshop on Computational Tools for Compact Star Astrophysics Ganil, Caen, France, February 8-16, 2010 (2010), arXiv: 1003.5015 [gr-qc].

[38] M. Alcubierre, *Introduction to 3+1 numerical relativity*, Oxford University Press, Oxford, 2008.

[39] E. Gourgoulhon, *3+1 formalism and bases of numerical relativity* (2007), arXiv: gr-qc/0703035 [gr-qc].

[40] R. L. Arnowitt, S. Deser, and C. W. Misner, *The Dynamics of general relativity*, Gen. Rel. Grav. **40** (2008) 1997–2027, arXiv: gr-qc/0405109 [gr-qc].

[41] J. W. York Jr., *Conformally invariant orthogonal decomposition of symmetric tensors on Riemannian manifolds and the initial-value problem of general relativity*, Journal of Mathematical Physics **14**.4 (1973) 456–464.

[42] J. W. York Jr., *Kinematics and dynamics of general relativity*, Sources of Gravitational Radiation, ed. by L. L. Smarr, 1979 83–126.

[43] R. C. Tolman, *On the Weight of Heat and Thermal Equilibrium in General Relativity*, Phys. Rev. **35** 8 (1930) 904–924.

[44] S. Bonazzola and E. Gourgoulhon, *Physics of sources of gravitational waves*, Proceedings of the International Summer School on Experimental Physics of Gravitational Waves (Urbino, Italy, 6-18 September 1999), ed. by M. Barone et al., World Scientific, 2000, p. 62–105.

[45] C. Palenzuela et al., *Beyond ideal MHD: towards a more realistic modelling of relativistic astrophysical plasmas*, Mon. Not. Roy. Astron. Soc. **394** (2009) 1727–1740, arXiv: 0810.1838 [astro-ph].

[46] E. Gourgoulhon and S. Bonazzola, *A formulation of the virial theorem in general relativity*, Class. Quantum Grav. **11**.2 (1994) 443.

[47] S. Bonazzola and E. Gourgoulhon, *A virial identity applied to relativistic stellar models*, Class. Quantum Grav. **11**.7 (1994) 1775.

[48] J. B. Hartle and K. S. Thorne, *Slowly Rotating Relativistic Stars. II. Models for Neutron Stars and Supermassive Stars*, Astrophy. J. **153** (1968) 807.

[49] J. B. Hartle, *Slowly Rotating Relativistic Stars. IX: Moments of Inertia of Rotationally Distorted Stars*, Astrophys. Space Sci. **24** (1973) 385–405.

[50] K. Konno, T. Obata, and Y. Kojima, *Flattening modulus of a neutron star by rotation and magnetic field*, Astron. Astrophys. **356** (2000) 234–237, arXiv: astro-ph/0001397 [astro-ph].

[51] L. Rezzolla, *Gravitational Waves from Perturbed Black Holes and Relativistic Stars* (2003), arXiv: gr-qc/0302025 [gr-qc].

[52] T. Regge and J. A. Wheeler, *Stability of a Schwarzschild Singularity*, Phys. Rev. **108** 4 (1957) 1063–1069.

[53] F. J. Zerilli, *Gravitational field of a particle falling in a schwarzschild geometry analyzed in tensor harmonics*, Phys. Rev. **D2** (1970) 2141–2160.

[54] B. Reina and R. Vera, *Revisiting Hartle's model using perturbed matching theory to second order: amending the change in mass*, Class. Quantum Grav. **32**.15 (2015) 155008, arXiv: 1412.7083 [gr-qc].

[55] A. M. Raghoonundun, *Exact Solutions for Compact Objects in General Relativity*, PhD thesis, University of Calgary (Canada), 2016, arXiv: arXiv:1604.08930 [gr-qc].

[56] K. Schwarzschild, *Über das Gravitationsfeld eines Massenpunktes nach der Einsteinschen Theorie*, Sitzungsber. preuss. Akad. Wiss. **7**.1 (1916) 189–196.

[57] K. Schwarzschild, *Über das Gravitationsfeld einer Kugel aus inkompressibler Flüssigkeit nach der Einsteinschen Theorie*, Sitzungsber. preuss. Akad. Wiss. **7**.1 (1916) 424–434.

[58] J. Oppenheimer and G. Volkoff, *On Massive Neutron Cores*, Phys. Rev. **55** (1939) 374.

[59] R. Tolman, *Static Solutions of Einstein's Field Equations for Spheres of Fluid*, Phys. Rev. **55** (1939) 364.

[60] F. Weber, *Pulsars as Astrophysical Laboratories for Nuclear and Particle Physics*, CRC Press, 1999.

[61] İ. Semiz, *OV or TOV?* (2016), arXiv: 1610.03049 [physics.hist-ph].

[62] R. Tolman, *Relativity, Thermodynamics, and Cosmology*, Oxford University Press, 1934.

[63] L. Herrera, *TOV or OV?, the whole story* (2016), arXiv: 1611.06364 [physics.hist-ph].

[64] P. J. Papasotiriou, V. S. Geroyannis, and S. A. Sanidas, *Numerical Methods for Solving the Relativistic Oppenheimer-Volkoff Equations*, Int. J. Mod. Phys. C **18** (2007) 1735–1746.

[65] L. Lindblom, *Determining the nuclear equation of state from neutron-star masses and radii*, Astrophys. J. **398** (1992) 569–573.

[66] L. Lindblom, *Phase transitions and the mass-radius curves of relativistic stars*, Phys. Rev. D **58**.2 (1998) 024008, arXiv: gr-qc/9802072 [gr-qc].

[67] S. Postnikov, *Topics in the Physics and Astrophysics of Neutron Stars*, Electronic Dissertation, Ohio University, 2010, retrieved from https://etd.ohiolink.edu/, 16.12.12 - 12:30.

[68] H. A. Buchdahl, *General Relativistic Fluid Spheres*, Phys. Rev. **116** 4 (1959) 1027–1034.

[69] S. Weinberg, *Gravitation and Cosmology: Principles and Applications of the General Theory of Relativity*, New York: Wiley, 1972.

[70] H. Bondi, *Massive Spheres in General Relativity*, **282**.1390 (1964) 303–317.

[71] M. S. R. Delgaty and K. Lake, *Physical acceptability of isolated, static, spherically symmetric, perfect fluid solutions of Einstein's equations*, Comput. Phys. Comm. **115** (1998) 395–415, arXiv: gr-qc/9809013 [gr-qc].

[72] A. M. Raghoonundun and D. W. Hobill, *The Geometrical Structure of the Tolman VII solution*, ArXiv e-prints (2016), arXiv: 1601.06337 [gr-qc].

[73] R. P. Kerr, *Gravitational Field of a Spinning Mass as an Example of Algebraically Special Metrics*, Phys. Rev. Lett. **11** 5 (1963) 237–238.

[74] L. C. Woods, *Physics of plasmas*, Wiley-VCH, Weinheim, 2004.

[75] L. Rezzolla and B. J. Ahmedov, *Electromagnetic fields in the exterior of an oscillating relativistic star - I. General expressions and application to a rotating magnetic dipole*, Mon. Not. R. Astron. Soc. **352**.4 (2004) 1161–1179.

[76] A. Jeffrey and H.-H. Dai, *Handbook of mathematical formulas and integrals*, 4. ed., Elsevier, San Diego, CA, 2008.

[77] P. Mészáros, *High-Energy Radiation from Magnetized Neutron Stars*, University of Chicago Press, 1992.

[78] K. Konno and Y. Kojima, *General Relativistic Modification of a Pulsar Electromagnetic Field*, Progress of Theoretical Physics **104** (2000) 1117–1127, arXiv: astro-ph/0011240 [astro-ph].

[79] O. Benhar et al., *Perturbative approach to the structure of rapidly rotating neutron stars*, Phys. Rev. **D72** (2005) 044028, arXiv: gr-qc/0504068 [gr-qc].

[80] J. M. Cohen, L. S. Kegeles, and A. Rosenblum, *Magnetospheres and pulsars with net charge*, Astrophys. J. **201** (1975) 783–791.

[81] A. F. Gutiérrez-Ruiz and L. A. Pachón, *Electromagnetically induced frame dragging around astrophysical objects*, Phys. Rev. D. **91**.12 (2015) 124047, arXiv: 1504.01763 [gr-qc].

[82] L. Herrera et al., *Frame dragging, vorticity and electromagnetic fields in axially symmetric stationary spacetimes*, Class. Quantum Grav. **23** (2006) 2395–2408, arXiv: gr-qc/0602040 [gr-qc].

[83] H. Reissner, *Über die Eigengravitation des elektrischen Feldes nach der Einsteinschen Theorie*, Ann. Phys. (Berlin) **355**.9 (1916) 106–120.

[84] G. Nordström, *On the Energy of the Gravitation field in Einstein's Theory*, Koninklijke Nederlandse Akademie van Wetenschappen Proceedings Series B Physical Sciences **20** (1918) 1238–1245.

[85] A. Komar, *Covariant Conservation Laws in General Relativity*, Phys. Rev. **113** 3 (1959) 934–936.

[86] G. Pappas and T. A. Apostolatos, *Revising the Multipole Moments of Numerical Spacetimes and its Consequences*, Phys. Rev. Lett. **108** 23 (2012) 231104.

[87] K. Yagi and N. Yunes, *Approximate universal relations for neutron stars and quark stars*, Phys. Rep. **681** (2017) 1–72, arXiv: 1608.02582 [gr-qc].

[88] S. Bonazzola and E. Gourgoulhon, *Gravitational waves from pulsars: emission by the magnetic-field-induced distortion.* Astron. Astrophys. **312** (1996) 675–690, arXiv: astro-ph/9602107 [astro-ph].

[89] S. Bonazzola and J.-A. Marck, *Pseudo-spectral methods applied to gravitational collapse. Frontiers in Numerical Relativity*, ed. by C. R. Evans, L. S. Finn, and D. W. Hobill, 1989 239–253.

[90] S. Bonazzola and J.-A. Marck, *Three-dimensional gas dynamics in a sphere*, Journal of Computational Physics **87** (1990) 201–230.

[91] P. Grandclément and J. Novak, *Spectral Methods for Numerical Relativity*, Living Rev. Relativity **12**.1 (2009).

[92] E. Gourgoulhon et al., *LORENE: **L**angage **O**bjet pour la **RE**lativité **N**umériqu**E***, 1997-2016, http://www.lorene.obspm.fr.

[93] M. Galassi, et al., *GNU Scientific Library - Reference Manual*, Edition 2.3, 09.12.2016, https://www.gnu.org/software/gsl/.

[94] W. H. Press et al., *Numerical Recipes: The Art of Scientific Computing*, 3rd ed., Cambridge University Press, 2007.

[95] W. Becker, *Neutron Stars and Pulsars*, Springer, Berlin, Heidelberg, 2009.

[96] J. M. Lattimer and M. Prakash, *Neutron star structure and the equation of state*, Astrophys. J. **550** (2001) 426, arXiv: astro-ph/0002232 [astro-ph].

[97] J. M. Heinzle, N. Rohr, and C. Uggla, *Spherically symmetric relativistic stellar structures*, Class. Quant. Grav. **20** (2003) 4567–4586, arXiv: gr-qc/0304012 [gr-qc].

[98] CompOSE - CompStar Online Supernovae Equations of State, *HS_DD2 (with electrons)*, http://compose.obspm.fr/spip.php?article21, 2017.04.24 - 14:10.

[99] S. Typel et al., *Composition and thermodynamics of nuclear matter with light clusters*, Phys. Rev. C **81**.1 (2010) 015803, arXiv: 0908.2344 [nucl-th].

[100] CompOSE - CompStar Online Supernovae Equations of State, *SFHO (with electrons)*, http://compose.obspm.fr/spip.php?article37, 2017.04.24 - 16:00.

[101] A. W. Steiner, M. Hempel, and T. Fischer, *Core-collapse Supernova Equations of State Based on Neutron Star Observations*, Astrophys. J. **774**, 17 (2013) 17, arXiv: 1207.2184 [astro-ph.SR].

[102] CompOSE - CompStar Online Supernovae Equations of State, *HS_FSG (with electrons)*, http://compose.obspm.fr/spip.php?article23, 2017.04.24 - 14:00.

[103] B. G. Todd-Rutel and J. Piekarewicz, *Neutron-Rich Nuclei and Neutron Stars: A New Accurately Calibrated Interaction for the Study of Neutron-Rich Matter*, Phys. Rev. Lett. **95** 12 (2005) 122501.

[104] S. Chandrasekhar and J. C. Miller, *On slowly rotating homogeneous masses in general relativity*, Mon. Not. Roy. Astron. Soc. **167** (Apr. 1974) 63–80.

[105] C. Posada, *Slowly rotating supercompact Schwarzschild stars*, â€ŽMon. Not. R. Astron. Soc. **468** (2017) 2128–2139, arXiv: 1612.05290 [gr-qc].

[106] H. A. Buchdahl, *General-Relativistic Fluid Spheres. III. a Static Gaseous Model*, Astrophys. J. **147** (1967) 310.

[107] P. G. Whitman, *Interior solutions for rotating fluid spheres*, Phys. Rev. D **32** 8 (1985) 1857–1862.

[108] V. C. A. Ferraro, *On the Equilibrium of Magnetic Stars*, Astrophys. J. **119** (1954) 407.

[109] K. Yagi and N. Yunes, *I-Love-Q relations in neutron stars and their applications to astrophysics, gravitational waves, and fundamental physics*, Phys. Rev. **D88**.2 (2013), arXiv: 1303.1528 [gr-qc].

[110] Wolfram Research, Inc., *Mathematica*, Version 11.1.1, Champaign, Illinois, 2017, http://www.wolfram.com/mathematica/.

[111] P. Haensel, J. L. Zdunik, and R. Schaefer, *Strange quark stars*, Astron. Astrophys. **160** (1986) 121–128.

[112] T. Nozawa et al., *Construction of highly accurate models of rotating neutron stars - comparison of three different numerical schemes*, Astron. Astrophys. **132** (1998) 431–454, arXiv: gr-qc/9804048 [gr-qc].

[113] M. D. Swesty, *Thermodynamically Consistent Interpolation for Equation of State Tables*, J. Comput. Phys. **127**.1 (1996) 118–127.

[114] M. Oertel et al., *Equations of state for supernovae and compact stars*, ArXiv e-prints (2016), arXiv: 1610.03361 [astro-ph.HE].

[115] S. Richers et al., *Equation of state effects on gravitational waves from rotating core collapse*, Phys. Rev. D **95**.6 (2017) 063019, arXiv: 1701.02752 [astro-ph.HE].

[116] T. Fischer et al., *Symmetry energy impact in simulations of core-collapse supernovae*, Eur. Phys. J. A **50**, 46 (2014) 46, arXiv: 1307.6190 [astro-ph.HE].

[117] S. Typel, M. Oertel, and T. Klaehn, *CompOSE - **Comp**Star **O**nline **S**upernovae **E**quations of State*, 2013-2017, http://compose.obspm.fr/.

[118] S. Typel, M. Oertel, and T. Klaehn, *CompOSE - CompStar Online Supernovae Equations of State*, ArXiv e-prints (2013), arXiv: 1307.5715 [astro-ph.SR].

[119] M. Hempel and J. Schaffner-Bielich, *A statistical model for a complete supernova equation of state*, Nucl. Phys. A **837** (2010) 210–254, arXiv: 0911.4073 [nucl-th].

[120] G. Baym, C. Pethick, and P. Sutherland, *The Ground State of Matter at High Densities: Equation of State and Stellar Models*, Astrophys. J. **170** (1971) 299.

Appendices

A Field equations of the Hartle-Thorne metric

In this appendix we present the raw field equations, which we used in this work to derive various structure equations. The $O\left(B^0\Omega^0\right)$, $O\left(B^0\Omega^1\right)$, $O\left(B^2\Omega^0\right)$ and $O\left(B^2\Omega^1\right)$ field equations are field equations of GR

$$\mathscr{E}_{\alpha\beta} \equiv G_{\alpha\beta} - 8\pi T_{\alpha\beta} = G_{\alpha\beta} - 8\pi\left(T^{(\mathrm{F})}_{\alpha\beta} + T^{(\mathrm{EM})}_{\alpha\beta}\right) = 0 \tag{A.1}$$

expanded to the corresponding order in the magnetic field B and angular velocity Ω. The ansatz for the metric and the energy-momentum tensor is described in Chap. 3.

We are mainly working with the field equations involving the mixed tensors $\mathscr{E}^{\alpha}{}_{\beta} = g^{\alpha\mu}\mathscr{E}_{\mu\beta}$ since they reduce to shorter expressions than their purely co- or contravariant counterparts.

The $O\left(B^1\Omega^1\right)$ Maxwell equations were derived and discussed in Sec. 3.4. We only present them in this appendix to have a complete succession of all field equations from $O\left(B^0\Omega^0\right)$ up to $O\left(B^2\Omega^1\right)$.

Computing field equations or in general higher objects (e.g. $\Gamma^{\alpha}_{\beta\gamma}$ or $R_{\alpha\beta}$) for a given metric in GR is straight forward but if done by hand a tedious and error-prone process. Computer algebra systems are very well suited to compute the needed higher objects fast and fail-safe. We wrote a short (~ 200 lines) MATHEMATICA [110] package to compute all needed higher objects for a given metric.

A.1 $O\left(B^0\Omega^0\right)$: Background equations

In $O\left(B^0\right)$ we used the following three field equations

$$\left(\mathscr{E}^{t}{}_{t}\right) : 1 + \mathrm{e}^{\lambda}\left(8\pi r^2\rho - 1\right) - r\lambda' = 0, \tag{A.2}$$

$$\left(\mathscr{E}^{r}{}_{r}\right) : -1 + \mathrm{e}^{\lambda}\left(1 + 8\pi r^2 P\right) - r\nu' = 0, \tag{A.3}$$

$$\left(\mathscr{E}^{\theta}{}_{\theta}\right) : 2r\nu'' + r(\nu')^2 + 2\nu' - \lambda'\left(2 + r\nu'\right) - 32\mathrm{e}^{\lambda}\pi r P = 0, \tag{A.4}$$

$$\left(\nabla_{\mu}\mathscr{E}^{r\mu}\right) : 2P' + (P+\rho)\nu' = 0. \tag{A.5}$$

Eq. (A.2) relates the energy density ρ to the g_{rr} metric potential λ. The second field eq. (A.3) relates the pressure to the two metric potentials. The third field eq. (A.4) involves a second derivative and the square of the first derivative of the g_{tt} metric potential ν but it contains only the pressure as source term. The pressure source term can be eliminated when adding $(4/r\mathscr{E}^{r}{}_{r})$ to $(\mathscr{E}^{\theta}{}_{\theta})$ which results in a structure equation for metric potentials only. This is the reason why it is often used to construct analytic interior solutions. The Euler eq. (A.5) on the other hand is very use full for deriving the TOV equations.

A.2 $O\left(B^0\Omega^1\right)$: Frame-dragging equation

There is only one nontrivial $O\left(\Omega^1\right)$ field equation which is related to the scalar product of the two Killing vectors ξ and χ

$$\left(\mathscr{E}^{\phi}{}_{t}\right) : \omega'' - \frac{4}{r}\left(\pi r^2\mathrm{e}^{\lambda}(P+\rho) - 1\right)\omega' + 16\pi\mathrm{e}^{\lambda}(P+\rho)(\Omega-\omega) = 0. \tag{A.6}$$

Using $\bar{\omega} = \Omega - \omega$ and the $O\left(B^0\right)$ eqs. (A.6) can be recast into the more common form

$$\bar{\omega}'' + \frac{1}{2r}\left(r(\nu'+\lambda') - 8\right)\bar{\omega}' + \frac{2}{r}(\nu'+\lambda')\bar{\omega} = 0. \tag{A.7}$$

A.3 $O\left(B^1\Omega^1\right)$: Maxwell equations

The field equations $\mathscr{E}_{\alpha\beta}$ only contain even powers of B and Ω in terms of a series expansion, since the energy-momentum tensor is even in B and Ω. In $O\left(B^1\right)$ we have l decoupled Maxwell eqs.

$$\left(-\nabla_\mu F_\phi{}^\mu + 4\pi J_\phi = 0\right) : \mathrm{e}^{-\lambda} a''_{\phi l} + \frac{1}{2}\mathrm{e}^{-\lambda} a'_{\phi l}\left(\nu' - \lambda'\right) - l(l+1)\frac{a_{\phi l}}{r^2} + 4\pi j_{\phi l} = 0. \tag{A.8}$$

In $O\left(B^1\Omega^1\right)$ we again recover l Maxwell eqs. which are coupled to the magnetic field and the frame-dragging frequency

$$\begin{aligned}\left(-\nabla_\mu F_t{}^\mu + 4\pi J_t = 0\right) :& \mathrm{e}^{-\lambda} a''_{tl} - \frac{1}{2r}\mathrm{e}^{-\lambda} a'_{tl}\left(r\nu' + r\lambda' - 4\right) - l(l+1)\frac{a_{tl}}{r^2} + 4\pi j_{tl} \\ &+ \frac{1}{r}\mathrm{e}^{-\lambda}\left(\omega(r\nu' - 2) - r\omega'\right)\left[\sum_n a'_{\phi n}\sin\theta\frac{d\mathrm{P}_n(\cos\theta)}{d\theta}\right]_l \\ &- \frac{2}{r^2}\omega\left[\sum_n n(n+1)\cos\theta\mathrm{P}_n(\cos\theta)\right]_l .\end{aligned} \tag{A.9}$$

In the scope of the present work we have only discussed configurations with $l = 1$ dipolar magnetic fields and the resulting induced $l = 0$ and $l = 2$ electric fields in detail.

A.4 $O\left(B^2\Omega^0\right)$: Perturbation equations

In our ansatz for the line element we separated the angular dependency from metric- and enthalpy-perturbations using $(m = 0)$-harmonics. Solutions for metric potentials and source term perturbations are by construction independent of the polar angle θ. To decouple equations for monopole $(l = 0)$ and quadrupole $(l = 2)$ perturbations without the need for additional algebraic manipulations we use the angles

$$P_2(\theta_{2,1}) \equiv 1 \Leftrightarrow \sin^2\theta_{2,1} = 0, \tag{A.10}$$

$$P_2(\theta_{2,0}) \equiv 0 \Leftrightarrow \sin^2\theta_{2,1} = \frac{2}{3}, \tag{A.11}$$

and the corresponding projections

$$(X)_{l=0} \equiv X|_{\theta=\theta_{2,0}}, \tag{A.12}$$

$$(X)_{l=2} \equiv X|_{\theta=\theta_{2,1}} - X|_{\theta=\theta_0}. \tag{A.13}$$

Using those projections is not necessary to derive decoupled equations for mono- and quadrupole perturbations but it is the most convenient way to do so since using different angles to obtain equivalent equations involves more algebra.

There are five nontrivial, linear independent field equations of $O\left(B^2\right)$: $\mathscr{E}^t{}_t$, $\mathscr{E}^r{}_r$, $\mathscr{E}^\theta{}_\theta$, $\mathscr{E}^\phi{}_\phi$ and $\mathscr{E}^r{}_\theta$. The $O\left(B^0\right)$ contributions have been eliminated from the following equations by using eqs. (A.2)-(A.5).

Using the projections (A.12) and (A.13) one can derive the following four independent, for $(l = 0)$ and $(l = 2)$ decoupled, equations from $\mathscr{E}^t{}_t$ and $\mathscr{E}^r{}_r$:

$$\left(\mathscr{E}^t{}_t\right)_{l=0} : -2r^2 m'_0 + 8\pi r^4\frac{d\rho}{dh}h_0 + \frac{2}{3}\left(2a_\phi^2 + \mathrm{e}^{-\lambda}r^2(a'_\phi)^2\right) = 0, \tag{A.14}$$

$$\begin{aligned}\left(\mathscr{E}^t{}_t\right)_{l=2} :& -2\mathrm{e}^{-\lambda}r^4\left(n''_2 - \nu''_2\right) + \mathrm{e}^{-\lambda}\left(r\lambda' - 6\right)r^3\left(n'_2 - \nu'_2\right) - 2r^2 m'_2 + 4r^2\left(h_2 - \nu_2\right) \\ &- 6\mathrm{e}^{\lambda} r m_2 + 8\pi r^4\frac{d\rho}{dh}h_2 + \frac{2}{3}\left(4a_\phi^2 - \mathrm{e}^{-\lambda}r^2(a'_\phi)^2\right) = 0,\end{aligned} \tag{A.15}$$

$$\left(\mathcal{E}^{r}{}_{r}\right)_{l=0} : 2\mathrm{e}^{-\lambda} r^3 n_0' - 2\left(1 + r\nu'\right) r m_0 - 8\pi r^4 (P+\rho) h_0 + \frac{2}{3}\left(2a_\phi^2 - \mathrm{e}^{-\lambda} r^2 (a_\phi')^2\right) = 0, \tag{A.16}$$

$$\begin{aligned}\left(\mathcal{E}^{r}{}_{r}\right)_{l=2} : &-\mathrm{e}^{-\lambda}\nu' r^4 n_2' + \mathrm{e}^{-\lambda}\left(2 + r\nu'\right) r^3 v_2' - 2r^2\left(n_2 + 2v_2\right) - 2\left(1 + r\nu'\right) r m_2 \\ &- 8\pi r^4 (P+\rho) h_2 + \frac{2}{3}\left(4a_\phi^2 + \mathrm{e}^{-\lambda} r^2 (a_\phi')^2\right) = 0.\end{aligned} \tag{A.17}$$

The field equation $\mathcal{E}^{r}{}_{\theta}$ only contains ($l = 2$) metric perturbations and one source term $-8a_\phi a_\phi'$:

$$\left(\mathcal{E}^{r}{}_{\theta}\right) : 6r^2 v_2' + 3r(r\nu' - 2) n_2 - 3\mathrm{e}^{\lambda}(r\nu' + 2) m_2 - 8a_\phi a_\phi' = 0. \tag{A.18}$$

The remaining two field equations, $\mathcal{E}^{\theta}{}_{\theta}$ and $\mathcal{E}^{\phi}{}_{\phi}$, are rather lengthy and on their own not very convenient to use but their difference leads to a very short and useful equation for the n_2 and m_2 metric potentials:

$$\left(\mathcal{E}^{\phi}{}_{\phi} - \mathcal{E}^{\theta}{}_{\theta}\right) : n_2 - \frac{\mathrm{e}^{\lambda}}{r} m_2 + \frac{2}{3}\mathrm{e}^{-\lambda}(a_\phi')^2 = 0. \tag{A.19}$$

The relativistic Euler equations, which encodes energy-momentum conservation, take the form of three nontrivial equations:

$$\left(\nabla_\mu \mathcal{E}^{r\mu}\right)_{l=0} : n_0' + h_0' - \frac{2j_\phi}{3\left(P+\rho\right) r^2} a_\phi' = 0, \tag{A.20}$$

$$\left(\nabla_\mu \mathcal{E}^{r\mu}\right)_{l=2} : n_2' + h_2' + \frac{2j_\phi}{3\left(P+\rho\right) r^2} a_\phi' = 0, \tag{A.21}$$

$$\left(\nabla_\mu \mathcal{E}^{\theta\mu}\right) : n_2 + h_2 + \frac{2j_\phi}{3\left(P+\rho\right) r^2} a_\phi' = 0. \tag{A.22}$$

Of the nine $O\left(B^2\right)$ eqs. (A.14)-(A.22), all except for eq. (A.15) were used in this work. We presented eq. (A.15) in this appendix for completeness only.

A.5 $O\left(B^2\Omega^1\right)$: Higher-order frame-dragging corrections

There is only one nontrivial $O\left(B^2\Omega^1\right)$ field equation which describes $O\left(B^2\right)$ corrections to the frame-dragging frequency in form of W_1 and W_3. Using projections similar to (A.12) and (A.13) it is possible to derive two decoupled equations

$$\begin{aligned}\left(\mathcal{E}^{\phi}{}_{t}\right)_{l=1} : &\mathrm{e}^{-\frac{\lambda}{2}-\frac{\nu}{2}} r^4 W_1'' - \frac{1}{2}\mathrm{e}^{-\frac{\lambda}{2}-\frac{\nu}{2}} r^3 W_1'\left(-8 + r\lambda' + r\nu'\right) - 2\mathrm{e}^{-\frac{\lambda}{2}-\frac{\nu}{2}} r^3 W_1\left(\lambda' + \nu'\right) \\ &+ S_0 + S_1 - S_2 = 0,\end{aligned} \tag{A.23}$$

$$\begin{aligned}\left(\mathcal{E}^{\phi}{}_{t}\right)_{l=3} : &\mathrm{e}^{-\frac{\lambda}{2}-\frac{\nu}{2}} r^4 W_3'' - \frac{1}{2}\mathrm{e}^{-\frac{\lambda}{2}-\frac{\nu}{2}} r^3 W_3'\left(-8 + r\lambda' + r\nu'\right) - 2\mathrm{e}^{-\frac{\lambda}{2}-\frac{\nu}{2}} r^3 W_3\left(5\mathrm{e}^{\lambda} + r\lambda' + r\nu'\right) \\ &+ S_2 + S_3 = 0,\end{aligned} \tag{A.24}$$

with

$$S_0 \equiv e^{-\frac{\lambda}{2}-\frac{\nu}{2}} r^3 \left(e^{\lambda} m_0' + r n_0'\right) \bar{\omega}' + e^{\frac{\lambda-\nu}{2}} r^2 m_0 \left(4\bar{\omega}\left(\lambda' + \nu'\right) + \left(-1 + r\lambda'\right)\bar{\omega}'\right) + 16 e^{\frac{\lambda-\nu}{2}} \pi r^4 h_0 \left(\frac{d\rho}{dh} + P + \rho\right)\bar{\omega}, \tag{A.25}$$

$$S_2 \equiv \frac{1}{5} e^{-\frac{\lambda}{2}-\frac{\nu}{2}} r^3 \left(e^{\lambda} m_2' + 5 r n_2' - 4 r v_2'\right) \bar{\omega}' + \frac{1}{5} e^{\frac{\lambda-\nu}{2}} r^2 m_2 \left(4\bar{\omega}\left(\lambda' + \nu'\right) + \left(-1 + r\lambda'\right)\bar{\omega}'\right) + \frac{16}{5} e^{\frac{\lambda-\nu}{2}} \pi r^4 h_2 \left(\frac{d\rho}{dh} + P + \rho\right)\bar{\omega}, \tag{A.26}$$

$$S_1 \equiv -\frac{24}{5} e^{\frac{\lambda-\nu}{2}} a_{t,2} a_\phi - \frac{16}{5} e^{\frac{\lambda-\nu}{2}} a_\phi^2 \omega + \frac{4}{5} e^{-\frac{\lambda}{2}-\frac{\nu}{2}} r^2 \left(5 a_{t,0}' - a_{t,2}'\right) a_\phi' - \frac{16}{5} e^{-\frac{\lambda}{2}-\frac{\nu}{2}} r^2 \omega \left(a_\phi'\right)^2, \tag{A.27}$$

$$S_3 \equiv -\frac{16}{5} e^{\frac{\lambda-\nu}{2}} a_{t,2} a_\phi - \frac{32}{15} e^{\frac{\lambda-\nu}{2}} a_\phi^2 \omega + \frac{4}{5} e^{-\frac{\lambda}{2}-\frac{\nu}{2}} r^2 a_{t,2}' a_\phi' + \frac{8}{15} e^{-\frac{\lambda}{2}-\frac{\nu}{2}} r^2 \omega \left(a_\phi'\right)^2. \tag{A.28}$$

B Equations of state

B.1 Incompressible relativistic fluid (IRF)

Arguably the simplest but thermodynamically consistent EoS is the one of an incompressible fluid. In the following we will derive the EoS in terms of the fluid log-enthalpy h of a cold incompressible relativistic fluid (IRF) of constant energy density

$$\rho(h) \overset{!}{=} \text{const.} \equiv \rho_c. \tag{B.1}$$

Integrating the fundamental relation $dP/dh = \rho + P$ with the boundary condition $P(h=0) = 0$ leads to:

$$P(h) = \rho_c(\mathrm{e}^h - 1). \tag{B.2}$$

Using eq. (B.2) we can derive an expression for the baryon number density

$$n_\mathrm{B} = \frac{dP}{d\mu} = \frac{dP}{\mu dh} = \frac{\rho_c}{m_\mathrm{B}}, \tag{B.3}$$

where we used the fundamental relation between the fluid log-enthalpy h and the baryon chemical potential $\mu = \mu_0 \mathrm{e}^h = m_\mathrm{B}\mathrm{e}^h$. We use a fixed baryon rest mass of$m_B = 931.192\,\mathrm{MeV}$ and characterize different IRF EoS by the only remaining parameter their constant density. Throughout this work we will frequently use the notation IRF($\rho_c\left[\mathrm{MeV\,fm^{-3}}\right]$).

The TOV eqs. can be integrated analytically when using an IRF EoS because of the very simple analytical form of this EoS. This particular solution of the TOV eqs. is called *interior Schwarzschild solution* [57] and we derived and discussed it in Sec. 3.2.4.

B.2 EoS of the Tolman VII interior solution (TVII)

We introduced and discussed Tolman VII interior solutions in Sec. 3.2.5. In this appendix we will focus on the corresponding EoS. In Sec. 3.2.5 we derived expressions for all thermodynamic quantities as functions of the dimensionless radial variable $s = r/R$. To derive an EoS relating those quantities in TVII configurations we begin with inverting the expression for the log-enthalpy from eq. (3.80):

$$\phi(h) = \operatorname{arcsec}\left[\frac{\mathrm{e}^h}{\cos\phi_1}\right]. \tag{B.4}$$

We now have a relation for the auxiliary function ϕ in terms of h. It is possible to analytically invert eq. (3.77a) to get a complicated expression for $s(\phi(h))$:

$$s(h) = \frac{\sqrt{18(3\mu-5)\sqrt{10-6\mu}\mu^{3/2}e^{2c_\phi+W(1)-2\phi(h)} - \frac{\sqrt{(10-6\mu)\mu}e^{-2c_\phi-W(1)+2\phi(h)}(6\mu(3\mu-5)+25Z)}{Z}} + 60(3\mu-5)\mu}{6\mu\sqrt{6\mu-10}}, \tag{B.5}$$

with the constants $W(1)$ from eq. (3.77b) and $c_\phi = \arctan\left(\sqrt{5-3\mu}/\sqrt{\mu\left(6/Z-12\right)}\right)$. Using the chain rule and the derivative ds/dh with the expressions for $P(s)$, $\rho(s)$ and $n_\mathrm{B}(s)$ from Sec. 3.2.5 we can provide a complete EoS for TVII configuration in h in form of

$$P(h) = P(s(h)), \tag{B.6a}$$

$$\frac{dP(h)}{dh} = \frac{dP(s)}{ds}\frac{ds(h)}{dh}, \tag{B.6b}$$

$$\rho(h) = \rho(s(h)), \tag{B.6c}$$

$$\frac{d\rho(h)}{dh} = \frac{d\rho(s)}{ds}\frac{ds(h)}{dh}, \tag{B.6d}$$

$$n_\mathrm{B}(h) = n_\mathrm{B}(s(h)), \tag{B.6e}$$

$$\frac{dn_\mathrm{B}(h)}{dh} = \frac{dn_\mathrm{B}(s)}{ds}\frac{ds(h)}{dh}. \tag{B.6f}$$

This EoS scales in the central pressure the same way the IRF EoS does. Apart form this, EoS of TVII configurations are special in the sense that there are no equilibrium configurations that lie on the same EoS. Every TVII configuration has its unique EoS determined by the choice of ρ_c, h_c and m_B. Throughout this work we will frequently use the notation $\mathrm{TVII}_\mu(\rho_c\left[\mathrm{MeV\,fm^{-3}}\right])$. The left panel of Fig. B.1 illustrates that fact. The EoS of three $\mathrm{TVII}_1(473)$ configurations with identical central pressure and mean baryon rest mass are distinct. They are not related by a scale and do not follow a common curve.

When considering sequences with constant compactness/central log-enthalpy but differing central density the EoS are related linearly in ρ_c. For the TVII EoS there is no obvious unique way of specifying the EoS. Choosing sequences of constant central density is a natural choice for the IRF EoS and doing the same for TVII EoS allows to describe sequences with differing compactness. In the scope of this work we choose this view because we want to discuss NS with differing Z. Considering different choices of a fixed quantity to distinct between TVII EoS is possible and depending on the application better suited [55, 72].

In the right panel of Fig. B.1 we compare $\mathrm{TVII}_1(473)$ to the other EoS used in this work for a $Z = 0.15$ NS. By construction of $\mathrm{TVII}_1(473)$ the EoS is very similar to the SFHo's EoS but TVII EoS are in general well suited to model the high density regime of hadronic EoS.

The EoS and the algebraic structure of the TVII solution presented in this work is different from the one used by A. M. Raghoonundun in [55, 72]. We derived the complete EoS in h and not only $P(\rho)$. For computations in the scope of this work $P(\rho)$ is not sufficient we need the full EoS: all thermodynamic quantities and their derivatives. Implementing this EoS numerically is straight forward using eqs. (B.5) and (B.6) but one has to be aware of one property of our form of the TVII solution. The auxiliary function $W(s)$ from eq. (3.77b) is a mapping $W : [0,1] \to \mathbb{C}$ but the imaginary parts of $W(1)$ and $W(s)$ are always equal. All thermodynamic quantities and metric potentials for that matter depend on the difference $W(1) - W(s)$ only and they are always real. When implementing the EoS it is however necessary to use complex data types and functions when working with W.

B.3 Relativistic polytropes (Poly)

In the previous section we introduced the IRF EoS. Another yet more flexible class of simple analytical EoS are relativistic polytropes (Poly). The pressure of a relativistic polytrope is related to the baryon number density

$$P(n_\mathrm{B}) = \kappa\rho_0\left(\frac{n_\mathrm{B}}{n_{\mathrm{B},0}}\right)^\gamma \equiv K n_\mathrm{B}^\gamma, \tag{B.7}$$

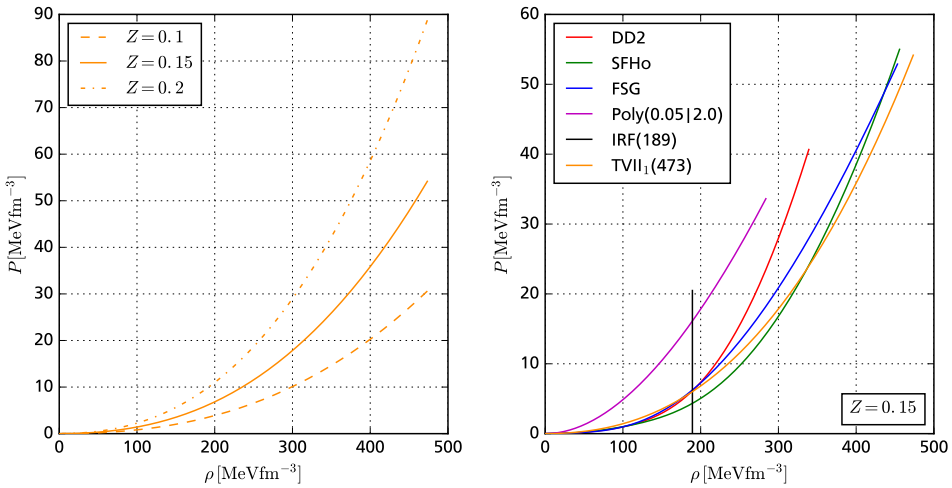

Figure B.1: EoS in form of pressure over energy density inside different equilibrium configurations. On the left we have three configurations with TVII$_1$(473) EoS with varying compactnesses and on the right we have six $Z = 0.15$ configurations with different EoS.

with a polytropic/adiabatic index γ, a dimensionless pressure coefficient κ and two arbitrary number- and energy densities $n_{\mathrm{B},0}$ and ρ_0. This definition is similar to the one presented in [18] and is consistent with the definition [97, 111] of a relativistic adiabatic index γ

$$\gamma \equiv \frac{\rho + P}{P} \frac{dP}{d\rho}. \tag{B.8}$$

Using eq. (B.7) and the Gibbs-Duhem-Relation at zero temperature one can derive a relation between energy density and baryon density

$$\rho(n_{\mathrm{B}}) = m_{\mathrm{B}} n_{\mathrm{B}} + \frac{K n_{\mathrm{B}}^{\gamma}}{\gamma - 1}. \tag{B.9}$$

With eqs. (B.7) and (B.9) one can derive an expression for the log-enthalpy h

$$h(n_{\mathrm{B}}) = \log\left[\frac{P(n_{\mathrm{B}}) + \rho(n_{\mathrm{B}})}{m_{\mathrm{B}} n_{\mathrm{B}}}\right] = \log\left[1 + \frac{\gamma}{\gamma - 1} \frac{K n_{\mathrm{B}}^{\gamma - 1}}{m_{\mathrm{B}}}\right] \tag{B.10}$$

which can be inverted to yield

$$n_{\mathrm{B}}(h) = \left[\frac{m_{\mathrm{B}}}{K} \frac{\gamma - 1}{\gamma} \left(\mathrm{e}^{h} - 1\right)\right]^{\frac{1}{\gamma - 1}}. \tag{B.11}$$

Eq. (B.11) together with eqs. (B.7) and (B.9) resemble the complete relativistic polytropic EoS in the log-enthalpy h.

The speed of sound as a function of n_{B} is given by

$$c_s(n_{\mathrm{B}})^2 \equiv \frac{dP}{d\rho} = \frac{dP}{dn_{\mathrm{B}}} \frac{dn_{\mathrm{B}}}{d\rho} = \frac{K(\gamma - 1)\gamma n_{\mathrm{B}}^{\gamma}}{m_{\mathrm{B}}(\gamma - 1) n_{\mathrm{B}} + K\gamma n_{\mathrm{B}}^{\gamma}} \tag{B.12}$$

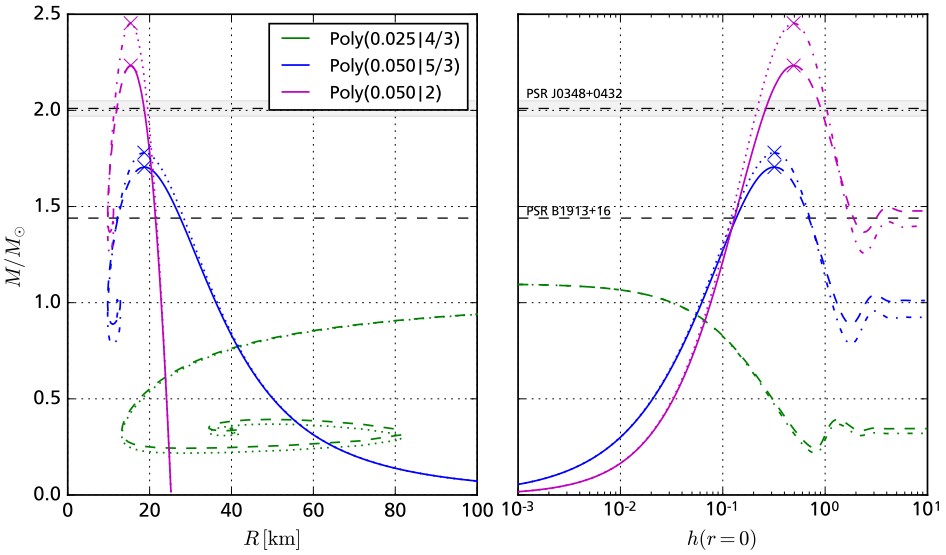

Figure B.2: Gravitational (solid lines) and baryonic mass (dotted lines) over stellar radius (left) and over central log-enthalpy h for three different Poly EoS. Dashed and dash-dotted configurations are unstable. Crosses mark stable equilibrium configurations with maximum mass.

and its $n_\mathrm{B} \to \infty$ limit is

$$\lim_{n_\mathrm{B}\to\infty} c_s(n_\mathrm{B})^2 = \gamma - 1. \tag{B.13}$$

Physical and causal relativistic polytropes have $\gamma \in (1,2]$. For $\gamma < 1$ the pressure contributions to ρ are negative and sound speeds can become imaginary. In the case $\gamma = 1$ the given expressions are singular. A solution for an $\gamma = 1$ polytrope is possible but the resulting EoS is not physical. For $\gamma > 2$ the EoS become acausal ($c_s > 1$) at high baryon densities while the $\gamma = 2$ polytropes asymptotically approach the causal limit $c_s = 1$.

For our numerical computations we adopt values used in LORENE: $m_\mathrm{B} = 931.192\,\mathrm{MeV}$, $n_{\mathrm{B},0} = 0.1\,\mathrm{fm}^{-3}$ and $\rho_0 = m_\mathrm{B} n_{\mathrm{B},0} = 93.119\,\mathrm{MeV\,fm}^{-3}$. Once those parameters are fixed different Poly EoS are characterized completely by their dimensionless pressure coefficient κ and their polytropic/adiabatic index γ. Throughout this work we will frequently use the notation Poly($\kappa\,|\,\gamma$) .

Fig. B.2 shows the $M-R$ and $M-h$ curves for three different Poly EoS and there are several features worth mentioning.

- With increasing polytropic index the overall compactness of the configurations increases.
- For $\gamma = 4/3$ there are no stable configurations since $\partial M/\partial h < 0\,\forall h$ and the gravitational binding energies are negative ($M_\mathrm{B} - M < 0$).
- The $\gamma = 5/3$ polytrope has a stable branch and for $h \to 0$: $M \to 0$ and $R \to \infty$.
- Poly(0.050|2) has a stable branch and an interesting low h asymptotic: for $h \to 0$: $M \to 0$ but $R \to 25.2\,\mathrm{km}$.
- All three polytropes show a spiral structure for high h: the individual $M-R$-curves converge towards an EoS-dependent point (R_O, M_O).

J. M. Heinzle et al. presented an in-depth discussion of stellar structure for relativistic polytropes in their paper [97]. They introduced four theorems describing the mass-radius properties of Poly EoS,

which we just phenomenologically presented here.

We will conclude this section about Poly EoS with specifying their scaling properties. The thermodynamic quantities of two relativistic polytropes I and I with $m_{\mathrm{I}} = m_{\mathrm{II}}$ and $\gamma_{\mathrm{I}} = \gamma_{\mathrm{II}} \equiv \gamma$ are related by

$$S_{\mathrm{I}}^2 \left(n_{\mathrm{B}}^{\mathrm{I}}(h), P_{\mathrm{I}}(h), \rho_{\mathrm{I}}(h)\right)^T = S_{\mathrm{II}}^2 \left(n_{\mathrm{B}}^{\mathrm{II}}(h), P_{\mathrm{II}}(h), \rho_{\mathrm{II}}(h)\right)^T , \tag{B.14}$$

with

$$S_{\mathrm{I}}^2 = K_{\mathrm{I}}^{\frac{1}{\gamma-1}} \text{ and } S_{\mathrm{II}}^2 = K_{\mathrm{II}}^{\frac{1}{\gamma-1}}. \tag{B.15}$$

Due to that scaling, solutions of the TOV eqs. with EoS I and II are related for configurations with the same central log-enthalpy $h(r = 0)$

$$r_{\mathrm{I}}(h)/S_{\mathrm{I}} = r_{\mathrm{II}}(h)/S_{\mathrm{II}}, \tag{B.16}$$
$$z_{\mathrm{I}}(h) = z_{\mathrm{II}}(h). \tag{B.17}$$

The associated global parameters are related

$$R_{\mathrm{II}} = \frac{S_{\mathrm{II}}}{S_{\mathrm{I}}} R_{\mathrm{I}}, \tag{B.18}$$
$$M_{\mathrm{II}} = \frac{S_{\mathrm{II}}}{S_{\mathrm{I}}} M_{\mathrm{I}}, \tag{B.19}$$
$$Z_{\mathrm{II}} = Z_{\mathrm{I}}, \tag{B.20}$$
$$M_{\mathrm{B}}^{\mathrm{II}} = \frac{S_{\mathrm{II}}}{S_{\mathrm{I}}} M_{\mathrm{B}}^{\mathrm{I}}. \tag{B.21}$$

As a result of eqs. (B.16) and (B.18) $s = r/R$ is scale invariant and in combination with eqs. (B.17) and (B.20) the metric potentials in terms of s are identical for I and II

$$\nu_{\mathrm{I}}(s) = \nu_{\mathrm{II}}(s) \ \forall s \in [0, \infty), \tag{B.22}$$
$$\lambda_{\mathrm{I}}(s) = \lambda_{\mathrm{II}}(s) \ \forall s \in [0, \infty). \tag{B.23}$$

For the HT quantities similar scaling relations arise as a natural consequence of the scaling effects of the background star.

Introducing polytropic units would be advantageous when dealing extensivly with this kind of EoS. But since we are using only Poly(0.05|2) in the main part of this work we did not compute nor present results in polytropic units.

B.4 Tabulated/interpolated realistic EoS: DD2, SFHo and FSG

In this section we present the interpolation method we used for tabulated EoS as well as the three tabulated EoS we used in this work.

In order to provide a thermodynamically consistent EoS from a tabulated EoS we use the method proposed by T. Nozawa et al. [112] and M. D. Swesty [113]. For an Eos provided as a table of $\left(n_{\mathrm{B}}, P, \rho\right)$ data points we first compute h for the data points. After that we generate two splines: a hermite spline through $\left(\log_{10} P, \log_{10} h\right)$ and a linear spline through $\left(d \log_{10} P / d \log_{10} n_{\mathrm{B}}, \log_{10} h\right)$. Between the first two data points we do not use the $\log_{10}$-interpolations since they are singular for $P = 0$ and $h = 0$.

EoS	$n_{B,s}\left[\mathrm{fm}^{-3}\right]$	K [MeV]	J [MeV]	L [MeV]
DD2	0.1491	242.7	31.67	55.03
SFHo	0.1583	245.4	31.57	47.10
FSG	0.1482	229.5	32.56	60.43

Table B.1: Nuclear matter properties of the general purpose EoS DD2, SFHo and FSG [98, 100, 102]

Between the first two points we use splines through (P,h) and a linear spline through $\left(dP/dn_{\mathrm{B}},h\right)$. We adapt the interpolation order of the hermite spline accordingly to the density of data points. For the tabulated EoS obtained from CompOSE we use a cubic spline at high densities, a quadratic one at lower densities and at very low densities we use a linear spline.

Using the Gibbs-Duham relation we can construct all thermodynamic quantities at interest from the two splines $(dP/dn_{\mathrm{B}})(h)$ and $P(h)$ when additionally using the derivative $(dP/dh)(h)$ provided by the hermite spline. This method guaranties a thermodynamic consistent EoS, meaning an EoS satisfying the Gibbs-Duham relation, even between the given data points. This interpolation method in the log-enthalpy is advantageous to us since we need P, ρ, n_{B} and their derivatives as functions of h.

For more details on the explicit implementation of this method we refer to the reference manual of the LORENE library [92]. Our implementation is very similar to the one of the `Eos_tabul` class. We modified this class to have an identical implementation of our interpolation scheme in LORENE and in our code.

An extreme variety of tabulated EoS for cold NS matter is publicly available. Those EoS vary from the matter content they try to describe to the methods that where used to obtain them. For an excellent overview we recommend the recent review paper of M. Oertel et. al. [114] from 2016.

In the scope of this work we have decided to use three so called *general purpose EoS*. General purpose EoS cover the full thermodynamical parameter range needed for involved astrophysical simulations. They give pressure, energy- and baryon-density and even information on composition as a function of temperature, charge fraction and baryon-density. For a detailed discussion of this kind of EoS we refer the reader to [114–116]. The three EoS we use can be obtained from CompOSE [117]. For describing cold NS matter we computed the cold β-equilibrium EoS of those general purpose EoS using `compose.f90` code [117, 118].

The three EoS we use are based on the extended nuclear statistical equilibrium (NSE) model of Hempel and Schaffner-Bielich (HS) [119]. The HS model describes a mixture of nucleons, electrons and nuclei in NSE. Unbound nucleons and their interactions are described with a relativistic mean field (RMF) method using different parameterizations. Around seven thousand nuclei are considered and described by a classical Maxwell-Boltzmann gas. Apart from light nuclei like d, t, h and α, heavy nuclei ranging from slightly above the proton- to slightly below the neutron drip line are included. Experimental data for those nuclei is used if it exists and missing data is obtained from nuclear structure calculations. Several medium effects like Coulomb energies by the surrounding electron gas, excited states and excluded-volume effects are included in the HS model.

The three EoS we use are all based on the HS model but use different RMF-parameterizations. They include protons, neutrons, electrons and nuclei (npeN).

- The DD2 EoS [98][(5)] uses the RMF parameter set of S. Typel et al. [99]. It is a stiff EoS with a high maximum mass at rather large radii.

(5) Since we originally obtained the EoS data files the CompOSE web page was relaunched and the urls to the individual EoS changed. As of 2017.06.21 all three EoS can be found on this page `http://compose.obspm.fr/table/family-subg/4/7/`.

- The SFHo EoS [100] is based on RMF parameters of A. W. Steiner, M. Hempel and T. Fischer [101]. The SFHo parametrization was specially optimized to be consistent with latest NS mass and radius constraints.
- The FSG Eos [102] uses RMF parameters of B. G. Todd-Rutel and J. Piekarewicz [103]. It is a soft EoS which does not reach NS masses above $\sim 1.7 M_\odot$.

All three EoS fulfill latest constraints from nuclear physics experiments. The experimental value for the nuclear saturation density is $n_{\mathrm{B},s} \sim 0.16\,\mathrm{fm}^{-3}$. Nuclear incompressibility from the experiment expected to be $K = 240 \pm 20\,\mathrm{MeV}$. Experimental data is compatible with nuclear symmetry energies J between 28 and 34 MeV and a symmetry slope parameter L between 20 and 120 MeV. References and definitions for those parameters can be found in e.g. [115]. The corresponding values for the three EoS can be found in Tab. B.1.

Fig. B.4 displays the relation between various thermodynamic properties for different EoS.

DD2 generates a high pressure at a given energy-density and is therefore considered as stiff, while FSG generates a lower pressure and is considered soft. SFHo has a medium stiffness between DD2 and FSG.

The sound speeds of DD2 and FSG are causal for all tabulated values. SFHo becomes acausal at very high pressures but for those pressures the NS configurations are already unstable.

For low densities all the tabulated EoS become extremely similar since the different parametrizations of the nuclear interaction have very limited impact on the low density regime of the EoS.

Fig. B.3 shows the complete mass-radius and mass-central baryon-density curves for all three tabulated EoS and for the analytic ones introduced previously.

At low baryon-densities $n_\mathrm{B}(0) \lesssim 10^{-8}\,\mathrm{fm}^{-3}$ equilibrium configurations of the tabulated EoS are on a self-bound planet branch. With a rather high maximum planet mass of $0.38\,M_\odot$. The low temperature, low pressure asymptotic of those general purpose EoS is microscopically not fully realistic. The EoS can not describe the exotic phases and crystalline structures [1, 114] of a realistic NS crust and they do not approach $n_{\mathrm{B,Fe}}$ for $P \to 0$. For a detailed description of the crust one would need to use an extra EoS for the crust like BPS [120]. For all discussions within this work such a detailed model of the NS crust is not necessary and we use the plain general purpose EoS only.

For central densities below $1.3 \times 10^{-6}\,\mathrm{fm}^{-3}$ stable configurations are on a white dwarf (WD) branch stabilized by the degeneracy pressure of the electron gas. The maximum mass on this WD branch is $0.96\,M_\odot$ with a corresponding radius of 1554 km. Those values are rather low for realistic WD but since DD2, SFHo and FSG do not describe WD matter that is to be expected.

The stable NS branch begins for $n_\mathrm{B}(0) \gtrsim 0.8 \times 10^{-2}\,\mathrm{fm}^{-3}$ beyond the neutron drip line. Stable configurations on the NS branch are stabilized by the degeneracy pressure of the nucleons and the strong repulsive component of the nuclear interaction at short ranges. Properties of configurations on this branch are discussed in Sec. 5.1.

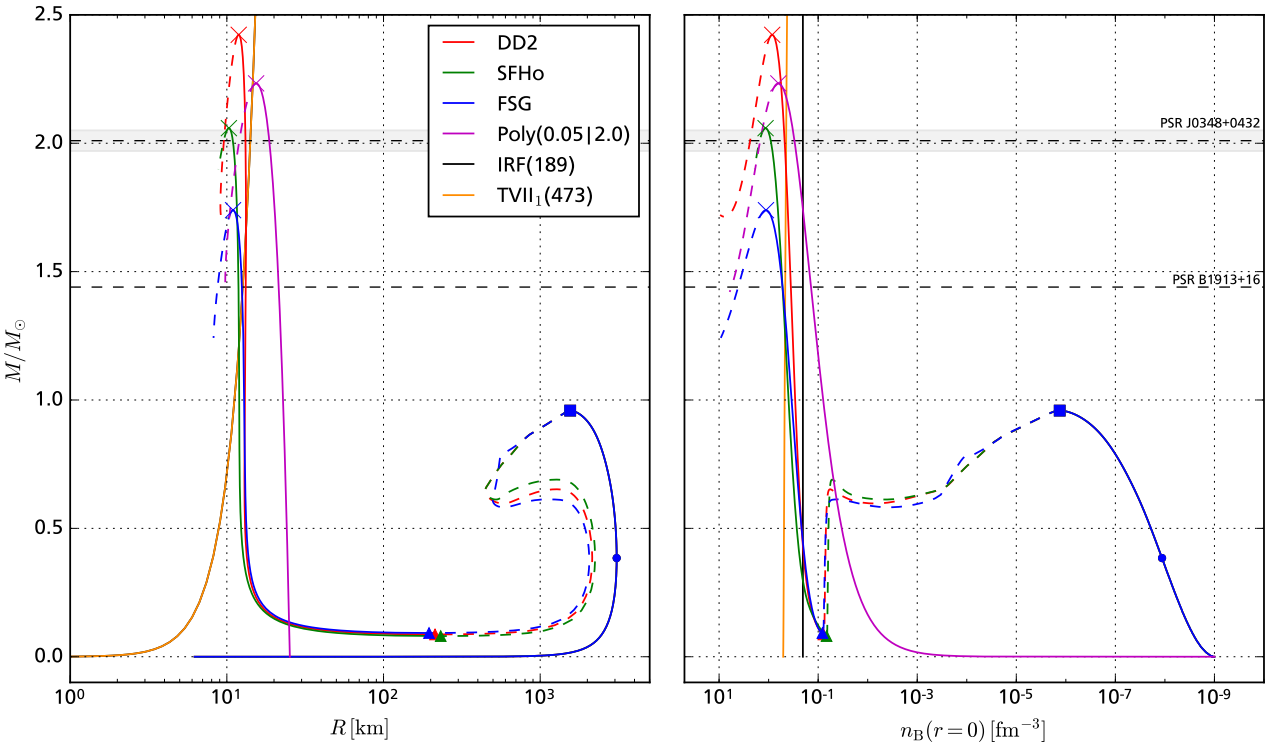

Figure B.3: Mass-radius (left) and mass-central baryon-density (right) curves for the tabulated general purpose EoS DD2, SFHo and FSG. For comparison we included the analytic EoS Poly(0.05|2) , IRF(189) and TVII$_1$(473) . Crosses denote the NS with maximum mass, triangles denote the onset of the stable NS branch, squares mark the WD with maximum mass and the points denote the onset of the self-bound planet branch.

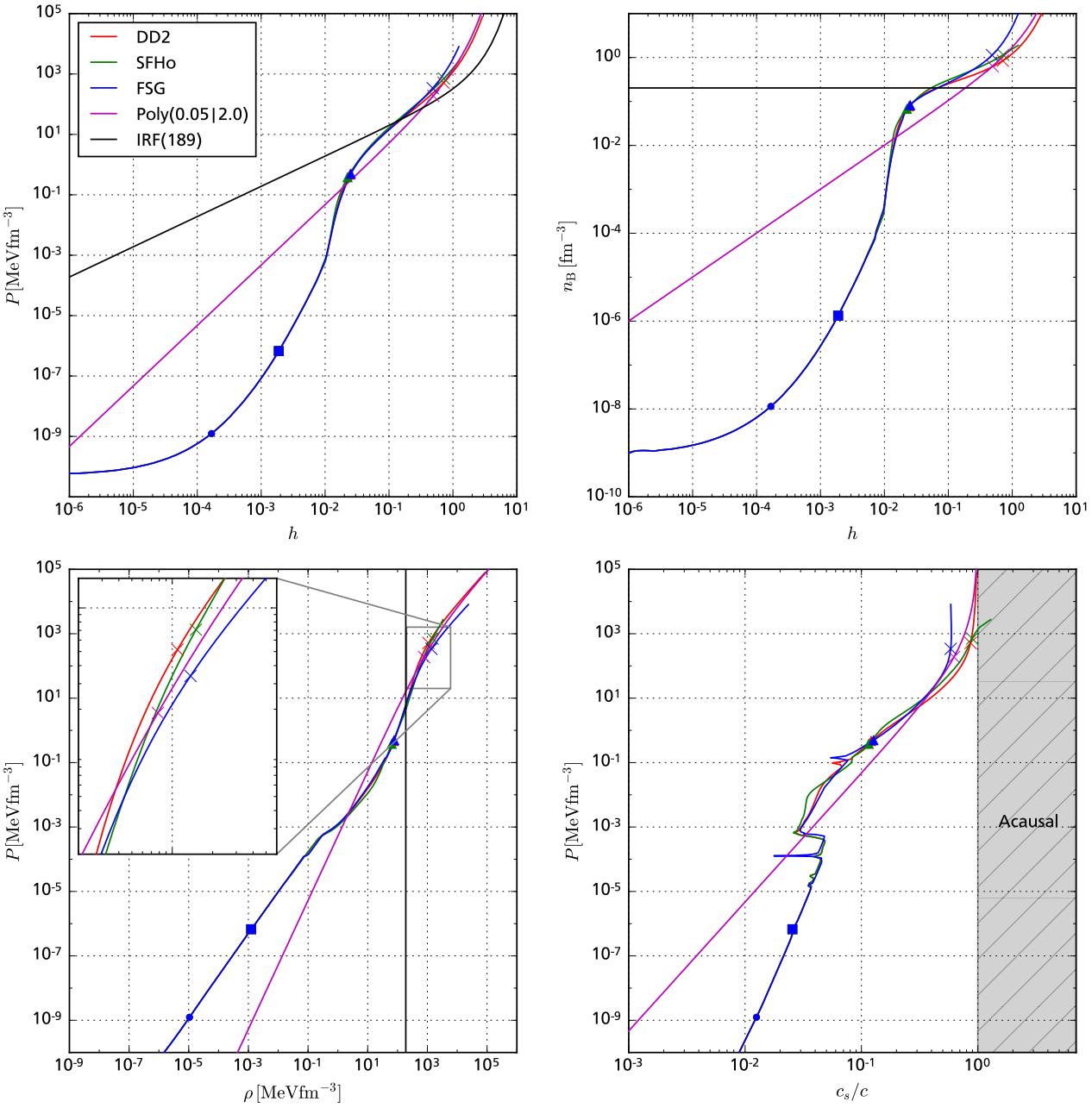

Figure B.4: Pressure over log-enthalpy (top-left), baryon-density over log-enthalpy (top-right), pressure over energy-density (bottom-left) and pressure over speed of sound (bottom-right) for the tabulated, general purpose EoS DD2, SFHo and FSG. For comparison we included the analytic EoS Poly(0.05|2) and IRF(189) . The markers denote the central values corresponding to the special equilibrium configurations marked in Fig. B.3.